Development of co-immobilization hydrogel of anaerobic digestion microbes with conductive material and evaluation of its anaerobic digestion performance

2025 年 3 月

Stella Chan On San

Contents

Acknowledgements

I would like to express my deepest gratitude to my supervisor, Professor Junichi Ida, for his unwavering support, encouragement, and guidance, not only in my research but also in my life as an international student in Japan over the past six years. It has been an honor to learn from and work with such an inspiring mentor. Thank you for believing in my potential, even when I couldn't see it myself.

I would also like to extend my sincere thanks to my co-supervisors, Professor Kiyohiko Nakasaki and Professor Tatsuki Toda, for their time, effort, and valuable insights on my Ph.D. thesis. Their comments and suggestions have been instrumental in shaping my research.

A special thanks to Professor Tatsushi Matsuyama and Dr. Mitsuhiko Koyama for their insightful feedback and guidance, which helped me refine my research plans and achieve better results.

To Dr. Kento Nishi, thank you for your mentorship and support throughout my entire academic journey, from my bachelor's days through to the completion of this Ph.D. Your guidance in experimental planning, result discussions, thesis writing, and preparation for international conferences has been invaluable. I am also deeply grateful for your continuous care for my well-being.

I would like to acknowledge the members of Professor Toda's CRET team and the Institute of Plankton Eco-engineering for their generosity in sharing knowledge and lending apparatus, which enabled me to complete my research. I am also thankful to the Hokubu Sludge Treatment Center for providing the experimental materials necessary for this study.

Last but certainly not least, I would like to thank my parents, Mr. Chan Weng Choy and Mrs. Beh Cha Boh, and my sister, Sheila Chan On Lei, for their constant encouragement

and unwavering support throughout my Ph.D. journey. I could not have overcome the challenges of this journey without their love and belief in me.

Finally, I am eternally grateful to Dr. Daisaku Ikeda and Mrs. Ikeda, the founders of Soka University, for creating an environment where I could thrive both academically and personally during my time in Japan. Their heartfelt encouragement has been a constant source of strength and inspiration throughout my life. I am profoundly thankful for the opportunity to build lasting friendships with people from all around the world. Although Dr. Ikeda is no longer with us, I will continue to carry his spirit in my heart and remain forever grateful to him. Thank you, Dr. Daisaku Ikeda, for your enduring legacy and inspiration.

Abstract

Anaerobic digestion (AD) is known for its low-cost, environmentally friendly organic wastewater treatment method. Recently, the direct interspecies electron transfer (DIET) mechanism has been receiving great attention as it can accelerate the AD process. In general, H_2 converted by acetogen acts as an electron transfer mediator through diffusion to methanogen to produce CH_4 is a rate-limiting step owing to the slow diffusion rate of H_2. Recently, it has been reported that the addition of conductive materials (CM) into the AD bioreactor could act as a bridge to promote direct interspecies electron transfer (DIET) between exoelectrogenic bacteria and methanogens. However, even with the addition of CM, DIET cannot occur unless exoelectrogenic bacteria have grown to a certain extent. Furthermore, by looking at the DIET phenomena from the perspective of powder technology, because the bacteria and CM can be regarded as particles, all three (exoelectrogenic bacteria, methanogens and CM) must be in contact with each other for DIET to prevail. However, due to the flow of water in a dispersed condition, the contact efficiency between the three is relatively low leading to low electron transfer efficiency. In addition, continuous addition of CM is needed due to the washout of CM together with the effluent when operated in a continuous process. To address these challenges, we developed a "co-immobilized hydrogel of AD microbes and CM" using polyvinyl alcohol (PVA) to enhance DIET by improving its contact efficiency, an approach which has never been done before.

First, before developing the co-immobilized hydrogel, we evaluated three CMs—granular activated carbon (GAC), multi-walled carbon nanotubes (MWCNTs), and polyaniline (PANI)—using two substrates, sodium propionate and ethanol, to identify optimal culturing conditions and the best CM for immobilization (Chapter 2). Results showed that sodium propionate had no effect on increasing the methane production rate, even with the addition of

CMs. However, with ethanol as a substrate, *Geobacteraceae*, an exoelectrogenic bacterium, was enriched, and DIET was enhanced, resulting in faster methane production rate. The order of *Geobacteraceae* abundance (GAC > MWCNTs > PANI > Control) corresponded with a higher rate of methane production, implicating that abundance of *Geobacteraceae* could directly improve the AD performance. Therefore, culturing AD microbes using ethanol as a substrate is an important factor in promoting the DIET mechanism.

Next, we explored four immobilization methods from previous studies on gas-producing bacteria to determine the best method for AD microbe immobilization (Chapter 3). Most methods failed due to the small porosity of the synthesized hydrogel which entrapped the produced biogas, leading to system acidification and hydrogel damage/rupture within seven days of the AD experiment. However, the freeze-thawing method for synthesizing PVA-cryogel with macropores showed promising results; with good biogas permeability, no inhibition in AD performance or deformation of the hydrogel was observed, making it the chosen method for immobilization and was further optimized for better performance (Chapter 4). Optimization involved adjusting the biomass content from 30% to 80% (w/w) and varying CM concentration from 0.5 to 3.0 g L^{-1}. Although GAC showed the best performance in chapter 2, MWCNTs were eventually selected as the CM for co-immobilization due to easier and more successful immobilization with lesser MWCNTs concentration needed compared to GAC. The results show that a biomass content of 30% combined with 1 g L^{-1} MWCNTs shortened the stabilization period and improved hydrogel durability compared to other conditions and was therefore selected as the optimal condition.

Lastly, the optimized co-immobilized hydrogel was evaluated in the AD batch experiment, along with the dispersed sludge as control and dispersed sludge with MWCNTs addition as the conventional DIET method. The results shows that the methane production rate for the co-immobilized hydrogel was 2.5-fold and 1.9-fold faster than that of the control

(dispersed sludge) and conventional DIET (dispersed sludge with MWCNTs addition), respectively. Microbial analysis indicated the enrichment of functional microbes such as *Anaerolineacea*, *Sedimentibacteraceae, Rhodocyclaceae* and *Methanothrichaceae,* which may be involved in the DIET under the co-immobilized conditions. Additionally, the presence of predicted functional *pilA* and multiheme c-type cytochrome genes analyzed by PICRUSt2 suggest the prevalence of DIET. These findings suggest that the co-immobilized hydrogel method significantly enhances methane production rates through improved contact efficiency between AD microbes and CMs. This approach demonstrates potential for advanced continuous AD processes, enabling smoother performance even under higher organic loading rate conditions.

Chapter 1

General introduction

1.1 Organic waste and wastewater treatment

With the rapid growth in human population and the expansion of industrial activities the generation of organic waste and wastewater has inevitably increased. Such waste contains high levels of organic matter, and if released directly into the environment, it can lead to water pollution, eutrophication and ecosystem disruption (Beristain-Cardoso et al., 2011). Therefore, effective treatment is essential to mitigate further disruption to the ecosystem. Various technologies have been developed and employed for decades to treat such organic waste. For example, landfilling and incineration are commonly used for solid organic waste. Although these methods have been widely implemented, both have significant environmental drawbacks. Landfills not only consume valuable land resources but are also recognized as a major source of anthropogenic greenhouse gas (GHG) emission, primarily due to the substantial quantities of CH_4 and CO_2 released during the decomposition of waste material deposited in these sites (Kumar, 2004). On the other hand, while incineration treatment process is very efficient as it burns 90% of the initial waste, it is expensive, unsuitable for wet waste, and produces harmful byproducts such as acid gases, carcinogenic dioxin, nitrogen oxides (NOx), sulfur oxides (SOx), and ash containing heavy metals (Jacob et al., 2021, Khan et al., 2022).

In terms of wastewater treatment, the aerobic wastewater treatment process is widely used. Aerobic treatment is a biological process that utilizes oxygen to breakdown organic matter and remove pollutants such as nitrogen and phosphorus from wastewater (Ahmad et al., 2019). While this treatment method is efficient and produces minimal reject water, it requires significant energy input, primarily due to the need for continuous oxygen supply (Karolinczak et al., 2021). It has been reported that aeration is identified as the most energy-demanding operation in the wastewater

treatment plants, representing about 75% of the total energy usage (Rosso et al., 2008). Furthermore, the aerobic process generates a considerable amount of excess sludge, and its treatment and disposal constitute around 60% of the plant's operating costs, thereby increasing the overall operational expenses (Divyalakshmi et al., 2015). Additionally, aerobic treatment results in the production of CO_2, a major contributor to global warming. Given these drawbacks, while these treatment methods are effective, it is not a sustainable option considering current environmental and energy challenges.

Conversely, methane fermentation, also known as anaerobic digestion (AD), has gained much interest in treating both solid and liquid organic waste due to its low energy requirements and the ability to produce renewable biogas, offering a more sustainable and cost-effective solution. AD is a biological process that breaks down organic waste in the absence of oxygen. Thereby, AD has many advantages compared to aerobic treatment, such as lower energy requirements, as no energy is required for oxygenation. Moreover, it generates significantly less excess sludge (6 to 8 times less compared to aerobic process) resulting in reduced costs for sludge treatment and disposal (Ghangrekar & Behera, 2014). This lower biomass production also decreases nutrient requirements, while the breakdown of organic matter generates biogas (CH_4 and CO_2), which is captured and converted into a valuable renewable energy source (Muralikrishna & Manickam, 2017). Further details on the process of AD will be outlined in the next section.

1.2 Organic waste and wastewater treatment by Anaerobic Digestion

As mentioned on the above section, Anaerobic Digestion (AD), is a cost-effective and environmental friendly technology for organic waste treatment though microbial interactions. The process converts high-molecular-weight organic compounds into CH_4 and CO_2 through the four key phases: hydrolysis, acidogenesis, acetogenesis, and methanogenesis, all occurring in the absence of oxygen (**Figure 1-1**). During hydrolysis, complex organic matters is first broken down by hydrolysis bacteria into simpler molecules like sugars and amino acids. These intermediates are further broken down by acidogenic bacteria in the acidogenesis phase, converting them into volatile fatty acids

(VFAs) and alcohols. Next, the acetogenic bacteria oxidize the VFAs and alcohols into H_2, CO_2, and acetate. Finally, methanogenesis —the slowest but most crucial step— produces CH_4 and CO_2 through two major pathways where: (1) acetate is converted into CH_4 and CO_2, and (2) H_2 and CO_2 are converted into CH_4 and H_2O. In addition to these classical pathways, alternative microbial processes, such as homoacetogenesis and acetate oxidation, also play significant roles in CH_4 production under certain conditions (Angelidaki & Batstone, 2010). Homoacetogenesis is a process in which homoacetogenic bacteria reduce CO_2 using H_2 to produce acetate. This process competes with hydrogenotrophic methanogens for H_2 consumption, but it also provides additional acetate which can be utilized by acetoclastic methanogens to produce CH_4. On the other hand, acetate oxidation involves syntrophic acetate-oxidizing bacteria (SAOB) that oxidize acetate into H_2 and CO_2. Reports indicate that this pathway becomes dominant under thermodynamic constraints (e.g., thermophilic conditions or high ammonia concentrations) or when acetoclastic methanogens are inhibited (Pan et al., 2020). The H_2 and CO_2 produced during acetate oxidation are subsequently converted into CH_4 by hydrogenotrophic methanogens. These alternative pathways are particularly important in stabilizing AD systems when microbial competition or unfavourable environmental condition hinder the efficiency of classical methanogenesis. Overall, the biogas typically consists of 50-75% CH_4 and 25-50% CO_2 (Li et al., 2019). The advantage of this process is that the produced methane gas can serve as a renewable energy source, reducing carbon emission by providing electricity, heat, or even converting into biofuel (Zaks et al., 2011). Additionally, the remaining digestate which contains valuable nutrients such as nitrogen and phosphorus could repurposed as biofertilizers or used to cultivate microalgae, which has garnered much interest in the recent years (Milano et al., 2016).

However, even with such advantages, AD faces several operational challenges, particularly in between the acetogenesis and methanogenesis reaction. In the conventional AD process, acetogens convert H_2 or formic acid, which acts as an electron transfer mediator facilitating the production of CH_4 by hydrogenotrophic methanogens (Gahlot et al., 2020). Previous research has found that the hydrogen concentration must be kept low (H_2 $<10^{-4}$ atm) to maintain thermodynamically feasible

conditions for fermentative bacteria to sustain the fermentation process (De Bok et al., 2004). However, the slow diffusion rate of H_2 is a rate-limiting step in this process (Zhang et al., 2019). When applying a high organic loading condition, the accumulation of H_2 ($H_2 > 10^{-4}$ atm) inhibits the acetogenic reaction. This leads to the accumulation of VFAs, resulting in the acidification of the digester and leading to a failure of AD, as methanogens are highly sensitive to low pH (Ye et al., 2012, Zhang et al., 2019). Therefore, even though a high organic loading rate (OLR) is more favorable in an AD process owing to its smaller-footprint digester and lower heating cost, low OLRs are often necessary to maintain appropriate hydrogen levels and ensure stable AD operation, representing a key challenge in the process.

1.3 Direct Interspecies Electron Transfer (DIET) in Anaerobic Digestion

To address this challenge, recent discoveries have revealed that the direct interspecies electron transfer (DIET) mechanism can rapidly convert VFAs to methane gas. Unlike the conventional AD, which transfer electrons to methanogens via H_2 (**Figure 1-2 (A)**), DIET bypasses the need for H_2 production. Instead, it facilitates direct electron transfer from exoelectrogenic bacteria to methanogens using biological conductive nanowires (**Figure 1-2 (B)**), membrane-bound electron transfer protein (**Figure 1-2 (C)**), or non-biological conductive materials (**Figure 1-2 (D)**) (Park et al., 2018). The exoelectrogenic bacteria are defined as bacteria that can transport electrons across their plasma membranes for extracellular electron transfer.

Conductive nanowires, or also known as e-pili, are pilin proteins frequently found on cell surfaces, playing crucial roles in bacterial movement, conjugation, and surface adhesion (Sharma et al., 2018). The phenomena of DIET occurrence through conductive nanowire (**Figure 1-2 (B)**) were first found by Morita et al., 2011 with the observation of *Geobacter* sp. aggregated in a microbial granule which was electrically conductive in the up-flow anaerobic sludge blanket (UASB) (Morita et al., 2011). The conductive nanowire act as a bridge to transfer electrons directly from the exoelectrogenic bacteria to methanogens, while the methanogens use the received electrons, carbon

dioxide and hydrogen ion to generate the methane gas. Recent reports also proposed a hypothesis on explaining the electron transfer mechanism of the conductive nanowires, suggesting that these nanowires conduct electricity due to the overlapping $\pi - \pi$ orbital of the aromatic amino acids in their structure (Sharma et al., 2018, Nguyen et al., 2021). Many studies have also shown that *Geobacter* species can promote DIET to the *Methanothrix* (previously known as *Methanosaeta*) or *Methanosarcina* using the conductive nanowires (Chen et al., 2014, Rotaru et al., 2014). Thereby, these are among the most well-known syntrophic bacteria and methanogens involved in the DIET mechanism.

As for DIET via membrane bound electron transfer protein mechanism (**Figure 1-2 (C)**), this process functions similarly by transferring electrons directly to the methanogens, but without the presence of conductive nanowires. This mechanism was discovered by Ha et al., 2017, where electron transfer occurred in aggregates of *Prosthecochloris aestaurii* and *Geobacter sulfurreducens* without the observation of conductive nanowires. Additionally, in a microbial fuel cell experiment, *G. sulfurreducens* was observed to be attached to electrodes while transferring electrons. The electron transfer was facilitated by multiheme outer-surface c-type cytochromes, which appears to be responsible for the electron transfer and are expected to participate in DIET (Richter et al., 2009; Lovley, 2017). Thereby, to achieve effective DIET via membrane bound electron transfer protein, the exoelectrogenic bacteria's membrane must be in extremely proximity to the electron-accepting methanogen's membrane, allowing for easier electron transfer between the two membranes (Dubé & Guiot, 2015). However, to date, only one c-type cytochromes, the *OmcS* cytochrome of *G. sulfurreducens*, has been studied in detail (Leang et al., 2010, Qian et al., 2011, Filman et al., 2019). Therefore, further research on the role of surface c-type cytochromes in DIET is needed to better understand this membrane-bound electron transfer mechanism. Nevertheless, compared to DIET via nanowire, which enables long-range electron transfer between microbes, DIET via membrane-bound electron transfer proteins is less commonly found in AD due to its limited practicality in many environments (Malvankar & Lovley, 2014).

Recent studies have also shown that, rather than relying solely on biological conductive nanowire or membrane bound electron transfer proteins, the addition of non-biological conductive materials (CMs) could act as a conductive bridge for the DIET (**Figure 1-2 (D)**). Due to their inherent characteristics—such as large specific surface area, high adsorption capacity, and excellent electrical conductivity— CMs offer the potential for achieving longer-distance electron transfer compared with DIET facilitated by biologically conductive nanowires (Jin et al., 2022). As a result, various CMs, including carbon- and iron-based materials, have been studied and demonstrated a significant enhancement in AD performance, including higher methane production rate, enhance process stability and shorten start-up/lag phase through the DIET process (Wang et al., 2021, Xiao et al., 2021). For instance, the addition of granular activated carbon (GAC) into the digestate could enhance the methane production rate by 2.5 times as compared to the conventional AD (Liu et al., 2012). Similarly, a study found that using magnetite can reduce lag time by nearly 1.5 times, and methane production increased three-fold than the conventional AD (Li et al., 2014). More recently, conductive polymers such as polyaniline nanorod have also been studied and have resulted in a two-fold increase in the rate of methane production (Hu et al., 2017). Additionally, most CMs exhibit higher conductivity than biological conductive nanowire (2–20 μS/cm), which can further enhance electron transfer between syntrophic species (Holmes & Smith, 2016). For instance, Liu et al. 2012 found that GAC improved syntrophic metabolism even in environments where DIET was already established via biological conductive nanowire, as GAC offers higher conductivity between cells leading to faster electron transfer. More importantly, DIET facilitated by CMs offers an ecological advantage over biologically mediated DIET, as it eliminates the need for additional energy for producing synthetic cellular appendages (conductive nanowires) (Kato et al., 2012). Therefore, DIET facilitated by non-biological CMs is generally more favorable than the biological mediated alternatives.

Overall, DIET offers distinct advantages over conventional hydrogen-mediated interspecies electron transfer in enhancing AD performance. Since H_2 is not involved in the DIET pathway, its

concentration does not inhibit the metabolic process. Moreover, mathematical modeling has shown that the rate of external electron transfer per cell pair through conductive nanowires in DIET is higher than that of H_2 diffusion transfers (44.9×10^3 e^- cell $pair^{-1}$ s^{-1} and 5.24×10^3 e^- $pair^{-1}$ s^{-1}, respectively), suggesting that DIET can enhance syntrophic conversion and stabilize AD processes even at high OLR conditions (Storck et al., 2015, Zhang et al., 2019). Furthermore, DIET is more energetically favorable than hydrogen-mediated processes, as bacteria can conserve their energy by eliminating the need for electron transformation to H_2 (Lovley, 2011). Research has also indicated that DIET could participate not only in acetogenesis and methanogenesis, but also in acetate oxidation and methanogenesis (conventional pathway: $CH_3COO^- + 2H_2O \rightarrow 2CO_2 + 4H_2$, $CO_2 + 4H_2 \rightarrow CH_4 + 2H_2O$. DIET pathway: $CH_3COO^- + 4H_2O \rightarrow 2HCO_3^- + 8e^- + 9H^+$, $1/2CO_2 + 4e^- + 4H^+ \rightarrow 1/2CH_4 + H_2O$) (Liu et al., 2012, Yang et al., 2019). Notably, various electron transfer mechanisms (via nanowires, membrane-bound proteins, or conductive materials) can coexist within the same microorganism. For example, with the addition of conductive materials, electrons can transfer first through nanowires or c-type cytochromes, then to the conductive materials, and finally to the methanogens. It should be noted that even with the prevalence of direct interspecies electron transfer (DIET), this mechanism is often observed in conjunction with hydrogen-mediated interspecies electron transfer (Wang et al., 2021).

1.4 Challenges in Anaerobic Digestion using Conductive Materials for Direct Interspecies Electron Transfer

As previously mentioned, the addition of CMs into AD digesters can induce DIET, thereby enhancing AD performance even at high OLR. As a result, various CMs have been extensively studied in the context of DIET mechanisms, progressing from batch to continuous reactor systems (Lei et al., 2016; Park et al., 2018; Zhang et al., 2020; Zhuang et al., 2020). Nevertheless, despite the addition of CMs, it is important to note that DIET cannot occur without the presence of exoelectrogenic bacteria. Many studies have shown that using ethanol as a substrate can facilitate the growth of exoelectrogenic bacteria such as the well-known *Geobacter* sp. (Rotaru et al., 2014a; Jin

et al., 2022). Ethanol has often been used in pre-culture conditions, and some studies suggest using ethanol-type fermentation substrates, such as polysaccharides, to enhance DIET efficiency (Liu et al., 2012; Zhao et al., 2016a). Despite the limited number of studies, DIET has also been successfully demonstrated using simpler substrates, such as propionate and butyrate, instead of ethanol. Given that propionate is a major VFA in digesters, it is crucial to investigate whether exoelectrogenic bacteria can thrive on propionate and enhance AD through DIET without the need for ethanol enrichment.

At an overview, to date, most studies related to DIET have only focused on exploring more efficient CMs or substrates (as mentioned above) to improve the DIET performance. However, aside from the type of CM and substrate, another factor may play a crucial role in facilitating DIET. From the viewpoint of particle technology, to transfer the electrons between particles, the particles need to be in contact. In that case, to achieve efficient electron transfer between particles, it is important to increase contact efficiency between particles. Since microbes and CM can be regarded as particles, even with the presence of exoelectrogenic bacteria, all three particles of exoelectrogenic bacteria, methanogens, and CMs must be in contact with each other to transfer electrons, for DIET to prevail. However, in the conventional continuous operation such as the Continuous Stirred Tank Reactor (CSTR) combined with DIET, low contact efficiency is evident, as the positions of AD microbes and CMs constantly change owing to stirring of wastewater flow, leading to reduced direct electron transfer efficiency. Another commonly used continuous reactor, the Upflow Anaerobic Sludge Blanket (UASB) process has essentially the same problem. Thus, improving the contact efficiency between all three particles of exoelectrogenic bacteria, methanogens, and CMs is crucial to improve electron transfer between the particles and to achieve more efficient DIET. So far, there has been no research from this viewpoint in AD related research using the mechanism of DIET. Therefore, this research will be focusing on the approach from this perspective to improving the AD process, which highlights its uniqueness and originality of my research.

Another significant bottleneck is the application of CMs in continuous operations, such as CSTRs or UASB reactors, where CMs are prone to washout and are difficult to recover due to their

insufficient density for settling, leading to a significant reduction in efficiency (Baek et al., 2023; Zhang et al., 2023).To maintain the DIET efficiency, continuous CM addition is required to compensate for their loss, but this approach increases costs and necessitates a comprehensive environmental impact assessment of CMs nanopollution. Notably, nanoparticles can be toxic to the environment when released, as their small size allows for persistence, bioaccumulation, and the disruption of cellular functions in organisms, potentially leading to long-term ecological harm (Martínez et al., 2020). Additionally, if a high concentration of CMs is washed out, it can increase the volume of biosolids requiring disposal and handling, further elevating operating costs (Gahlot et al., 2020). Furthermore, although studies have shown that the addition of CMs to AD can promote microbial growth on their surfaces, including methanogens involved in DIET (Qin et al., 2017), the continuous loss of these microbes, along with the CMs, remains unresolved, even with the continuous addition of CMs. Therefore, improving contact efficiency between CMs and microbes while retaining CMs in the reactor is a critical challenge that must be addressed for the feasible application of DIET mechanisms in the AD process to enhance the performance. However, this challenge has yet to be fully explored.

1.5 Solution proposal and research objective

Recently, microbial cells have been immobilized in hydrogels for the biotreatment of wastewater to overcome the limitations of process instability in long-term operation and microbe retention in bioreactors. The immobilization of microbial cells has many advantages, including providing higher biomass, reusing cells, resistance to toxic chemicals, and preventing microbe washout (Bouabidi et al., 2018). Several studies have shown that immobilizing microbial cells can improve the removal efficiency of water contaminants (Al-Zuhair & El-Nass, 2011, Kadimpati et al., 2012, Dong et al., 2014). However, research on immobilizing AD microbes within the hydrogels remains limited. Furthermore, in the limited available studies, all have focused on immobilizing AD microbes via the adsorption methods rather than using entrapment methods (Wenjie et al., 2008,

Pandey & Sarkar, 2017, Sitthi et al., 2020). Despite the great performance, adsorption methods require a preculturing period to facilitate the attachment of AD microbes to the hydrogel, which can be time-consuming. In contrast, immobilizing AD microbes via entrapment methods in hydrogel may potentially offer more advantages, such as maintaining high microbial concentrations, enhancing resistance to toxic substances, and reducing preparation time (omitting the preculturing period), as reported in other studies that have immobilized microbes such as nitrifying bacteria and anammox (Bouabidi et al., 2018).

Therefore, this study proposes a novel approach to address challenges in improving DIET performance in the AD process, specifically enhancing contact efficiency between CM and AD microbes, which has not been explored to date. This approach involves the co-immobilization of AD microbes and CM in a hydrogel using the entrapment method **(Figure 1-3)**. Co-immobilizing AD microbes and CM not only enhances their contact efficiency by maintaining their proximity and fixing their position, leading to more efficient electron transfer from acetogens to methanogens but also prevents CM from washing out from the reactor **(Figure 1-4)**. More importantly, this novel approach eliminates the need for a lengthy preculturing period because the microbes and CM are initially immobilized (entrapped) inside the hydrogel. Applying this approach to continuous operation, such as in a CSTR, could potentially solve contact efficiency problems and can achieve easy solid–liquid separation and cell/CM recycling. In the case of the UASB reactor, the start-up stage for granulation process is expected to be omitted by using the proposed method, as hydrogel immobilization requires less time compared to granulation.

The present study aimed to evaluate the effect of the proposed co-immobilization method on batch methane production performance and demonstrate the effectiveness of this method before advancing to the continuous process. To achieve these goals, first, we evaluated various CMs and substrates to establish and select suitable conditions for DIET to enhance AD performance for the immobilization process (Chapter 2). Next, a suitable immobilization procedure for AD microbes into hydrogel was developed and optimized (Chapter 3 & 4). Finally, based on the obtained results,

simultaneous co-immobilization of AD microbes with selected CM prepared under optimized condition will be evaluated in a batch test using ethanol as substrate for its AD performance (Chapter 5).

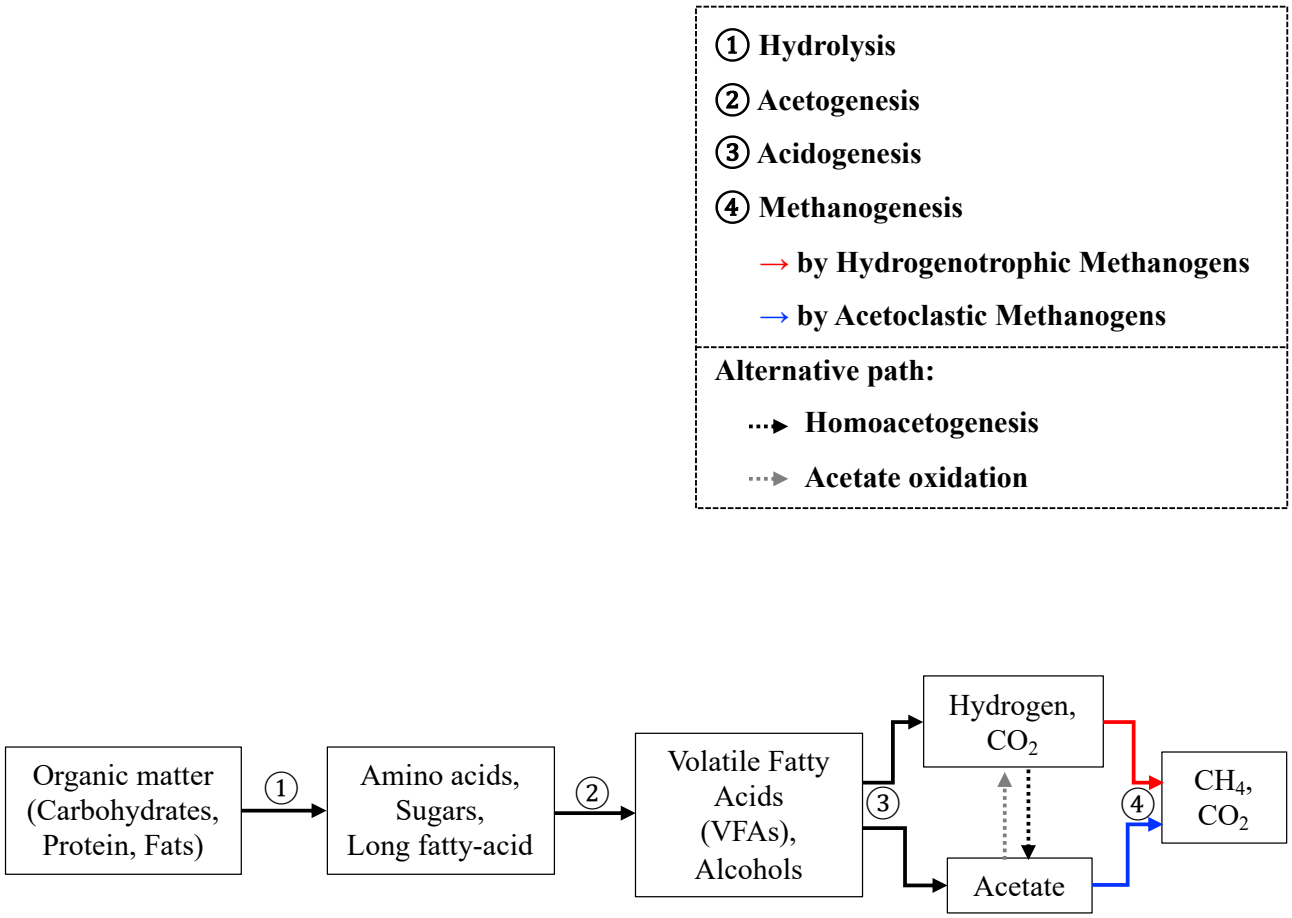

Figure 1-1. Degradation pathway of organic matters in anaerobic digestion

(A) Electron transfer via hydrogen

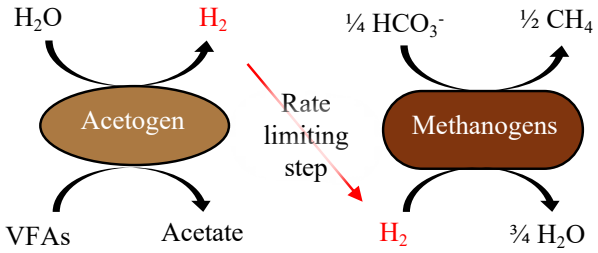

(B) Direct Interspecies Electron Transfer via Conductive nanowire

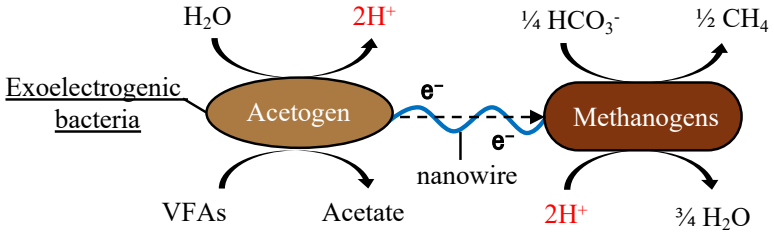

(C) Direct Interspecies Electron Transfer via Membrane-bound electron transfer protein

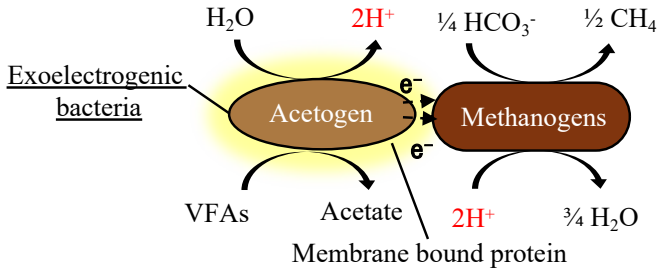

(D) Direct Interspecies Electron Transfer via Conductive Material

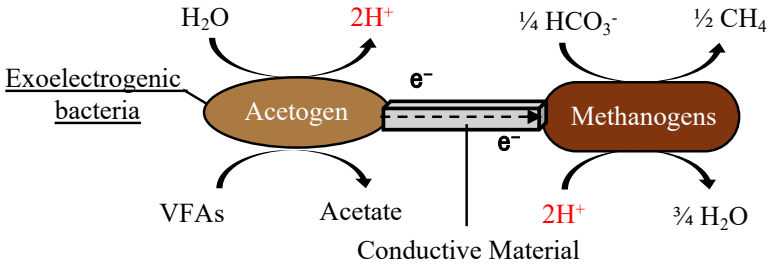

Figure 1-2. Traditional anaerobic digestion pathway through (A) Electron transfer via hydrogen, and the three mechanisms of DIET (B) DIET via Conductive nanowire (C) DIET via Membrane bound electron transfer protein (D) DIET via Conductive Materials

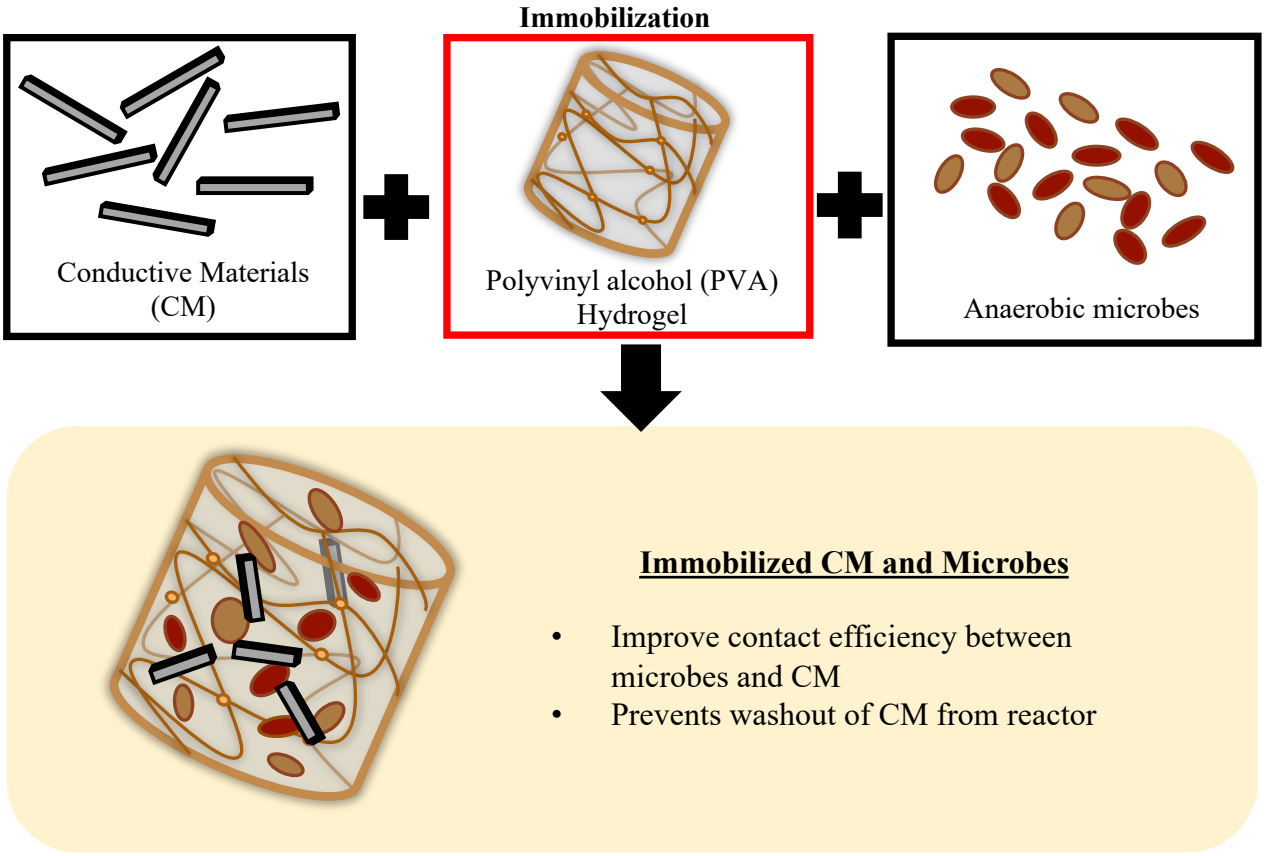

Figure 1-3. Proposal of co-immobilizing Conductive Materials (CMs) and Anaerobic Microbes together

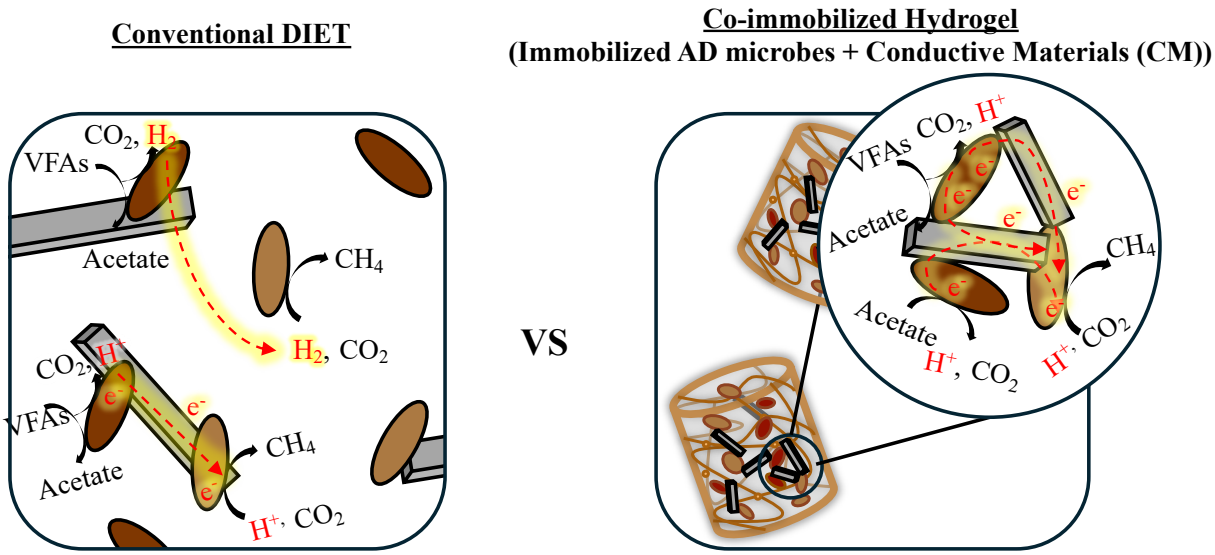

Figure 1-4. Comparison of conventional direct interspecies electron transfer (DIET) using conductive materials (CM) and the proposed co-immobilization of AD microbes and CM for enhanced electron transfer

Chapter 2

Establishing the culturing condition and selecting CM suitable for DIET to occur and to enhance the methane production performance

2.1 Background/Overview of Experiment 1

As introduced in Chapter 1, the addition of conductive materials (CM) to anaerobic digestion (AD) has received considerable attention because it could enhance the methane production rate through the direct interspecies electron transfer (DIET) mechanism. Consequently, many researchers have been investigating the effects of various types of CMs on methane production performance to determine the CM's optimal dosage concentrations. However, direct comparisons of different CMs' effects on methane fermentation under identical experimental conditions remain limited. To achieve effective DIET, it is understood that not only the type of CM but also the type of substrate is an important factor. Rotaru et al. (2014a) reported that *Geobacter* sp., a well-known exoelectrogenic bacterium which considered as one of the most effective microorganisms for DIET, was enriched when ethanol was used as the substrate. Other studies that utilized DIET to improve methane fermentation have also used ethanol as a substrate or added it during the preculture of microorganisms to enhance its efficiency (Liu et al., 2012, Rotaru et al., 2014b, Storck et al., 2015). However, although limited, there have been studies on DIET reporting successful utilization of simpler substrates, such as propionate and butyrate, aside from ethanol (Viggi et al., 2014, Zhang & Lu, 2016, Wang et al., 2020). Since propionate is one of the major volatile fatty acids (VFAs) products in the digester, it is worth studying whether exoelectrogenic bacteria can grow or maintain their growth under propionate substrate conditions and enhance methane fermentation performance via DIET without requiring ethanol enrichment. Thus far, no studies have directly compared different CM additions under the same experimental conditions, especially considering the combined effect of CMs and substrates.

In this chapter, three different types of CM—granular activated carbon (GAC), multi-walled carbon nanotubes (MWCNTs), and polyaniline (PANI)—were selected to evaluate their effects on

the methane production rate in two sets of batch experiments: one using sodium propionate and the other using ethanol as the substrate. The three CMs were chosen based on their high methane production rates reported in previous studies, as summarized in **Table 2-1**. It should also be noted that, instead of using the same concentration of each CM for comparison, all CMs were used at their optimal concentrations as reported in the literature. Since the optimal dosage of many CMs has been established, it is worth comparing different CMs at their optimal dosage under identical experimental conditions to understand the effect of optimized CM concentration on AD performance. As the DIET mechanism occurs only between acetogens and methanogens, propionate (a commonly generated VFA intermediate) was used as a substrate for comparison with ethanol. Additionally, to clarify the differences in methane production efficiency, the effects of the culture medium on the microbial community were also evaluated. Through this experiment, the most suitable CM and substrate will be chosen for use in subsequent studies.

2.2 Materials and Methods

2.2.1 Sludge, Substrate, and Conductive Materials (CMs)

Anaerobic sludge was collected from a mesophilic AD sludge biogas plant (6800 m^3) treating domestic sewage in the Hokubu Sludge Treatment Center in Yokohama, Japan. The collected sludge was left to degas at 37°C for approximately 4 days, to remove residual substrate in the inoculum. Two batch tests were conducted. In the first (Study I) sodium propionate was used as substrate and in the other (Study II) ethanol was used as substrate, along with trace elements and vitamin solution additions in both studies which were described by Morita et al., 2011. The components of the trace element solution were as follows: 0.5 g L^{-1} $MnSO_4 \cdot H_2O$, 0.1 g L^{-1} $FeSO_4 \cdot 7H_2O$, 0.04 g L^{-1} $NiCl_2 \cdot 6H_2O$, 0.05 g L^{-1} $CoCl_2 \cdot 6H_2O$, 0.13 g L^{-1} $ZnCl_2$, 0.01 g L^{-1} $CuSO_4 \cdot 5H_2O$, 0.1 g L^{-1} $AlK(SO_4)_2 \cdot 12H_2O$, 0.01 g L^{-1} H_3BO_3, and 0.025 g L^{-1} $Na_2MoO_4 \cdot 2H_2O$. The components of the vitamin solution were as follow: 0.002 g L^{-1} biotin, 0.005 g L^{-1} pantothenic acid, 0.0001 g L^{-1} B-12, 0.005 g L^{-1} -aminobenzoic acid, 0.005 g L^{-1} thioctic acid, 0.005 g L^{-1} nicotinic

acid, 0.005 g L^{-1} thiamine, 0.005 g L^{-1} riboflavin, 0.01 g L^{-1} pyridoxine HCl, and 0.002 g L^{-1} folic acid. The total solid (TS) and total volatile solid (VS) contents in the sludge were 24.3 g L^{-1} and 19.1 g L^{-1} for study I and 27.1 g L^{-1} and 23.2 g L^{-1} for study II.

Three different CMs: GAC, MWCNTs, and PANI were compared in this study. The GAC (20×50 mesh) was purchased from the Ueda Environmental Solution Company, Japan. MWCNTs (NC-7000, diameter = 9.6 nm, length = 1.5 μm, 90% purity) was purchased from the Nanocyl Company, Belgium. PANI was synthesized by interfacial polymerization according to the method proposed by Hu et al.,2019. Briefly, 1.6 mL of aniline solution was added to 100 mL chloroform solvent to obtain 1 M aniline solution. Ammonium persulfate (APS) of 8.22 g was dissolved in 100 mL deionized water. The APS solution was then dripped into the aniline solution and placed in Erlenmeyer flask at 25 °C. The aniline was polymerized for 2 h until the color of the solution changed from opaque to dark green. After polymerization, PANI was obtained by vacuum filtration and washed with acetone and deionized water 10 times for 10 mins each. The PANI was then dried in an electrical furnace at 70°C for 12 h. The resulting sample was analyzed using a Fourier transform infrared spectroscopy (FT-IR; IRPrestige-21, Shimadzu, Japan). This result (included in section 2.3.1) indicated the successful synthesis of PANI in the emeraldine salt state. Specific surface area and pore volume of the three CMs were analyzed by a surface area and porosity analyzer (ASAP2020, Shimadzu, Japan). All CMs were vacuumed to eliminate any oxygen remaining in the pores of CMs, to prevent any toxicity towards the microbes prior to the methane fermentation experiment.

2.2.2 Biomethane potential (BMP) test

The Biomethane potential (BMP) test was carried out in a batch operation using an automatic methane potential test system (AMPTS® II, BPC Instruments, Sweden). Reactor vessels of identical 500 mL medium bottles were used, each inoculated with 300 mL of AD sludge. Three different CMs with different concentration were added to reactors as follows: (1) 20 g L^{-1} GAC, (2) 1.0 g L^{-1} MWCNTs, and (3) 0.6 g L^{-1} PANI prepared as in section 2.2.1. The concentration of CM used in this

study were regarded as optimal for the most efficient methane production rate according to the literature (Hu et al., 2017, Zheng et al., 2020, Tiwari et al., 2021). For each condition, experiments were carried out in triplicate. As a control, a set of triplicate reactors was prepared without any CM addition. For all condition, the substrate was added in a 2:1 AD sludge to substrate ratio on volatile solid (VS) basis (Substrate for Study I: Sodium propionate, Study II: Ethanol), together with 3.0 mL of the trace element and vitamin solutions described in section 2.2.1. To obtain the net biogas production values from each batch, the blank reactor, in which no substrate was added, was also set up in triplicate, and the resulting biogas amount was subtracted from those of the other conditions.

All reactors were incubated at 37 $\pm$ 1 °C and stirred intermittently with 10 s mixing and 10 s resting at 100 rpm. In study I, the first cycle was carried out for 7 days after adding the sodium propionate substrate. After the first cycle, the same amount of sodium propionate was added again to perform the second cycle for a subsequent 10 days. Study II was conducted using ethanol as the substrate. In the case of Study II, cycles 1 and 2 were carried out in the same way as in study I. For Study II only, an additional 14-day cycle was conducted by adding ethanol during cycle 3. To avoid possible air contamination and achieve an anaerobic environment, N_2 gas was introduced to the reactors for 1–2 min before starting the experiment. The produced biogas during the experiment was first transported to a CO_2 stripping unit filled with 3.0 M NaOH, and the remaining biomethane was measured using a methane volume measuring device based on the principles of liquid displacement and buoyancy. For both study I and II, sampling and pH measurements were performed every 5 days throughout the experiment.

2.2.3 Analysis

Total solids (TS) and VS were measured using the American Public Health Association standardized methods, with detailed procedure provided in the **Appendix A** (American Public Health Association, 2005). The methane gas volume was automatically measured by AMPTS® II. pH was measured using a pH meter (B-212, HORIBA, Japan). Volatile fatty acids (VFAs) were analyzed

using a high-performance liquid chromatography (HPLC) detector (SPD-6AV, Shimadzu, Japan) equipped with the Shodex, KC-811 column, Waters, 600E for pump A and Senshu Scientific, SSC-3461 for pump B. The column temperature was kept at 60 °C. As mobile buffer phase, 3.0 mM of perchloric acid was used in the pump A at a flow rate of 1.0 mL min^{-1}. For the mobile buffer phase in pump B, a mixed solution of 2.0 mM sodium hydroxide, 15 mM disodium hydrogen phosphate, and 0.2 mM bromothymol blue was used at a flow rate of 1.0 mL min^{-1}. The ethanol content was analyzed using a gas chromatography with a flame ionized detector (FID) (GC-2014, Shimadzu, Japan) equipped with a BX-100 60/80 glass column. The temperatures in the injector, detector, and column were maintained at 250°C, 110°C, and 110°C, respectively. Nitrogen was used as carrier gas at a flow rate of 35 mL min^{-1}.

2.2.4 Scanning electron microscope (SEM) observation

The morphology of each CM before and after the methane fermentation experiment was observed using a scanning electron microscope (SEM) (JSM-7500, JEOL, Japan). The pre-treatment for the sample after methane fermentation experiment was carried out using the same method proposed by Salvador et al., 2017. In detail, the CM samples taken after the experiment were fixed in 2.5% (v/v) glutaraldehyde for at least 2 h and then washed with 0.1 M phosphate buffer solution (pH 7) for 15 min per wash, thrice. Samples were dehydrated by using ethanol through a sequence of increasing concentrations (10%, 25%, 50%, 75%, 90% and 100% (v/v)) for 20 min durations each. The last dehydration step (100% ethanol) was repeated for another 30 min and then the product was dried in a desiccator overnight. Finally, the samples were mounted on sample holders and coated with osmium for 5 s in a sputter coating unit (HPC-1S, Vacuum device, Japan). The accelerating voltage used was 10.0 kV.

2.2.5 Microbial composition

The initial and final sludge samples before and after the methane fermentation experiment under each condition were taken and immediately stored in a freezer at -20°C. Microbial analysis was performed using the method reported by Koyama et al., 2019. In detail, the bacterial DNA was extracted from the sludge samples using an ISOIL for Beads beating kit (319-06201, Nippon Gene Co., Ltd., Japan.). The 16S V3-V4 region was amplified using forward primer [5'-TCGTCGGCAGCGTCAGATGTGTATAAGAGACAGCCTACGGGNGGCWGCAG-3′] and reverse primer [5′-TCTCGTGGGCTCGGAGATGTGTATAAGAGACAGGACTACHVGGGTATCTAATCC-3′]. The PCR reaction was carried out using an automated thermal cycler (PCR thermal cycler dice, TaKaRa, Japan.) The PCR product was purified using the Wizard® SV Gel and PCR Clean-Up System quick protocol (Promega, USA). Dual indices were attached to the amplicon PCR product and Illumina sequencing adapters using the Nextera XT Index Kit. Index PCR product were purified using Agencourt AMPure XP beads (Beckman Coulter, USA). The mixed library was paired-end-sequenced with Illumina MiSeq system 2x300 bp) following the Illumina sequencing protocols. The raw reads were filtered based on purity with chastity values >0.6 using the Illumina MiSeq accessory software, and demultiplexed with bcl2fastq (ver. 1.8.3) Koyama et al., 2019, whereas the demultiplexed sequences were analyzed with QIIME2-2020.11 Bolyen et al., 2019. Sequences were denoised using DADA2 with the following parameters: trim left-f = 17, trim left-r =20, trunc-len-f = 260, trunc-len-f = 260, trunc-len-r = 220. The taxonomy was assigned to the representative sequences of OTUs by using a Naïve Bayes classifier pre-trained on SILVA release 138 clustered at 99% identity. Phylogenetic Investigation of Communities by Reconstruction of Unobserved States (PICRUSt2) package was conducted to predict the functional genes and corresponding biochemical pathways using the marker genes within 16 S rRNA sequences Douglas et al., 2020. All raw sequencing data has been deposited to the DDBJ Sequence Read Archive under the accession number DRA015671.

2.2.6 Calculations: Methane production rate data analysis

Since the activity of microbes are correlated to the biogas production, the cumulative methane gas production was fitted by the modified Gompertz model equation (Equation 1) to obtain the methane gas production rate and the lag phase (Lay et al., 1998).

The modified Gompertz model equation is as follows:

$$f(t) = P \times exp\left(-exp\left(\frac{e \cdot R_m}{P} \times (l - t) + 1\right)\right) \quad \text{Eq. 1}$$

where $f(t)$, P, R_m and l are cumulative methane production (mL) at time t, maximum cumulative methane production (mL) at the end of the incubation, maximum methane production rate (mL day^{-1}) and lag phase (day), respectively.

2.3 Result & Discussion

2.3.1 Characterization of synthesized PANI

Figure 2-1 shows the FT-IR spectrum of the synthesized PANI (polyaniline). The characteristic peaks of PANI at 1566 cm^{-1} and 1483 cm^{-1} correspond to the stretching vibrations of C=C in N=Q=N and N-B-N (Q: quinoid ring, B: benzenoid ring), respectively (Hu et al., 2019). It is important to note that while PANI can exist in three oxidation states—pernigraniline, emeraldine, and leucoemeraldine—only the emeraldine state exhibits significant electrical conductivity (Hu et al., 2017). Previous studies have reported that the key peaks of PANI in its emeraldine salt state appear at 1560 cm^{-1} and 1480 cm^{-1} (Yang et al., 2011). In this study, the observed peaks at 1566 cm^{-1} and 1483 cm^{-1} confirm the successful synthesis of PANI in the emeraldine salt state.

2.3.2 Characterization of Conductive Materials

Table 2-2 shows the results of the three CMs analyzed by ASAP2020, which reveal that GAC

had the highest specific surface area followed by MWCNTs and PANI, while MWCNTs showed the highest pore volume followed by GAC and then PANI. As the added concentration of each CM in the bioreactor is different (20 g L^{-1} GAC, 1.0 g L^{-1} MWCNTs, 0.6 g L^{-1} PANI), the total BET surface area and the total pore volume of CMs in the reactor were also calculated based on the quantity of each CM introduced and are summarized in **Table 2-2**. Both, the total BET surface area and the pore volume in the reactor, were highest for the GAC, followed by MWCNTs and then PANI. MWCNTs exhibited the largest pore diameter, followed by PANI then GAC. As microbial attachment with CM is necessary for DIET to occur, the CM's surface area and pore volume are important parameter. Greater surface area and pore volume could provide a more suitable habitat for microbes to attach easily, which assists the DIET mechanism. Based on these results, it is expected that more microbial attachment would occur with GAC, followed by MWCNTs, and then PANI.

The SEM images of CMs before and after the methane fermentation experiment are shown in **Figure 2-2**. As compared to the CMs before the experiment **(Figure 2-2 (A–C)),** microbial attachment is observed in all CMs following the experiment when viewed under the same magnification **(Figure 2-2 (D-F)).** Although GAC has been reported to have a high affinity for microbes (Bertin et al., 2004, Nageeb, 2013) it should be noted that microbial attachment was observed only on the rough surfaces near or in the pores of the GAC **(Figure 2-2 (D))** while little or no attachment of microbes was observed on the smooth surface (photo is not shown but similar to **Figure 2-2 (A)**). In contrast, as the MWCNTs and PANI both have rough surfaces, agglomerated sludge was observed around the CM on most of the surfaces for both cases **(Figure 2-2 (H,I))**. This tight agglomeration could be due to rougher surfaces and greater pore sizes attributed to MWCNTs and PANI compared to GAC, which could assist microbial attachment. Dense microbial surface packing was especially notable in the case of MWCNTs **(Figure 2-2 (E))**. As the MWCNTs has a long fibre-like structure, the aggregate of MWCNTs has a complicated and rough surface and high pore volume compared to the GAC. These unique properties could have provided a scaffold for easy microbial attachment. In addition, it has been reported that the CNT can easily form agglomerates

with sludge owing to their highly hydrophobic nature (Brar et al., 2010), and these are likely the reasons for much denser microbial attachment for MWCNTs than the GAC and PANI. This indicates that it is not only the surface area and pore volume, but also the surface properties of CMs that could affect microbial attachment.

2.3.3 Methane fermentation results

Cumulative methane production over time for Study I with propionate as the substrate is shown in **Figure 2-3**. No significant difference in the methane production rate was observed between the MWCNTs and control conditions in cycles 1 and 2. In comparison, the GAC and PANI experiments revealed slower methane fermentation in both cycles. This indicates that despite the addition of CMs, no enhanced methane fermentation was observed with propionate as substrate. Furthermore, for reasons not fully understood, the addition of CMs, especially GAC and PANI, was found to cause the slower methane fermentation.

Based on the results of VFA (acetate) concentration and pH **(Figure 2-4)**, the slower methane fermentation in GAC and PANI conditions is likely due to the inhibition of acetogen activity, rather than methanogen as there was no accumulation of acetate or drop in pH. The reason for the slower methane production in the GAC condition has not yet been confirmed, but as GAC is known for its superior absorption ability (Ahmed & Rothenberger, 2014), some toxic contaminants might have been absorbed on the GAC before the experiment, which may have led to the inhibition of acetogen. In the case of PANI, one possible reason for this could be attributed to minor remnants of chloroform, used during PANI synthesis. Chloroform has been observed to inhibit the acetogen bacteria (Knight et al., 2011). Although the PANI was washed thoroughly after synthesis, it is possible that a small amount of chloroform remained attached to the PANI, which caused acetogen inhibition. Therefore, before conducting Study II, PANI was once again synthesized using the same methods, but washed more carefully and thoroughly. Other CMs were also washed thoroughly to remove any unwanted substances which may have attached to the CMs prior to Study II.

The progression of cumulative methane gas production for the Study II when ethanol was used as substrate is shown in **Figure 2-5**. The result showed no significant differences for all the conditions in cycle 1. However, different methane production performances were observed in cycle 2, and the conditions with CM addition exhibited an improved and faster methane production than the control condition. However, the methane production rate of control in cycle 2 can be seen slower than in cycle 1, suggesting that the control condition might not be acclimating well with ethanol substrate. To obtain a result where the control was also acclimated, methane fermentation was further extended to cycle 3 over 14 days for Study II. In cycle 3, methane production for the control became faster up until day 3 than in the cycle 2, after which it slowed down. The reason for the sudden slowdown has not yet been clarified, but the drastic drop in pH and the accumulation of acetate in the reactor only for the control condition **(Figure 2-6)** indicates that the activity of methanogens was inhibited. To compare the methane gas production rate and lag time for each condition in both the Studies I and II, the modified Gompertz equation (Equation 1) was fitted to the cumulative methane production curves in the 2nd cycle and the results are shown in **Table 2-3**.

Despite the addition of CMs, the results indicate no improvement in the rate of methane production with propionate as the substrate (Study I). The result from study II, on the other hand shows that with ethanol as the substrate, the addition of CMs improved the methane production rate, and as compared to the control, the addition of GAC resulted in the highest methane production rate, followed by MWCNTs and PANI. The methane production rate for the GAC condition was approximately 2.3-fold higher than that for the control, while the MWCNTs and PANI conditions were approximately 1.9 and 1.3 folds higher, respectively. However, as can be observed in **Figure 2-5 (A)**, the effect of CM addition on the rate of methane production was not observed in cycle 1 even in Study II. This may indicate that microbes need to acclimatize to ethanol, and it takes a certain period of time for DIET to occur. Furthermore, the lag time for the CM-added conditions were approximately 0.1–2.4 days, which was shorter than that for the control which was approximately 3.3 days. As reported by Gahlot et al., 2020, while adapting to a new environment, fast growing microbes

tend to have a shorter lag phase than slow growing microbes. This means that the addition of CMs may help stimulate microbial growth attached to the CMs, which leads to shortening the acclimation time needed. In contrast the control condition showed a longer lag phase in cycle 2 when compared to the CMs-added conditions, and even to that for the control in cycle 1 as shown in **Figure 2-5 (B)**.

To examine the reason, time course changes in ethanol, acetate, and pH in cycles 1–3 of Study II are summarized in **Figure 2-6**. **Figure 2-6 (B-i)** shows that the control condition had a slower ethanol breakdown in cycle 2 than in cycle 1. This may indicate that inhibition of acetogen bacteria had occurred, leading to a slower ethanol breakdown, whereas the results for other CMs additions showed that it could help relieve the inhibition of acetogen bacteria. This may be due to the CMs providing scaffolds for microbes to grow on, and that this helped to acclimate faster for ethanol substrate. In the case of control, the time needed for the metabolic activity for cell growth (especially with exoelectrogenic bacteria) was longer, which resulted in a longer lag time in cycle 2. It has been reported that the lag phase can be considered as an occurrence of metabolic activity as the cells are preparing to grow (Bertrand, 2019).

It should be noted that the added amount of each CM in the present study was determined based on previously cited references, which identified the optimum amount for each CM to achieve a maximum improvement in methane production rate. Therefore, the amounts of added CMs were not the same, and were 20, 1.0, and 0.6 g L^{-1} for the GAC, MWCNTs and PANI, respectively (Hu et al., 2017, Zheng et al., 2020, Tiwari et al., 2021). In terms of the total BET surface and the total pore volume in the reactor **(Table 2-2)**, the GAC showed the highest values, followed by the MWCNTs and PANI. The order corresponds to the order of faster methane fermentation and a shorter lag phase. In addition, based on the SEM observation in **Figure 2-2**, microbial attachment was also confirmed in all CM added condition. Since the DIET mechanism can only occur when microbes are in contact with the CM, the result suggest that greater total surface area and larger total pore volume could aid more microbial attachment, contributing to faster methane fermentation rate and shorten lag time via DIET. However, despite the total surface area and total pore volume for the GAC being more than

120 times and 14 times larger, respectively, than those for the MWCNTs, which had the second fastest methane fermentation rate, the methane production rate for the GAC was only approximately 1.2 times faster than that for MWCNTs. This may be related to the results from the SEM, in which microbes were observed to attach only to the rough surface of GAC and not to the smooth surface. Furthermore, the total surface area and the total pore volume for the MWCNTs are more than 6 times and 22 times larger than those for the PANI, but the methane production rate for the MWCNTs was only approximately 1.5 times faster than that for the PANI. Therefore, the relationship between the methane production rate and total surface area/pore volume is not proportional. However, as mentioned earlier, the surface and pores are directly related to the ability of microbes to attach and grow, as well as transfer electrons through the attached surface. Therefore, it is reasonable to assume that a larger surface area and pore volume would have a positive influence on the rate of methane production.

2.3.4 Microbial composition

The microbial communities in the Study I and II; before and after the experiments, are shown in **Figure 2-7**. The numbers of clean reads for each study condition were as follows; 3323 (Before experiment), 3444 (Control), 3293 (GAC), 3406 (MWCNTs), 3359 (PANI) for Study I, 2933 (Before experiment), 3525 (Control), 3280 (GAC), 3430 (MWCNTs), 3348 (PANI) for Study II, respectively. It should also be noted that the VS for each condition **(Table 2-4)** before and after the experiment did not show a large difference, meaning the total amounts of bacteria and archaea in terms of VS in each condition were approximately the same. In Study I, when propionate acid was used as a substrate, *Anaerolineaceae* and *Methanosaetaceae* were the dominant bacterial and archaea families before and after the experiment, respectively. Several reports have shown that *Anaerolineaceae* were dominant with *Methanosaetaceae* when degrading propionate, suggesting that these microbes play an important role in propionate degradation and biogas production (Puengrang et al., 2020). *Syntrophobacteraceae,* which also contributes to degrading propionate, was only detected in all

conditions after the experiment. A higher relative abundance of *Syntrophobacteraceae* was observed for the CM-added conditions, except for the PANI. This indicates that the GAC and MWCNTs addition may have contributed to enhancing the growth of *Syntrophobacteraceae*. As to the microbes related to DIET, *Pseudomonadaceae*, which is known to be an exoelectrogenic bacteria, was found only in the sample taken before the experiment (Barua & Dhar, 2017), and was not found in any of the conditions thereafter. The results indicate that despite the addition of various kinds of CMs, propionate acid as the sole carbon source was unable to encourage the growth of *Pseudomonadaceae* or any other exoelectrogenic bacteria. A very small relative abundance of *Geobacteraceae* (0.57%) was simultaneously detected after the experiment only in the GAC-added condition. As stated earlier, *Geobacter,* which is one of the exoelectrogenic bacteria capable of donating electrons through its conductive nanowire, is a genus of *Geobacteraceae*. Several reports have shown that the *Geobacteraceae* was able to contribute to the DIET as an electron-donating bacterium (Zhang et al., 2017, Zhuang et al., 2018). The reason for *Geobacteraceae* only growing in the GAC condition is likely owing to the high BET surface area of GAC compared to other CMs **(Table 2-2)**. It has been reported that the high surface area of GAC could not only promote microbial attachment but also enhance microbial growth (Liu et al., 2012). However, owing to the relatively small amount of *Geobacteraceae*, there was no significant change in the methane production rate. While these results may stem from the mild toxicity (from possible toxic contaminant discussed in section 2.2.3) which could affect the acetogens, they also suggest that certain abundance of exoelectrogenic bacteria is necessary to significantly enhance methane production. Overall, the use of propionic acid as a substrate appears ineffective, even with the addition of conductive material (CM).

In contrast, when ethanol was used as a substrate in Study II, the dominant bacterial family both before and after the experiment was *Cloacimonadaceae*, a bacterium known to be an anaerobic mesophilic acetogen (Lee et al., 2018). As for microbes related to the DIET, no exoelectrogenic bacteria were detected before the experiment, but *Geobacteraceae* was detected in all conditions after the experiment, with GAC having the highest abundance (2.561%), followed by MWCNTs (0.904%),

PANI (0.836%) and then the control (0.766%). This suggests that the ethanol could induce the growth of *Geobacteraceae* similar to the results from previous studies (Zheng et al., 2015, Zhang et al., 2017, Zhuang et al., 2018). Another exoelectrogenic bacteria, *Desulfuromonadaceae,* which are closely related to *Geobacteraceae* both phylogenetically and functionally, was only detected in the MWCNTs (1.312%) and PANI (5.227%) added conditions (Lonergan et al., 1996). This may suggest that the MWCNTs and PANI could enhance the growth of *Desulfuromonadaceae*. Although no study has reported whether *Desulfuromonadaceae* plays a role in the DIET mechanism, there is a possibility that it could serve as an electron-donating bacteria as it is closely related to *Geobacteraceae*. This may explain the relatively high methane production rate, despite the low relative abundance of *Geobacteraceae* for the MWCNT and PANI condition. Hence, further study of microbes participating in DIET needs to be considered in our future work.

In study II, *Methanosaetaceae* were found to be dominant archaea family before and after the experiment. Interestingly, the increase in the relative abundance of *Methanosaetaceae* was observed only in the CM-added conditions, where the relative abundance of *Methanosaetaceae* before the experiment was approximately 5.5%, which increased to approximately 9.6% for GAC, 6.9% for MWCNTs and 10% for PANI. The relative abundance of *Methanosaetaceae* in the control after the experiment was 5.4%, that is, essentially the same as before the experiment. Previous studies have shown that *Methanosaeta*, a genus of *Methanosaetaceae* is one of the two methanogens capable of directly receiving electrons in the DIET (Rotaru et al., 2013, Rotaru et al., 2014b) In addition, it has been reported that the DIET can preserve cell energy as microbes do not need to form biological conductive nanowire when CM is added. Therefore, the DIET mechanism could help enrich its syntrophic methanogens (Zhao et al., 2016b, Holmes et al., 2017). These results suggest that the DIET was enhanced in the CM-added conditions by utilizing the CMs to transfer electrons to *Methanosaetaceae,* rather than using a less energetically favorable fermentative metabolism of generating hydrogen.

As mentioned earlier, the abundance of the DIET related to exoelectrogenic bacteria,

Geobacteraceae is enhanced by the addition of CMs in the order of GAC>MWCNTs>PANI>Control. This corresponds to the order of higher methane production rates in Study II. Enrichment of *Methanosaetaceae* was also found only for the CM-added conditions. These results indicate that the use of ethanol as a substrate, combined with CM addition, is important to help the growth and enrichment of the DIET-related exoelectrogenic bacteria, *Geobacteraceae*, and electrotrophic methanogen, *Methanosaetaceae,* which contributes to achieving an improved methane production performance in the AD process.

2.3.5 Predicted functional gene abundance related to methanogenic pathway for DIET presence analysis

To further examine if DIET occurred in Study II, the normalized abundance of genes that encode the key enzymes related to both of hydrogenotrophic and acetoclastic methanogenic pathways based on the KEGG (Map:00680) was predicted by PICRUSt2 and is shown in **Figure 2-8 (A)** (Yin et al., 2018, Zhao et al., 2019). In the hydrogenotrophic pathway, formylmethanofuran dehydrogenase (EC: 1.2.99.5) showed the most abundant gene encoded. Formylmethanofuran dehydrogenase is known to be the first enzyme in the hydrogenotrophic (carbon dioxide reduction) pathway as shown in **Figure 2-8 (B)** (Holmes et al., 2017). Especially for the CM-added conditions, the abundance of genes that encoded the key enzymes for the hydrogenotrophic pathway was higher than those for the control. Another gene to note is ferredoxin hydrogenase (EC: 1.12.7.2), which plays a key role in oxidizing H_2 to provide electrons for the reduction of CO_2 to CH_4 (Palacios et al., 2021, Rossi et al., 2022). The results indicate that the abundance of EC:1.12.7.2 genes in the GAC and MWCNTs conditions is higher than those in the Control and PANI conditions, suggesting activation of the CO_2 reduction pathway in the GAC and MWCNTs conditions. However, under the DIET mechanism, the abundance of EC:1.12.7.2 is expected to decrease, as electrons are directly transferred to methanogens, bypassing the need for H_2 oxidation. In a previous study by Li et al. (2022), the relative abundance of EC:1.12.7.2 was indeed lower in DIET-dominated conditions compared to the control.

Although not shown in the current results, raw data indicate that *Methanosaetaceae*—a group capable of participating in DIET—did not contribute to this gene in any of the condition. Instead, the only archaea contributing to this gene were *Methanospirillum*, which were found exclusively in the GAC and MWCNTs conditions. *Methanospirillum* is known to be hydrogenotrophic methanogens, utilizing CO_2 reduction pathway to produce CH_4 (Joshi et al., 2018). These findings suggest that the higher abundance of EC:1.12.7.2 in the GAC and MWCNTs conditions is attributed to *Methanospirillum* activity via a non-DIET CO_2 reduction pathway. In contrast, the gene encoded acetate-CoA ligase (EC:6.2.1.1) was detected with the highest abundance in acetoclastic pathway for all the conditions. It has been reported that there are two pathways to convert acetate conducted by different methanogens. *Methanosarcina* uses acetate kinase (EC: 2.7.2.1) and phosphate acetyltransferase (EC: 2.3.1.8), whereas *Methanosaeta* uses acetate-CoA ligase (EC:6.2.1.1) to convert acetate to acetyl-CoA (Smith & Ingram-Smith, 2007, Liu & Whitman, 2008). Although neither acetate kinase nor phosphate acetyltransferase (EC: 2.7.2.1 and EC: 2.3.1.8) was detected, it is reasonable since *Methanosarcina* was not detected in our experiment as outlined in the previous section. In contrast similar to the result for the enzyme in hydrogenotrophic (carbon dioxide reduction) pathway, as compared to the control, a 1.2–1.3 fold increase in abundance of the gene encoding acetate-CoA ligase enzyme was observed for the CM-added conditions. It should be noted that referring to the microbial composition result in our study, *Methanosaetasaea* which is an acetate-utilizing methanogen, was the dominant methanogen as compared to H_2-utilizing methanogens. However, since the abundance of genes that encoded the formylmethanofuran dehydrogenase (EC: 1.2.99.5) was higher than the acetate-CoA ligase (EC:6.2.1.1), it may suggest the methanogenesis completed by the hydrogenotrophic (carbon dioxide reduction) pathway could be dominant in all four conditions. Although these results seemingly contradict each other, it could support the presence of DIET. It has been reported that when *Methanosaeta* species were accepting electrons via DIET to produce methane, genes encoding enzymes in hydrogenotrophic were highly expressed at the transcription level (Rotaru et al., 2013). Meaning, *Methanosaeta* (an acetoclastic methanogen) could

utilizes the red-colored pathway to generate CH_4 when DIET is prevailed, instead of using the common blue-colored pathway depicted in **Figure 2-8 (B)**.

However, since the abundance of genes which encoded key enzymes predicted in **Figure 2-8 (A)** did not only belong to *Methanosaetasaea* sp. but also from the total archaea detected, the abundance of formylmethanofuran dehydrogenase and acetate-CoA ligase genes assigned to only *Methanosaetasaea* was extracted from **Figure 2-8 (A)** and is shown in **Figure 2-9**. As can be seen from the figures, all CM-added conditions showed an improved abundance of both the hydrogenotrophic (EC:1.2.99.5) and the acetoclastic enzyme (EC:6.2.1.1) when compared to the control. This aligns with a study reported by Rotaru et al., 2014b. This suggest that the *Methanosaetasaea* species were actively involved in the DIET mechanism through the reduction of carbon dioxide to methane under the CM-added conditions. However, the PANI conditions shows a higher abundance of functional genes than the GAC and MWCNTs conditions, even though the added concentration was the least. The reason for this result is still unknown and therefore further studies on determining the mechanism that enriches functional genes and how it affects the AD performance should be made. Also, it should be noted that the results only demonstrate the predicted functional genes, therefore future studies on the metatranscriptome are required to explore the activity enzyme at expression levels.

2.4 Conclusion

In this study, the combined effect of substrate type and CM addition on the improvement of methane fermentation was evaluated using propionate and ethanol as substrates and GAC, MWCNTs, and PANI as CMs. No improvement in methane production was observed when sodium propionate was used as a substrate, despite the addition of CMs of any type. The results from microbial composition analysis show that propionate as substrate could not enrich or maintain the growth of exoelectrogenic bacteria, and DIET could not be established. When ethanol was used as a substrate, a considerable improvement in the methane production rate and lag phase shortening for the CM-added cases was observed when compared to the control. There was a 2.3-, 1.9- and 1.2-fold increase in the rates for the GAC, MWCNTs, and PANI, respectively as compared to the control. Together with the results of microbial composition analysis and SEM observation, it was revealed that ethanol could aid the enrichment of exoelectrogenic bacteria, *Geobacteraceae*. The resulting higher relative abundance of *Geobacteraceae* related to DIET is likely the reason for the higher methane production rates. Based on the physicochemical characterizations of CMs, large total surface area and pore volume combined with surface roughness could facilitate microbial attachment, thereby contributing to the growth of *Geobacteraceae* as well as the efficient contact between microbes and CMs. Based on these results, we suggest that the following order may affects the DIET mechanism. First, since DIET requires the presence of exoelectrogenic bacteria, selecting an appropriate substrate is crucial and ethanol can effectively enriched exoelectrogenic bacteria. Second, the addition of CM, particularly with high surface area and pore volume, further promoted the enrichment of exoelectrogenic bacteria. Lastly, the increased abundance of exoelectrogenic bacteria lead to improved methane production performance. Overall, these results show that the combination effect of substrate and CM is very important for DIET to improve methane fermentation performance, and that ethanol as substrate with GAC as CM was the most effective combination tested. Thereby, ethanol was selected as the substrate for subsequent studies to promote the growth of exoelectrogenic

bacteria, facilitating more efficient DIET. As for the selection of CM, GAC was initially selected based on the high methane production rate performance from this study, however, was change to MWCNTs which also shows a good AD performance even at a small concentration amount. The reason for using MWCNTs will be further discussed in Chapter 4.

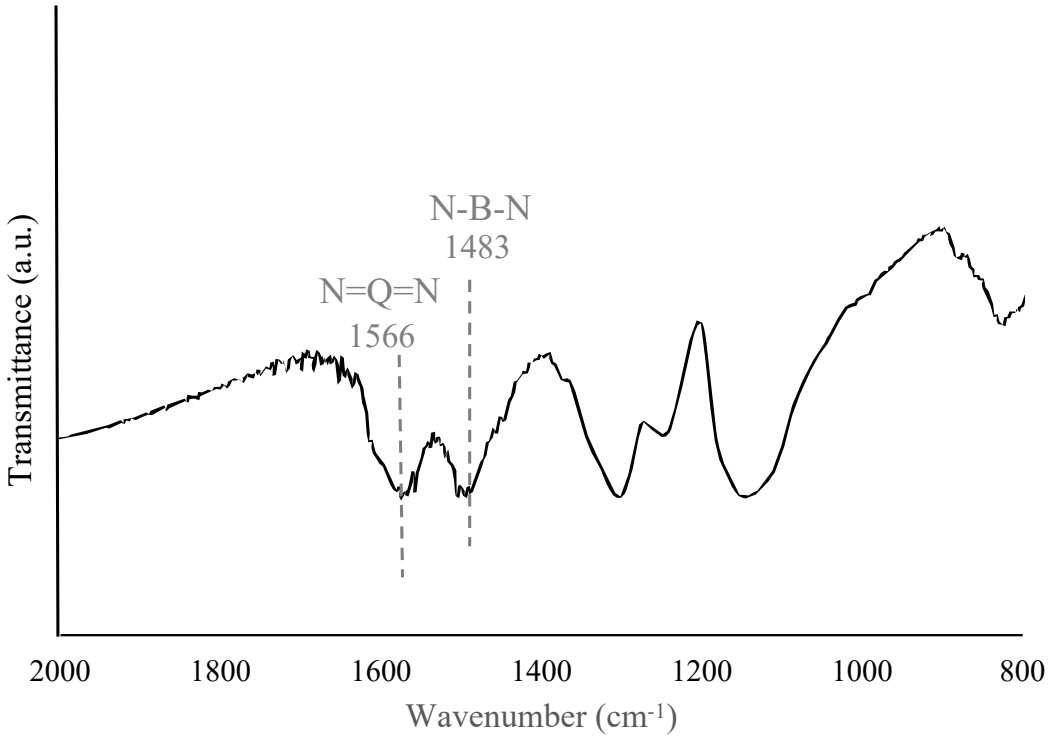

Figure 2-1. FTIR spectrum of synthesized PANI

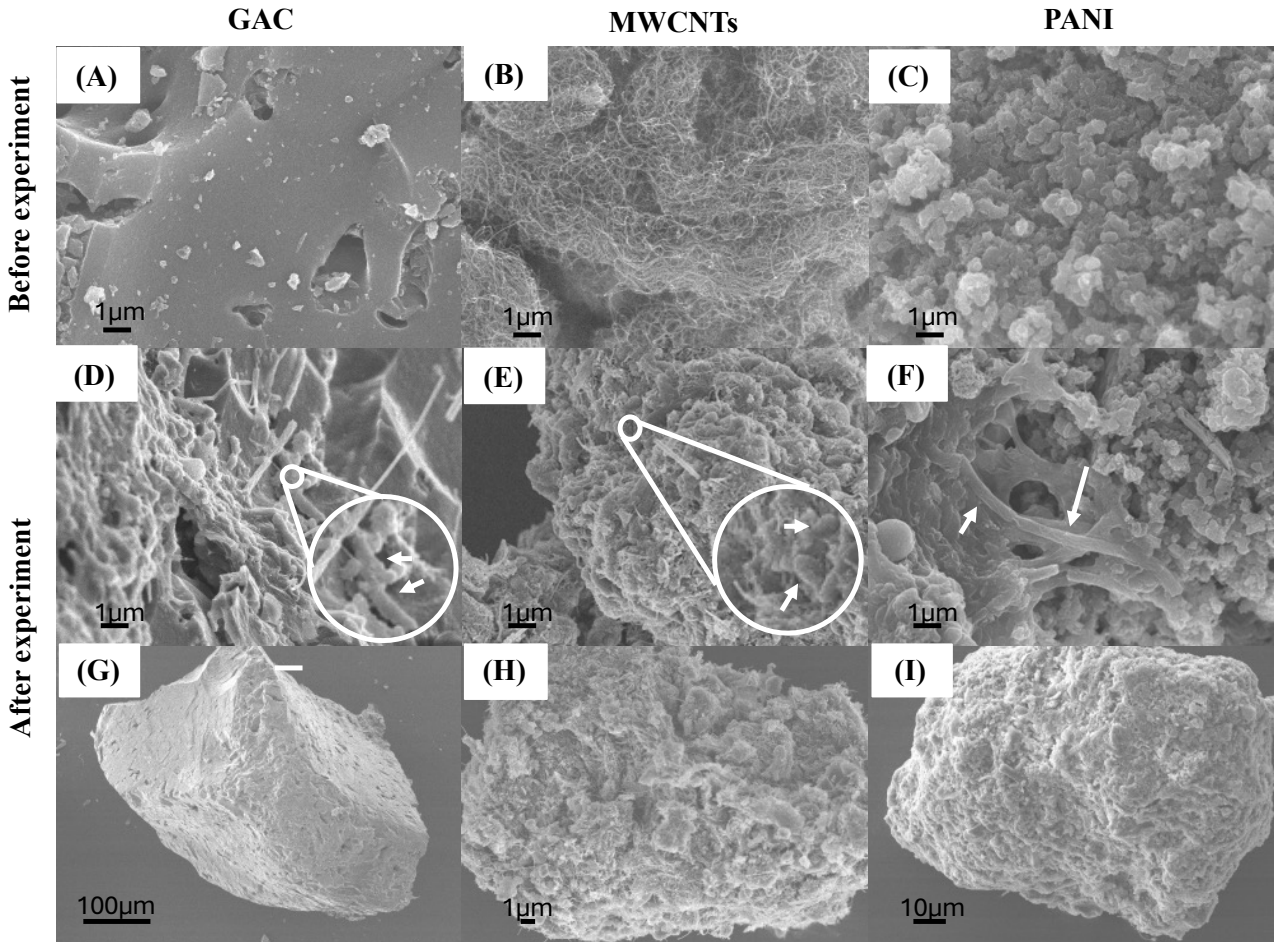

Figure 2-2. Scanning electron micrograph of granular activated carbon (GAC), multiwalled carbon nanotubes (MWCNTs), and polyaniline (PANI) in before the experiment at 8000 times magnification (A-C), after the experiment in 8000 times magnification (D-F), and after the experiment in smaller scale magnification respectively.

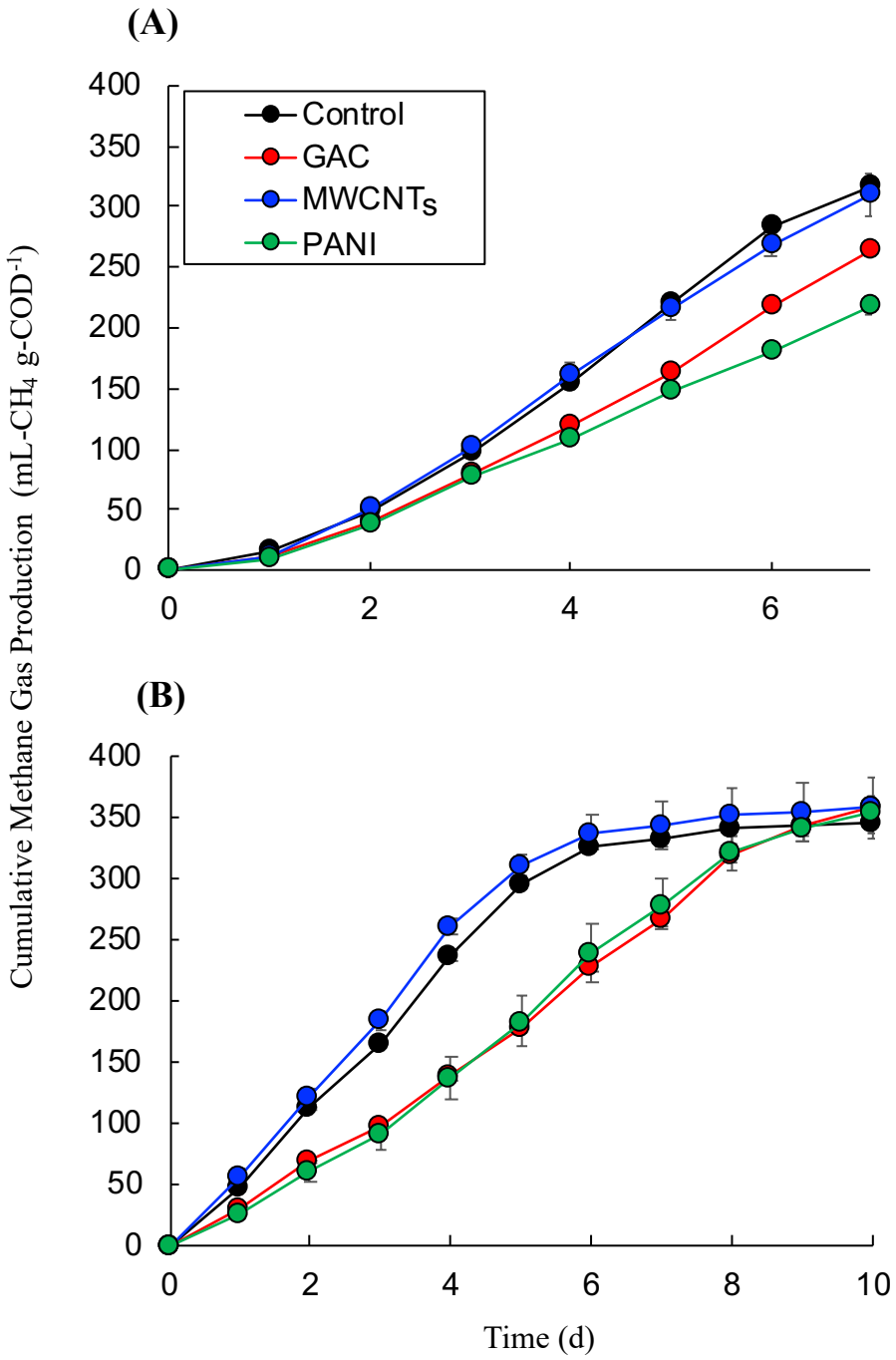

Figure 2-3. Cumulative methane gas production with propionate (Study I) used as substrate in (A) Cycle 1 and (B) Cycle 2

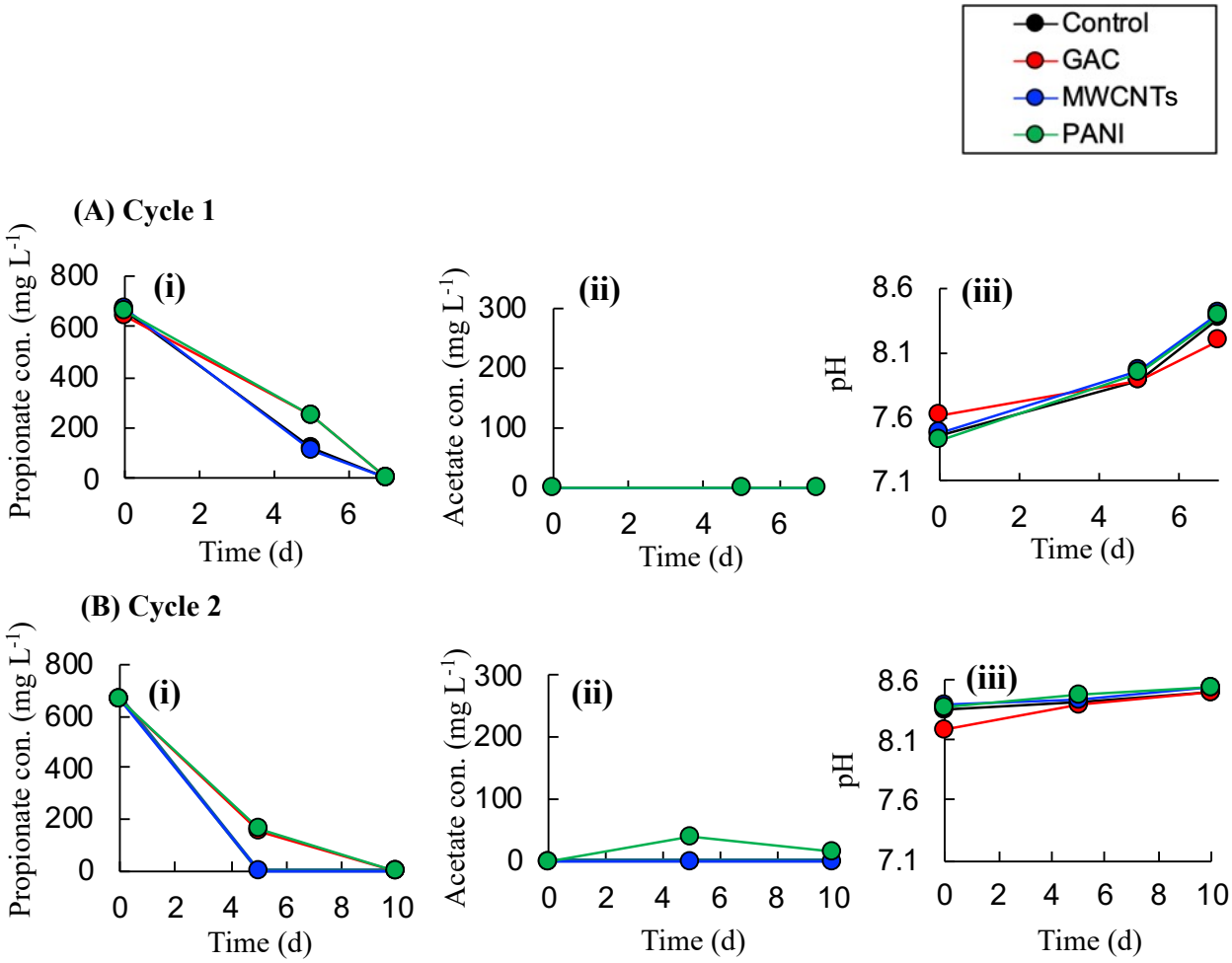

Figure 2-4. Propionate concentration, acetate concentration and pH of all condition in Study I's (A) Cycle 1 and (B) Cycle 2

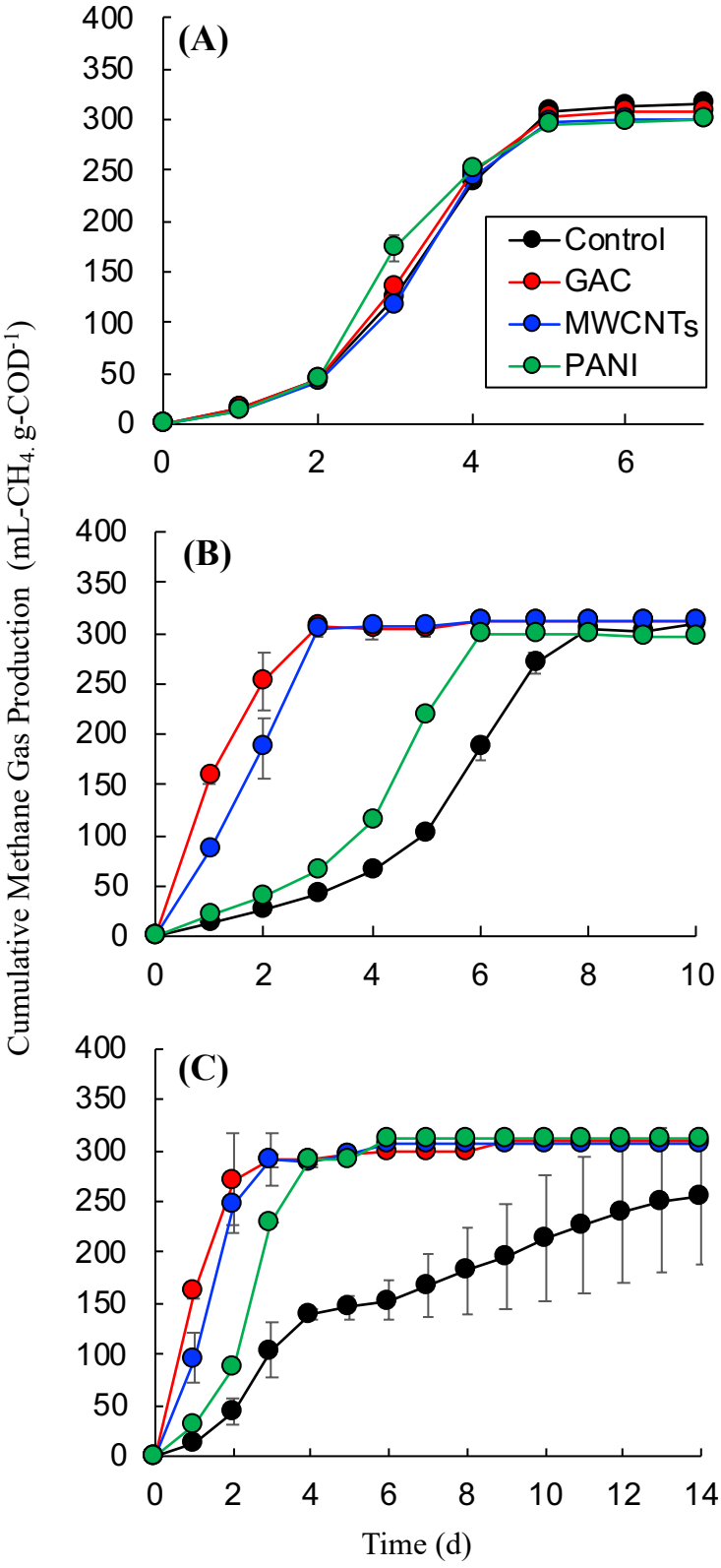

Figure 2-5. Cumulative Methane Gas Production with Ethanol (Study II) used as substrate in (A) Cycle 1, (B) Cycle 2 and (C) Cycle 3

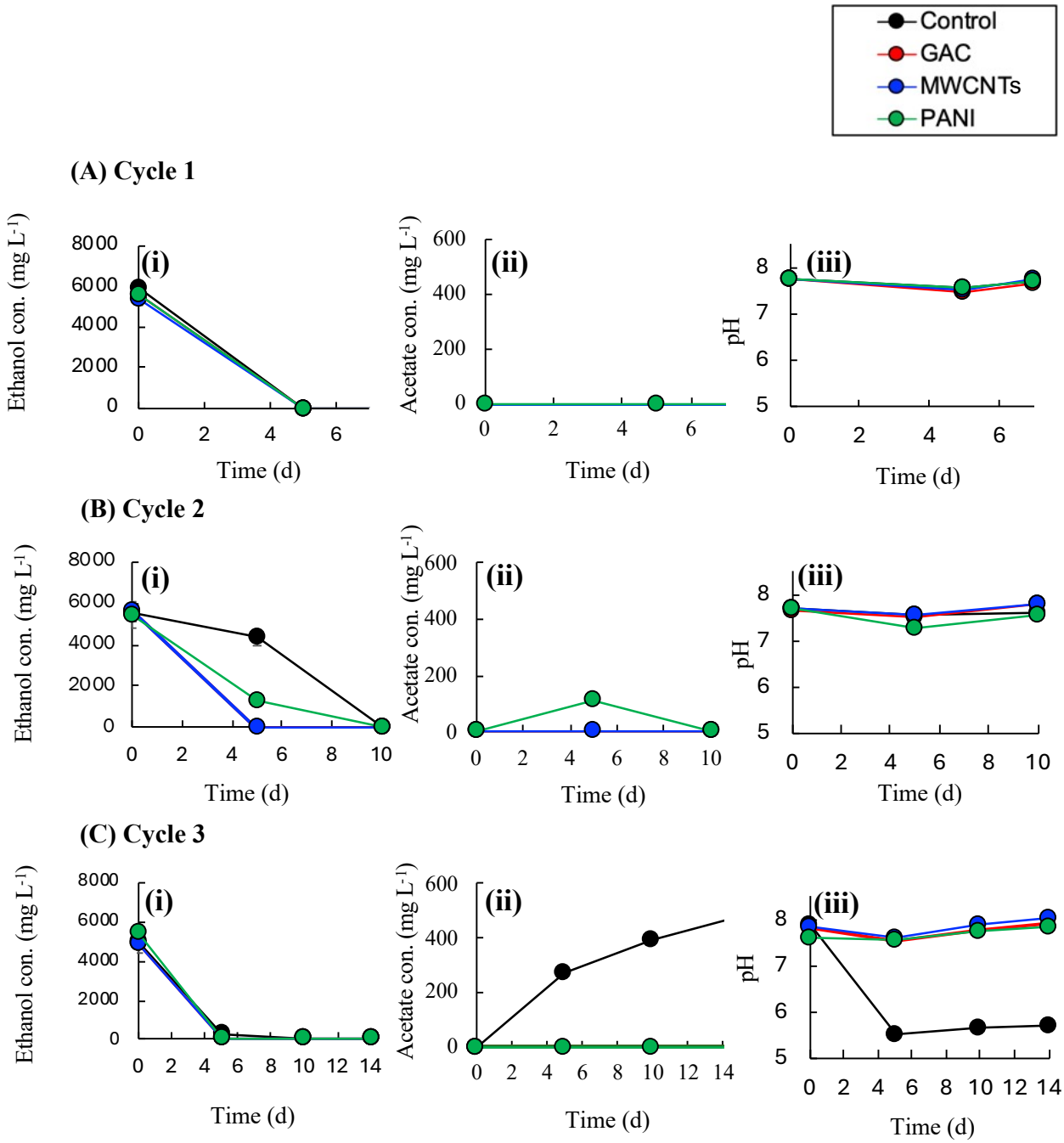

Figure 2-6. Ethanol concentration, acetate concentration and pH of all condition in Study II's (A) Cycle 1, (B) Cycle 2 and (C) Cycle 3

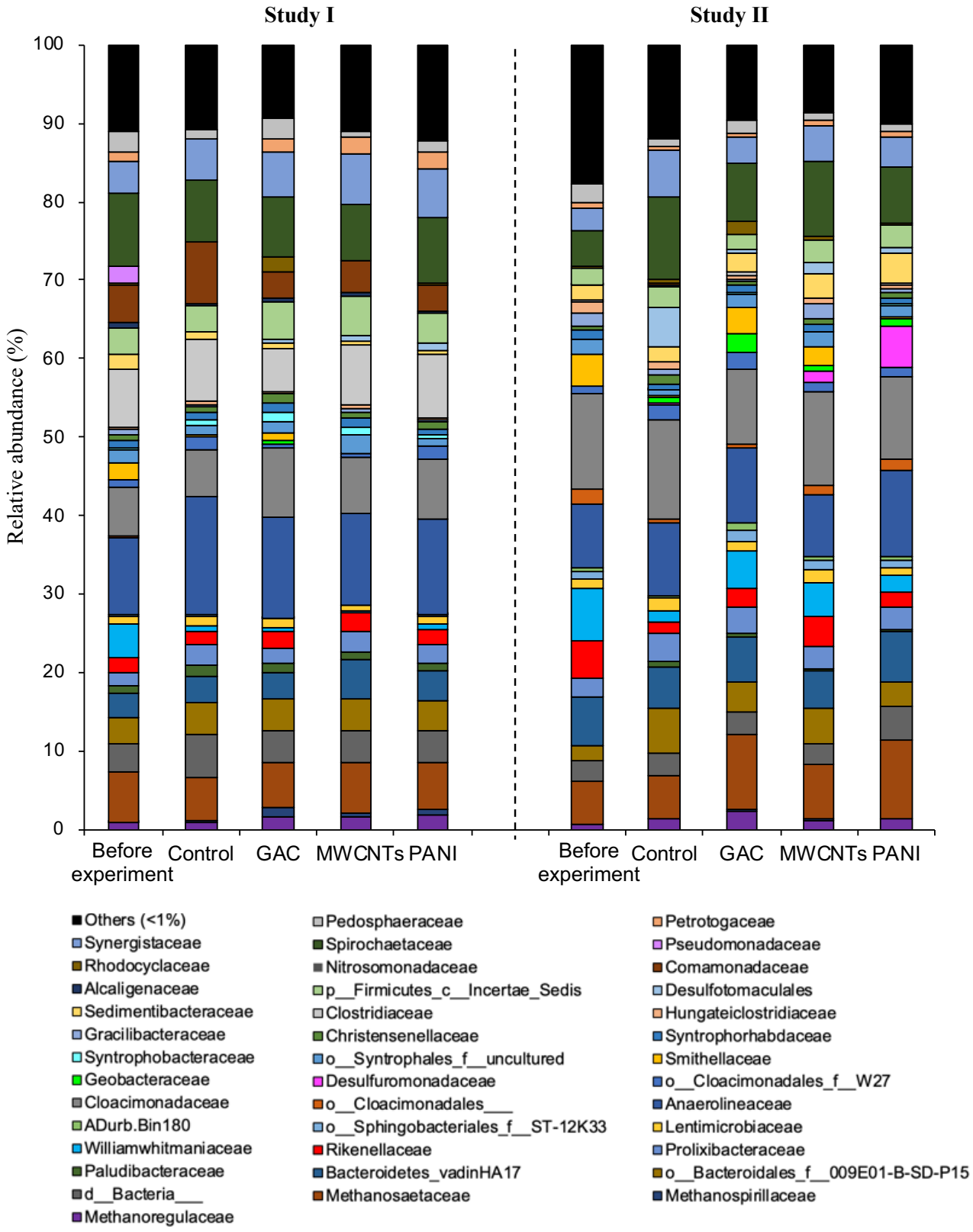

Figure 2-7. Relative abundance of microbial communities at the family level in Studies I & II

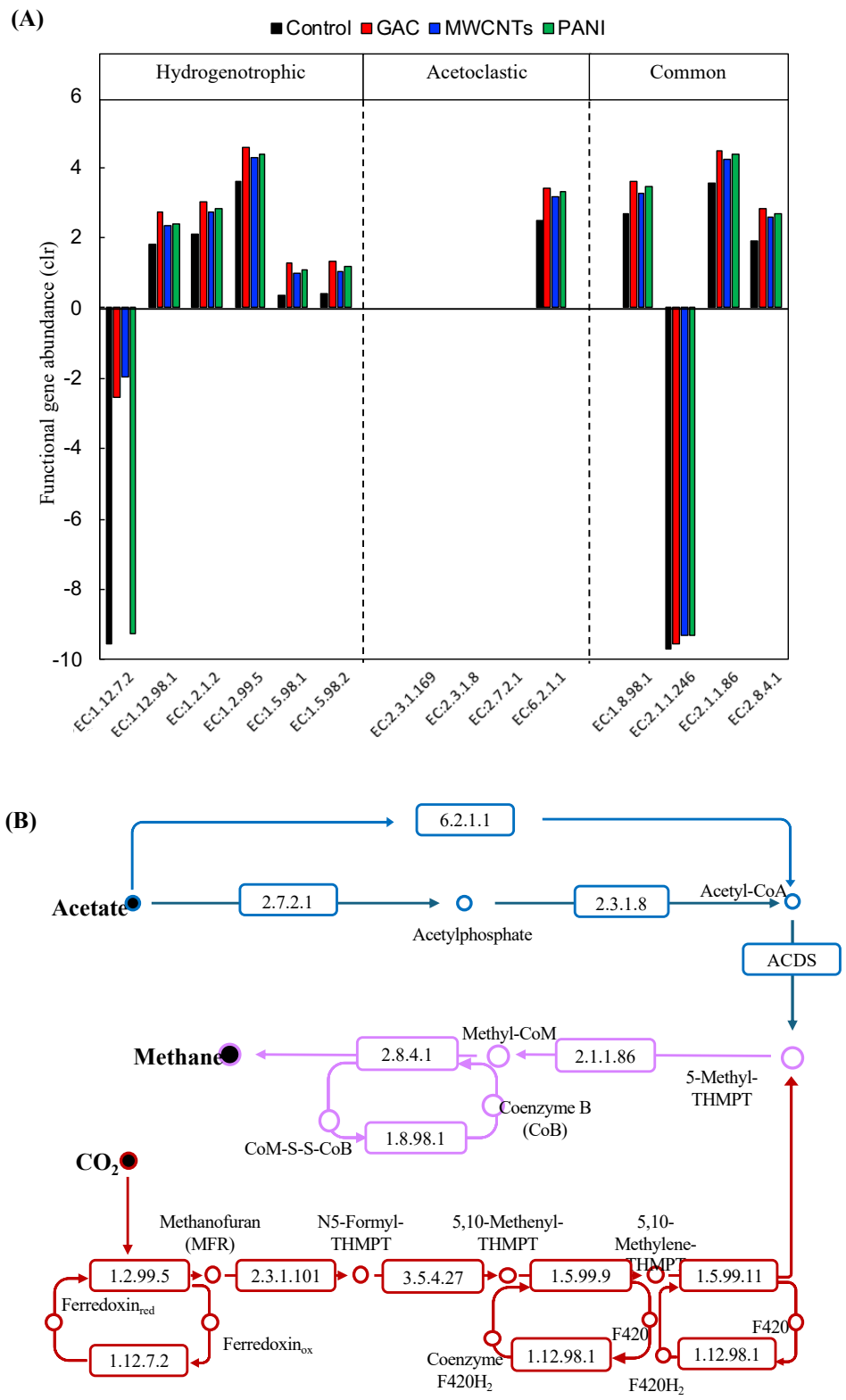

Figure 2-8. (A) Clr-transformed predicted functional gene abundance related to methanogenic pathway, (B) Methanogenic pathway according to KEGG (MAP: 00680). Figure was drawn based on previous studies (Yin et al., 2018, Zhao et al., 2019)

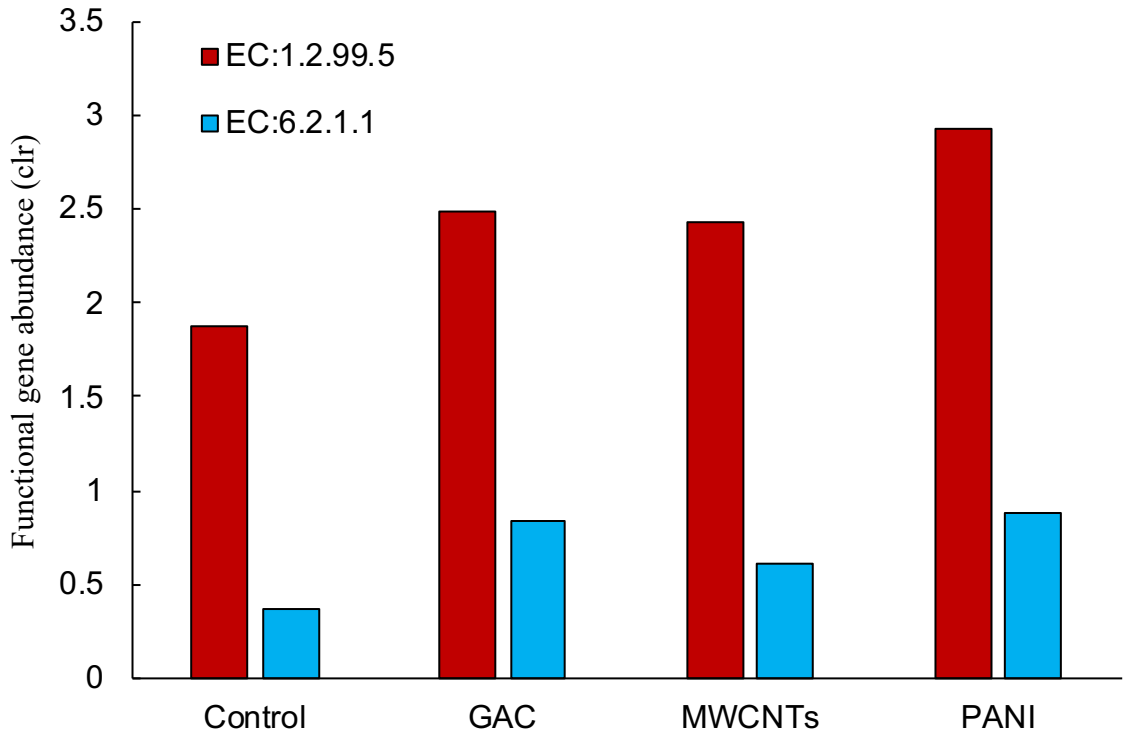

Figure 2-9. Abundance of enriched acetoclastic and hydrogenotrophic genes assigned to *Methanosaetasaea*

Table 2-1. Overview of research on enhancement of anaerobic digestion performance using conductive materials

Conductive Material	particle size (μm)	Concentration (g/L)	Substrate	Methane improvement	Reference
Magnetite	0.001 - 0.3	0.01 to 20	Acetate, Ethanol, Benzoate, Butyrate and Propionate	1.3 to 3.6	Baek et al., 2015; Zhang & Lu, 2016
Iron Oxide nanoparticle	0.002	0.8	Beet sugar industrial water	1.3	Ambuchi et al., 2017
Hematite	500 - 2000	25	Acetate, Ethanol, Benzoate, Sludge	1.3 to 2.2	Kato et al., 2011; Zhuang et al., 2015
Stainless Steel	500 - 2000	25	Synthetic water	1.3	Li et al., 2017
Polyaniline Nanorod	0.25 - 3	1.2	Sucrose	2	Hu et al., 2017
Graphene	-	0.03 to 2.0	Ethanol, Synthetic wastewater	1.2 to 1.5	Tian et al., 2016
Multi-walled Carbon Nanotube	0.010 - 0.2	0.1 to 5.0	H_2/CO_2, Acetate, Butyrate, Beet sugar industrial wastewater	1.1 to 17	Salvador et al., 2017; Zheng et al., 2020
Graphite	6 - 25	12 to 132	Synthetic complex waste and wastewater	1.0 to 1.3	Dang et al., 2016
Granular Activated Carbon	841 - 2000	3.3 to 25	Acetate, Ethanol, Butyrate, Propionate, Glucose, Synthetic brewery wastewater, Synthetic dairy wastewater, Activated sludge	1.1 to 18	Yan et al., 2017; Liu et al., 2012; Dang et al., 2016
Carbon Felt	-	3 to 30 pieces	Glucose and synthetic complex waste	1.1	Dang et al., 2016
Carbon Cloth	-	10 to 20 pieces	Ethanol, Synthetic wastewater, Leachate from municipal solid waste incineration, Organic fraction of municipal solid, Synthetic complex waste	1.1 to 10	Dang et al., 2016; Chen et al., 2014

Table 2-2. Brunauer-Emmett-Teller (BET) Surface Area and Porosity data

	GAC	MWCNTs	PANI
BET surface area (m^2/g)	1329.3	215.70	17.540
Total BET surface area of particle in reactor (m^2)	7975.7	64.710	10.520
Pore volume (cm^3/g)	0.435	0.605	0.044
Total Pore volume in reactor (cm^3)	2.610	0.1815	0.0079
Pore diameter (nm)	3.13	11.22	9.99

Granular activated carbon, GAC; multiwalled carbon nanotubes, MWCNTs; and polyaniline, PANI; Brunauer-Emmett-Teller, BET

Table 2-3. Kinetic Parameter of Study I & II of Cycle 2 result fitted into Gompertz equation

	P (mL g-COD^{-1})	R_{max} (mLg-COD^{-1} day^{-1})	*l* (day)	R^2
Study I				
Control	351.87	77.09[a]	0.63	0.99
GAC	405.35	48.23[b]	1.04	0.99
MWCNTs	362.34	81.76[a]	0.54	0.99
PANI	386.99	52.73[b]	1.27	0.99
Study II				
Control	324.61	75.37[a]	3.3	0.99
GAC	310.06	175.12[b]	0.14	0.99
MWCNTs	314.91	141.135[b]	0.46	0.99
PANI	305.26	95.82[a]	2.4	0.99

Means followed by the same letter are not statistically different according to One-way ANOVA, Tukey-Kramer test at $P \leq 0.01$, based on the results from each study.

Table 2-4. VS (Volatile Solid) content of each condition for before and after the experiment in both Study I & II

		Before experiment	After experiment			
			Control	GAC	MWCNTs	PANI
Study I	VS ($g\ L^{-1}$)	19.1 ±0.29	20.1 ±0.35	19.7 ±0.27	20.8 ±0.25	19.3 ±0.26
Study II	VS ($g\ L^{-1}$)	23.2 ±0.21	22.9 ±0.27	24.3±0.19	23.8 ± 0.24	32.2 ± 0.20

Chapter 3

Establishing suitable immobilization method for AD microbes into hydrogel

3.1 Background/Overview of Experiment 2

Research on immobilizing microbial cells into hydrogel for biotreatment has been advancing in recent years as it offers many advantages such as preventing microbial washout, achieving high microbial retention in reactors, providing resistance to toxic chemicals with low cost in hydrogel synthesis and its material (Bouabidi et al., 2018). For instance, high-rate denitrification with a maximum nitrogen removal rate of 5.1 kg-N m^{-3} d^{-1} was achieved by immobilizing heterotrophic denitrifying bacteria in polyethylene glycol (PEG) hydrogel, which enhanced biomass retention in the bioreactor even with a short hydraulic retention time (HRT) without biomass loss (Isaka et al., 2012). Another example involved entrapping nitrifying bacteria in alginate hydrogel combined with carbon black as a light-shielding material to mitigate photoinhibition in microalgae-nitrifying bacteria consortia (Nishi et al., 2020). Similarly, research on immobilizing annamox bacteria in hydrogel has gained popularity, as it could enhances nitrogen removal rates through high cell retention in the bioreactor and shortens its start-up time (Wang et al.,2021).

Due to the numerous advantages of wastewater biotreatment through microbial cell immobilization as mentioned above, recent research has explored the application of hydrogel immobilization for AD microbes. For example, the use of polyvinyl alcohol (PVA) hydrogel in a UASB reactor has been shown to enhance granular formation, resulting in reduced VFA concentrations in the effluent compared to conditions without the addition of PVA hydrogel (Wenjie et al., 2008). Similarly, studies have demonstrated that applying PVA hydrogel for immobilization in a two-stage packed-bed reactor treating high-strength particulate waste improved hydrolytic reactor performance by increasing VFA production by up to 31% (Pandey & Sarkar, 2017). However, current research has predominantly focused on immobilizing AD microbes using adsorption methods, with

limited to no studies investigating immobilizing AD microbes in hydrogel using the entrapment method (Wenjie et al., 2008, Pandey & Sarkar, 2017, Sitthi et al., 2020). This scarcity is likely due to the challenges posed by biogas (CH_4 and CO_2) production, which makes stable immobilization difficult to achieve. While immobilization of AD microbes using the adsorption method has shown excellent performance, it requires a preculturing phase to facilitate microbial attachment to the hydrogel, which can be time-consuming. In contrast, entrapment methods for immobilizing AD microbes in hydrogel offer advantages, including maintaining high microbial concentrations, improving resistance to toxic substances, and eliminating the need for a preculturing period. These benefits have been reported in studies involving the immobilization of other microbes, such as nitrifying bacteria and anammox (Bouabidi et al., 2018). Therefore, in this chapter, the establishment of a suitable immobilization method for AD microbes using the entrapment method was initially attempted without the addition of conductive materials (CM).

In this study, four different immobilization methods were tested and evaluated. The methods and materials selected for immobilization are based on previous studies involving both non-gas-producing bacteria and gas-producing bacteria (e.g., anammox and biohythane). First, short-term incubation experiments were conducted to screen potential immobilization methods and materials suitable for subsequent microbial activity and biogas permeability tests. The selected methods were then applied in longer incubation tests to evaluate their durability. Based on the results, the most suitable immobilization method was chosen for the co-immobilization of AD microbes with CM in the following experiments.

3.2 Methods and Materials

3.2.1 Immobilization method

Before immobilization, the biomass and supernatant of the anaerobic sludge obtained from the Hakubu Sludge Treatment Center (Yokohama, Japan) were separated by centrifugation at 4000 rpm for 15 min using a centrifuge machine (Beckman Coulter, Allegra X-30R Centrifuge). The supernatant of the sludge was collected and placed in the refrigerator at 4℃ until further usage. The remaining biomass was immobilized using the following four methods stated below. After immobilizing the AD sludge, the initial amount of the supernatant liquid was added back to the reactor in which the AD sludge-immobilized hydrogel was inoculated.

Method A:

The first method was performed according to the methods of Tuyen et al. 2018 and Nishi et al. 2020 **(Figure 3-1 (A))**. In brief, 100 mL of the solution containing 12 w/v% PVA (Polyvinyl alcohol 25-100; Kuraray Co., Ltd, Japan) and 2 w/v% sodium alginate (80~120 cP; Wako 1st Grade, FUJIFILM Wako Pure Chemical Cooperation, Japan) was autoclaved (TOMY, BS-235) at 121℃ for 20 min. After cooling to 37℃, the solution was mixed with 100 mL of the condensed biomass obtained from centrifugation. The mixture was dripped into a crosslinking solution of saturated $B(OH)_3$ and 2% (w/v) $CaCl_2$ to form spherical beads. The beads were crosslinked in the $B(OH)_3/CaCl_2$ solution for 1-3 h, then transferred to 0.5 M Na_2SO_4 solution for further crosslinking for 1 h. The beads were collected and washed with deoxygenated distilled water in magnetic stirrer at 400 rpm for 24 h. The sample obtained using method A is referred to as "PVA-SA."

Method B:

The second method was performed as described by Kurayama et al. 2019 **(Figure 3-1 (B))**. The centrifuged biomass was first mixed with an equal volume of a solution containing 7.5% polyvinylpyrrolidone (PVP, K85-95; Across Organics, USA) and 2 M $CaCl_2$ to obtain the core

solution. The core solution was then added to a vigorously stirred 1 w/v% sodium alginate (80~120 cP; Wako 1st Grade, FUJIFILM Wako Pure Chemical Cooperation, Japan) solution to form capsules. After dripping the core solution, the capsule-containing solution was continuously stirred for another 10 min to complete capsule formation. In addition, using the same procedure as described above, but with the addition of 1.5 w/v% chitosan (Chitosan 100; Wako Pure Chemical Industries, Ltd., Japan) to the core solution, another type of capsule was prepared. The capsules were then collected and washed with distilled water for 30 min. The obtained capsules are referred to as "Alginate capsule" for the former condition and for the later condition with chitosan addition, they are referred to as "Alginate-chitosan capsule."

Method C:

The third immobilization method was performed according to the method reported by Ta et al. 2020 **(Figure 3-1 (C))**. In detail, 10 g-VS (Volatile Solid) biomass concentration was first mixed with 100 mL solution containing 3% (w/v) κ-carrageenan (Tokyo Chemical Industry Co. Ltd., Japan) and 1.5% (w/v) gelatin (Wako Pure Chemical Industries, Ltd., Japan). The mixed solution was then pumped into a silicon pipeline with a diameter of 4 mm which was partly submerged in cold water at 4℃ to form a solid gel matrix. The solid gel matrix was consistently cut into a length of 15 mm to create a cylinder-shaped hydrogel. Then, they were immersed into a 0.3 M KCl solution for 2 h to strengthen their mechanical property and then stored at 4℃ for 24 h before usage. The resulting hydrogel is referred to as "KC-gelatin."

Method D:

The final immobilization method was performed according to Senko et al. 2019 **(Figure 3-1 (D))**. Briefly, the concentrated biomass obtained from centrifugation was mixed with a 10% (w/v) PVA (Polyvinyl alcohol 25-100; Kuraray Co. Ltd, Japan) aqueous solution to achieve a biomass concentration of 30% (w/w) and the final composition of 7% (w/v) PVA. The mixed solution was

pipetted into the 96-well microplates and then placed into a freezer at -20℃ for 24 h. Finally, they were thawed at room temperature. The resulting PVA-cryogel will be referred to as "PVA-cryogel."

3.2.2 Experimental set up

The methane fermentation experiment was carried out within a short-term inoculation period of seven days. Each immobilized hydrogel prepared using the four different methods was inoculated into a 300 mL working volume of 500 mL medium bottle with ethanol used as the substrate. Only for method A's experiment, the methane gas volume was measured automatically by the automatic methane potential test system (AMPTS® II, BPC Instruments, Sweden), while the biomethane from other condition (Method B-D) was collected using a gasbag and the volume of methane was measured by using a 60 mL syringe. It should be noted that the biogas produced during the batch experiment was transported to a 3.0 M NaOH solution for CO_2 stripping, and the remaining biomethane was captured using a gasbag. Since all microbes were immobilized in a new environment, a sludge to substrate ratio of 3:1 (VS-based) was applied to prevent the inhibition in methane fermentation during the acclimation phase. All reactors were incubated at 37℃ with a stirring rate of 100 rpm. Before the starting the experiment, all reactors were purged with N_2 gas for 1-2 min to attain an anaerobic phase. Basic analytical parameters, such as methane production and pH, were measured to determine the successful operation of the AD process under different immobilized conditions. In addition, the time-course change in shape and the rupture and/or flotation of the hydrogel were carefully monitored.

Based on the obtained results, a suitable immobilization method that resulted in a successful AD process in the short-term experiment will be further tested in an extended inoculation of three weeks using the same experimental setup to monitor the hydrogel's durability.

3.3 Result and Discussion

Method A

Figure 3-2 shows the cumulative methane gas production and pH change for the PVA-SA crosslinked in boric acid and $CaCl_2$ for 3 h. The PVA-SA condition showed higher methane gas production than the control condition from day 0 to 2. However, methane production for the PVA-SA condition slowed down, and the production rate for the control became faster than that for the PVA-SA after day 3. The possible inhibition of the AD process under the PVA-SA conditions could be due to the pH change. The pH was monitored every 2 days throughout the experiment, and the results showed significant decrease in pH from day 2 to pH 5.7 under the PVA-SA condition. It has been reported that the pH in an AD process can be tolerated in the range of 6.5 to 8.0 (Cioablă et al., 2012), however, a pH lower than 6.5 could lead to the inhibition of the process. **Figure 3-3** shows images of the hydrogel at the beginning (A) and at the end of the experiment (B). As can be observed, not only the flotation of the hydrogel but also the swelling of the hydrogel due to the biogas entrapment was developed for the method A's immobilization. The swelling under the PVA-SA condition was probably due to the long crosslinking time, which increased the density of the outer layer of the spherical hydrogel, leading to the formation of smaller pores. Because methanogens are gas-releasing archaea, the limited small pore size could interfere with the gas produced to permeate, resulting in biogas being trapped inside the hydrogel. The increased partial pressure of biogas could cause inhibition of acetogenesis and methanogenesis reactions, leading to the accumulation of VFA and a pH drop. Therefore, the PVA-SA immobilization method A was attempted once again by decreasing the crosslinking time to allow the formation of larger pores in the hydrogel to enhance the biogas permeability.

Figure 3-4 shows the cumulative methane gas production and pH change when the PVA-SA hydrogels were crosslinked in boric acid and $CaCl_2$ solutions for 1h, 1h 30min, and 2 h, respectively. Although a slight improvement in methane production was observed with the decrease in crosslinking time, the overall trends were similar to the previous results, where all the PVA-SA

conditions had a faster methane production rate until day 2, and the rates were surpassed by that of the control condition after day 3. Regarding pH, all conditions showed a value within the optimum range for the AD process. However, despite better pH results, the experiment was stopped on day 4 because of the severe agglomeration of the PVA-SA hydrogel beads observed under all the immobilized conditions **(Figure 3-5)**. This is most likely due to insufficient crosslinking time. According to previous studies, although PVA is known to agglomerate easily owing to its sticky nature, this can be suppressed by adding a small amount of sodium alginate (Wu & Wisecarver, 1992; Van Pham & Bach, 2014). However, in this study, even though the sodium alginate was added, it could leak out from the hydrogel over time owing to insufficient crosslinking. Another possible reason is that the lack of crosslinking in both the PVA and alginate caused the gel-to-sol transition to form a large sticky lump in the middle. Therefore, to solve the agglomeration problem, the PVA-SA immobilization method A was tried again by using different PVA:SA ratios of 5:1 and 4:1 (a higher alginate ratio as compared to the original condition, PVA:SA ratio of 6:1) with a crosslinking time of 1 h.

Figure 3-6 shows images of the PVA-SA hydrogels with different PVA:SA ratios. Even after changing the PVA:SA ratio, agglomeration was observed again starting on day 2 and became even more severe with time. Based on this result, another question was raised regarding whether agglomeration would still occur without the addition of AD sludge to the hydrogel. To confirm this, the PVA-SA hydrogel was synthesized without the addition of AD sludge with different crosslinking times of 1, 2, and 3 h for comparison. Interestingly, without the addition of AD sludge, no agglomeration of the PVA-SA hydrogel was observed even after continuous stirring for 6 days **(Figure 3-7)**. This indicates that agglomeration occurred only when the AD sludge was immobilized in the hydrogel. One possible reason is the release of uncrosslinked PVA polymer from the hydrogel accompanied by biogas production, which could result in agglomeration through the bridging of the gel beads. On the other hand, it has been reported that *Bacteroidetes*, one of the most popular acidogens bacteria in AD could degrade various polysaccharides (Kabisch et al., 2014, Lapebie et al.,

2019). According to a previous study by Springael (2019), when AD microbes were immobilized in a 1.3% alginate-containing hydrogel, the entire matrix was broken down in only 7-13 days even without any additional carbon source. In this study, the prepared hydrogels contained only 1% alginate, which may lead to faster degradation. Therefore, another possible reason for the agglomeration observed in this study is that alginate, a natural polysaccharide derived from seaweed, is biodegraded by AD microbes, leading to agglomeration using the remaining PVA. Therefore, although PVA is known for its low biodegradable properties (Chiellini et al., 2003), the high biodegradability of alginate may limit its performance in AD systems. In addition, the immobilization method A requires the use of boric acid as a crosslinking agent, which is highly unfavourable because it is toxic to microbes owing to its low pH (Van Pham & Bach, 2014). Therefore, the Method A was concluded not suitable for immobilizing AD microbes.

Method B

In the previous immobilization experiment using method A, it was discovered that alginate could be degraded by one of the AD microbes (Kabisch et al., 2014). Therefore, in addition to the ongoing search for an alternative to alginate as a material for immobilization, an alternative method using encapsulation in alginate was also attempted. Polyvinylpyrrolidone (PVP) is a nontoxic polymer used as a thickener for capsule synthesis and reported to be able to improve bacterial adhesion (Pilarska et al., 2018). Furthermore, other studies have shown that the addition of chitosan to AD sludge can help accelerate the granulation process, as chitosan can act as an extracellular polymeric substance (EPS)-like substance to promote the agglomeration of AD microbes (Ariyavongvivat et al., 2015). Based on the understanding, a hypothesis was made for as follows; when AD sludge is encapsulated(immobilized) together with PVP and chitosan in the capsule made of alginate, if the AD sludge could form granule in relatively short time, the AD sludge may remain intact with each other due to the accelerated formation of AD granules even after alginate capsule is degraded with time **(Figure 3-8)**. Because the sludge is tightly attached to PVP and chitosan, the

granulation process may be accelerated. Also, because alginate is known to have a more porous shell structure than PVA (Roquero et al., 2021), it may permeate out the biogas produced by the encapsulated AD microbes. However, if the degradation of alginate is faster than the granulation of AD microbes, the hypothesis does not work. Therefore, in method B, the encapsulation of AD sludge was attempted under two conditions. Under one condition, the AD sludge was immobilized using alginate and PVP without the addition of chitosan to observe the required time for microbes to degrade alginate. In contrast, AD sludge was immobilized using alginate and PVP with the addition of chitosan to observe whether chitosan could help the sludge stay intact even if alginate was degraded.

Figure 3-9 shows the results of methane production and pH change with time for the two encapsulation conditions using method B. The methane fermentation experiment was stopped on day 2 as inhibition was observed due to the rupture of the capsule, resulting in a sudden drop in pH for both conditions **(Figure 3-9 (B), Figure 3-10).** In this study, although the pore size of alginate is known to be larger than that of PVA, it was not large enough for biogas to permeate, and the structure was not strong enough to withstand the biogas pressure, thus leading to rupture of the capsule and a low pH as a result. In the case of the alginate-chitosan capsules, gas permeation seemed lower on day 1, and the pH dropped even more severely than in the alginate capsules. This was likely due to the formation of a dense capsule shell, caused by the electrostatic interaction between negatively charged alginate and positively charged chitosan (Baysal et al., 2013), which resulted in an undesirably smaller pore size in the capsule membrane. Therefore, it is concluded that the encapsulation method B was also not suitable for AD microbes immobilization.

Method C

In this study, the immobilization method reported for biohythane production experiments was used (Ta et al., 2020). **Figure 3-11** shows the results of methane production and pH changes over time for the obtained KC-gelatin hydrogel. As shown in the pH results, the pH decreased from the optimal range to a range where inhibition of the AD process could possibly occur. Additionally, the

hydrogel could not be observed from day 2 onwards **(Figure 3-12)**; therefore, the methane fermentation experiment was stopped on day 3. To understand if the hydrogel was degraded by the AD microbes or other factors, the hydrogel was once gain synthesized without the addition of AD sludge and then inoculated at 37℃ in an isothermal bath while being continuously stirred at 100 rpm as a blank condition. The results show that even without the addition of AD sludge, the hydrogel was slowly dissolved over time and had completely disappeared by the end of day 2 **(Figure 3-13).**

κ-carageenan is known as a thermally reversible gel and the addition of cation could help improve the strength of the hydrogel (Wang et al., 2018). As reported, the cation concentration could affect the gelling temperature of κ-carageenan and when 0.1 M of KCl was used, the shape of the hydrogel remained intact even at 55℃ without being dissolved. However, in this study, eventhough 0.3 M of KCl was used to strengthen the cross-linkages, the hydrogel was completely dissolved by day 3. This is probably due to the addition of gelatin which has an average melting point of 31.7-34.2℃ (Mad-Ali et al., 2017). Interestingly, the experiment by Ta et al. (2020) was successful, as the hydrogel, made from κ-carrageenan and gelatin, remained intact for 100 days at 37°C without dissolving or degrading. However, the hydrogel used in this study dissolved completely. One possible reason may be the different molecular weights of gelatin used compared to those used in Ta et al. (2020). Another possible reason for the success of Ta et al. (2020) was the addition of KOH for pH adjustment throughout the experiment. The OH^- ions assisted in balancing the pH from becoming too acidic, whereas K^+ ions assisted in maintaining the cross-linkage of the hydrogel. In this study, no pH adjustments or additional K^+ ions were made, and the hydrogel could not remain intact. Overall, the pH results in this study showed a value below the tolerable range even when the hydrogel was semi-intact until day 2, indicating poor gas permeability **(Figure 3-11 (B)).** This result was also observed in Gardin & Pauss, 2001, where AD sludge immobilized in κ-carrageenan hydrogel trapped the biogas, preventing its release. The study further reports that the addition of gelatin to κ-carrageenan allowed partial biogas permeation, as some microbes consumed the gelatin, altering the hydrogel's matrix and porosity. Although κ-carrageenan, gelatin, and the crosslinking agent are non-toxic to

microbes, the biodegradation of hydrogel could lead to the shifts in the microbial community, which may be unfavourable. Therefore, the materials and methods for immobilizing AD in this experiment (Method C) are also concluded to be incompatible with the AD system.

Method D

Figure 3-14 shows the results of cumulative methane production, and the pH change with time for AD sludge immobilized in PVA cryogel. The results show favourable methane production and a tolerable range of pH fluctuation for the AD process throughout the seven days of the experiment, with no floatation or rupture of the hydrogel observed. This indicates a successful AD process under these sludge immobilization conditions. Therefore, the experiment was extended to approximately 3 weeks to examine the durability of the hydrogel and the result is shown in **Figure 3-15**.

Besides the first cycle, the results from both cycle 2 and 3 show that the control and hydrogel conditions had similar biogas production curves and final production amounts at the end of each cycle **(Figure 3-15)**. The lower methane production in the first cycle may be due to the sudden transition of the AD microbes from a mobile environment to an immobilized state within the PVA hydrogel, which requires an acclimation period. Overall, the results indicate that the biogas could be permeated smoothly from the hydrogel, and no inhibition was observed in the hydrogel condition. The pH measurements throughout the three cycles also showed favourable and appropriate pH change behaviour, indicating a successful AD process. Therefore, immobilization method D was selected for the co-immobilization of AD sludge. For AD microbes, because the substrate was suddenly changed to ethanol, they needed time to acclimate to the new environment. However, from the 1st cycle, the pH fluctuation was in the appropriate range, and it seems that acclimatization was smooth from the beginning. Because the ratio of sludge to substrate was 3:1 (VS-base) in this experiment, it may be possible to start using a higher substrate loading condition by using a sludge to substrate ratio of 2:1 (VS-base) in the evaluation of methane fermentation of the co-immobilized hydrogel. Additionally,

no rupture or significant damage was observed for the hydrogel compared to the control, and the ratio of floated hydrogel was less than 10% **(Figure 3-16)**. At the end of cycle 3, the hydrogel was removed to check for any rupture or damage; with no significant change in shape was observed **(Figure 3-16 (B))**. Compared to the other methods tested before, the PVA-cryogel prepared by the freeze-thawing method showed a successful AD process. One of the main reasons for the success of the process was the macropore size of the PVA-cryogel, which allowed the biogas to permeate smoothly. The PVA-cryogel is formed by physical crosslinking, briefly explained in **Figure 3-17**. Upon freezing the PVA-solution, the formation of ice crystals pushes the PVA polymer chain to get close together. Due to the close contact of the PVA polymer chain, hydrogen bonding occurs and is further strengthened by ice crystallization, providing a network with structural integrity even after thawing. It has been reported that the movement of macromolecules is usually slow, and not all PVA chains are involved in crosslinking in one cycle of the freeze-thaw process, providing macropores to be formed (Adelnia et al., 2021). In addition, since no crosslinking agent was needed for the formation of the hydrogel, no toxic or excess nutrients were given to the microbes during hydrogel preparation. In addition, it has been reported that the PVA-cyrogel exhibits a higher mechanical strength than a chemically crosslinked PVA hydrogel, as the mechanical load can be distributed along the crystallites of the three-dimensional structure, and therefore shows good durability of the hydrogel in this study (Hassan & Peppas, 2000). Regarding the biocompatibility of the PVA-cryogel, it has been reported that PVA can act as a cryoprotectant that prevents cell death upon freeze-thawing and helps maintain cell viability (Senko et al., 2019). Additionally, PVA is known for its slow biodegradability, suggesting its potential for long-term use in continuous operation (Chiellini et al., 2003). These results indicate that, among the four immobilization methods, method D is more suitable for AD microbes immobilization. Therefore, in the following co-immobilization study, immobilization using method D was applied to evaluate the AD performance.

3.4 Conclusion

In this chapter, four different immobilization methods and materials were tried to immobilize the AD sludge, aiming to achieve successful methane production while preserving the shape and function of the hydrogel. The results obtained in this chapter are summarized in **Table 3-1**. Methods A to C shows failures in the AD process. For Method A, an extended crosslinking time resulted in a smaller pore size of the hydrogel, which hindered gas permeability and ultimately led to hydrogel rupture. Conversely, a shorter crosslinking time caused insufficient crosslinking in the hydrogel's core, resulting in agglomeration upon biogas production. For Method B, the alginate capsule's poor mechanical strength was insufficient to withstand the biogas pressure when being produced, and its limited porosity hindered effective gas diffusion, contributing to capsule rupture. Method C hydrogel was completely dissolved from day 2 onwards, which may be due to the addition of gelatin, and the absence of K^+ ions in the bioreactor post-synthesis. Even so, when the hydrogel remained intact, it still shown unsuitable for immobilizing AD microbes, as biogas could not be efficiently permeated out from the hydrogel. Lastly, Method D, which utilizes the freeze-thawing technique for immobilizing AD sludge in PVA hydrogel, demonstrated successful AD processes with excellent gas permeability from the while maintaining optimal pH, durability, and biocompatibility. These results indicate that Method D is suitable for AD microbes' immobilization, thereby selected for co-immobilizing of AD microbes and the selected conductive materials (CM) in chapter 2.

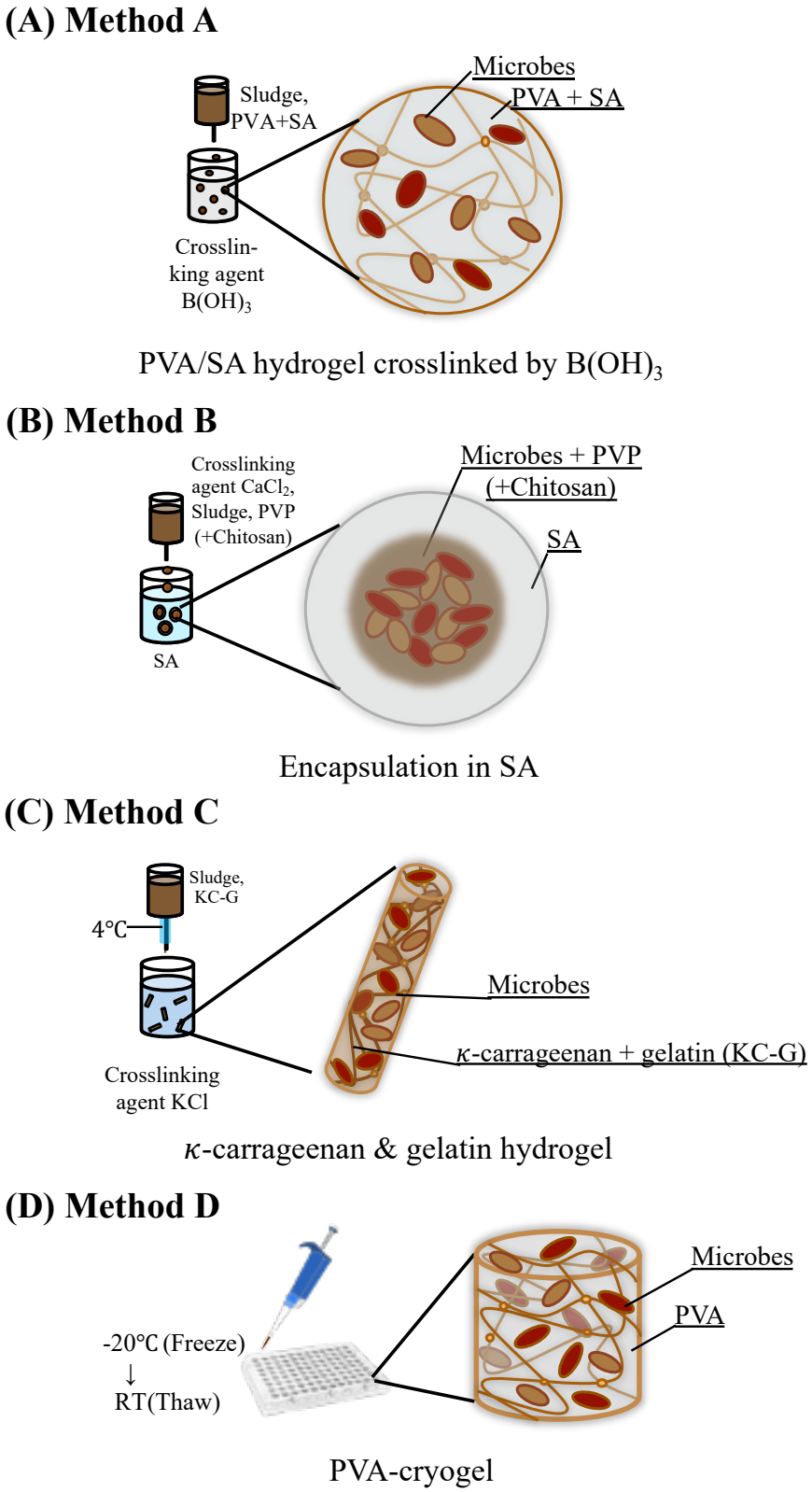

Figure 3-1. Schematic diagram of immobilizing AD sludge in (A) Method A, (B) Method B, (C) Method C and (D) Method D

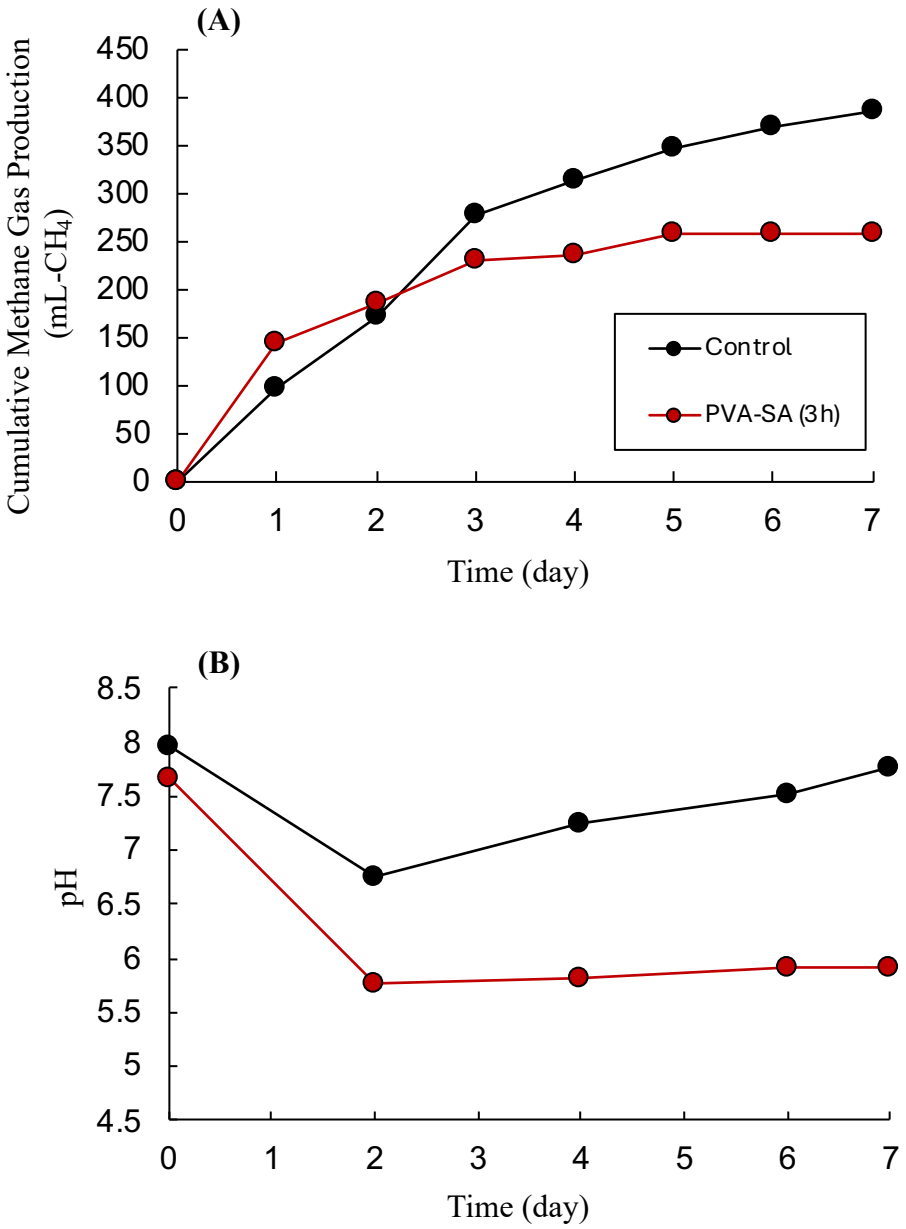

Figure 3-2. (A) Cumulative methane gas production and (B) pH of dispersed AD sludge and sludge immobilized in PVA-SA crosslinked at 3h

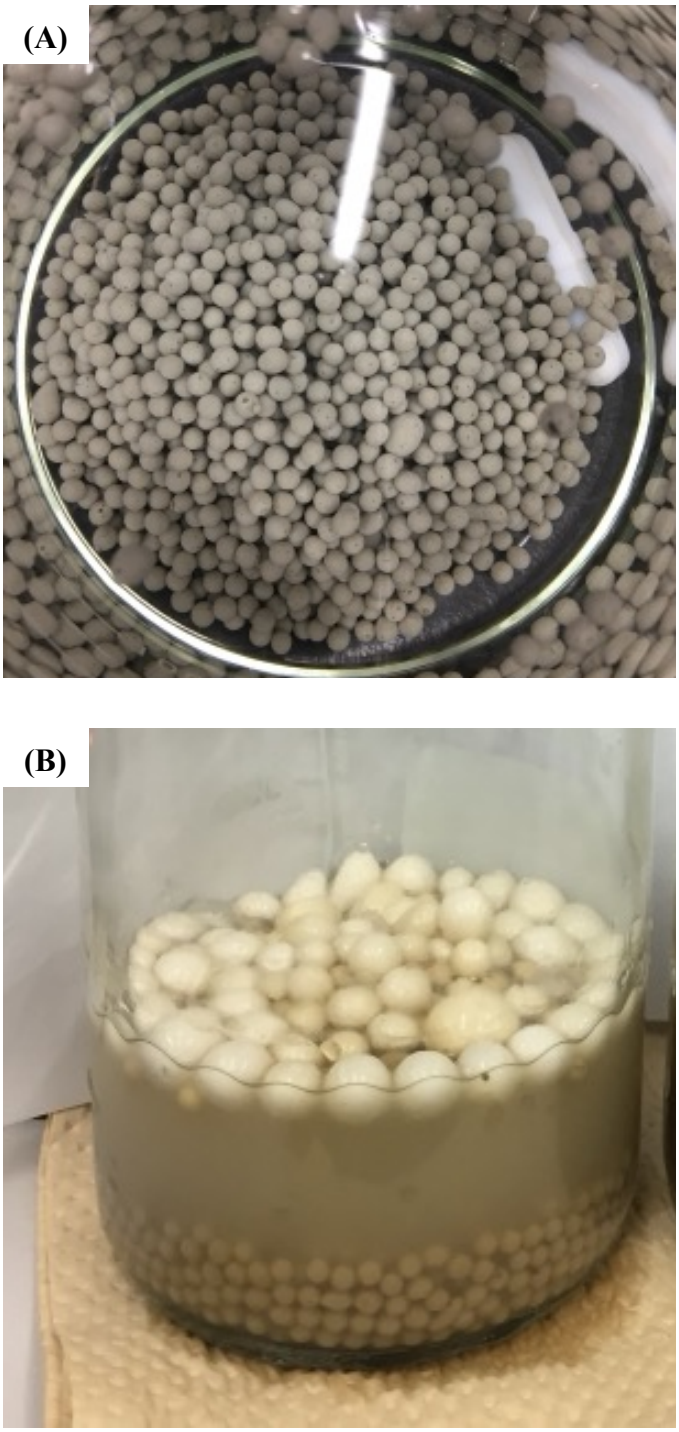

Figure 3-3. Immobilized AD sludge in PVA-SA crosslinked for 3h at the beginning of the experiment and (B) at the end of the experiment

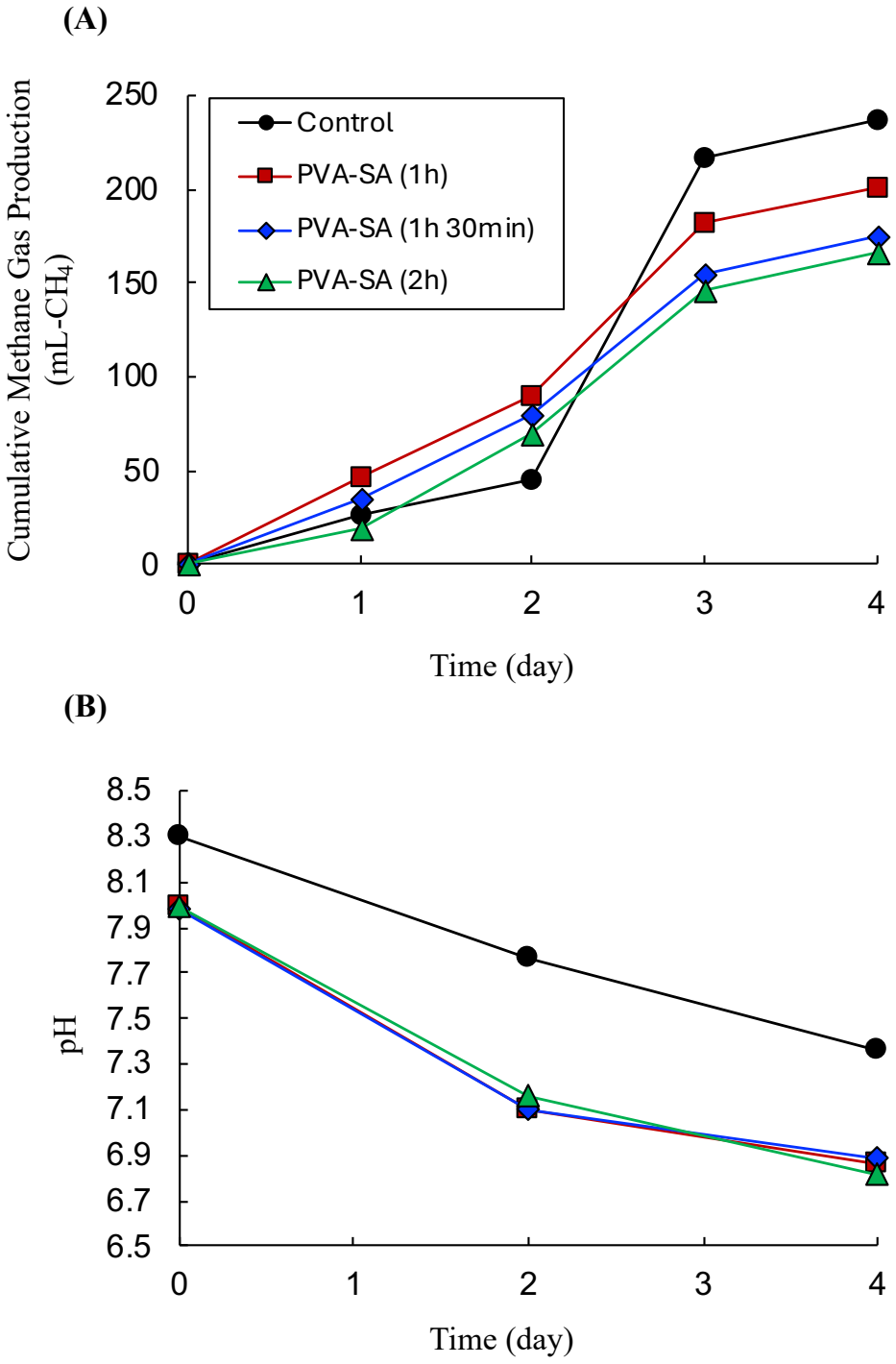

Figure 3-4. (A) Cumulative methane gas production and (B) pH of dispersed AD sludge and sludge immobilized in PVA-SA crosslinked at different time

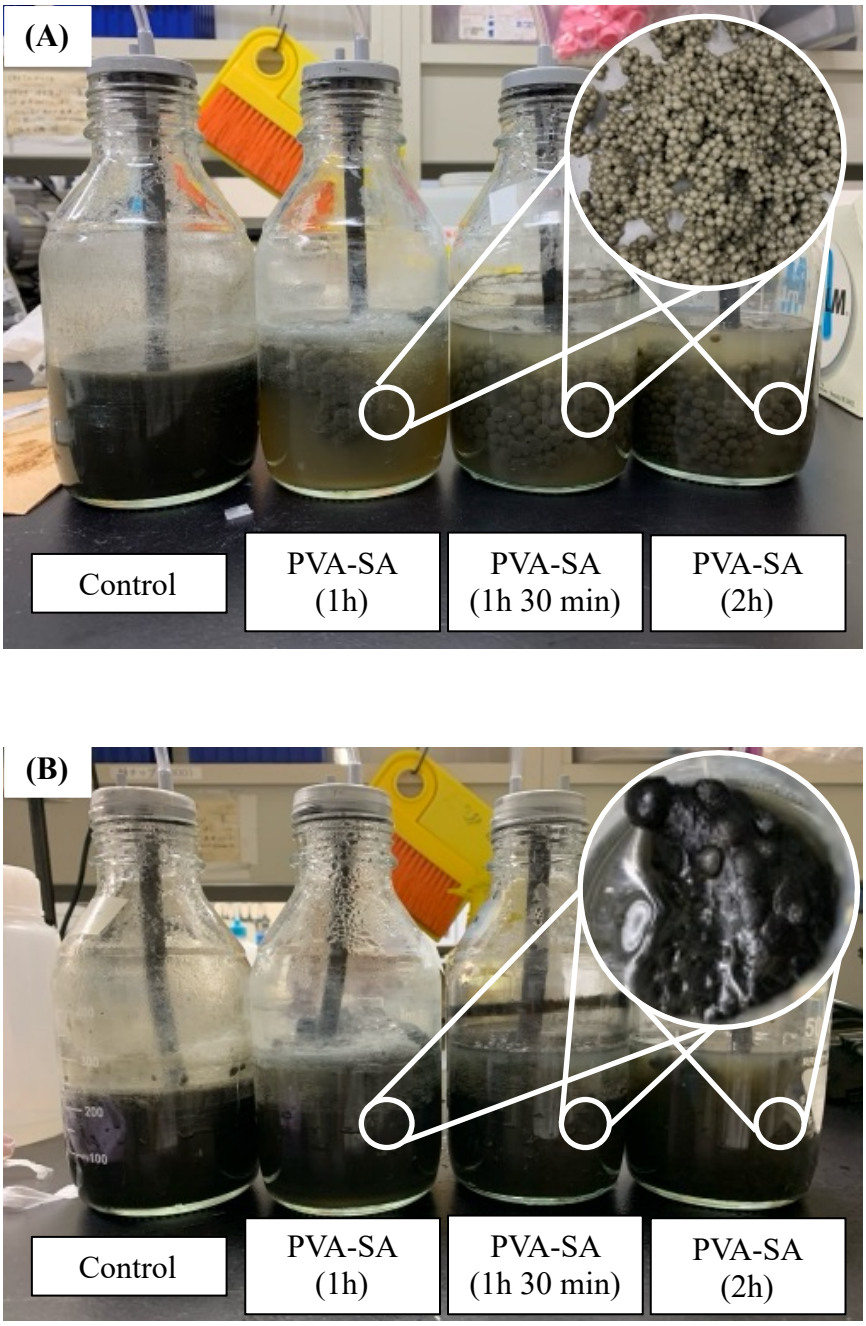

Figure 3-5. Different crosslinking time of PVA-SA hydrogel at (A) the beginning and (B) the end of the experiment.

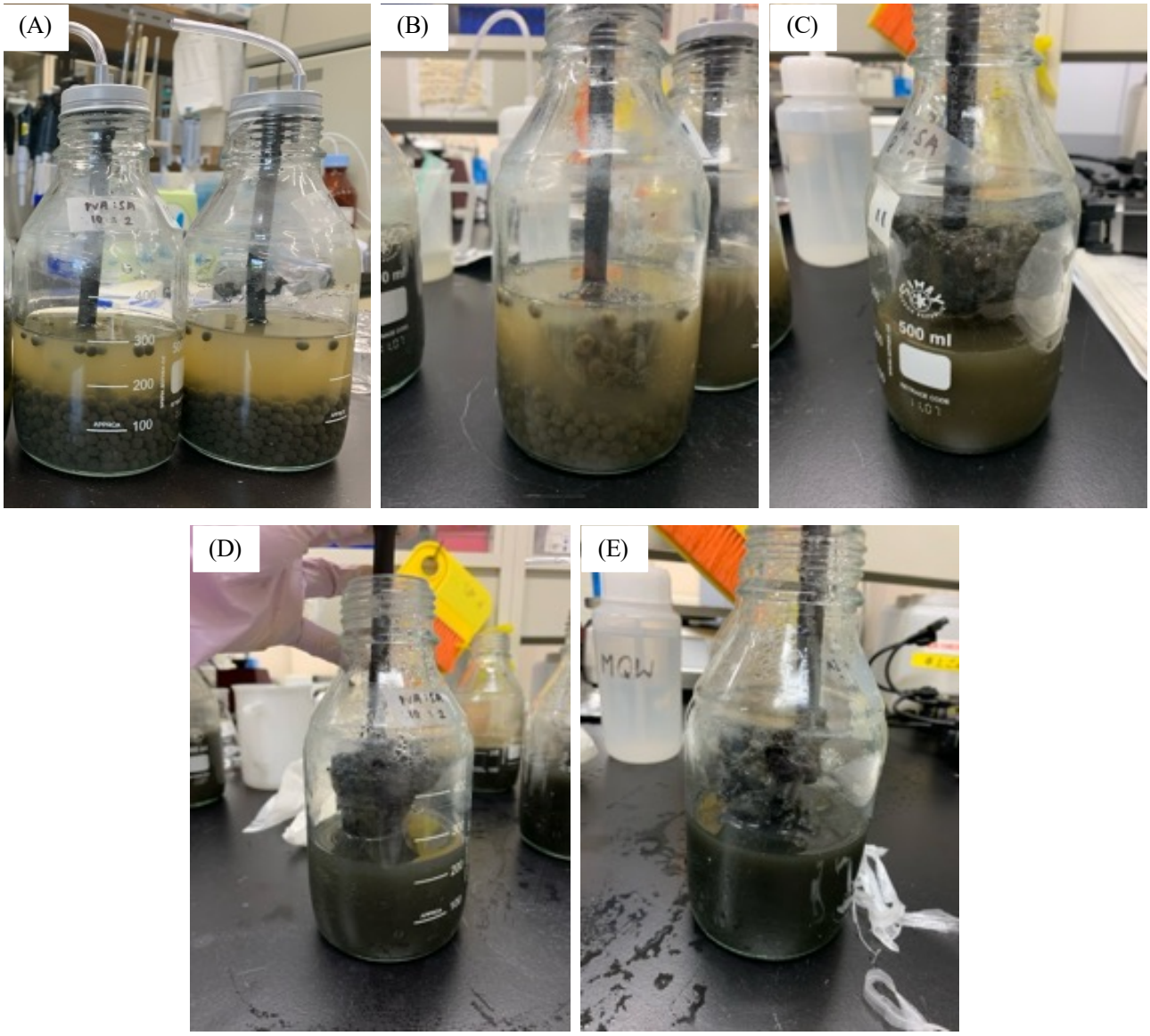

Figure 3-6. Images of hydrogel with different PVA:SA ratios at (A) the beginning, (B) 5:1 on day 2, (C) 4:1 on day 2, (D) 5:1 on day 4, and (E) 4:1 on day 4 of the experiment

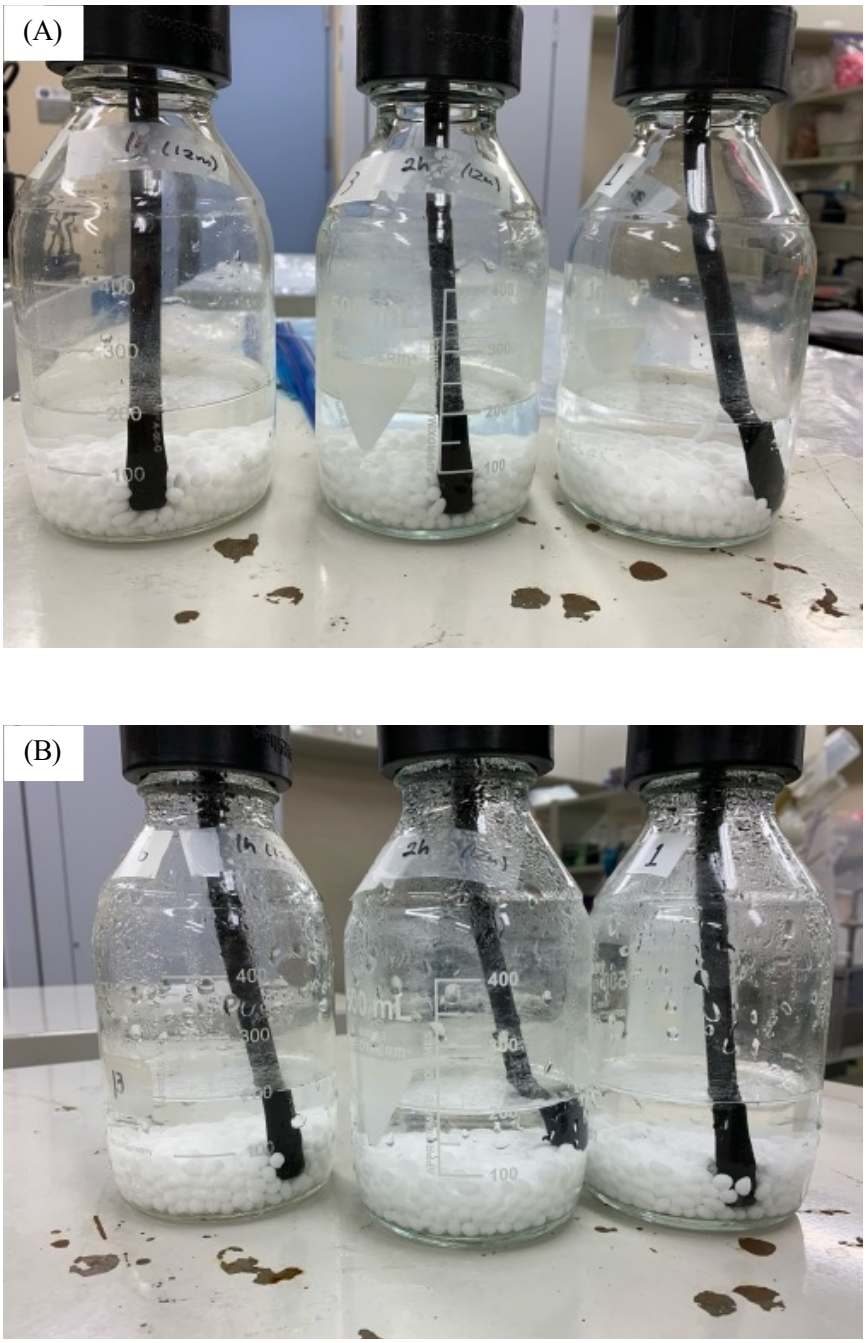

Figure 3-7. Image of PVA-SA hydrogel synthesized without AD sludge at different crosslinking times: (A) Beginning and (B) end of the experiment on day 6

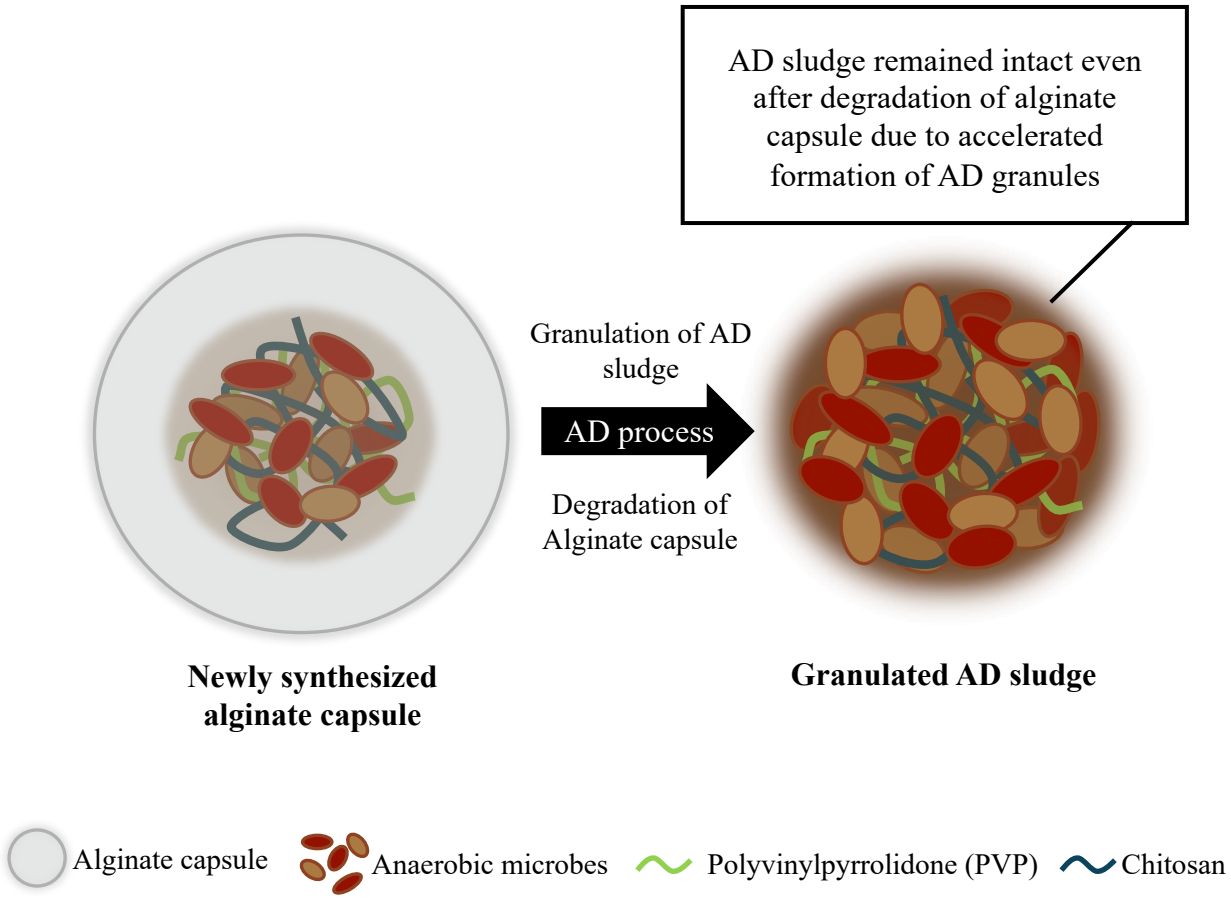

Figure 3-8. Concept diagram of AD sludge encapsulated in alginate with PVP and Chitosan in AD process

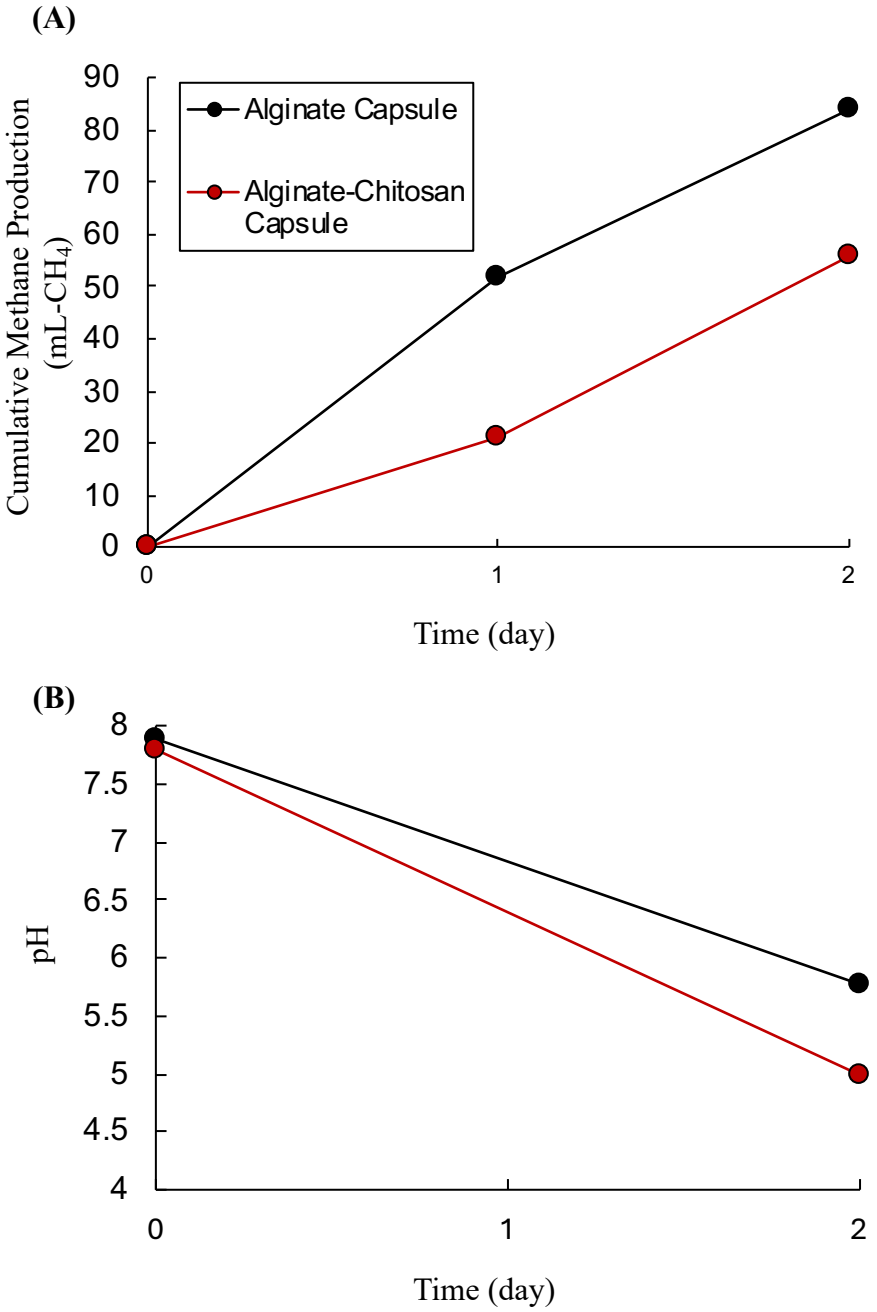

Figure 3-9. (A) Cumulative methane gas production and (B) pH of AD sludge encapsulated in alginate and chitosan

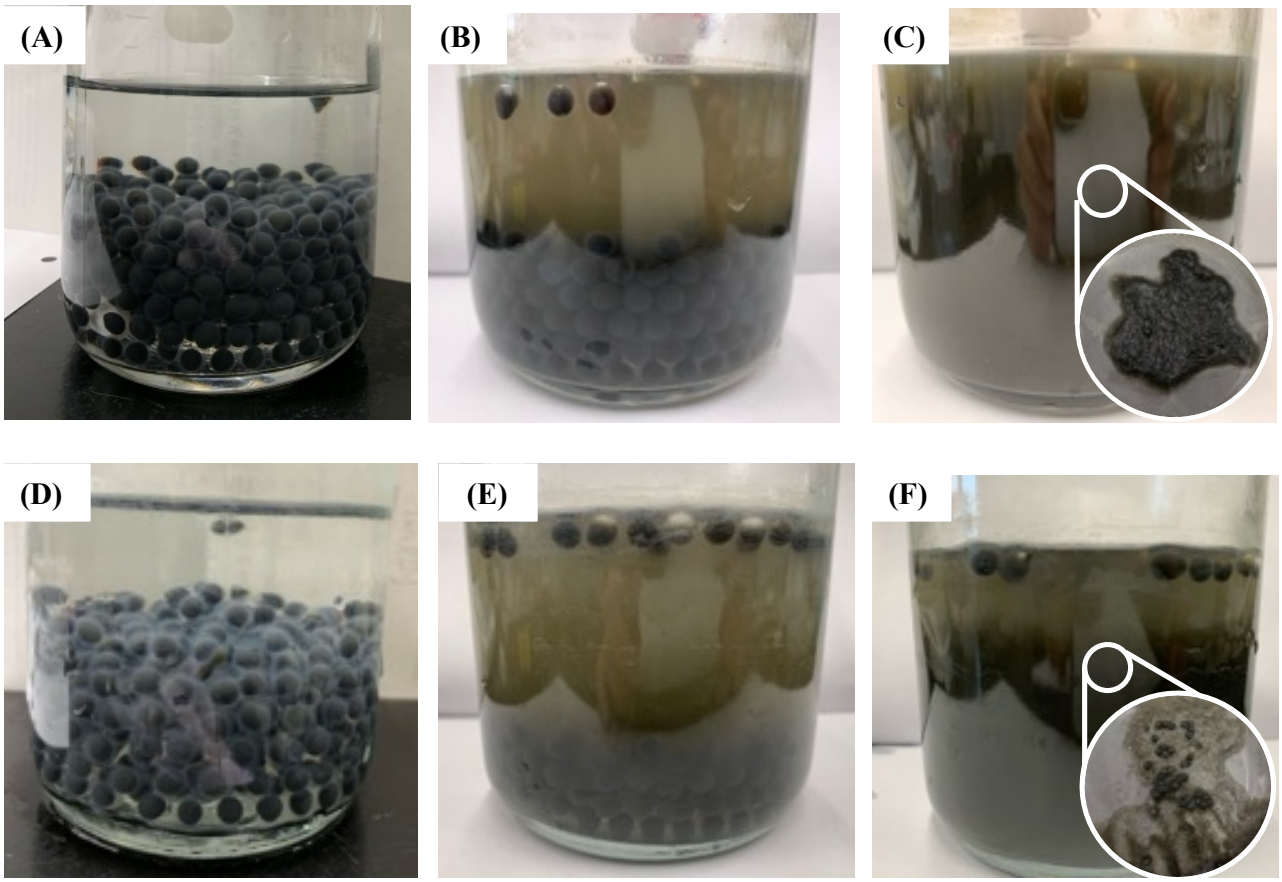

Figure 3-10. Images of AD sludge encapsulated in alginate in (A) day 0, (B) day 1, (C) day 2 and encapsulation in alginate with addition of chitosan in (D) day 0, (E) day 1, (F) day2

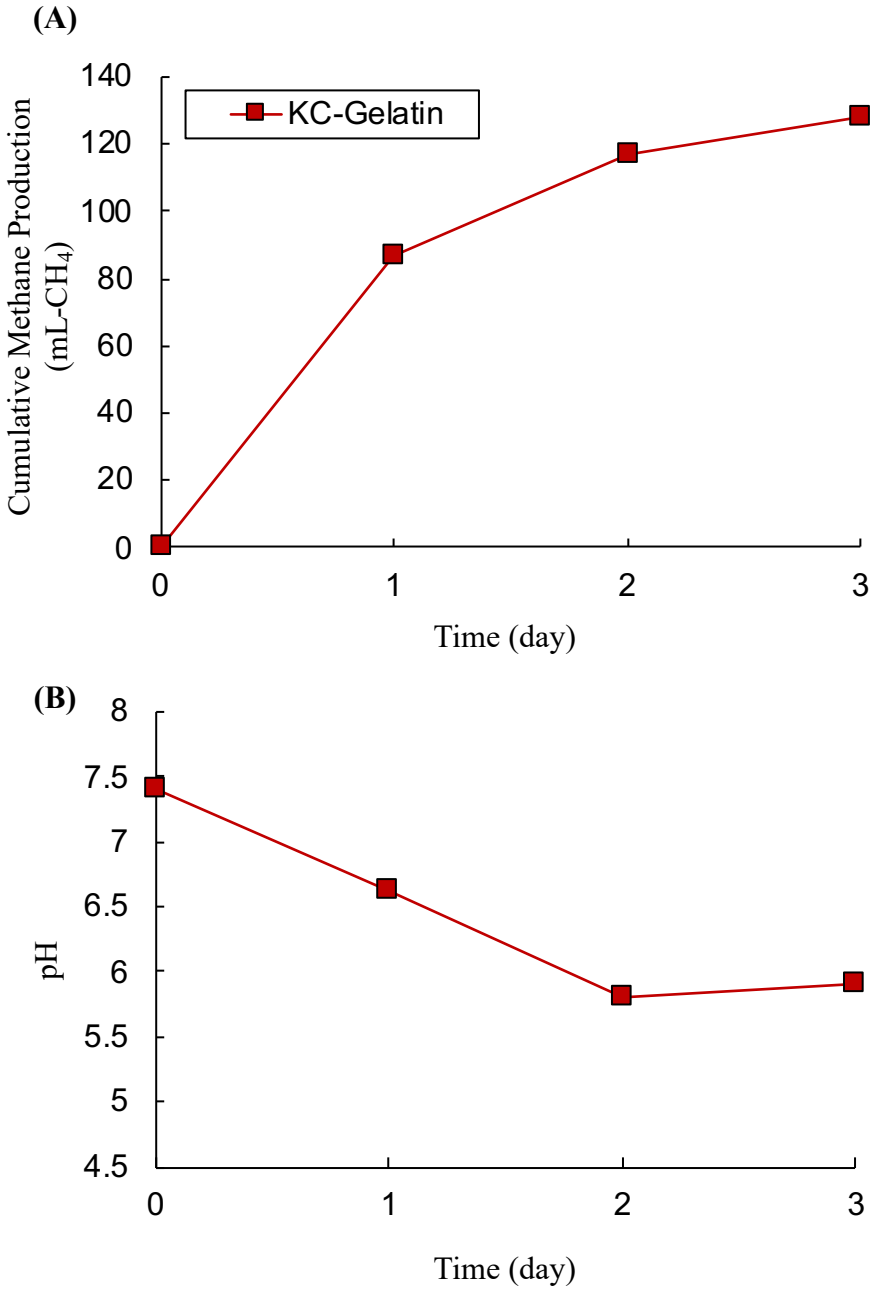

Figure 3-11. (A) Cumulative methane gas production and (B) pH of AD sludge immobilized in κ-carrageenan and gelatin

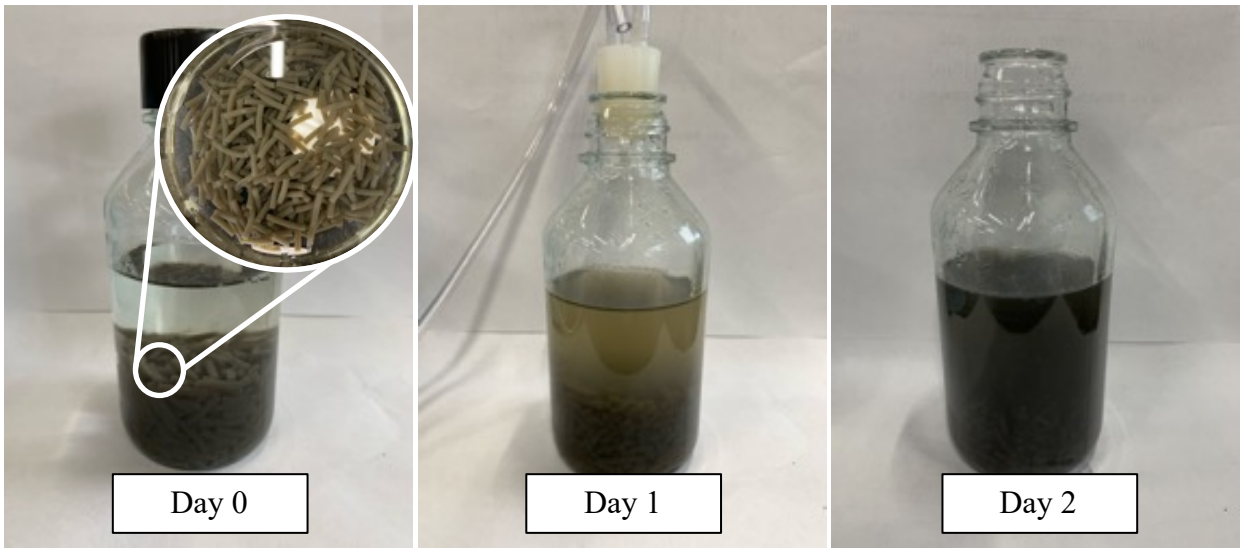

Figure 3-12. Image of AD sludge immobilized in κ-carrageenan and gelatin throughout the experiment

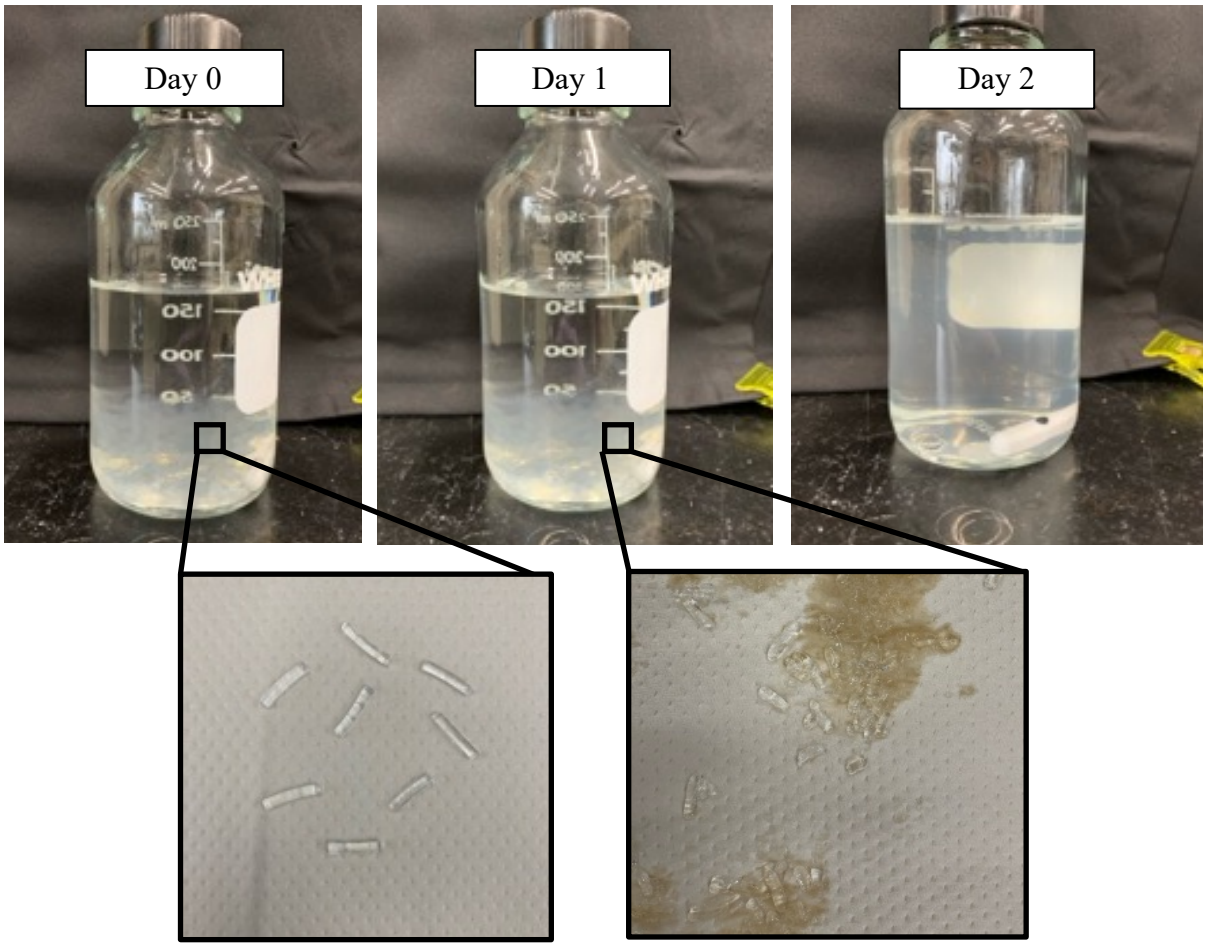

Figure 3-13. Image of κ-carrageenan and gelatin hydrogel without AD sludge inoculated at 37℃

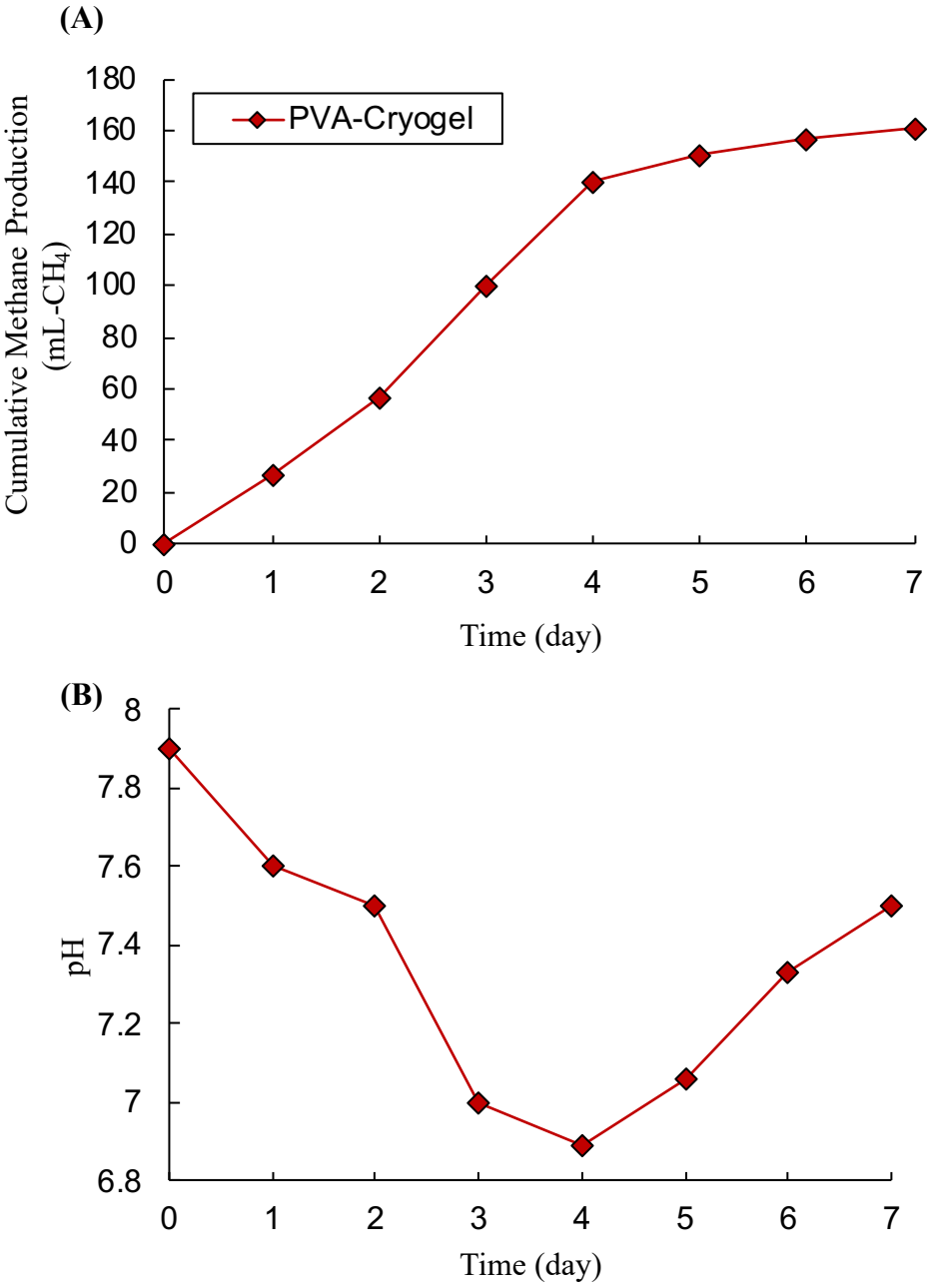

Figure 3-14. (A) Cumulative methane gas production and (B) pH of AD sludge immobilized in PVA-cryogel

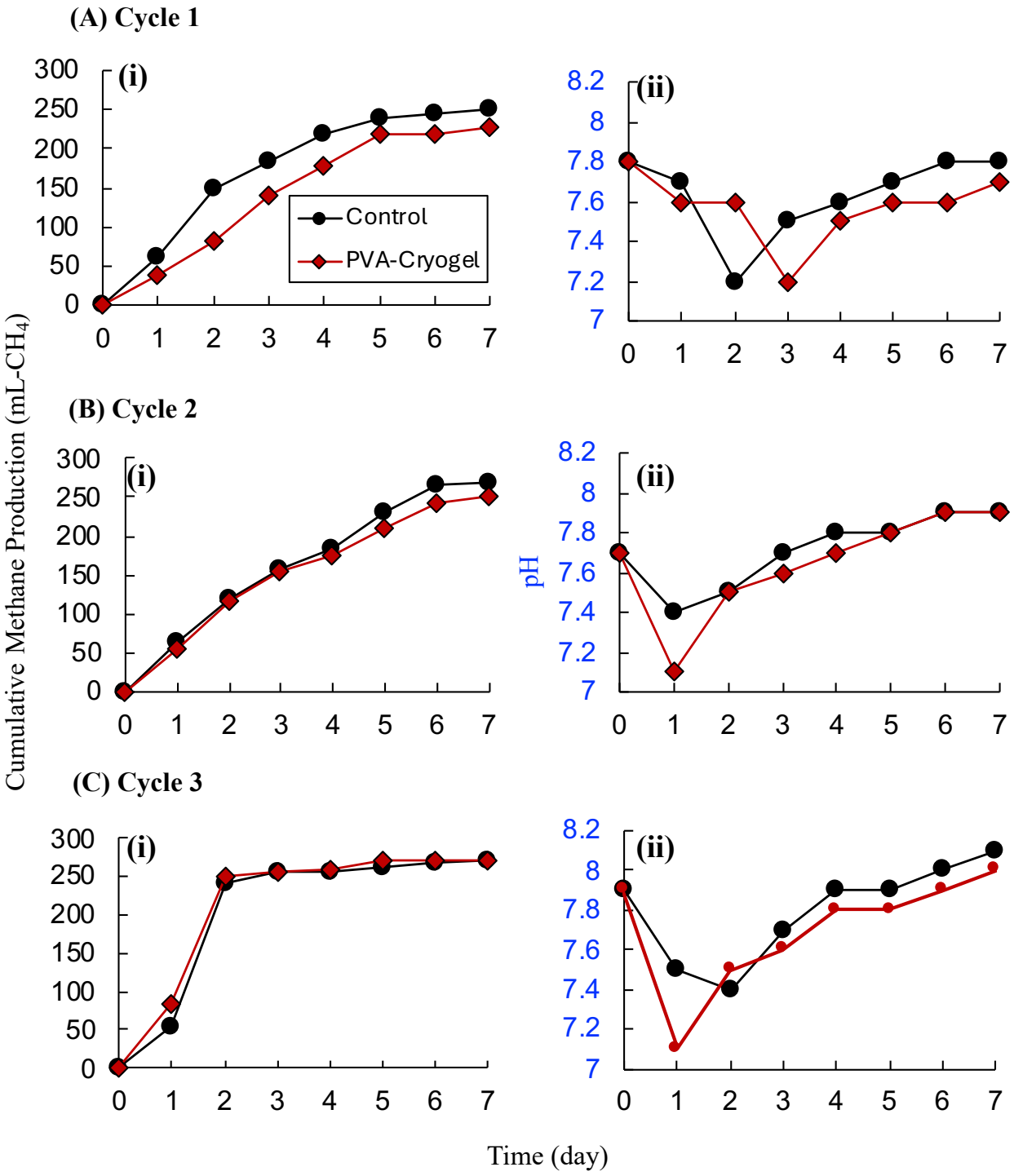

Figure 3-15. Cumulative methane production and pH of AD sludge immobilized in PVA-cryogel in (A) Cycle 1, (B) Cycle 2, and (C) Cycle 3

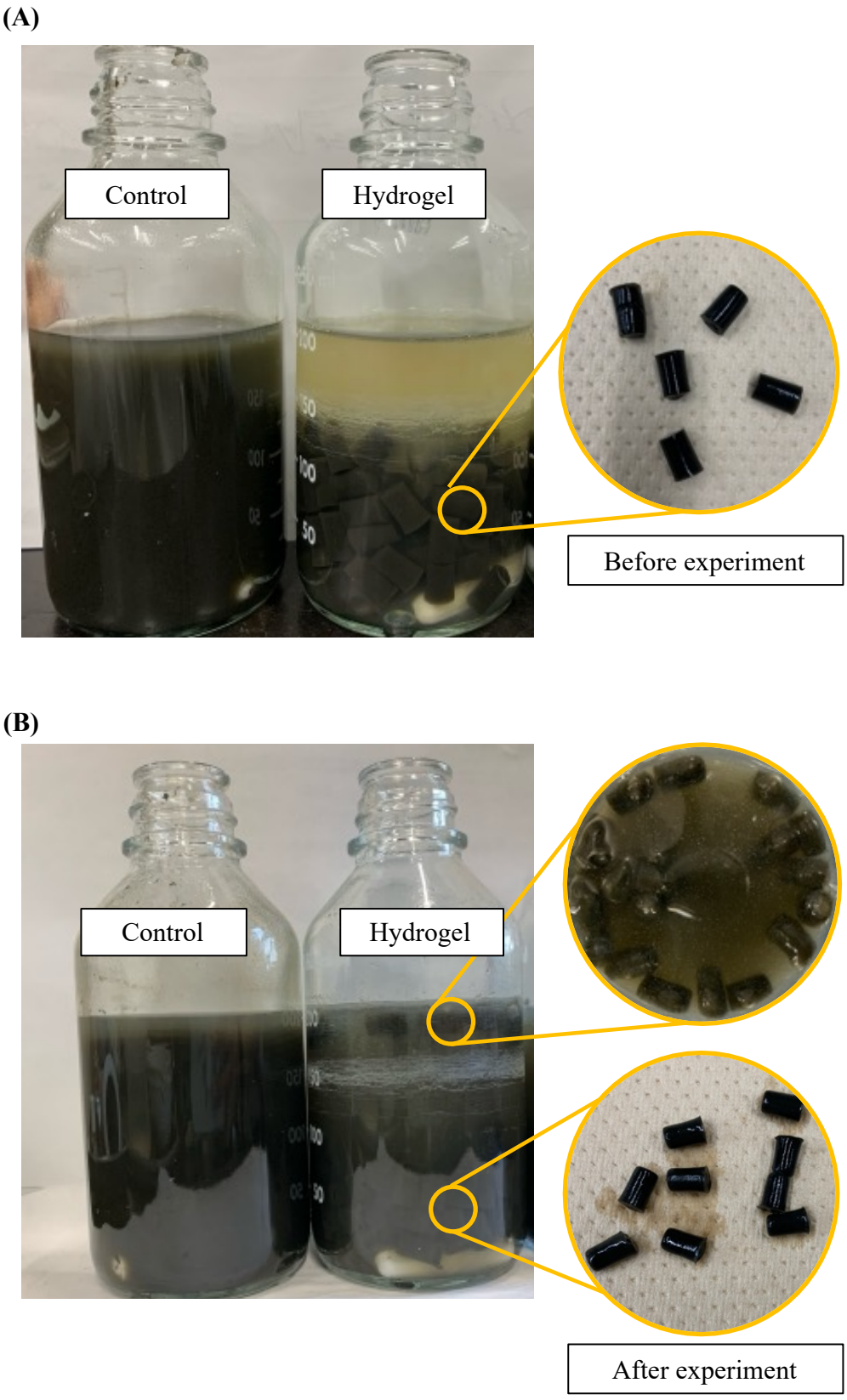

Figure 3-16. Image of AD sludge immobilized in PVA-cryogel in (A) before and (B) after the experiment

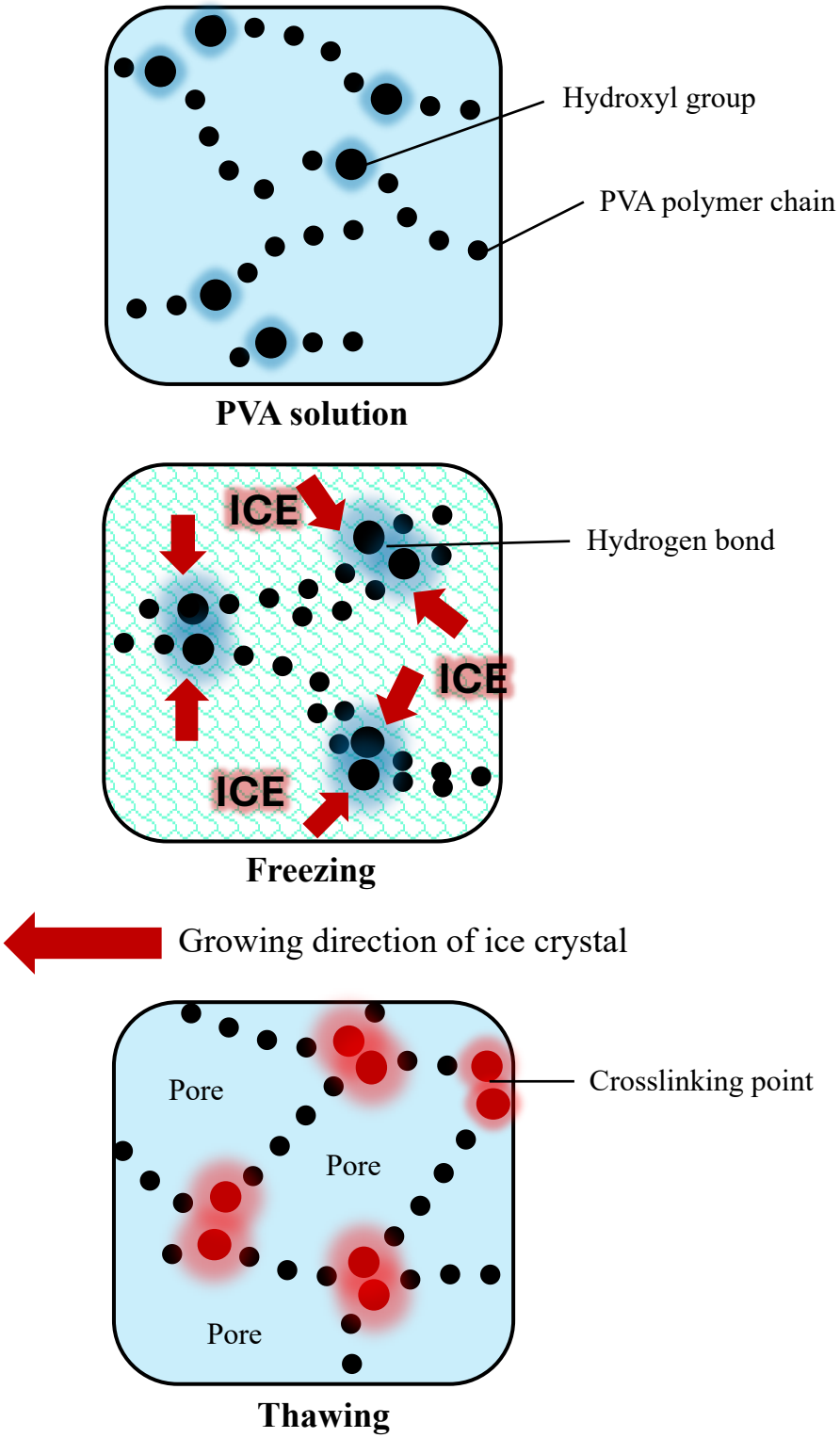

Figure 3-17. Mechanism of PVA-Cryogel formation via freeze-thawing

Table 3-1. Summary of four different immobilization method tested in the AD system

	Successful AD process	**Biogas Permeability**	**Maintain of neutral pH**	**Dura -bility**	**Low biodegra -dability**
Method A Boric Acid PVA-SA	×	×	×	×	△
Method B Encapsulation in SA	×	×	×	×	×
Method C κ-carrageenan & gelatin	×	×	×	×	×
Method D PVA-cryogel	○	○	○	○	○

Chapter 4

Optimization of co-immobilized hydrogel

4.1 Background/Overview of Experiment 3

In the previous chapter (Chapter 3), the immobilization method for AD microbes was established. Before evaluating the AD performance of the co-immobilized hydrogel, the preparation conditions were optimized to achieve better results. This optimization aimed to improve the hydrogel's performance in the AD process using the immobilization method outlined in Chapter 3. As discussed in the introduction, direct interspecies electron transfer (DIET) requires DIET-related microbes to attach to conductive nanowires or non-biological conductive materials (CMs) to occur. Thereby, naturally, immobilizing a high biomass (microbial) concentration within the hydrogel could facilitate DIET more easily. However, immobilizing excessive biomass content may weaken the hydrogel's mechanical strength, affecting durability when use in long-term experiments. Conversely, insufficient biomass content could reduce the contact between microbes and CMs, leading to inefficient electron transfer or even intermediate substrate transfer. Similarly, the concentration of CMs also influences AD performance; an excess amount could reduce the hydrogel durability, while an insufficient amount will lead to inefficient DIET. Therefore, optimizing both biomass content and CM concentration within the hydrogel is essential.

In this chapter, the optimization of the co-immobilized hydrogel is examined in two studies. In Study I, the biomass content is optimized by changing the biomass volumes to 30%, 50%, and 80% (w/w) within the hydrogel. The optimized biomass content is then used to determine the appropriate amount of CMs, which are varied from 0.5 to 3.0 g L^{-1} in Study II.

4.2 Materials and Methods

4.2.1 Inoculates and cultivation media

The mesophilic anaerobic sludge from Hokubu Sludge Treatment Centre in Yokohama, Japan, was utilized as the inoculum for this batch experiment. For both experimental study, ethanol was used as substrate along with the addition of trace elements and vitamin solution similar to the one used in chapter 2. The sludge's total solid (TS) and volatile solids (VS) content inoculated were 7.47 g L^{-1} and 5.57 g L^{-1} for Study I, and 6.6 g L^{-1} and 4.4 g L^{-1} for Study II, respectively.

4.2.2 Preparation of hydrogel

The hydrogel optimization was conducted using the immobilization method established in Chapter 3. Briefly, the AD sludge was centrifuged at 4000 rpm for 15 min using a Beckman Coulter Allegra X-30R centrifuge to separate the biomass from the supernatant. The supernatant was stored at 4℃ for later use, while the biomass was mixed with an aqueous PVA (Polyvinyl alcohol 25-100; Kuraray Co., Ltd, Japan) solution to achieve a final composition of 7% (w/v) PVA. The mixture (PVA and biomass) was then pipetted into 96-well microplates, frozen at -20℃ for 24 h, and subsequently thawed at room temperature to form the hydrogel.

In Study I, the hydrogel was synthesized following the above procedure under three conditions only by changing the used biomass content to 30%, 50%, and 80% (w/w) for comparison. These hydrogels are referred to as "30% Biomass," "50% Biomass," and "80% Biomass," respectively. Despite the varying biomass contents, it should be noted that all hydrogels maintained a consistent final composition of 7% (w/v) PVA. Additionally, it should be noted that CM are not added in study I. In Study II, multi-walled carbon nanotubes (MWCNTs) were added as CM for immobilization together with the optimized amount of AD sludge in study I in the hydrogel. The hydrogel preparation followed the same procedure as described above, except for one step in which the MWCNTs were first mixed with the AD sludge until a homogeneous mixture was achieved before being combined

with the aqueous PVA solution. Four variations of co-immobilized hydrogel were prepared, with MWCNTs (NC-7000, diameter = 9.6 nm, length = 1.5 μm, 90% purity; Sambreville, Belgium) concentrations of 0.5 g L^{-1}, 1.0 g L^{-1}, 2.0 g L^{-1}, and 3.0 g L^{-1}. For comparison, a control hydrogel without MWCNTs was also prepared. It is important to note that all hydrogels synthesized in Study II contained a consistent biomass content of 30%, which was identified as the optimal biomass content in Study I.

4.2.3 Biomethane potential test

The biomethane potential (BMP) test was performed in batch mode using the automatic methane potential test system (AMPTS® II, BPC Instruments, Sweden). In Study I, three conditions were tested with different biomass contents: (1) 30% Biomass, (2) 50% Biomass, and (3) 80% Biomass. Although the hydrogel's biomass content varied across these conditions, the amount of biomass in each condition was carefully calculated to ensure equal sludge inoculation. In Study II, five different conditions were prepared to optimize the MWCNTs concentration in the co-immobilized hydrogel: (1) Control (hydrogel with immobilized AD sludge only), (2) 0.5 g L^{-1} MWCNTs, (3) 1.0 g L^{-1} MWCNTs, (4) 2.0 g L^{-1} MWCNTs, and (5) 3.0 g L^{-1} MWCNTs. All conditions were performed in triplicate. All reactors were inoculated with the prepared hydrogels and the initially separated supernatant along with an additional 200 mL of deoxygenated distilled water to achieve a final working volume of 300 mL. Ethanol was used as a substrate with a sludge-to-substrate ratio of 2:1 based on VS, along with the addition of 0.5 mL of trace element and vitamin solution. All reactors were incubated at 37°C with slow stirring at 50 rpm to prevent mechanical damage to the hydrogels. The experiment was conducted in three cycles, with the operation in which cycle transition were conducted when the biogas production ceased for three consecutive days. After the complete conversion of ethanol, the next cycle began by re-feeding ethanol(substrate) without changing the medium. It should be noted that only for Study I, the experiment was extended to a fourth cycle by replacing the medium from cycle 3 before re-feeding with ethanol. In both studies,

pH measurements were carried out only at the start and the end of each cycle. Before the experiment, nitrogen gas was flushed through the reactors for 1–2 mins to achieve anaerobic conditions. Biogas produced during the batch operation was directed to a 3.0 M NaOH solution to strip CO_2, and the remaining methane volume was measured using a liquid displacement and buoyancy-based method.

4.2.4 Analysis method

The total solids (TS) and volatile solids (VS) were measured according to the standardized methods outlined by the American Public Health Association (American Public Health Association, 2005). Biomethane yield was automatically recorded every 24 h using the AMPTS® II system, and pH measurements were conducted with a pH meter (Bettler Toledo, S220-Basic). To determine the amount of biomass and MWCNTs that may have leaked out from the originally immobilized hydrogel, the medium from all conditions was collected at the end of the experiment, dried at 105°C for 3-5 days, and weighted at the end of the experiment for study I & II.

The mechanical strength of the hydrogel before and after the experiment was also assessed using a tabletop material testing instrument (A&D Co., Ltd., Japan) via a compression test with a 50 N load cell. During the test, cylindrical hydrogel samples (10 mm in height, 6 mm in diameter) were placed between self-leveling plates and compressed at a rate of 10 mm min^{-1}. Young's modulus was calculated from the slope of the stress-strain curve within the initial linear range of 5–15%. To ensure accuracy, the measurements were averaged across at least five different hydrogel samples for each condition in both study I & II.

4.2.5 Calculations: Methane production rate

The cumulative methane production from each study was fitted using the modified Gompertz equation (Equation 1) to estimate both the methane production rate and the lag phase, as this model is commonly used to correlate microbial activity with biogas generation. The modified Gompertz

equation is as follows:

$$f(t) = P \times exp\left(-exp\left(\frac{e \cdot R_m}{P} \times (l - t) + 1\right)\right) \qquad \text{Equation 1}$$

In this equation, $f(t)$ represents the cumulative methane production (mL) at time t, P is the maximum cumulative methane production (mL) achieved by the end of the incubation, R_m is the maximum methane production rate (mL day^{-1}) and l refers to the lag phase (days).

4.3. Results and Discussion

4.3.1. Study I: Optimization of biomass content in hydrogel

In Study I, the biomass content in the hydrogel was varied to 30%, 50%, and 80% with the aim of achieving a higher methane production rate by reducing the distance between microbes in the hydrogel, which could facilitate faster intermediate transfer and/or efficient DIET. At the same time, maintaining the shape and durability of the hydrogel was a priority. However, hydrogel preparation for the condition with 80% biomass could not be achieved due to the high viscosity of the solution. The increased biomass content in the PVA aqueous solution resulted in excessive viscosity, making it difficult to process, pour, and mold the material into the 96-well microplate. Consequently, only the 30% and 50% biomass conditions were evaluated.

Figures 4-1 and **Table 4-1** shows the cumulative methane gas production and methane production rate for both biomass amount conditions across the cycles. Both conditions show similar cumulative methane production at the end of each cycle, indicating that AD proceeded successfully in both cases. Nevertheless, both conditions also show a similar methane production rate, which is contrary to our hypothesis, and it indicates that increasing the immobilized biomass concentration from 30% to 50% did not result in a higher methane production rate. Additionally, a significant observation was the noticeable leakage of immobilized biomass into the medium solution for all conditions as the experiment progressed (**Figure 4-2;** depicts the 30% biomass concentration but all

conditions were similar). While continuous stirring may contribute to biomass leakage due to the collision between the stirrer and hydrogel beads, which could gradually damage the beads' surface, the extent of this damage was unlikely under this study's conditions as the stirring rate was set up to only 50 rpm. In contrast to a preliminary failed AD experiment—where no biogas was produced even after 7 days under similar stirring rates— no leakage of immobilized biomass from the hydrogel into the medium was observed (**Figure 4-3**). This suggest that the biomass leakage from hydrogel is likely driven by the release of biogas from the immobilized microbes in hydrogel.

Given this result, biomass leakage could potentially hinder the AD process in a continuous operation. Therefore, it was important to quantify the leaked biomass and evaluate whether its removal would impact methane production efficiency. At the end of cycle 3, the medium solution containing leaked biomass from both conditions was completely replaced with fresh medium. The same amount of ethanol as in cycles 1-3 was fed, and the process was evaluated in cycle 4. This step was designed to assess whether the volume of leaked biomass was large enough to affect the AD process when removed. The results of cumulative methane production and methane production rate of cycle 4 is shown in the **Figures 4-1(D)** and **Table 4-1**. The result indicates that even after removing the leaked biomass from hydrogel, the AD process continued smoothly, implying that the amount of leaked biomass was relatively small. It should be pointed out that the 30% biomass showed approximately 1.7 times faster methane fermentation rate. Additionally, the leaked out biomass from hydrogel in cycle 3 was collected, dried at 105°C, and weighed. The results **(Figure 4-4)** revealed a significant difference between the two conditions: the 50% biomass condition leaked 1.6 times more biomass than the 30% condition. As discussed in Chapter 3, the PVA-cryogel preparation relies on hydrogen bonding (crosslinking) between the PVA polymer chains during the freezing process (Tsou et al., 2016). The addition of biomass can interfere with crosslinking density, as biomass may disrupt the formation of a uniform and strong PVA crosslinking network. Thereby, even with a consistent final PVA concentration of 7% in both hydrogels, increasing the biomass content likely increased the porosity of the hydrogel, leading to greater biomass leakage in the 50% biomass condition.

Nevertheless, calculations showed that the leaked biomass accounted for only 8.5% of the total for the 30% biomass condition and 11.4% for the 50% biomass condition. This means after the leaked biomass was removed at the end of cycle 3, the 30% biomass contained a higher biomass amount in the hydrogel than that for the 50% biomass. Therefore, the reason for the higher methane production rate for the 30% biomass may be due to the higher biomass retention in the hydrogel. Nevertheless, it is important to mention that the removal of the leaked biomass had no significant impact on the methane production performance likely due to relatively small leakage for both condition (**Figure 4-1 (D)**).

Figure 4-5 shows the appearance of hydrogel before and after the experiment. As can be seen, both appearance of hydrogel prepared with 30% and 50% biomass before the experiment looks the same as they were moulded from the 96-well microplate. After the experiment, no significant change in shape of the hydrogel was seen with 30% biomass conditions, however a noticeable change in shape of the hydrogel was observed for the 50% biomass hydrogel condition. This is probably due to the leaked-out biomass from hydrogel as observed in **Figure 4-4**. To further verify the durability of the hydrogels, the elastic modulus values of the hydrogels before and after the experiment were measured, and the result is shown in **Figure 4-6**. The results show a difference in the elastic modulus even before the experiment, where the 30% biomass conditions showed approximately 1.2 times higher elastic modulus than that for the hydrogel of the 50% biomass. The results indicate that increasing the biomass content reduces the mechanical strength of the hydrogel, which is likely due to the interference with PVA-crosslinking as discussed above. After the experiment, the 30% biomass conditions showed about a 16% drop in mechanical strength compared to that of the hydrogel before the experiment, while the 50% condition was unmeasurable due to the change in the shape of the hydrogel (**Figure 4-5**). These results showed that increasing the biomass content from 30% to 50% not only resulted in no apparent enhancement in the methane production rate but also contributed to higher biomass leakage and lower durability even in such a short period of time, which is not favourable. Thereby, the 30% biomass amount immobilized in hydrogels was determined to be the

optimized biomass amount.

4.3.2. Study II: Optimizing the Conductive Materials concentration in hydrogel

In Chapter 2, the results show that granular activated carbon (GAC) as CM yielded the highest methane production rate compared to the other two tested CMs. Thereby, GAC was initially selected for co-immobilization with AD sludge in hydrogel. However, the co-immobilization was unsuccessful, as almost all the GAC was settled at the bottom of the hydrogel, with some particles even detaching from it (**Figure 4-7 (A)**: depicts prepared hydrogel without biomass for visualization purposes). This is likely due to the large particle size of GAC (20×40 mesh, approximately 297-841μm), which facilitated its settling in the 96-well microplate during hydrogel synthesis. As discussed earlier, the formation of cross-linkages within the PVA hydrogel occurs when the PVA chains are brought into proximity, facilitating hydrogen bond formation during the freezing procedure (Tsou et al., 2016). The inclusion of additional materials within the PVA solution can interfere with this crosslinking formation. When GAC was added, its high concentration (20 g L^{-1}) and fast sedimentation resulted in too high accumulation of GAC at the bottom of the hydrogel disrupting the crosslinking process. This contributed to a brittle lower section where most of the GAC was not effectively immobilized within the hydrogel. In contrast, when multi-walled carbon nanotubes (MWCNTs) were immobilized, the distribution of MWCNTs within the hydrogel was seemingly uniform while maintaining the hydrogel shape compared to when GAC was used **(Figure 4-7 (B))**. Given that the MWCNTs has a smaller size (diameter: 9.6 nm, length: 1.5 μm) compared to GAC, it can reduce its impact on disrupting the crosslinking process. Additionally, the results from Chapter 2 revealed that although the amount of MWCNTs used was only 1/20 of that of GAC, the methane production rate achieved was approximately 83% of that obtained with GAC. Therefore, based on these considerations, MWCNTs were selected for preparing the co-immobilized hydrogel.

Similar to Study I, the concentration of MWCNTs can influence AD performance when immobilized. An excessive amount of MWCNTs may reduce the durability of the hydrogel, while an

insufficient amount could limit the effectiveness of DIET. To evaluate this, MWCNTs concentrations were varied from 0.5 to 3.0 g L^{-1} in the hydrogel. **Figure 4-8** shows the cumulative methane production over cycles 1 to 3. In cycle 1, the complete ethanol conversion to methane took approximately 13 days for all conditions, likely due to the microbes acclimating to the new immobilized environment and substrate. As the cycles progressed, the time needed for ethanol conversion to methane decreased, indicating that the microbes successfully acclimatized to using ethanol as substrate. **Table 4-2** shows the methane production rates results. In cycle 1, the conditions with added MWCNTs exhibited rates about 1.2-1.5 times faster than that of the control (AD sludge immobilized in hydrogels without MWCNTs). Many previous DIET research has shown that adding CMs can accelerate the acclimatization phase or achieve faster stabilization (Wang et al., 2021, Xiao et al., 2021). Thus, despite the small differences in the methane production rate, the added MWCNTs likely contributed to the increased rates compared to the control. In cycle 2, all conditions showed faster methane production rates compared to cycle 1 as acclimatization continued. No significant differences in rate were observed compared to the control, except for the 1.0 g L^{-1} MWCNTs condition, in which the methane production rate was approximately 1.3 times faster than that of the control (149 mL g-COD^{-1} day^{-1} for the 1.0 g L^{-1} MWCNTs and 112 mL g-COD^{-1} day^{-1} for the control). By cycle 3, all conditions had similar rates (143-158 mL g-COD^{-1} day^{-1}) to the 1.0 g L^{-1} MWCNTs condition in cycle 2 with no significant difference. In the study by Zhao et al., 2015 a more pronounced difference in methane production rates was observed between CM-added and non-added conditions under high-OLR, whereas no significant difference was noted under low-OLR conditions. This is likely because, when the hydrogen partial pressure in the reactor becomes high at the high OLR condition, the degradation of VFAs through the traditional pathway requires more Gibbs energy, whereas DIET does not require additional energy since it bypasses the need for hydrogen production and oxidation (Mei et al., 2018, Wang et al., 2021). However, this study was conducted under a low-OLR condition (with a 2:1 sludge-to-substrate ratio), which may explain the lack of significant difference observed in cycle 3. Although the statistical tests (Tukey-Kramer) showed no significant

differences across the conditions, the 1.0 g L^{-1} MWCNTs appeared to achieve faster stabilization.

Similar to Study I, biomass leakage was observed in all conditions. The medium solutions were collected at the end of cycle 3 and dried at 105°C to measure biomass leakage. Notably, for conditions with MWCNTs, the dry weight included both leaked biomass and MWCNTs, which could not be separated. The results showed no significant difference in biomass leakage compared to the control for the conditions with up to 1.0 g L^{-1} MWCNTs **(Figure 4-9)**. However, significant leakage was observed in the 2.0 and 3.0 g L^{-1} MWCNTs conditions, where the leakage was approximately 2.1 and 1.8 times higher than that of the control, respectively. Additionally, calculations indicated that 78.5% and 81.3% of biomass were retained in the hydrogel for the 2.0 and 3.0 g L^{-1} MWCNTs conditions, respectively, compared to >87% retention for the conditions with hydrogel up to 1.0 g L^{-1} MWCNTs addition at the end of cycle 3. After the experiment, no noticeable changes were observed in the hydrogel structure for MWCNTs concentrations up to 1.0 g L^{-1}, while hydrogels with more than 1.0 g L^{-1} MWCNTs showed deformation where they became "thinner" and surface roughness could be seen **(Figure 4-10)**. Similarly to study I, higher concentrations of MWCNTs can interfere with PVA-crosslinking leading to an increase in pore size of the hydrogel. Based on these results, the addition of MWCNTs at concentrations exceeding 1.0 g L^{-1} likely leads to greater agglomeration of MWCNTs, resulting in increased leakage of both biomass and MWCNTs from the hydrogel. **Figure 4-11** illustrates the elastic modulus of each hydrogel before and after the experiment. Before the experiment, no significant changes in mechanical strength were observed for MWCNTs concentrations up to 3.0 g L^{-1}. After the experiment, hydrogels with 2.0 and 3.0 g L^{-1} MWCNTs deformed **(Figure 4-10)**, making them unmeasurable. In contrast, conditions with up to 1.0 g L^{-1} MWCNTs showed only a slight decrease in mechanical strength, with no significant difference from the control.

These results suggest that adding MWCNTs at concentrations up to 1.0 g L^{-1} does not significantly alter the hydrogel's properties (porosity and mechanical strength) compared to the control's hydrogel. Thereby, considering the methane production rates, stabilization time, hydrogel

durability, and biomass leakage, the optimal condition for the co-immobilized hydrogel was determined to be 1.0 g L^{-1} of multi-walled carbon nanotubes (MWCNTs) combined with 30% biomass.

4.4. Conclusions

In this chapter, the optimization of the hydrogel was conducted by adjusting the biomass volume to 30%, 50%, and 80% in Study I, and varying the concentration of MWCNTs from 0.5 to 3.0 g L^{-1} in Study II. In Study I, only the 30% and 50% biomass hydrogel conditions were able to be evaluated, as the 80% biomass hydrogel could not be prepared due to its excessive viscosity. The results indicated that the 30% biomass hydrogel maintained its shape and exhibited higher biomass retention, whereas the 50% biomass hydrogel lost its structural integrity due to greater biomass leakage after just four consecutive cycles. Notably, increasing the biomass content in the hydrogel did not enhance the methane production rate; therefore, the 30% biomass hydrogel condition was selected for evaluation in Study II.

In Study II, GAC was initially tested for immobilization within the hydrogel; however, this attempt was unsuccessful due to its large particle size and the necessity of high concentration in hydrogel, which interfered with the crosslinking process. Consequently, MWCNTs were utilized for immobilization instead. The addition of MWCNTs up to 1.0 g L^{-1} did not significantly alter the hydrogel's properties, including its durability and mechanical strength when compared to the control hydrogel (without MWCNTs). However, at MWCNTs concentrations of 2.0 g L^{-1} and 3.0 g L^{-1}, a noticeable change in shape and approximately double the biomass leakage were observed compared to the control. This suggests that higher concentrations of MWCNTs and/or an increase in biomass amount (in Study I), may interfere with the PVA-crosslinking, leading to an unwanted increase in pore size which could affect the hydrogel's durability and cell retention. Regarding the methane production rate, no significant differences were observed among the different conditions possibly due to the low-OLR. Nevertheless, the incorporation of 1.0 g L^{-1} MWCNTs in hydrogel facilitated faster

stabilization compared to the other conditions. Consequently, the optimized condition of 30% biomass with 1.0 g L^{-1} MWCNTs was selected for further evaluation in the batch AD experiment presented in the next chapter.

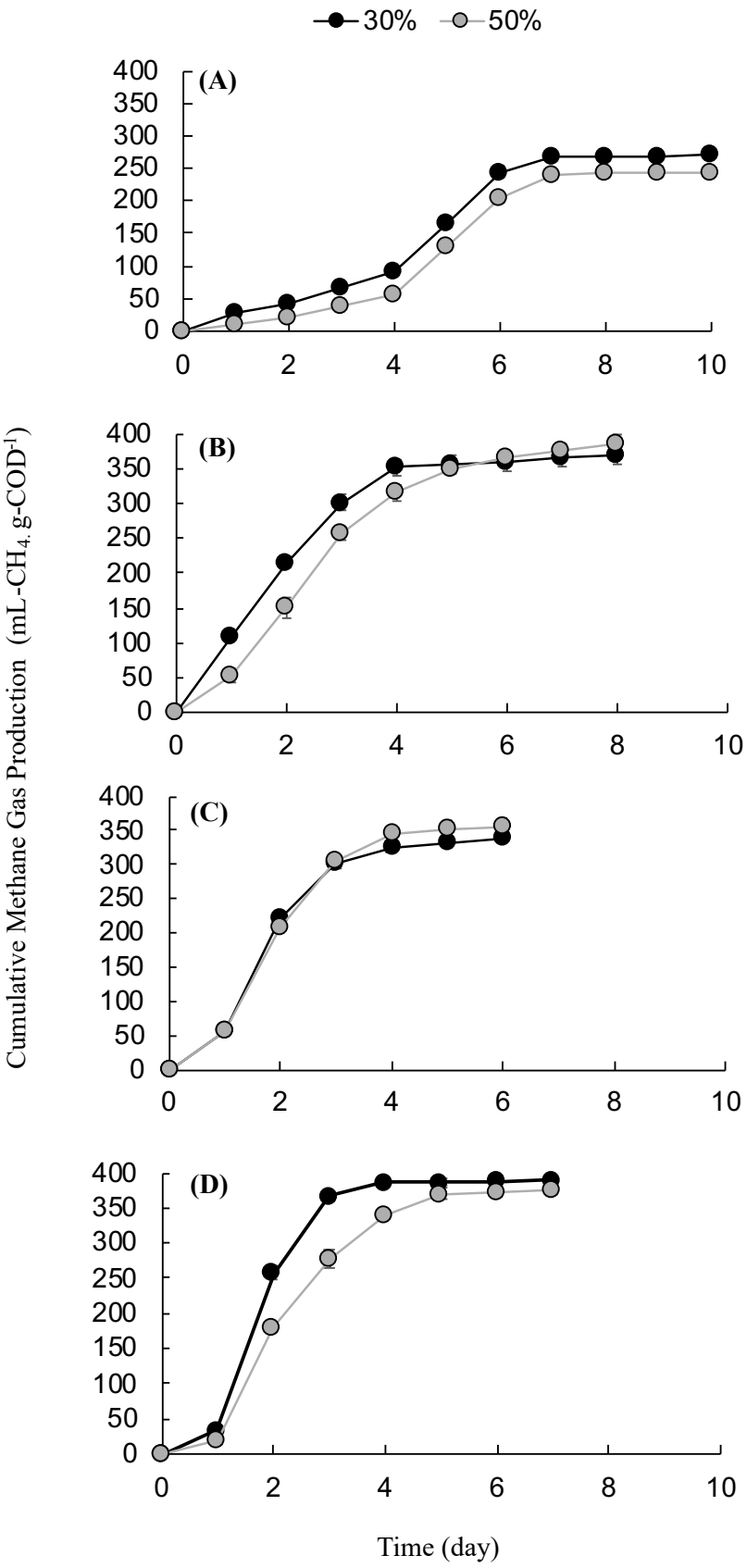

Figure 4-1. Cumulative Methane Production in (A) Cycle 1, (B) Cycle 2, (C) Cycle 3 and (D) Cycle 4

(A) Before experiment:

(B) After experiment:

Figure 4-2. Change in the color of the medium during the AD experiment: (A) before and (B) after the experiment. (Figure depicts the 30% biomass concentration but all conditions were similar)

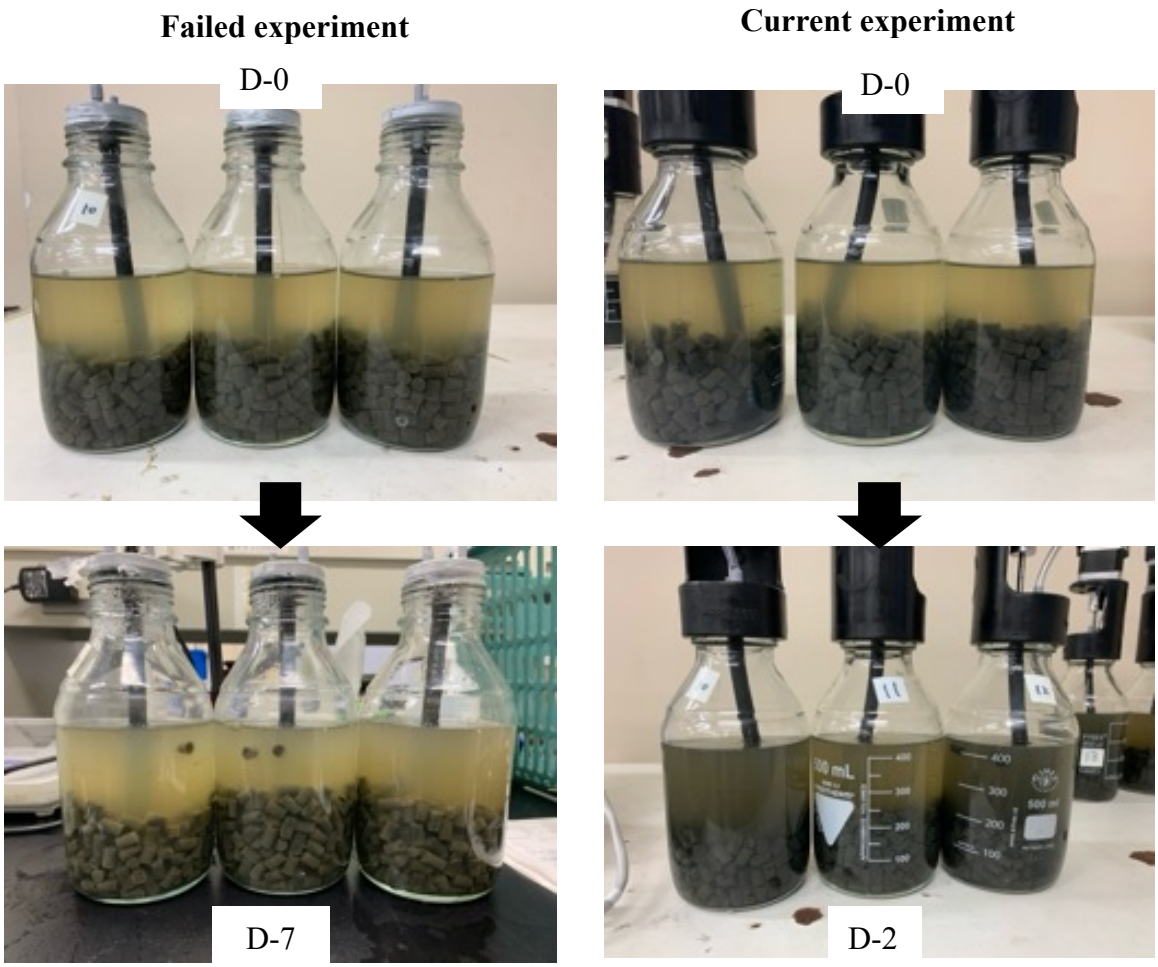

Figure 4-3. Image of hydrogel in reactor for the past failed preliminary experiment and current experiment

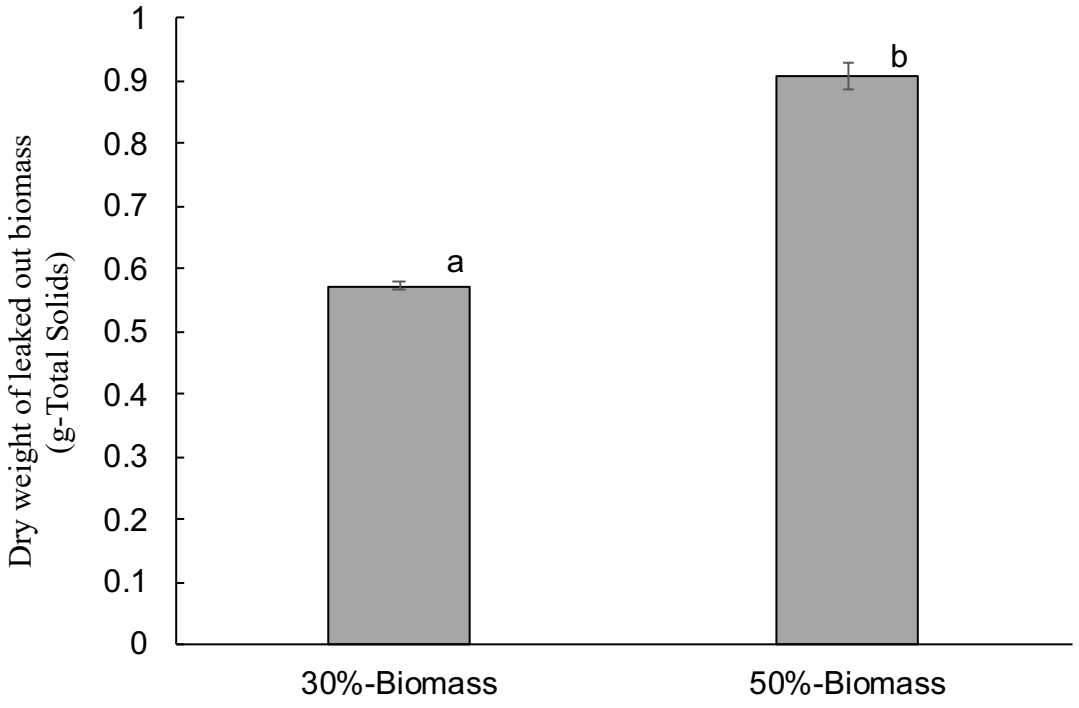

Figure 4-4. Dry weight of total leaked out biomass in Study I.

*Means followed by the same letter are not statistically different according to One-way ANOVA, Tukey-Kramer test at $P \leq 0.01$.

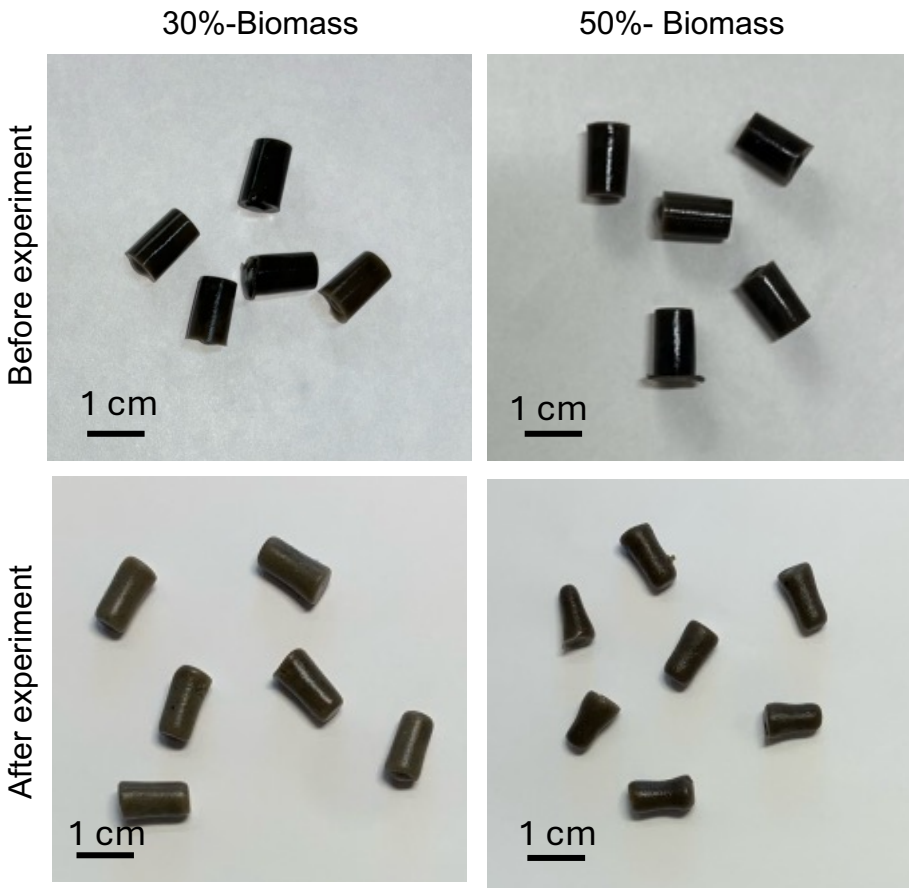

Figure 4-5. Image of hydrogel containing 30% and 50% biomass in before and after the experiment

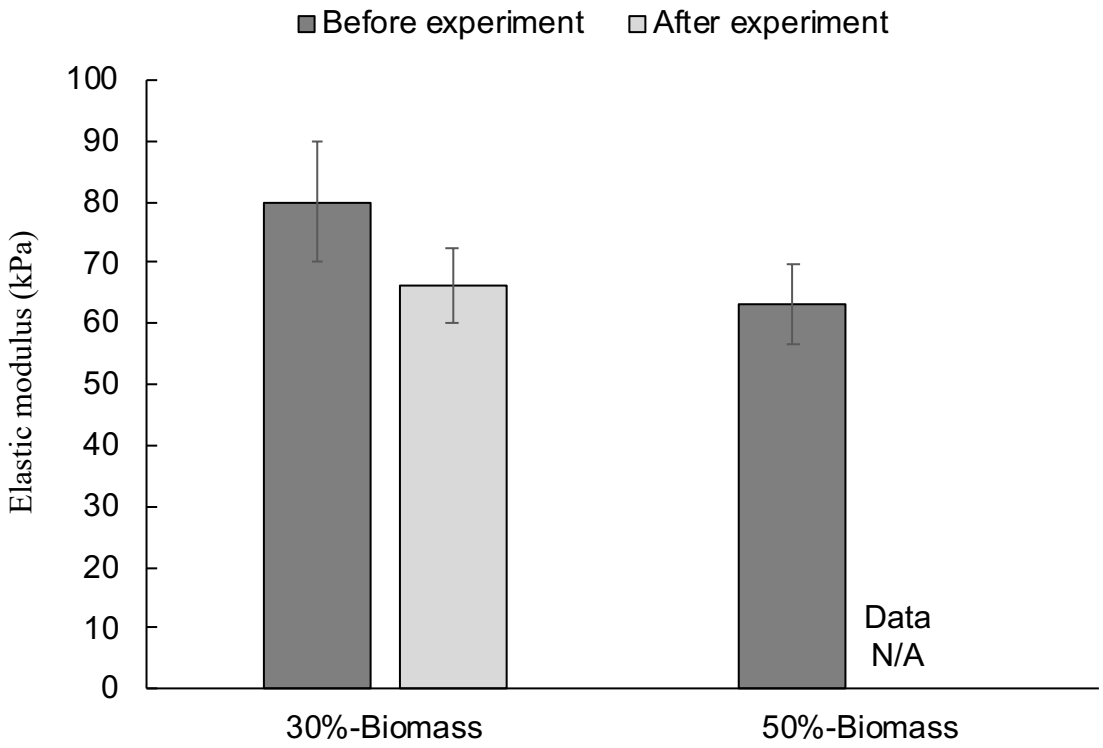

Figure 4-6. Elastic modulus of hydrogel before and after the experiment in Study I.

(A) GAC immobilized in hydrogel

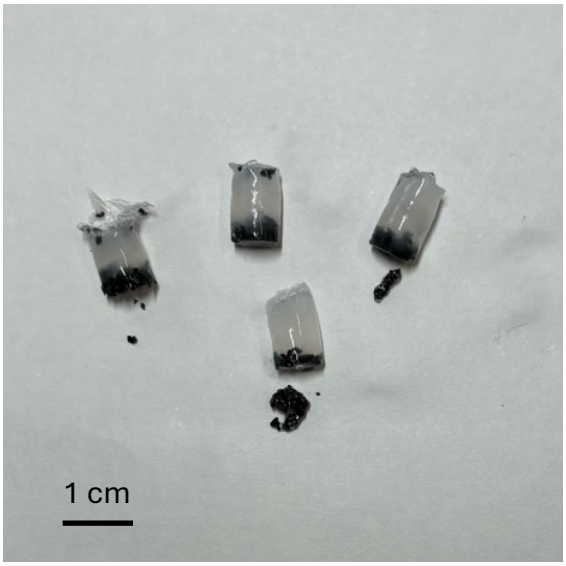

(B) MWCNTs immobilized in hydrogel

Figure 4-7. Image of PVA hydrogel immobilization: (A) GAC without the addition of biomass and (B) MWCNTs with biomass.

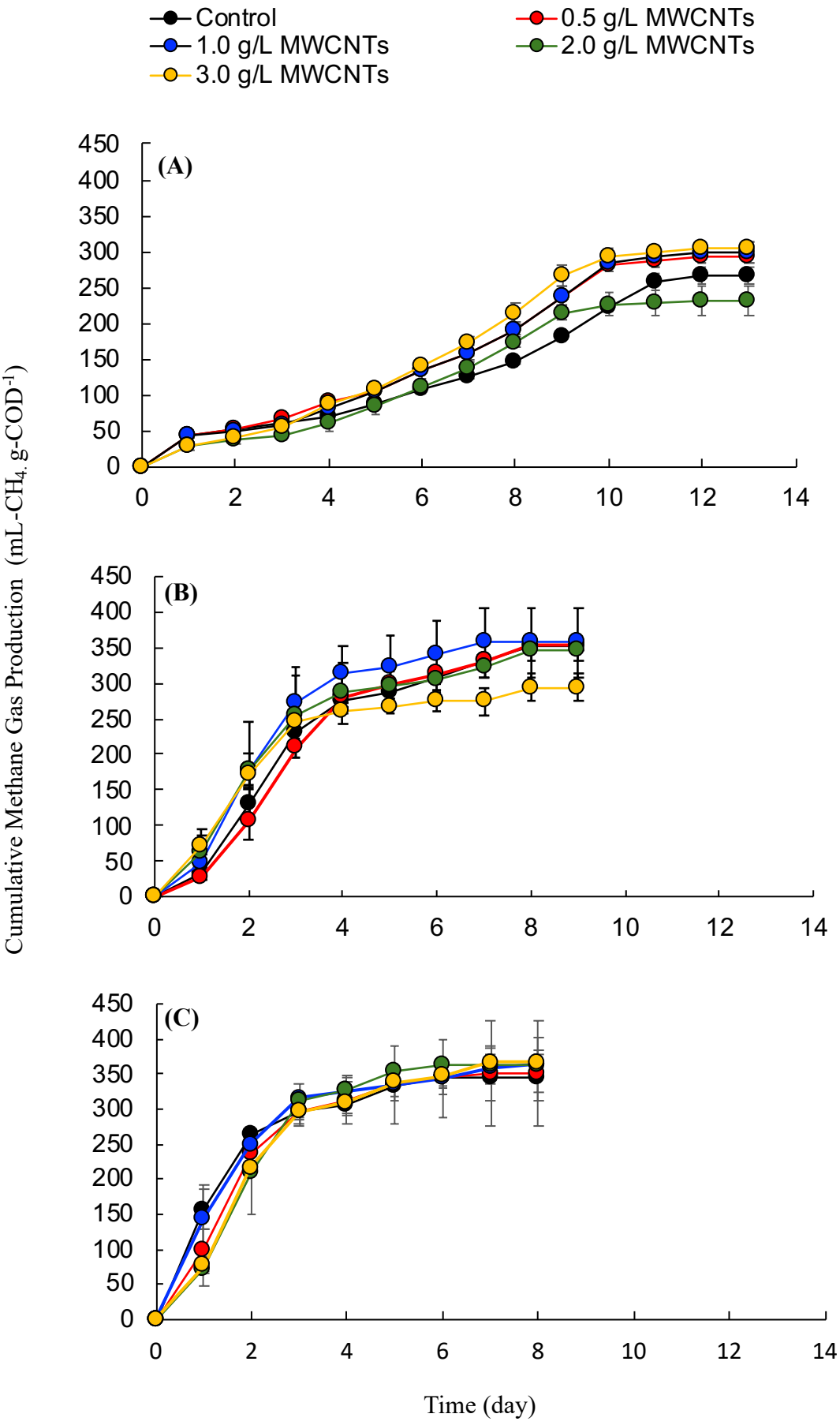

Figure 4-8. Cumulative Methane Gas Production in (A) Cycle 1, (B) Cycle 2 and (C) Cycle 3

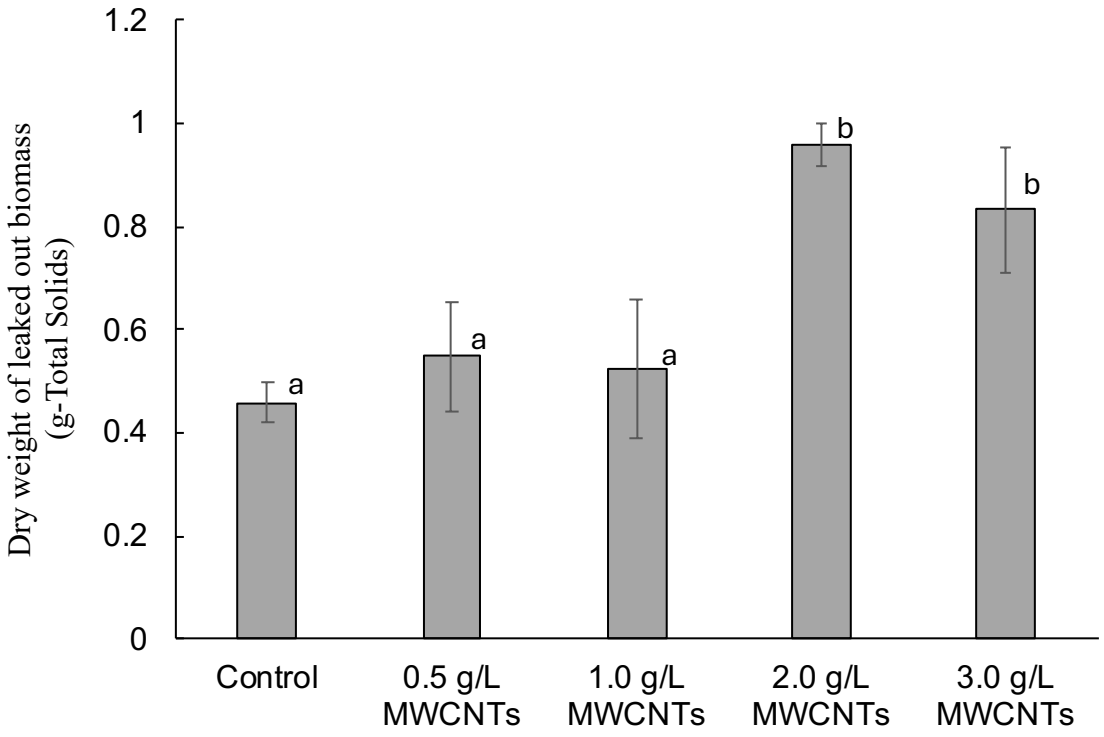

Figure 4-9. Dry weight of total leaked out biomass in Study I.

*Means followed by the same letter are not statistically different according to One-way ANOVA, Tukey-Kramer test at P≤0.01.

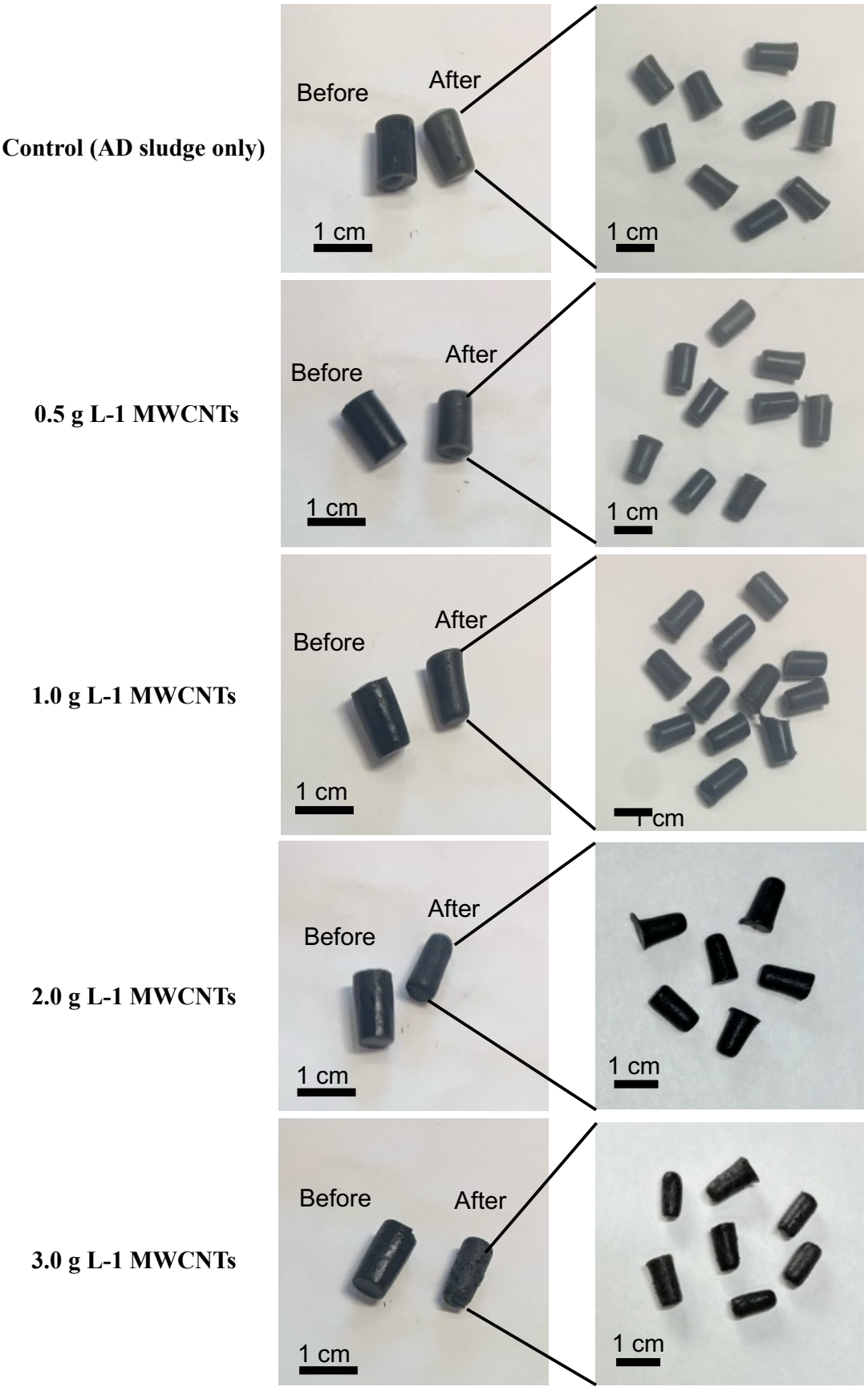

Figure 4-10. Image of hydrogel with MWCNTs varied from 0.5-3.0 g L^{-1} in before and after the experiment

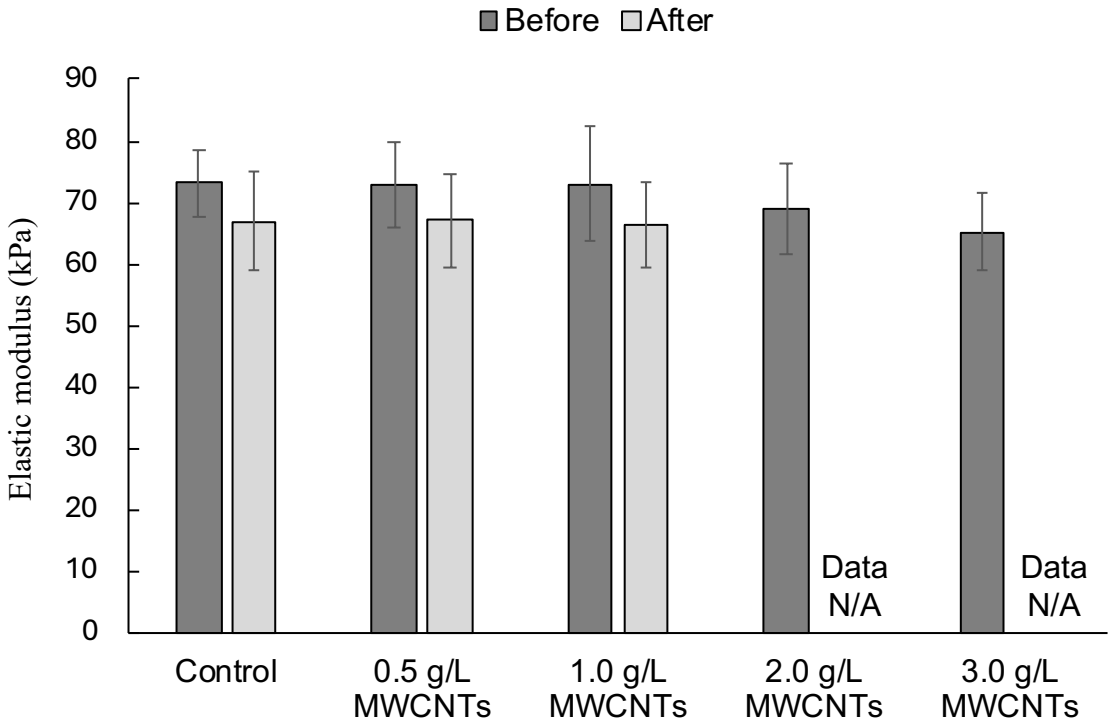

Figure 4-11. Elastic modulus of hydrogel before and after the experiment in Study II.

Table 4-1. Kinetic Parameter from Cycle 1, 2, 3 & 4 of Study I fitted to the Gompertz equation

	P (mL g-COD^{-1})	R_{max} (mLg-COD^{-1} day^{-1})	*l* (day)	R^2
		Cycle 1		
30% Biomass	280.10	63.99[a]	2.11	0.98
50% Biomass	254.40	79.59[a]	3.2	0.99
		Cycle 2		
30% Biomass	368.09	129.62[a]	0.24	0.99
50% Biomass	382.63	111.58[a]	0.62	0.99
		Cycle 3		
30% Biomass	335.29	174.32[a]	0.69	0.99
50% Biomass	356.87	162.11[a]	0.69	0.99
		Cycle 4		
30% Biomass	389.15	257.91[a]	0.94	0.99
50% Biomass	375.06	154.30[a]	0.92	0.99

*Means followed by the same letter are not statistically different according to One-way ANOVA, Tukey-Kramer test at $P \leq 0.01$, based on the results from each cycle.

Table 4-2. Kinetic Parameter from Cycle 1, 2 & 3 of Study II fitted to the Gompertz equation

	P (mL g-COD^{-1})	R_{max} (mL g-COD^{-1} day^{-1})	*l* (day)	R^2
Cycle 1				
Control	359.296	23.91[a]	1.06	0.98
0.5 g L^{-1} MWCNTs	348.23	30.18[a]	1.07	0.98
1.0 g L^{-1} MWCNTs	350.02	31.68[a]	1.36	0.99
2.0 g L^{-1} MWCNTs	256.05	29.23[a]	1.71	0.98
3.0 g L^{-1} MWCNTs	338.77	36.88[a]	1.74	0.99
Cycle 2				
Control	313.06	112.90[a]	0.72	0.99
0.5 g L^{-1} MWCNTs	328.12	114.78[a]	1.03	0.99
1.0 g L^{-1} MWCNTs	345.37	149.53[a]	0.67	0.99
2.0 g L^{-1} MWCNTs	313.18	102.61[a]	1.00	0.99
3.0 g L^{-1} MWCNTs	313.86	111.83[a]	0.63	0.99
Cycle 3				
Control	344.19	149.32[a]	0.26	0.99
0.5 g L^{-1} MWCNTs	343.74	152.86[a]	0.29	0.99
1.0 g L^{-1} MWCNTs	349.39	148.08[a]	0.08	0.99
2.0 g L^{-1} MWCNTs	361.19	158.19[a]	0.53	0.99
3.0 g L^{-1} MWCNTs	355.34	143.94[a]	0.38	0.99

*Means followed by the same letter are not statistically different according to One-way ANOVA, Tukey-Kramer test at $P \leq 0.01$, based on the results from each cycle.

Chapter 5

Evaluation of optimized co-immobilized hydrogel in AD process

5.1 Background/Overview of Experiment 4

Chapter 2 demonstrated that using ethanol as a substrate efficiently promotes the growth of exoelectrogenic bacteria, leading to higher DIET performance when CMs are added. Among the three CMs evaluated, MWCNTs were selected for co-immobilization due to their promising results in methane production, even with small additions, and their size, which is suitable for immobilization. In Chapter 3, the immobilization method for AD microbes was successfully established using the freeze-thawing technique, and the hydrogel condition was further optimized in Chapter 4. In this chapter, the AD sludge and MWCNTs were co-immobilized using the established freeze-thawing method and optimized conditions to evaluate their effect in the AD batch experiment, with ethanol as the substrate. The changes in microbial composition were also examined.

The AD batch experiment was conducted under four conditions of (1) Dispersed sludge, (2) Dispersed sludge with the addition of MWCNTs (conventional DIET), (3) Immobilized AD sludge in hydrogel with no addition of MWCNTs and (4) the co-immobilized hydrogel containing MWCNTs and AD sludge, for comparison. As a hypothesis, the proposed co-immobilized AD sludge & MWCNTs hydrogel will achieve a higher methane production rate as compared to the addition of MWCNTs into the dispersed sludge, due to the close contact of CMs and microbes through immobilization.

5.2 Materials and Methods

5.2.1 Inoculates and cultivation media

Mesophilic anaerobic sludge used to treat domestic sewage at the Hokubu Sludge Treatment Centre in Yokohama, Japan, was employed as the inoculum in the batch experiment. Prior to conducting the batch experiment, the sludge was left at 37°C for 4 d to naturally degas and for the removal of residual organic matter in the inoculum. Ethanol was used as a substrate to promote the growth of exoelectrogenic bacteria for efficient DIET (Chan et al., 2023). Trace elements and vitamin solutions were also added along with the substrate, as described by Morita et al. 2011 The components of the trace element solution were as follows: 0.5 g L^{-1} $MnSO_4 \cdot H_2O$, 0.1 g L^{-1} $FeSO_4 \cdot 7H_2O$, 0.04 g L^{-1} $NiCl_2 \cdot 6H_2O$, 0.05 g L^{-1} $CoCl_2 \cdot 6H_2O$, 0.13 g L^{-1} $ZnCl_2$, 0.01 g L^{-1} $CuSO_4 \cdot 5H_2O$, 0.1 g L^{-1} $AlK(SO_4)_2 \cdot 12H_2O$, 0.01 g L^{-1} H_3BO_3, and 0.025 g L^{-1} $Na_2MoO_4 \cdot 2H_2O$. The components of the vitamin solution were as follow: 0.002 g L^{-1} biotin, 0.005 g L^{-1} pantothenic acid, 0.0001 g L^{-1} B-12, 0.005 g L^{-1} -aminobenzoic acid, 0.005 g L^{-1} thioctic acid, 0.005 g L^{-1} nicotinic acid, 0.005 g L^{-1} thiamine, 0.005 g L^{-1} riboflavin, 0.01 g L^{-1} pyridoxine HCl, and 0.002 g L^{-1} folic acid. The total solid (TS) and volatile solid (VS) contents in the inoculated sludge were 7.36 and 5.9 g $L^{-1,}$ respectively.

5.2.2 Preparation of co-immobilized hydrogel

The co-immobilized hydrogel was prepared using the freeze–thaw method which was established in chapter 3 and optimized condition established in chapter 4. First, 1.0 g L^{-1} of MWCNTs (NC-7000, diameter = 9.6 nm, length = 1.5 μm, 90% purity; Sambreville Belgium) was added into 100 mL of AD sludge and mixed using a magnetic stirrer until homogenous. Then the sludge was centrifuged at 4000 rpm for 15 min to separate the biomass and supernatant. The supernatant was collected and refrigerated at 4°C until further usage. The concentrated biomass obtained by centrifugation was mixed with a 10% (w/v) PVA (Polyvinyl alcohol 25-100; Kurary Co., Ltd, Japan) aqueous solution homogeneously to achieve a biomass concentration of 30% (w/w). The mixed solution was pipetted into 96-well microplates and placed in the freezer at –20°C for 24 h.

Subsequently, the frozen samples were thawed at room temperature to obtain the "co-immobilized hydrogel" in a cylindrical shape (10 mm high, 6 mm diameter). For comparison, hydrogel without any MWCNTs was also prepared, following the same procedure described above; this was referred to as "hydrogel." Note that DIET-related bacteria were not isolated and immobilized; instead, all microbes present in the AD sludge—including hydrolysis bacteria, acidogens, acetogens, and methanogens—were immobilized within the hydrogel.

5.2.3 Biomethane potential test

The biomethane potential test experiment was conducted in a batch operation using the automatic methane potential test system (AMPTS® II, BPC Instruments, Sweden). Four different conditions were prepared in triplicate as follows: (1) control (dispersed sludge only), (2) MWCNTs (dispersed sludge + dispersed 1 g L^{-1} MWCNTs), (3) hydrogel (immobilized sludge only), and (4) co-immobilized hydrogel (sludge + 1 g L^{-1} co-immobilized MWCNTs). Under the control and MWCNTs conditions, the reactor was inoculated with 100 mL of AD sludge and 200 mL of deoxygenated distilled water to obtain a final working volume of 300 mL.

For the hydrogel and co-immobilization conditions, the reactor was inoculated with the prepared hydrogel and initially separated supernatant, which was then adjusted to 100 mL of AD sludge along with 200 mL of deoxygenated distilled water; this was done to achieve the same conditions as the control, considering the reactor's total sludge amount and concentration. Ethanol was used as the substrate with a sludge-to-substrate ratio of 2:1 (VS-based), along with 0.5 mL of trace element and vitamin solution (Section 5.2.1). All the reactors were incubated at 37°C with 50 rpm of slow stirring to prevent the hydrogels from being damaged by agitation. The experiment was conducted in three cycles of 8 d per cycle. Each reactor was fed at the beginning of each cycle, and pH measurements and sampling were conducted every 2 d. Prior to the experiment, N_2 gas was introduced into all reactors for 1–2 min to achieve an anaerobic environment. The biogas produced during the batch experiment was transported to a 3.0 M NaOH solution for CO_2 stripping, and the

remaining biomethane was measured using a methane volume based on the principles of liquid displacement and buoyancy.

In addition to the above conditions, a comparison between (1) the dispersed sludge condition and (5) the freeze-thawed dispersed sludge condition was conducted using the setup shown in **Figure 5-1** where biomethane was captured in the gasbag instead of being measured by the AMPTS system. This additional condition was included because the freeze-thaw procedure used in the immobilization method may have a negative effect on the AD microbes. To assess the impact of the freeze-thaw treatment on AD sludge, it was also evaluated in the dispersed condition in addition to the hydrogel condition. The experiment followed the same procedure and duration as described for the immobilized condition.

5.2.4 Analysis method

Total solids (TS) and VS were measured using the American Public Health Association standardized methods, with detailed procedure provided in the **Appendix A** (American Public Health Association, 2005). Biomethane yield was measured automatically every 24 h by AMPTS® II and pH was measured using a pH meter (Bettler Toledo, S220-Basic). Ethanol and VFAs were analyzed via gas chromatography using a flame ionization detector (Shimadzu Gas Chromatography, GC-2014) equipped with a BX-100 60/80 glass column and a Unisole F-200 30/60 glass column. For ethanol analysis, the injector, detector, and column temperatures were maintained at 250°C, 110°C, and 110°C, respectively, and N_2 was employed as the carrier gas at a flow rate of 32 mL min^{-1}. For VFA analysis, the injector, detector, and column temperature were maintained at 200°C, 140°C, and 140°C, respectively, with N_2 as the carrier gas at a flow rate of 35 mL min^{-1}. The total organic carbon was analyzed by a total organic carbon analyzer (Shimadzu, TOC-L CPH/CPN).

5.2.5 Morphology

The morphologies of the blank hydrogel (without immobilizing bacteria) and hydrogel and co-immobilized hydrogel after methane fermentation were observed using a scanning electron microscope (SEM) (JSM-7500, JEOL, Japan). The hydrogel and co-immobilized hydrogel samples were collected at the end of the experiment and fixed in a 1% (v/v) glutaraldehyde solution. The samples for SEM observations were prepared using the high-pressure water freeze–fracture method (Satani et al., 2020). In brief, two pressure vessels in which the samples and water were placed to ensure the exclusion of air were immersed in water. A copper ring was used to prevent pressure leakage between the vessels. Subsequently, the pressure vessels were positioned in the external frame and securely fastened by tightening the screws with a torque wrench exerting a force of 40 Nm. Then, the external frame, which accommodated the pressure vessels, was frozen in liquid nitrogen for 2 min, and the samples were taken out by loosening the screw when the temperature reached –60°C. The hydrogel sample was cleaved using a blade guided along the surface of the copper packing and lightly tapped with a plastic hammer. Finally, the cleaved sample was vacuum-dried at –12°C using a water freeze-dryer (FD6510, Sun Technologies). The dried samples were mounted on a sample holder and coated with osmium for 5 s in a sputter-coating unit (HPC-1S; Vacuum Device, Japan). The accelerating voltage used in the SEM observation was 10.0 kV.

5.2.6 Determination of microbial composition

The sludge samples collected before and after the methane fermentation experiment under each condition were immediately frozen at –20°C. Microbial analyses were performed as described by Koyama et al. 2019. DNA was extracted from sludge samples using the ISOIL for Beads Beating Kit (319-06201, Nippon Gene Co., Ltd., Japan). The 16S V3-V4 region was amplified using the forward primer [5’-TCGTCGGCAGCGTCAGATGTGTATAAGAGACAGCCTACGGGNGGCWGCAG-3′] and

reverse primer [5′-TCTCGTGGGCTCGGAGATGTGTATAAGAGACAGGACTACHVGGGTATCTAATCC-3′]. PCR was performed using an automated thermal cycler (PCR Thermal Cycler Dice; TaKaRa, Japan). The PCR product was purified using the Wizard® SV Gel and PCR Clean-Up System quick protocol (Promega, USA). Dual indices and Illumina sequencing adapters were attached to the amplicon PCR products using the Nextera XT Index Kit. The index PCR product was purified using the Agencourt AMPure XP beads (Beckman Coulter). The resulting library was subjected to paired-end sequencing using the Illumina MiSeq system, with 2 × 300 bp reads following Illumina sequencing protocols. Raw reads were filtered based on purity, requiring chastity values >0.6, using Illumina MiSeq accessory software. The demultiplexed sequences were further analyzed using QIIME2-2020.11. Sequences were denoised using DADA2 with the following parameters: trim left-f = 17, trim left-r =20, trunc-len-f = 260, trunc-len-f = 260, and trunc-len-r = 220. Taxonomy was assigned to representative sequences of operational taxonomic units using a Naïve Bayes classifier trained on the Greengenes2 database. Phylogenetic Investigation of Communities by Reconstruction of Unobserved States (PICRUSt2) package was conducted to predict the functional genes and corresponding biochemical pathways using the marker genes within 16 S rRNA sequences Douglas et al., 2020. All raw sequencing data were deposited in the DDBJ Sequence Read Archive under the accession number DRA017797.

5.2.7 Calculations

5.2.7.1 Analysis of methane production rate

The cumulative methane gas production of each test was fitted to the modified Gompertz model equation (Equation 1) to estimate the methane gas production rate and lag phase, given the well-established correlation between microbial activity and biogas production (Lay et al., 1998).

$$f(t) = P \times exp\left(-exp\left(\frac{e \cdot R_m}{P} \times (l - t) + 1\right)\right) \qquad (1)$$

where $f(t)$, P, R_m, and l are the cumulative methane production (mL) at time t, maximum

cumulative methane production (mL) at the end of the incubation period, maximum methane production rate (mL d^{-1}), and lag phase (d), respectively.

5.2.7.1 Calculation of proximity of microbes in dispersed and immobilized conditions

To determine the proximity of the biomass (microbes) in both dispersed and immobilized conditions, the concentration of sludge was calculated using the following Equation 2,

$$\text{Concentration of biomass (\%)} = \frac{\text{Volume of biomass (mL)}}{\text{Total volume (of Hydrogel or Dispersion (mL))}} \times 100 \quad (2)$$

in which the volume of biomass refers to the amount of biomass used in this study (33.3 mL obtained after centrifugation), and the total volume is defined as 111 mL for the biomass-immobilized hydrogel and 300 mL for the biomass-containing dispersion.

5.3. Results and Discussion

5.3.1 Methane production

The time course of cumulative methane gas production in the three cycles is shown in **Figure 5-2**. In cycle 1, a significant difference in the methane production rate was observed between the dispersed sludge conditions of the control and MWCNTs and the immobilized conditions of the hydrogel and the co-immobilized hydrogel. One possible reason for this could be that the freezing and subsequent thawing treatment negatively impacted microbes, as many researchers have reported that freezing can lead to lethal conditions for microbes owing to the damage to the cell membranes being damaged by the intracellular growth of ice crystals (Hu et al., 2011). Another possible reason could be the negative impact of a new and different environment on microbes owing to their confinement in the PVA hydrogel. In cycle 2, the methane production behavior was almost the same for all conditions throughout the experiment, indicating that the microbes in the immobilized conditions could have acclimatized and recovered from the damage caused by freezing. Finally, in

cycle 3, a difference in methane production rates was observed, and the order was as follows: Control < MWCNTs < Hydrogel < Co-immobilized Hydrogel.

The results showed that co-immobilizing MWCNTs and AD sludge in a confined space in the hydrogel enhanced the methane production rate, possibly through the effective expression of DIET. Furthermore, the microbes in the immobilized condition require approximately two weeks to fully acclimatize and recover from the immobilization from freezing–thawing. In the previous study of Sitthi et al. 2020, activated carbon, used as CM, was first immobilized into the hydrogel matrix. The hydrogel was then inoculated into the AD sludge to immobilize the AD microbes using the adsorption method for 45 days before use. In our study, although the microbes needed a recovery time due to slight inhibition in the freeze-thaw procedure, the results showed that the duration for recovery and acclimatization was significantly shorter than 45 days. Moreover, as the microbes were initially immobilized (entrapped) in the hydrogel, the time required for microbial immobilization in the hydrogel was much shorter and completed within a day during hydrogel synthesis.

Figure 5-3 shows the ethanol, acetate, and pH results for all conditions in cycles 1–3. In cycle 1, a faster acetogenesis reaction occurred under both immobilized conditions than under dispersed conditions **(Figure 5-3 (A-i)).** However, acetate accumulation was observed in both immobilization conditions from days 2 to 4 **(Figure 5-3 (A-ii)).** A pH decrease was also observed for the immobilized conditions from days 2 to 4 **(Figure 5-3 (A-iii))**, which agrees with the results for acetate. However, the pH change was still in a tolerable range for the methanogens. To determine whether the inhibition of methanogens, which led to the accumulation of acetate, was caused by the freeze-thaw process or the immobilization itself, a freeze-thaw treatment was also applied to the dispersed sludge condition. The results of this treatment are shown in **Figure 5-4**. Similarly to the results of the immobilized condition in **Figure 5-3**, the freeze-thawed condition showed faster ethanol consumption, and accumulation of acetate as compared to the control. As discussed on the above too, many researchers have shown that freezing microbes could lead to lethal condition for microbes due to the damage of cell membrane caused by the intracellular growth of ice crystal (Thomashow, 1998, Hu et al., 2011,

Bhattad et al., 2017). However, there were also studies that showed that upon freezing and thawing the AD sludge, the activity of microbes was found unaffected due to the excretion of extracellular polymers substance (EPS) (Huang et al., 1996, Örmeci & Vesilind, 2001). These results indicate that the effect of freeze–thaw treatment can differ depending on the type of microbes. In this study, the time course change in the ethanol and acetate concentrations in cycle 1 suggest that the freeze–thaw treatment had a positive effect on acetogens, but a negative effect on methanogens. The negative effect dominated the process, resulting in slower methane production under immobilization conditions. Further detailed research is needed to gain a more comprehensive understanding of the underlying metabolism and mechanisms driving the increase in acetogenesis upon freeze–thawing.

With respect to the methane yield results in cycle 1 in **Figure 5-2(A)**, a lower methane yield was observed under the immobilized conditions compared with the dispersed sludge conditions. However, the results in **Figure 5-3(A-i, ii)** indicate that most of the ethanol and acetate were degraded by the end of cycle 1 under all conditions, including the immobilized conditions. Additionally, this result is consistent with the results from the immobilization trials in chapter 3, where cycle 1 exhibited slower and lower methane production compared to the control **(Figure 3-15 (A-i))**. Therefore, the low methane yield under the hydrogel and co-immobilized hydrogel conditions were probably due to the small inhibition from the freeze-thaw process and suggests that carbon was assimilated during the growth of microbes in the first cycle. However, the results of the following cycles **(Figure 5-3 (B-ii & C-ii))** indicated that microbes in the immobilized conditions were not severely inhibited because the accumulation of acetate was suppressed as the cycle continued.

The modified Gompertz equation (Equation 1) was fitted to the cumulative methane production curve for all three cycles to obtain the methane gas production rate and lag time. The kinetic parameters obtained for all cycles are listed in **Table 5-1**. The results indicate that, in cycle 1, the dispersed conditions (control and MWCNTs) exhibited a higher methane production rate than the immobilized conditions (hydrogel and co-immobilized hydrogel). This is likely due to the lower methane production by the slight inhibition in the immobilized conditions, potentially caused by the

freeze–thaw process. In cycle 2, no significant changes in methane production rates were observed across all conditions. In contrast, in cycle 3, a significant difference in methane production rates were observed between all the conditions.

Previous studies have suggested that exoelectrogenic bacteria must reach a certain level of growth for DIET to prevail (Zhao et al., 2015). A significant difference between the methane production rates of the conditions was observed only in cycle 3, which suggests that the growth of DIET-related bacteria under the MWCNTs, hydrogel and co-immobilized hydrogel conditions may have reached a level conducive to DIET after two weeks/cycles of cultivation. Based on these results, we believe that the adaptation of microbes in immobilized conditions generally occurs during the following three phases: in the initial phase (cycle 1), the microbes may experience a stress response following freeze-thawing as they recover from the minor damage (caused by freeze-thawing) while adjusting to new physico-chemical conditions. In the second phase (cycle 2), the microbes start to recover from this damage and gradually acclimatize, optimizing their metabolic pathways to utilize available substrates more effectively within the hydrogel, resulting in increased acetate conversion rate compared to cycle 1. Finally in cycle 3, with the proliferation of DIET-related bacteria to a sufficient level, DIET prevails more effectively, leading to an enhanced AD performance.

In cycle 3, the methane production rates for the MWCNTs, hydrogel, and co-immobilized hydrogel were approximately 1.3, 1.4, and 2.5 times higher than those of the control condition. Compared with the MWCNTs condition (dispersed sludge with MWCNTs), which is the conventional DIET method, the co-immobilized hydrogel demonstrated an approximately 1.9 times higher methane production rate. In addition, the lag times for the MWCNTs, hydrogel, and co-immobilized hydrogel were approximately 4.2, 7.8, and 13.6 times shorter than that of the control condition.

Calculations showed that the biomass concentrations in the immobilized and dispersed conditions were 30% (v/v) and 11.1% (v/v), respectively, indicating that proximity between the microbes in the immobilized condition was 2.7 times greater than that in the conventional dispersed

condition. This means that the distance between microbes and CM was much closer in the immobilized conditions. Furthermore, because the fluid inside the hydrogel was not intensively disturbed by external stirring, the positions of microbes and CM were relatively well maintained unless the microbes moved to a more suitable environment, such as the surface of CM. As mentioned in the introduction, DIET can only occur when CM are in contact with DIET-related bacteria and archaea Gahlot et al., 2020. Therefore, the above-mentioned two factors contributed to achieving more efficient contact between the microbes and CM and enhancing the methane production rate by facilitating the smooth transfer of electrons to their syntrophic partners. Another possible reason is the presence of exoelectrogenic bacteria within the hydrogel at a close distance, which may have promoted DIET by enabling electron flow through biological nanowires or membrane-bound pathways instead of through the CM, thus improving the overall efficiency. The proximity of microbes also likely contributed to shortening the lag phase because of the transfer of various intermediates to their syntrophic partner was smoother. These processes could have provided a faster methane production rate and shorter lag phase for the co-immobilized hydrogel condition than for the conventional DIET.

Interestingly, the methane production rate of the hydrogel condition was faster than that of the MWCNTs condition. This could be due to the possible DIET prevalence through biological nanowires or membrane-bound pathways, or faster intermediates transfer caused by the close distance in the hydrogel. However, the methane production rate of the co-immobilized condition was 1.8 times faster than the hydrogel condition, indicating that the addition of MWCNTs further promoted efficiency of DIET.

5.3.2 Pre- and post-experiment hydrogel characteristics

At the end of cycle 3 of the AD batch experiment, the hydrogel and co-immobilized hydrogel were carefully sampled to observe whether rupture or damage occurred. Similar to the results in chapter 3 and 4, no ruptured or damaged hydrogels were observed after the three cycles of batch

experiments. Throughout the 3-week batch experiment, floatation of the hydrogel was occasionally observed, and such floated hydrogels were screened out when floatation was <10% **(Figure 5-5)**. This indicates that most hydrogels exhibited good permeability to the biogas produced. **Figure 5-6** shows the appearance of the hydrogel and co-immobilized hydrogel before and after the experiment. Although some surface roughness was observed for the samples, no significant deformation, cracking, or deficit was observed in the shape of the hydrogel compared with the as-prepared hydrogel. Although a much longer-term evaluation is needed before applying the proposed method for continuous operation, the results from the 3-week study show that the freeze–thaw method could be a promising method for co-immobilizing gas-producing microbes and conductive materials.

SEM was also used to observe the colonization of microbes inside the hydrogel and co-immobilized hydrogel at the end of the experiment. A blank hydrogel (without microbial or MWCNTs immobilization) was prepared and observed to distinguish between these differences. The cross-section of the blank hydrogel with a 3D network structure and abundant pores is shown in **Figure 5-7 (A&B)** and the cross-section of the hydrogel after the experiment is shown in **Figure 5-7 (C)**. Microbes were also observed in the hydrogel pores. Notably, instead of microbes being attached to the surface of the hydrogel, these were immobilized in a spiderweb-like form in the pores. Although a fibrous structure was also observed in the co-immobilized hydrogel, its spiderweb-like structure appeared to be different. In the hydrogel, microbes were connected through a fibrous network, which is likely formed by the excretion of EPS or pili by the microbes themselves **(Figure 5-7 (D))**.

Because it is still unknown that if EPS was excreted during hydrogel preparation or during the AD experiment, EPS evaluation is needed in future studies. Nevertheless, the increase in methane production rate under the hydrogel condition **(Table 5-1; cycle 3)** may have been due to the connection between the microbes within the hydrogel through EPS or nanowire, as observed, which functioned as a bridge for electron transfer. Meanwhile, in the co-immobilized hydrogel, MWCNTs were trapped in a spider web-like structure formed by the microbes **(Figure 5-7 (E))**; this showed

efficient contact between the microbes and MWCNTs while fixed in the co-immobilized hydrogel, which further enhanced the electron transfer leading to faster methane production rate **(Table 5-1; cycle 3).**

5.3.3 Microbial composition

The microbial communities before and after the experiment are shown in **Figure 5-8**. Before the experiment, the main bacterial families identified were *Anaerolineaceae* (10.3%), *Cloacimonadaceae* (9.6%), and *VadinHA17_877549* (6.8%). After three weeks of experiment, the dominant community shifted marginally in the dispersed conditions (Control and MWCNTs) to *Anaerolineaceae* (12.3% and 11.8%), *Cloacimonadaceae* (9.8% and 8.2%), UBA8932 (7.3% and 6.3%), and GWA2-38-11 (6.9% and 6.0%) from the class level. *Anaerolineacea* utilizes carbohydrates and proteinaceous carbon sources under anaerobic conditions and has recently been reported to syntrophically oxidize acetate to methanogens (McIlroy et al., 2017, Wu et al., 2023). *Cloacimonadaceae*, an acetoclastic bacterium, can oxidize propionate in anaerobic cultures (Dyksma & Gallert, 2022). As ethanol was the main carbon source in this study and this comparison was only made within the short-term (3 weeks), the decrease in *Cloacimonadaceae* abundance compared with the control was considered to be reasonable and not drastic. However, the immobilized conditions exhibited a considerable change in the dominant bacterial composition and a significant increase in abundance was observed (particularly of *Anaerolineaceae* and *Methanotrichaceae*) compared with the dispersed conditions. In the immobilized conditions (hydrogel and co-immobilized hydrogel), the dominant bacteria were *Anaerolineaceae* (21.9% and 23.3%, respectively), *VadinHa17_877549* (10.1% and 10.0%, respectively), *Sedimentibacteraceae* (9.2% and 8.0%, respectively), and *Prolixibacteraceae* (6.6% and 6.0%, respectively). Some members of *Sedimentibacteraceae* can reduce iron, and the presence of ethanol can increase its abundance (Zhao et al., 2019). This could also be the reason for the increase in the abundance of *Sedimentibacteraceae* under dispersed conditions (from 1.4% before the experiment to 1.7% and 2.2% for the Control and MWCNTs,

respectively). However, the increase was more prominent under immobilized conditions. This result indicates that the immobilization treatment efficiently enriched and concentrated *Sedimentibacteraceae* when ethanol was used as the substrate.

Prolixibacteraceae and *VadinHA17_877549* belong to the *Bacteroidetes* phylum and are known to degrade complex organic compounds, such as polysaccharides, lignin, and proteins, into simpler compounds (Zhang et al., 2019). Although polyvinyl alcohol, which is a component of hydrogel, is also a polysaccharide that can act as a substrate for *Prolixibacteraceae* and *VadinHA17_877549*, previous reports have shown that it has a very low degradation rate, especially under anaerobic conditions (Pšeja et al., 2006). In other reports, adding starch to PVA improved the degradation efficiency in AD, demonstrating that the degradation of PVA by anaerobic microbes can occur with the help of starch (Pšeja et al., 2006). Therefore, the presence of PVA in this study may have contributed to the increased abundance of *Prolixibacteraceae* and *VadinHA17_877549.* However, it should be noted that long-term degradability tests were conducted in previous studies, while this study uses PVA hydrogels in a short-term batch experiment without adding starch. Moreover, the cumulative methane production (**Figure 5-2 (B, C)**) did not significantly differ from the dispersed condition and the shape and mechanical strength of the hydrogel at the end of the experiment (**Figure 5-6**) did not significantly change compared to before the experiment. Additionally, no other VFA intermediate except acetate was observed as the intermediate product from this short experiment; therefore, PVA degradation could be very limited.

As discussed in chapter 1 and 2, ethanol promotes the growth of *Geobacter* sp., which is a renowned exoelectrogenic bacterium capable of participating in DIET (Dubé & Guiot, 2017). In this study, ethanol as substrate was specifically used to enrich exoelectrogenic bacteria to provide a more efficient DIET performance (Chan et al., 2023). The abundance of *Geobacteraceae*, a family member of *Geobacter*, increased from 0% to 0.76% and 0.73% after the experiment under the control and MWCNTs conditions, respectively. Notably, no *Geobacteraceae* were found after the experiment under either immobilization conditions, indicating that cultivating *Geobacteraceae* in a dispersed

condition is easier than in the immobilized condition used in this study, possibly because the substrate ethanol is more evenly dispersed among the microbes in the dispersed condition compared with in the immobilized condition. Based on this result, it may be more effective to first cultivate the exoelectrogenic bacteria to a certain level before immobilizing them into the hydrogel rather than immobilizing them prior to cultivation, as this could lead to a more efficient DIET performance. Although *Geobacteraceae* were not detected under immobilized conditions, other bacteria, such as *Anaerolineaceae* and *Sedimentibacteraceae,* may have participated in DIET. *Anaerolineaceae* are known to be electroactive bacteria, and several studies have suggested that they can extracellularly transfer electrons to *Methanothrix* archaea (Xu et al., 2016). As mentioned earlier, *Anaerolineaceae* have recently been reported to syntrophically oxidize acetate in cooperation with methanogens (Wu et al., 2023). Since DIET has also been implicated in acetate oxidation and methanogenesis, it is likely that DIET may have occurred through acetate oxidation under immobilized conditions. Additionally, *Sedimentibacteraceae*, which possess the *pilA* protein for pili formation, are potential candidates for participating in the DIET mechanism and were enriched when ethanol was used as the substrate (Zhao et al., 2019). Therefore, the presence and increase of both *Anaerolineaceae* and *Sedimentibacteraceae* under immobilized conditions, along with the observed increase in methane production, could be evidence of DIET prevalence. Additionally, the result suggests that DIET may have occurred in two pathways: ethanol oxidation facilitated by *Sedimentibacteraceae*, and acetate oxidation facilitated by *Anaerolineaceae* to *Methanotrichaceae*, the family that includes *Methanothrix*.

Another microbe worth noting is *Rhodocyclaceae*, a family within the phylum *Proteobacteria*, which has been reported to favor ethanol as a substrate (Yuan et al., 2021). The abundance of *Rhodocyclaceae* increased from 0.9% to 3.3%, 2.1%, 2.1%, and 4.3% under the control, MWCNTs, hydrogel, and co-immobilized hydrogel conditions, respectively. Previous studies have suggested that *Rhodocyclaceae* can engage in DIET with *Methanosaeta*, now known as *Methanothrix*, in magnetite-mediated anaerobic digestion systems (Yang et al., 2015). Interestingly, while the addition of MWCNTs in the dispersed condition did not significantly enrich *Rhodocyclaceae*, a two-fold

enrichment was observed in the co-immobilized hydrogel condition compared to the hydrogel condition. One possible explanation for this is that co-immobilization enhances the contact efficiency between microbes and MWCNTs, thereby facilitating cell growth when DIET is prevalent, as reported (Mostafa et al., 2020). This may help explain the higher methane production rate in the co-immobilized condition, despite the similar relative abundances of *Anaerolineaceae* and *Sedimentibacteraceae* in the hydrogel condition.

Methanotrichaceae was the main archaea family observed under all conditions, both before and after the experiment. Previous studies have shown that *Methanothrix*, a genus of *Methanotrichaceae*, utilizes the acetate decarboxylation pathway for acetate dissimilation and the CO_2 reduction pathway when participating in DIET with exoelectrogenic bacteria (Holmes & Smith, 2016). Although the results are not shown, *Methanothrix* was the genus of the *Methanotrichaceae* family detected in this study. No obvious change in the abundance of *Methanotrichaceae* was observed before (8.6%) and after the experiment for the control (8.6%) and MWCNTs (8.1%) dispersion conditions. In contrast, the immobilized conditions showed a higher abundance of *Methanotrichaceae* after the experiment; in concrete, 17.6% in the hydrogel, and 17.1% in the co-immobilized hydrogel. Previous studies have demonstrated that *Anaerolineaceae* can transfer electrons extracellularly to *Methanothrix* (Xu et al., 2016). The increased abundance of *Anaerolineaceae* under immobilized conditions may indicate the prevalence of DIET. However, despite the addition of MWCNTs, there was no significant change in the abundance of *Methanotrichaceae* within the disperse (control vs MWCNTs) and immobilized (hydrogel vs co-immobilized hydrogel) conditions, which suggests that the addition of MWCNTs did not contribute to enriching *Methanotrichaceae*.

Methanoregulaceae was another methanogenic archaea detected in this study, and its abundance increased from 1.23% before the experiment to 1.5% and 2% for the dispersed control and MWCNTs conditions, respectively. In comparison, it decreased in the immobilized hydrogel (0.5%) and co-immobilized hydrogel (0.7%) conditions. Although not shown in the results, the genus

Methanolinea from the *Methanoregulaceae* family was detected in this study; this is a hydrogenotrophic methanogen that uses H_2 as an electron source to convert CO_2 into CH_4 (Sakai et al., 2012). Lee et al. 2016 reported that *Methanolinea* can engage in DIET when adhered to a conductive material. They also showed that adding GAC enriched *Geobacter* and *Methanolinea,* which actively participated in DIET, increased methane production (Lee et al., 2016). As described earlier, *Geobacteraceae* and *Methanoregulaceae* increased from 0 to 0.73% and from 1.23% to 2.0%, respectively, for the MWCNTs (dispersed) after the experiment, and the abundance of *Methanoregulaceae* was much higher for the MWCNTs than for the control. These results suggest that DIET may have prevailed and/or was enhanced in the dispersed MWCNTs condition compared with the control.

In summary, notable microbial community shifts better occurred under immobilized conditions compared with dispersed conditions, and this was likely influenced by their distinct physicochemical and spatial environments. These results suggest that immobilizing AD microbes in PVA hydrogel effectively enhances the enrichment and cultivation of functional microbes associated with DIET. Although the experiment in this study was conducted in a batch operation, the proposed immobilization technique shows promising properties for use in a continuous system, such as a UASB reactor, with reduced washout of the particles/microbes and possibly a faster start-up compared with the granulation process, as hydrogel preparation requires a much shorter time.

5.3.4. Predicted functional genes abundance related to methanogenic pathway and DIET related genes

To explore the prevalence of DIET, the normalized abundance of genes encoding key enzymes related to both hydrogenotrophic and acetoclastic methanogenic pathways (based on the KEGG pathway Map:00680) was predicted using PICRUSt2 and is shown in **Figure 5-9** (Yin et al., 2018, Zhao et al., 2019). In the hydrogenotrophic pathway, formylmethanofuran dehydrogenase (EC 1.2.99.5) was the most abundant enzyme-coding gene. As mentioned in Chapter 2,

formylmethanofuran dehydrogenase is known to be the first enzyme in the hydrogenotrophic (carbon dioxide reduction) pathway, as depicted in **Figure 5-10** (Holmes et al., 2017). The results in **Figure 5-9** show that all conditions exhibited a higher abundance of formylmethanofuran dehydrogenase than the control, especially for the immobilized conditions. Interestingly, the centered log ratio values for the ferredoxin hydrogenase (EC 1.12.7.2) gene were negative in all conditions except for the control. The gene abundance followed this order: Control > MWCNTs > Hydrogel > Co-immobilized hydrogel. The ferredoxin hydrogenase enzyme plays a crucial role in the hydrogenotrophic methanogenesis pathway, where H_2 serves as the electron donor for CH_4 production. In this pathway, H_2 is oxidized to protons and electrons, with the electrons subsequently used to reduce CO_2 to methane (Palacios et al., 2021, Rossi et al., 2022). However, when DIET is prevalent, the abundance of EC 1.12.7.2 is likely to decrease, as electrons are directly transferred to methanogens, bypassing the need for hydrogen as an intermediary electron carrier. In previous studies by Yin et al. (2017) and Li et al. (2022), the relative abundance of EC 1.12.7.2 was lower in DIET prevailed conditions compared to the control. Similarly, in this study, the abundance of EC 1.12.7.2 was lower in all conditions compared to the control. However, although not shown in the results, the raw data shows no DIET-participating methanogens (*Methanotrichaceae* and *Methanoregulaceae*) contributed in activating the EC 1.12.7.2 genes for all conditions. These results were similar to our previous results in chapter 2. The result suggests that DIET likely prevailed in all conditions, as the dominant archaea in all conditions were all DIET-participating methanogens with no EC 1.12.7.2 gene activation found, while the higher abundance of EC 1.12.7.2 in Control and MWCNTs conditions were likely contributed by other methanogens which are less than 1% abundance in the microbial community. Conversely, the acetate-CoA ligase (EC:6.2.1.1) gene was most abundant in the acetoclastic methanogenesis pathway, with all conditions exhibiting a higher abundance of this gene compared to the control, particularly in the immobilized conditions. Overall, the gene encoding formylmethanofuran dehydrogenase (EC:1.2.99.5) showed higher abundance than acetate-CoA ligase, suggesting that the hydrogenotrophic (carbon dioxide reduction) pathway likely dominated

methanogenesis in all four conditions, even though the dominant archaea in all conditions were *Methanotrichaceae* (acetate utilizing methanogen).

To further examine the contribution of each gene, the abundances of formylmethanofuran dehydrogenase (EC:1.2.99.5) and acetate-CoA ligase (EC:6.2.1.1) genes from each methanogen in all conditions were extracted and are presented in **Figure 5-11**. The result shows that all conditions and methanogens show a higher abundance in EC:1.2.99.5 genes than EC:6.2.1.1. In this study, only *Methanotrichaceae* is known to be acetoclastic methanogens (Zhou et al., 2023). Thereby, the result of higher EC:1.2.99.5 genes from *Methanoregulaceae* and others is reasonable as they are all hydrogenotrophic methanogens which reduces CO_2 to CH_4. On the other hand, although *Methanotrichaceae* is an acetoclastic methanogens, the abundance of EC:1.2.99.5 is higher than EC:6.2.1.1. As mentioned earlier in section 5.3.3, *Methanothrix*, a genus of *Methanotrichaceae*, utilizes the acetate decarboxylation pathway for acetate dissimilation and the CO_2 reduction pathway when participating in DIET with exoelectrogenic bacteria (Holmes & Smith, 2016). Previous reports have also shown that when *Methanothrix* were accepting electron via DIET, the genes encoding enzymes in hydrogenotrophic were highly expressed at the transcription level (Rotaru et al., 2013). In addition to the results shown in **Figure 5-11**, the predicted metabolic functions from PICRUSt2 were used to identify the methanogenesis pathways for all conditions based on the KEGG database, with the findings presented in **Figure 5-12**. These results align with those in **Figure 5-11** (predicted functional genes of EC:1.2.99.5 and EC:6.2.1.1), indicating that all conditions predominantly rely on the CO_2 reduction pathway. Although *Methanotrichaceae* (acetoclastic methanogen) is the dominant archaea across all conditions, the module representing the conversion of CO_2 to CH_4 (M00567) is the most abundant, accounting for more than 98% in all condition. This suggests that *Methanotrichaceae* were actively involved in the DIET mechanism under all conditions. Interestingly, while the differences are small, the relative abundance of the M00567 module varies slightly across the conditions: Control (98.2%), MWCNTs (99.3%), Hydrogel (99.9%), and Co-immobilized Hydrogel (99.9%). This result is consistent with the observed methane production rates across conditions,

which also followed the order Control < MWCNTs < Hydrogel < Co-immobilized Hydrogel (**Table 5-1**; Cycle 3). This correlation further implies that the addition of CMs and microbial immobilization enhances DIET efficiency, leading to faster electron transfer and increased methane production.

Figure 5-13 presents the centered-log-ratio of DIET-related gene abundances for *pilA* and multiheme c-type cytochrome, based on PICRUSt2 analysis across all conditions. Interestingly, the results show a higher abundance of *pilA* genes in the immobilized conditions (Hydrogel and Co-immobilized Hydrogel), whereas the abundance of multiheme c-type cytochrome was greater in the dispersed conditions (Control and MWCNTs). The results agree with the SEM observation as shown in **Figure 5-7**, where the spiderweb-like structure was observed only in the immobilized conditions. As mentioned in the introduction, several studies have suggested that the addition of CM can bypass the need for synthesizing conductive nanowires, thereby conserving cellular energy in a DIET environment (Kato et al., 2012, Liu et al., 2014 Shrestha & Rotaru, 2014). This observation supports the lower abundance of *pilA* and the higher abundance of multiheme c-type cytochrome in the MWCNTs condition. On the other hand, the higher abundance of *pilA* in the immobilized conditions is likely due to the proximity of microbes within the hydrogel matrix. Notably, previous studies using UASB reactors treating brewery waste have also reported an abundance of conductive nanowires observed in the sludge aggregates, indicative of DIET activity (Morita et al., 2011, Shrestha et al., 2014). These findings suggest that under immobilized conditions, DIET likely occurred primarily through conductive nanowires (for hydrogel condition) or via conductive nanowires with MWCNTs serving as a bridge for electron transfer (for co-immobilized condition). In contrast, in the MWCNTs dispersed condition, DIET was predominantly facilitated by membrane-bound electron transfer proteins, followed by CM transferring electrons to methanogens, rather than utilizing conductive nanowires as the electron transfer bridge. Nevertheless, it should be noted that the discussion is based on gene abundance predicted by PICRUSt2 analysis, and metatranscriptome analysis will be necessary in future studies to fully understand the active genes involved in the AD system.

5.3.5. Identified Challenges and opportunities for further research

Figure 5-14 shows the total organic carbon (TOC) levels in the reaction solution for all conditions before and after the batch experiment in cycle 1. Although the results from the immobilized conditions indicate that most intermediates from the substrate ethanol were degraded (**Figure 5-3**), unlike the dispersed condition (Control and MWCNTs), unusually high TOC values with approximately 4 to 5 times higher than the initial levels were observed. Additionally, when a portion of the reaction solution from the immobilized condition was sampled and stored in the freezer, hydrogel formation was observed **(Figure 5-15)**. This suggests that PVA polymer leaked from the hydrogel into the reaction solution, as dissolved PVA can form a hydrogel at low temperature. Given that PVA is a low-biodegradable organic substance (Magdum et al., 2013, Chou et al., 2010), the increase in TOC for the immobilized condition is most likely due to this leakage.

Since TOC and chemical oxygen demand (COD) are critical parameters in anaerobic digestion research, the leakage of PVA polymer into the effluent will undesirably affect these measurements. It is also important to note that in this study, the hydrogel was used immediately after synthesis without washing. Moving forward, establishing a washing procedure for the hydrogel will be necessary to remove excess unwanted polymer before its use.

5.4. Conclusions

In this study, the anaerobic digestion (AD) performance of co-immobilized hydrogel containing 1 g L^{-1} MWCNTs and AD microbes (Co-immobilized hydrogel) was evaluated alongside three other conditions: dispersed sludge (Control), 1 g L^{-1} MWCNTs added to dispersed sludge (MWCNTs), and immobilized AD sludge without MWCNTs (Hydrogel). The results for methane production rate followed the order: Control < MWCNTs < Hydrogel < Co-immobilized Hydrogel, with the proposed co-immobilized hydrogel achieving a 2.5-fold increase in methane production rate compared to the control and 1.9-fold increase compared to the conventional DIET using dispersed

MWCNTs. The microbes immobilized in the hydrogel required approximately one week to recover from the minor inhibition caused by the freeze-thaw process. Freezing AD microbes appeared to enhance acetogenesis but reduce methanogenesis, leading to an imbalance between the two processes that could inhibit methane fermentation due to a resulting drop in pH. Thus, it may be beneficial to use a lower ethanol substrate loading in the first cycle until the microbes recover from freeze-thaw damage. Microbial community analysis revealed the enrichment of DIET-functioning microbes, including *Anaerolineaceae*, *Sedimentibacteraceae*, *Rhodocyclaceae*, and *Methanothrichaceae* in the co-immobilized hydrogel condition. This enrichment is likely due to the enhanced proximity and contact efficiency between the microbes and MWCNTs, contributing to the possible improvement in DIET under co-immobilized conditions. Notably, the co-immobilized hydrogels exhibited sufficient durability throughout the 3-week experiment. While further long-term evaluations in continuous operation are necessary to gain deeper insights, this study highlights the potential of our proposed method as a promising strategy for enhancing AD performance in continuous operation, which may contribute to achieving a higher organic loading rate.

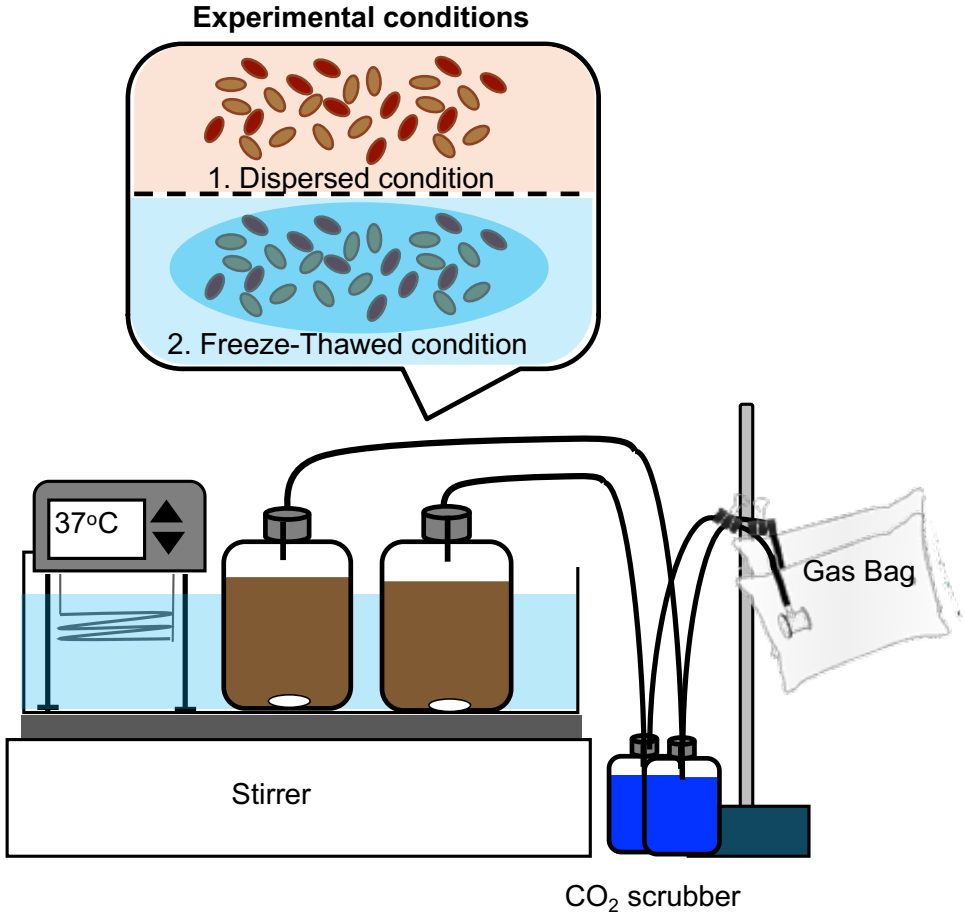

Figure 5-1. Schematic diagram of the setup for the additional AD batch experiment for freeze-thawed dispersed sludge condition

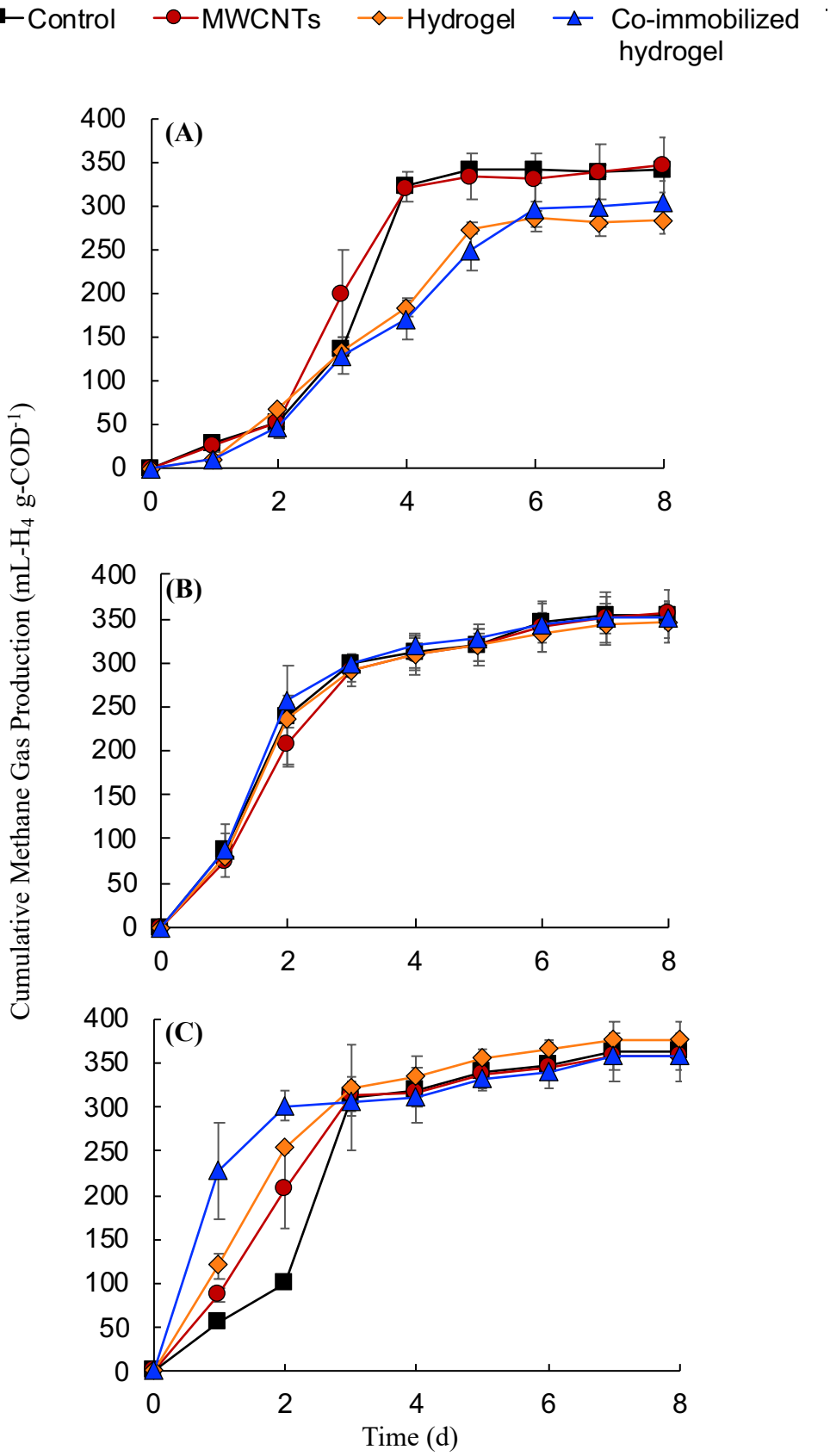

Figure 5-2. Cumulative methane gas production in (A) Cycle 1, (B) Cycle 2, and (C) Cycle 3

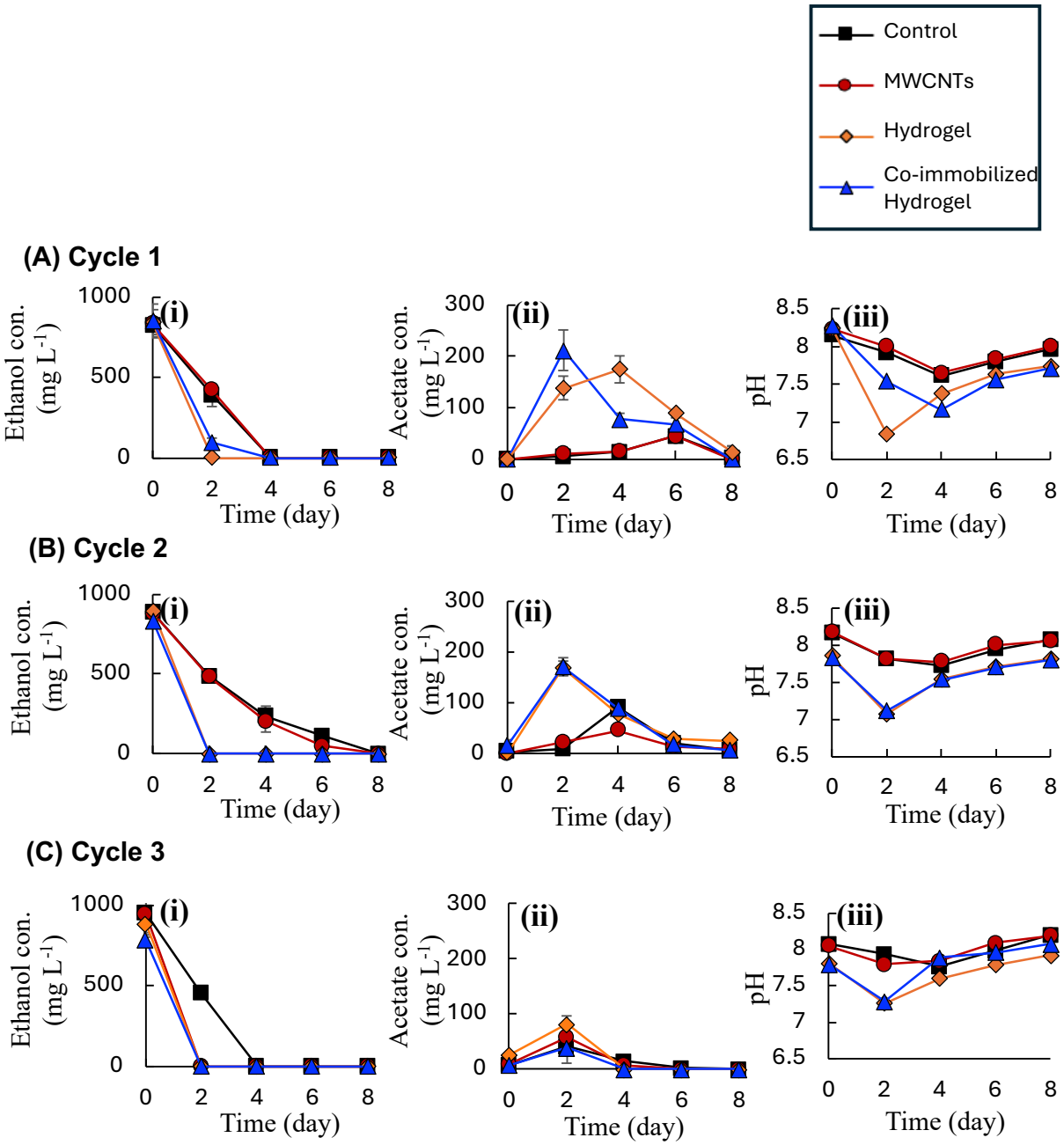

Figure 5-3. Ethanol concentration, acetate concentration and pH of all condition in (A) Cycle 1, (B) Cycle 2 and (C) Cycle 3

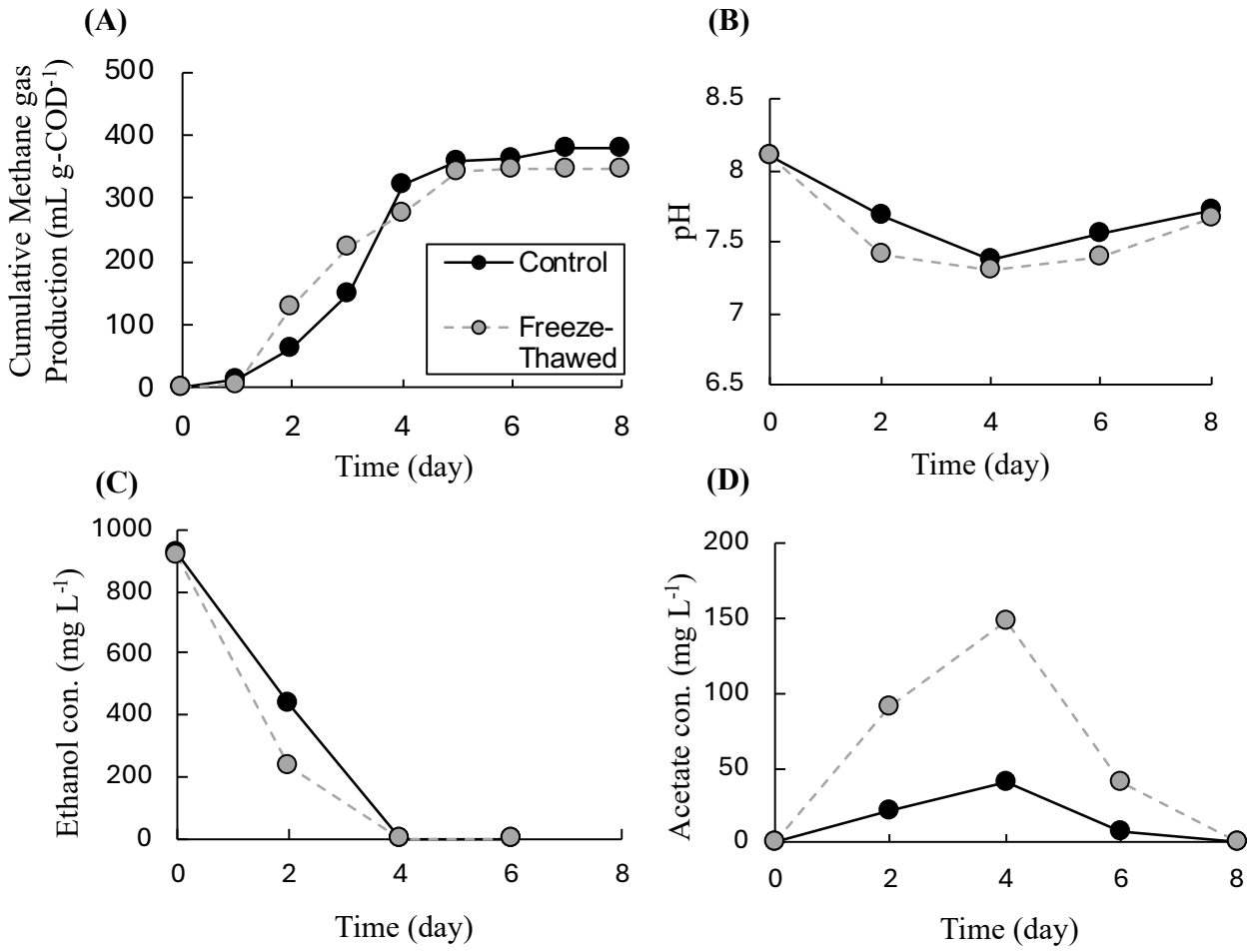

Figure 5-4. (A) Cumulative methane gas production, (B) Ethanol concentration, (C) Acetate concentration and (D) pH of result in Freeze-thawed AD sludge

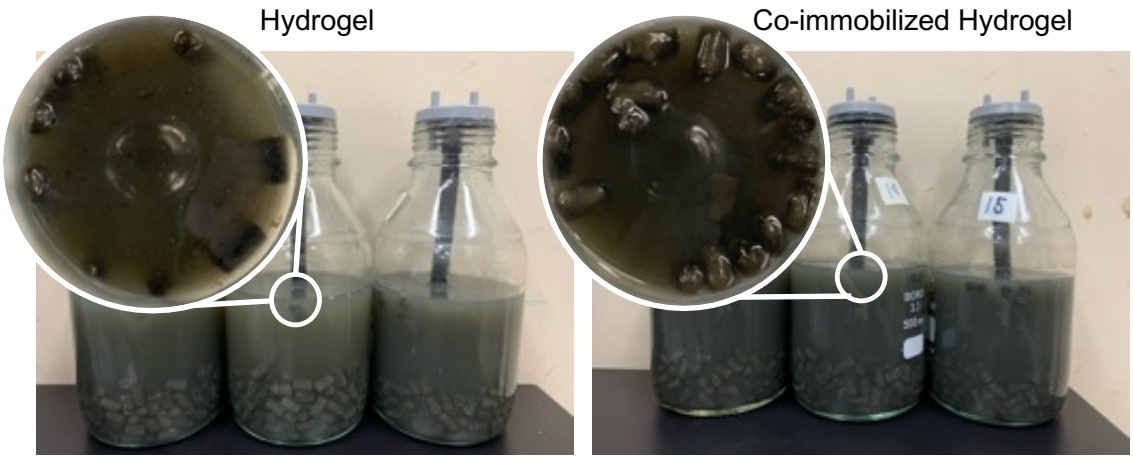

Figure 5-5. Image of hydrogel floatation at the end of the AD batch experiment

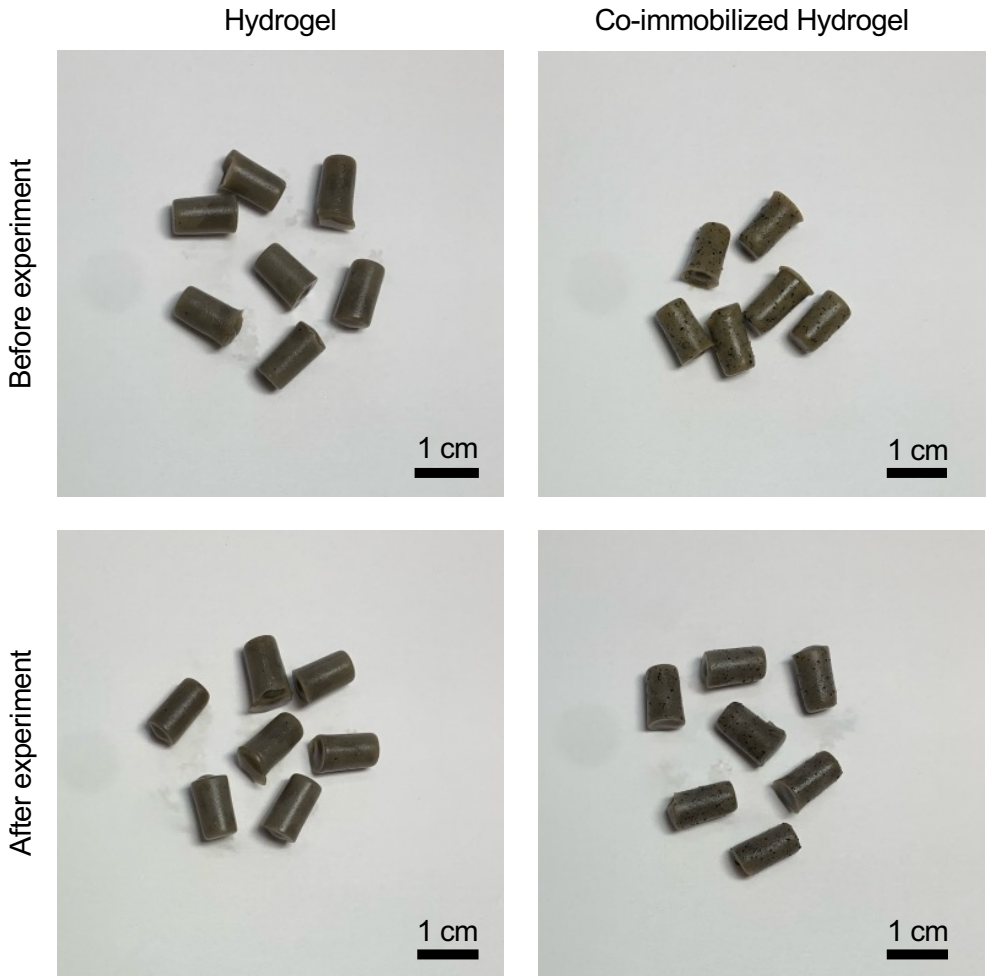

Figure 5-6. Image of hydrogel and co-immobilized hydrogel appearance in before and after the experiment

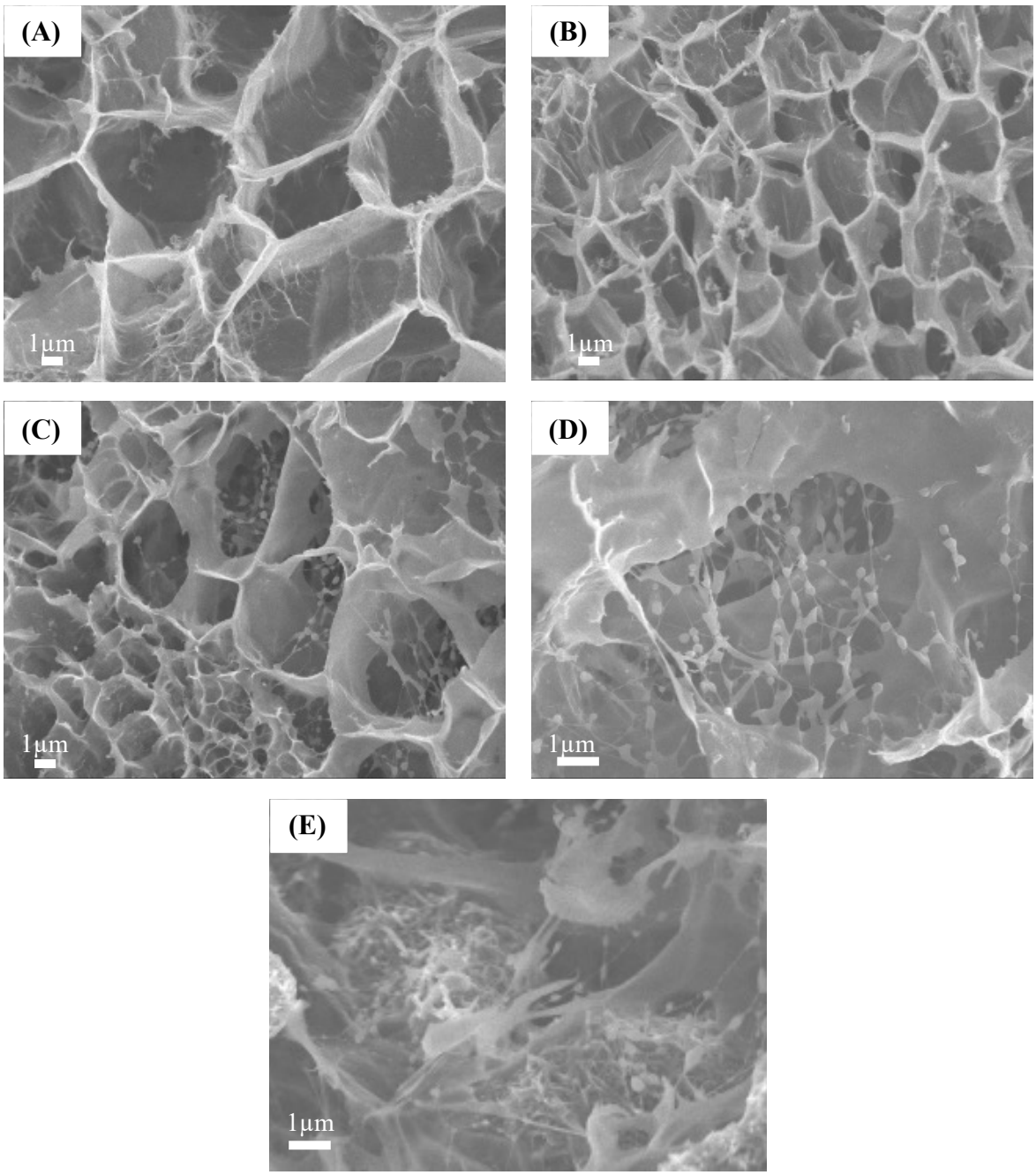

Figure 5-7. Scanning electron micrograph showing cross-section of Blank Hydrogel (A*)(B*), Hydrogel (C*) (higher magnification in panel D**), and Co-immobilized Hydrogel (E**)

* magnification at 5000 times; ** magnification at 1000 times

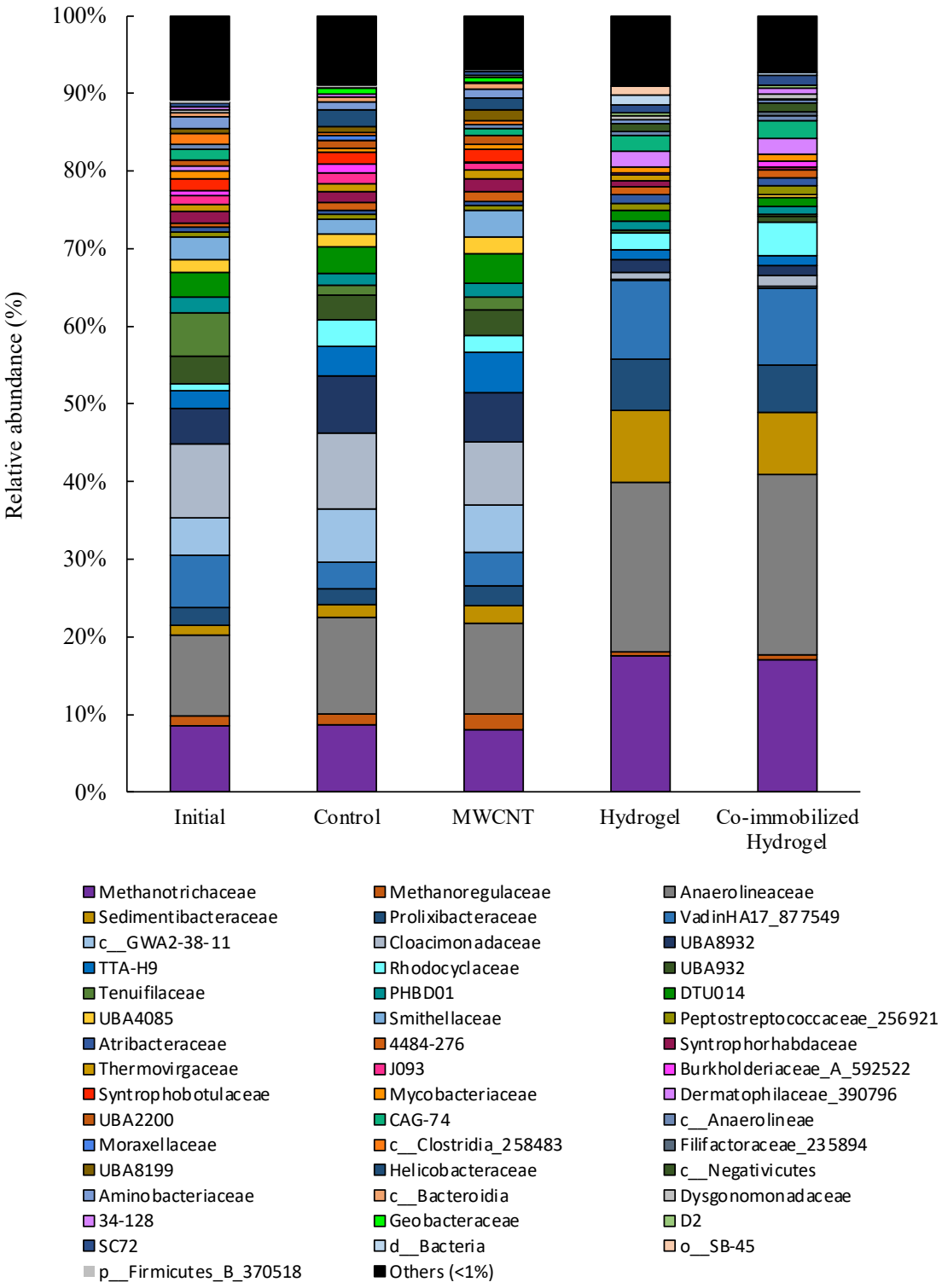

Figure 5-8. Relative abundance of microbial community at the family level in Before and After the experiment for all condition

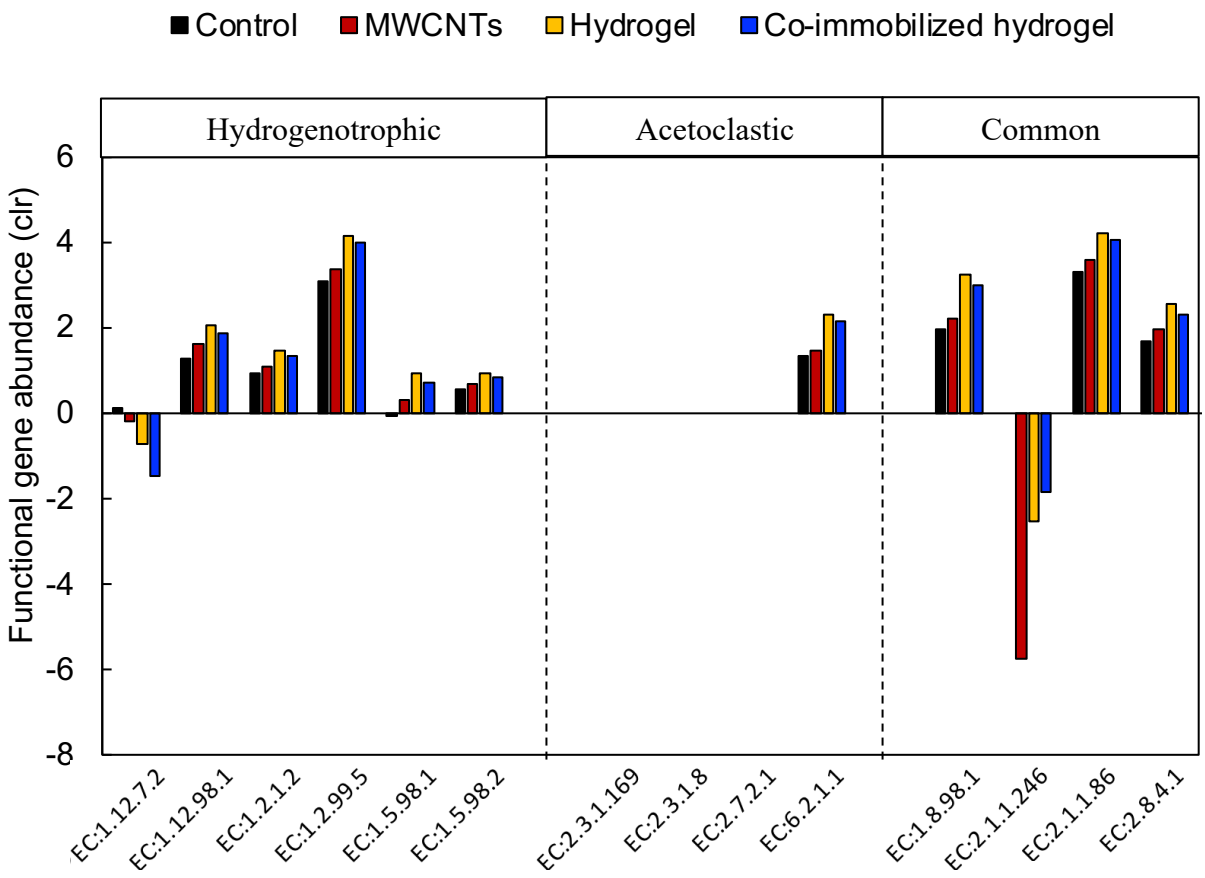

Figure 5-9. Clr-Transformed predicted abundance of functional genes associated with the methanogenic pathway

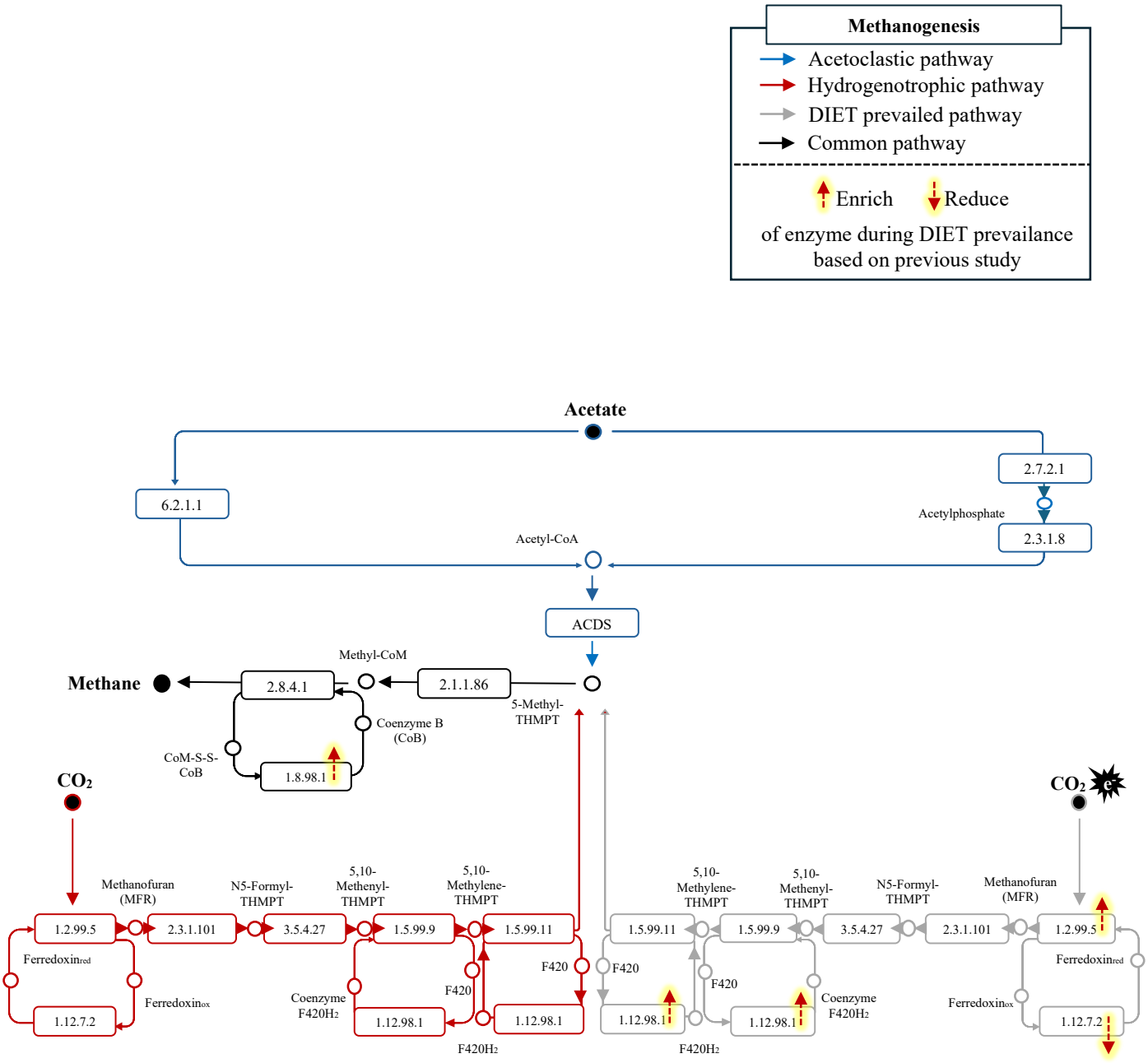

Figure 5-10 Methanogenic pathway according to KEGG (MAP: 00680). Note that possible enrichment and reduced enzyme abundance during DIET prevalence are based on previous DIET studies (Yin et al., 2017, Chen et al., 2022, Li et al., 2022, Wang et al., 2024)

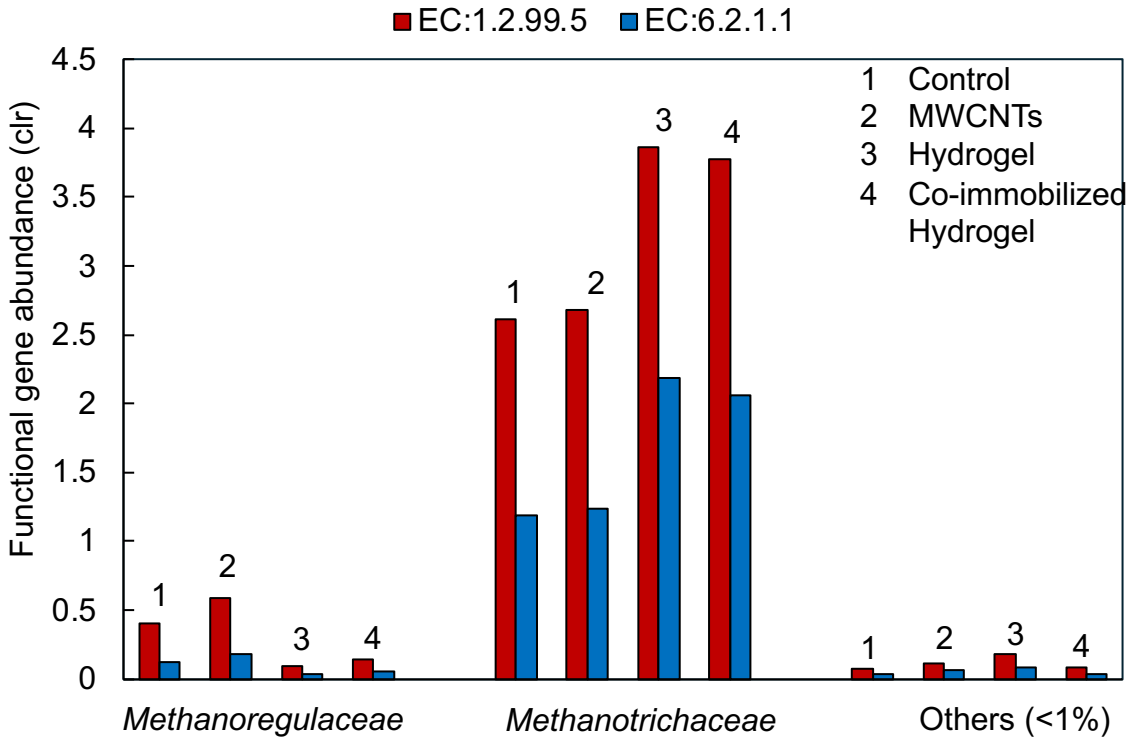

Figure 5-11. Abundance of enriched acetoclastic and hydrogenotrophic genes assigned to each methanogens

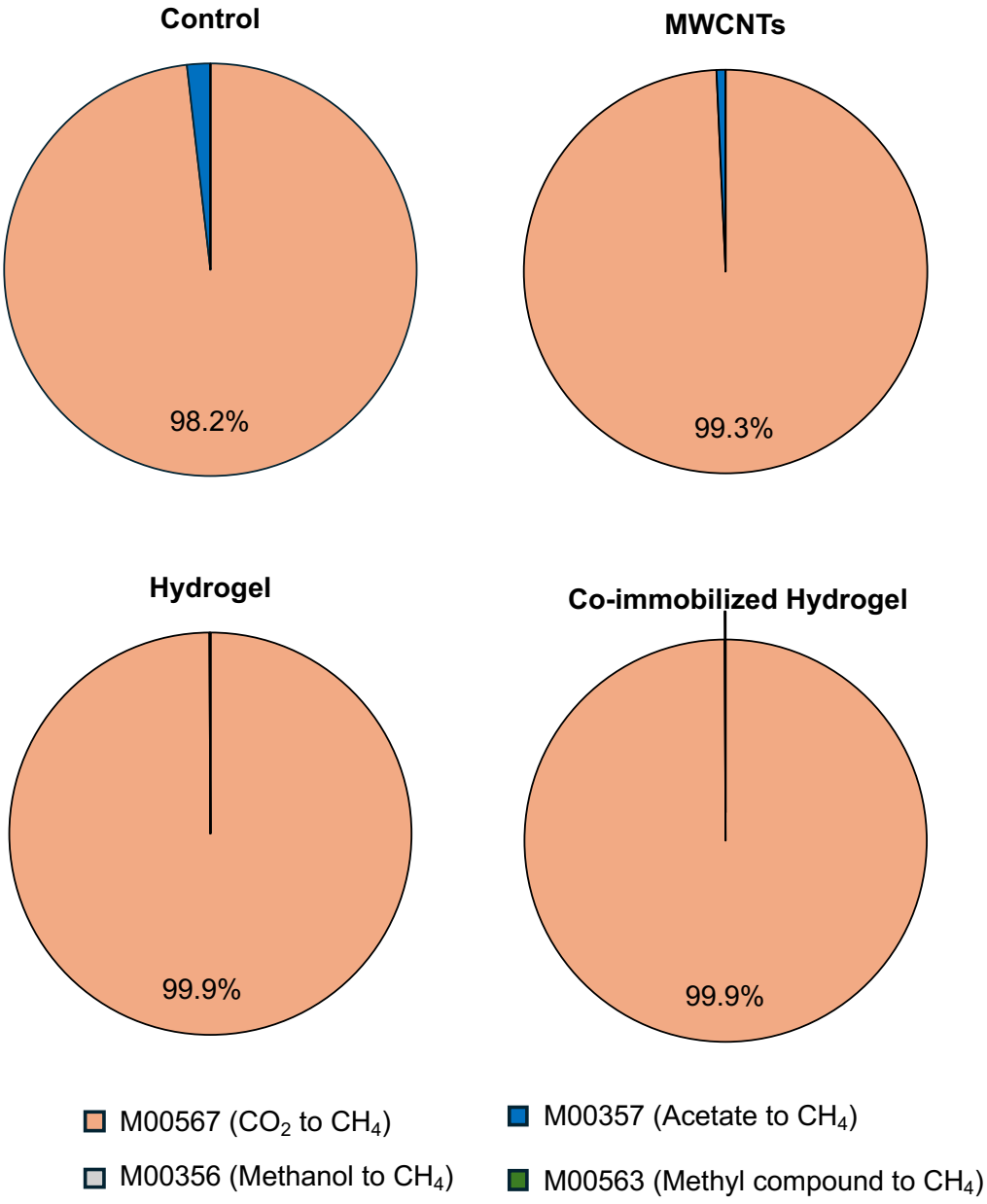

Figure 5-12. Predicted enriched KEGG modules associated with methanogenesis

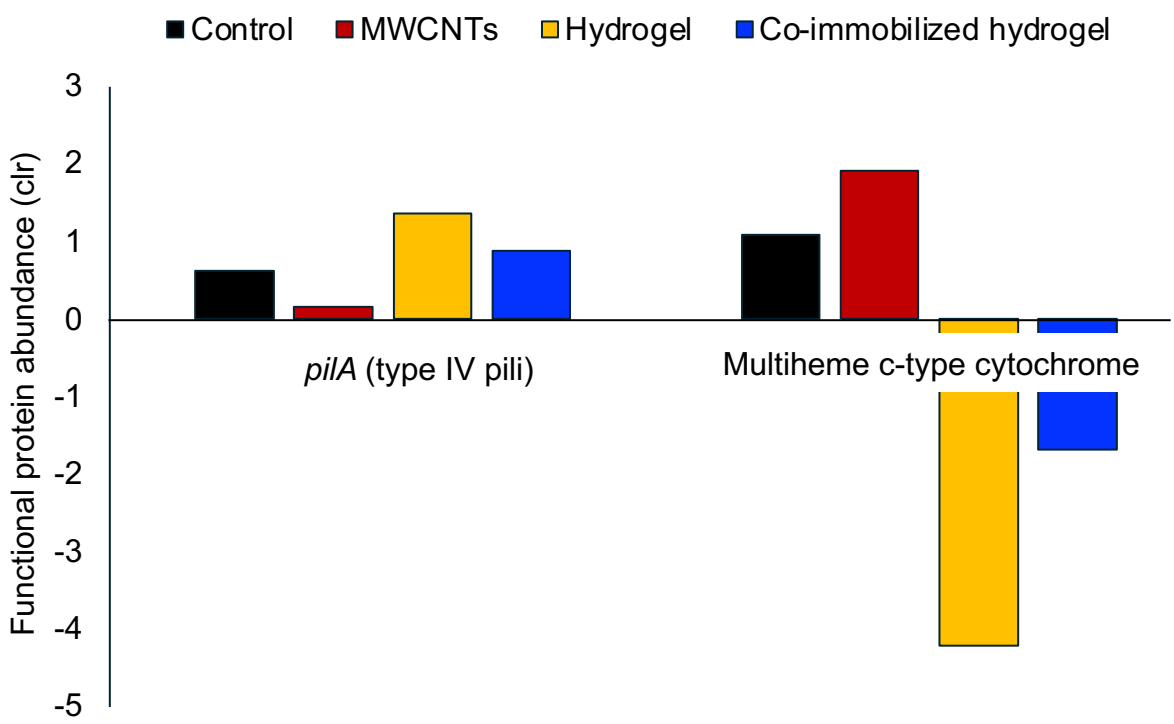

Figure 5-13. Clr transformed abundance of *pilA* and multiheme c-type cytochrome protein based on PICRUSt2 analysis

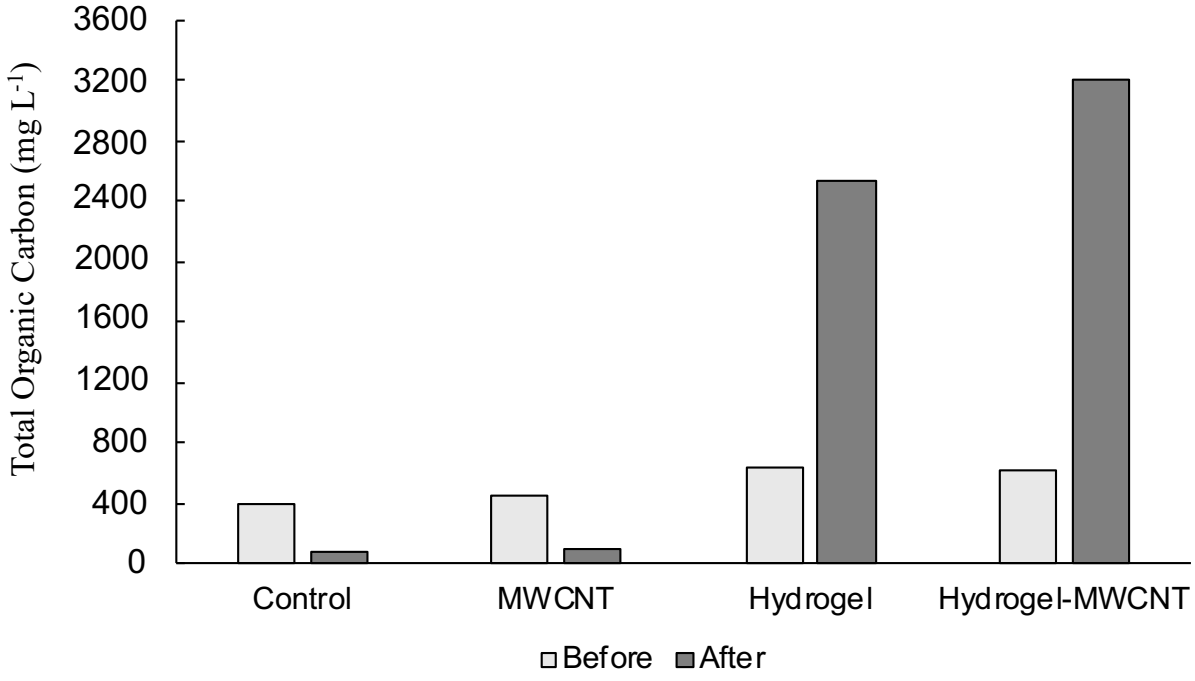

Figure 5-14. Total Organic Carbon of before and after the experiment in cycle 1

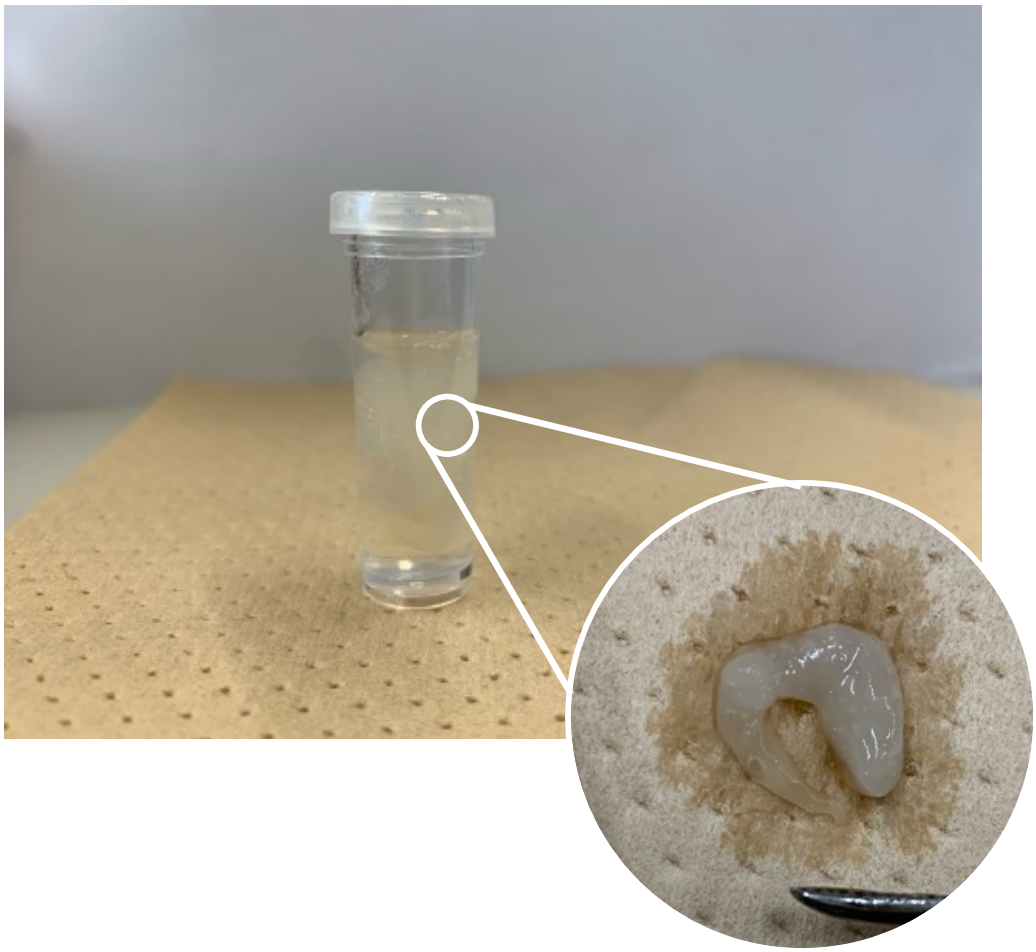

Figure 5-15. Image of hydrogel found in sampled bottle after freezing

Table 5-1. Kinetic parameter of Cycle 1,2 & 3 results fitted into Gompertz equation

	P (mL g-COD^{-1})	R_{max} (mLg-COD^{-1} day^{-1})	*l* (day)	R^2
Cycle 1				
Control	349	185[a]	2.10	0.99
MWCNTs	346	179[a]	1.78	0.99
Hydrogel	299	80[b]	1.26	0.99
Co-immobilized Hydrogel	328	75[b]	1.43	0.99
Cycle 2				
Control	341	151[a]	0.39	0.99
MWCNTs	344	131[a]	0.40	0.99
Hydrogel	334	154[a]	0.44	0.99
Co-immobilized Hydrogel	339	173[a]	0.47	0.99
Cycle 3				
Control	374	104[a]	1.64	0.98
MWCNTs	352	137[b]	0.39	0.99
Hydrogel	367	145[b]	0.21	0.99
Co-immobilized Hydrogel	332	264[c]	0.12	0.98

Means followed by the same letter are not statistically different according to One-way ANOVA, Tukey-Kramer test at $P \leq 0.01$, based on the results from each cycle.

Chapter 6

Conclusion and future perspective

In this study, the co-immobilization of anaerobic digestion (AD) microbes and multi-walled carbon nanotubes (MWCNTs) as a conductive material (CM) was explored to enhance the direct interspecies electron transfer (DIET) performance. In Chapter 2, three different CMs—granular activated carbon (GAC), MWCNTs, and polyaniline (PANI)—were evaluated using two substrates, sodium propionate and ethanol, to identify optimal culturing conditions and a suitable CM for immobilization. The results showed that when sodium propionate is used as substrate, no exoelectrogenic bacteria was enriched, nor changes in methane production rate was observed despite the addition of CM. On the other hand, ethanol promoted the enrichment of exoelectrogenic bacteria, specifically *Geobacteraceae*, and that the addition of CMs further amplified this effect. The higher relative abundance of *Geobacteraceae*, in conjunction with DIET, contributed to an accelerated methane production rate. Thus, even with the presence of CMs, efficient DIET only occurs with the presence of exoelectrogenic bacteria. The large surface area and pore volume of the CMs are likely the main contributors to the exoelectrogenic bacterial growth, enhancing DIET, which explains the methane production rate following the order of GAC > MWCNTs > PANI.

In Chapter 3, four different immobilization methods for AD sludge were tested, with the PVA-cryogel method (Method D: freeze-thawing) demonstrating superior biogas permeability, durability, and biocompatibility. These results confirmed that Method D is suitable for AD sludge immobilization. Additionally, the unnecessary of a crosslinking agent, combined with the simplicity of using only PVA for synthesis, makes this method advantageous, as it does not introduce toxins or excess nutrients to the microbes during immobilization. No significant inhibition of microbial activity was observed despite the freezing and thawing process, suggesting that long-term storage of AD sludge in the PVA-cryogel may be feasible while preserving microbial activity. The main drawback

of this method is likely the energy cost associated with freezing; however, this can potentially be offset by utilizing electricity generated from the biogas process. Additionally, the cost may be reduced when applied in continuous UASB operation, where the time and expense of long granulation periods can be eliminated. Nonetheless, a careful cost evaluation should be conducted following long-term operational testing.

Before applying the co-immobilized hydrogel in the AD system, the hydrogel was optimized by adjusting the biomass volume and the CM concentration in Chapter 4. Biomass volumes of 30%, 50%, and 80% were tested, but only 30% and 50% volumes could be prepared and evaluated. Interestingly, increasing the biomass volume did not enhance methane production rate; instead, it reduced the hydrogel's durability over a short period. Initially, GAC, which showed the best methane production rate in Chapter 2, was used for immobilization, but its large particle size made the process unsuccessful. Consequently, MWCNTs, which showed the second-best performance, were selected for immobilization due to their small particle size and smaller required amount for efficient DIET performance. The MWCNTs concentrations ranging from 0.5 g L^{-1} to 3.0 g L^{-1} were tested, and it was found that concentrations exceeding 1.0 g L^{-1} compromised hydrogel durability, whereas concentrations up to 1.0 g L^{-1} did not significantly alter the hydrogel's properties. Additionally, the 1.0 g L^{-1} MWCNTs condition showed a shorter acclimatization/stabilization period, likely due to the DIET mechanism. Therefore, the optimized hydrogel condition was determined to be a biomass volume of 30% with 1.0 g L^{-1} of MWCNTs.

Finally, in Chapter 5, the optimized co-immobilized hydrogel was evaluated in a batch AD experiment. The results showed that the proposed co-immobilized hydrogel improved the methane production rate by 2.5 times and 1.9 times compared to the control (dispersed sludge only) and conventional DIET (dispersed sludge with MWCNTs addition), respectively. This improvement is likely due to the efficient contact between microbes and MWCNTs. Interestingly, even by just immobilizing the AD microbes to the hydrogel could improve the methane production rate by 1.4 times compared to the control. This is likely because the distance between the microbes became

shorter allowing intermediates to be passed on smoothly to their syntrophic partner along with the prevalence of DIET via conductive nanowire.

Although this study demonstrated promising results, further research is necessary before practical application. This study was conducted only in batch operation; therefore, a long-term continuous experiment with varying OLRs should be performed to assess the practical applicability of the hydrogel. Such an experiment would also help determine the maximum organic loading rate the hydrogel can withstand and its capacity for retaining biomass and conductive materials (CMs) in the reactor. To address these gaps, we conducted a continuous experiment in a UASB reactor and a semi-continuous experiment with varying OLRs (detailed in Appendices B & C). In the UASB experiment, although the trial was discontinued due to the suboptimal reactor design, the results indicated that the proposed co-immobilized hydrogel technique not only accelerated the stabilization of biogas production but also retained more biomass in the reactor, making it a promising approach for long-term operation. In the semi-continuous experiment, the co-immobilized hydrogel successfully sustained high OLR conditions, reaching up to 21 g-COD L^{-1} day^{-1}. Additionally, it acted as a protective barrier against inhibitory substances such as free ammonia, shielding the microbes until a certain threshold. Interestingly, even the hydrogel condition without the addition of MWCNTs could achieved high OLR operation, further demonstrating the significant impact of hydrogel immobilization on enhancing AD performance. However, severe structural changes in the hydrogel were observed at the end of the experiment, suggesting that this immobilization technique may not be suitable for long-term use in a stirred reactor. Based on these findings from both semi and continuous experiment, the combined use of co-immobilized hydrogel in UASB reactors may prove more effective, as it retains more biomass and CMs while maintaining structural integrity longer than in stirred reactors. Therefore, a reevaluation of the proposed co-immobilized hydrogel in a properly designed continuous UASB reactor is necessary, as this would provide better insights into its practical applicability.

Besides the above experiment, other future work should be made. For instance, only ethanol

was used as a substrate in this study; other higher-molecular substrates to mimic the actual wastewater should also be evaluated to ensure broader practical applicability. For waste with high solid content, the co-immobilized hydrogel may not be suitable, but a hybrid approach—combining dispersed and immobilized microbes—may be able to overcome this challenge. In this case, dispersed microbes could mainly focus on hydrolysis and acidogenesis, while immobilized microbes could target acetogenesis and methanogenesis, where the DIET mechanism occurs. Thus, the ideal ratio of dispersed to immobilized sludge for high-solid-content waste treatment should be evaluated in future studies. Additionally, a comparison with other CMs such as Powdered Activated Carbon (PAC) and magnetite, which have smaller particle sizes than GAC is worth studying as MWCNTs can be very costly (Barua & Dhar, 2017).

In addition, this study uncovered a potential secondary pollution issue caused by the release of excess PVA polymers from the hydrogel. Therefore, establishing a washing method to remove excess PVA polymers prior to the start of experiments is necessary, as this leakage could affect effluent quality. While only basic microbial analysis along with prediction of functional genes by PICRUSt2 was conducted in this study to assess the occurrence of DIET, which is a common method for determining its prevalence (Dang et al., 2017, Liu et al., 2020, Zhang et al., 2021), further research on metatrasncriptome are crucial for confirming DIET through its enzyme activity in future continuous experiments, as this method has recently been recognized for its strong credibility (Wang et al., 2021).

Despite the remaining challenges as this proposed method is still at its early-stage development, this study demonstrates the potential and promising approach to enhancing AD performance through improved DIET. Implementing this approach in the Up-flow Anaerobic Sludge Blanket (UASB) could not only solve the contact efficiency issues from previous studies but also facilitate easier solid-liquid separation and cell reuse, this method could also address the washout problem and potentially eliminate the need for a prolonged start-up period for granulation, as hydrogel immobilization can be achieved within a few hours. The unique properties of the hydrogel

could further contribute to enhanced methane production even at high organic loading rates, reducing operational time and costs in both CSTRs and UASB reactors. Moreover, because the hydrogel is formed by crystallization through hydrogen bonding (Stauffer & Peppast, 1992; Hassan & Peppas, 2000), the PVA-hydrogel and AD sludge could be easily separated by dissolving the PVA at 70°C follow by centrifugation, allowing for the treated sludge to be collected as fertilizer. While the dissolved PVA could potentially be reused in future immobilization processes, offering both environmental and cost benefits. However, this method must be established to verify its applicability.

With all these potential future studies in mind, the findings of this research provide a foundational step toward realizing more efficient and sustainable anaerobic digestion processes, opening the door to enhanced methane production and broader practical applications in waste management and renewable energy generation.

Appendix A

Total solids and Volatile Solids measurement

The total solids (TS) and volatile solids (VS) in all experiments were measured using the methods from the American Public Health Association. In brief, a clean, dry aluminium cup was first weighed to record its initial weight (W_1). Next, 5 mL of sample (anaerobic digestion sludge) was added into the aluminium cup, and the combined weight of aluminium cup and sample (W_2) was recorded. The samples were dried at 105℃ for 12 h to remove all moisture, after which the cup and its contents were weighted again (W_3). The TS content was calculated using the following equation:

$$\text{Total solids (g L}^{-1}) = \frac{(W_3 - W_1)}{(W_2 - W_1)} \times 1000$$

For the VS measurement, the dried samples from the TS were subjected to 550℃ for 2 h to combust the organic material. Once cooled, the aluminium cup containing the remaining ash was weighed again (W_4). The VS content was calculated using the equation as follows:

$$\text{Volatile solids (g L}^{-1}) = \frac{(W_3 - W_4)}{(W_2 - W_1)} \times 1000$$

It should be noted that all measurement were done in triplicate to ensure accuracy. Desiccator was used during cooling steps before weighting to prevent any reabsorption of moisture.

Appendix B
Reports on proposed technique tried in UASB continuous experiment

Introduction

In the previous chapters, the proposed co-immobilization technique for AD microbes and CM demonstrated promising results, suggesting a potential improvement in DIET efficiency compared to the conventional approach (dispersed AD sludge + CM). However, these findings were based on short-term batch experiments, and further evaluation in long-term continuous AD operation is required for practical application. To address this, the co-immobilized hydrogel was tested in the continuous operation of an upflow anaerobic sludge blanket (UASB) reactor to assess its durability and determine the maximum OLR achievable, compared to the conventional DIET method. The UASB reactor was chosen due to its established effectiveness in promoting DIET, as previous studies have shown that microbial proximity to CM within this reactor configuration enhances electron transfer. Consequently, the UASB reactor is one of the most used systems in DIET research. However, as discussed in the introduction, a major challenge in UASB reactors remains the washout of sludge and CM, which can compromise reactor performance. This study also aims to investigate the ability of hydrogel immobilization to retain microbes and CM within the reactor, thereby mitigating washout issues compared to the conventional dispersed method.

Materials and Methods

Substrate and inoculum preparation

Mesophilic anaerobic sludge used to treat domestic sewage at the Hokubu Sludge Treatment Centre in Yokohama, Japan, was used as the inoculum for the semi-continuous experiment. The total solid (TS) and volatile solid (VS) contents of the sludge was 24.4 g L^{-1} and 17.2 g L^{-1}, respectively.

The substrate used in this study was an artificial wastewater by Zhao et al., 2015, with ethanol as the carbon source. The composition of the artificial wastewater is shown in **Table 1 (Appx B)**. Trace elements and vitamin solutions were also added along with the substrate, as described by Morita

et al. 2011. The components of the trace element solution were as follows: 0.5 g L^{-1} $MnSO_4 \cdot H_2O$, 0.1 g L^{-1} $FeSO_4 \cdot 7H_2O$, 0.04 g L^{-1} $NiCl_2 \cdot 6H_2O$, 0.05 g L^{-1} $CoCl_2 \cdot 6H_2O$, 0.13 g L^{-1} $ZnCl_2$, 0.01 g L^{-1} $CuSO_4 \cdot 5H_2O$, 0.1 g L^{-1} $AlK(SO_4)_2 \cdot 12H_2O$, 0.01 g L^{-1} H_3BO_3, and 0.025 g L^{-1} $Na_2MoO_4 \cdot 2H_2O$. The components of the vitamin solution were as follow: 0.002 g L^{-1} biotin, 0.005 g L^{-1} pantothenic acid, 0.0001 g L^{-1} B-12, 0.005 g L^{-1} -aminobenzoic acid, 0.005 g L^{-1} thioctic acid, 0.005 g L^{-1} nicotinic acid, 0.005 g L^{-1} thiamine, 0.005 g L^{-1} riboflavin, 0.01 g L^{-1} pyridoxine HCl, and 0.002 g L^{-1} folic acid. To prevent ethanol evaporation, the artificial wastewater was stored at 4℃ throughout the experiment.

Reactor design and operating condition

A self-constructed upflow anaerobic sludge blanket (UASB) reactor was used for the continuous experiment. The reactor had an internal diameter of 65 mm and a height of 480 mm. A schematic representation of the reactor design is shown in **Fig 1 (Appx. B)**. Four idential UASB reactors, each with a working volume of 1.2 L, were prepared under the same conditions described in Chapter 5, with the following experimental conditions: (1) Control (dispersed sludge only), (2) MWCNTs (dispersed sludge + 1 g/L MWCNTs), (3) Hydrogel (immobilized AD sludge only), and (4) Co-immobilized Hydrogel (immobilized sludge + 1 g/L MWCNTs). For the dispersed conditions (Control and MWCNTs), each reactor was initially inoculated with 600 mL of anaerobic sludge, followed by the addition of deoxygenated distilled water to reach a final working volume of 1.2 L. For the immobilized conditions (Hydrogel and Co-immobilized Hydrogel), the preparation followed the same procedure; however, the 600 mL of dispersed AD sludge was first immobilized using the method described in Chapter 5. The immobilized sludge was then introduced into the reactor along with the initial separated supernatant and deoxygenated distilled water, achieving a final working volume of 1.2 L.

To establish anaerobic conditions, all reactors were purged with N_2 gas for 30 mins before initiating the experiment. A mantle heater was wrapped around each UASB reactors to maintain a

constant operating temperature of 37℃. The artificial wastewater was continuously pumped into the reactors using a peristaltic pump (EYELA, MP-2000), ensuring an equivalent influent flow rate across all conditions. The hydraulic retention time (HRT) was maintained at 1.8 days throughout the experiment. The initial organic loading rate (OLR) was set at 1.0 g-COD L^{-1} day^{-1} and was gradually increased until AD failure was observed, allowing for the determination of the maximum achievable OLR for each condition. It should be noted that a 20-day acclimation phase was conducted before the main experimental phase to enhance the microbial activity. During the acclimation phase, all washed out biomass in the effluent was collected by centrifugation and returned to the reactor to maintain a consistent biomass concentration. After the acclimation period, biomass was no longer returned to the reactor to assess the biomass retention capacity of each condition in the UASB reactor. Except for biogas production sampled every day, other sampling was conducted three times per week, including biogas composition, influent and effluent VFAs, reactor's sludge and effluent's pH.

Analytical parameter

TS and VS were measured using the standardized methods of the American Public Health Association (American Public Health Association, 2005) while pH was measured using a pH meter (Bettler Toledo, S220-Basic). Biogas production was collected daily using gas bags, and the volume was measured with a 1.0 L syringe. The composition of the biogas was analyzed by gas chromatography (Shimadzu Gas Chromatography, GC-2014) equipped with a thermal conductivity detector and an Active Carbon 30/60 packed column. The injector, detector, and column temperatures were maintained at 120°C, 120°C, and 100°C, respectively. The detector current was set to 65 mA, and argon was used as the carrier gas at a flow rate of 40 mL min^{-1}.

Effluent samples were analyzed for ethanol and VFAs concentrations using gas chromatography (Shimadzu Gas Chromatography, GC-2014) equipped with a BX-100 60/80 glass column and a Unisole F-200 30/60 glass column. For ethanol analysis, the injector, detector, and column temperatures were set to 250°C, 110°C, and 110°C, respectively, with nitrogen as the carrier

gas at a flow rate of 32 mL min^{-1}. For VFA analysis, the injector, detector, and column temperatures were set to 200°C, 140°C, and 140°C, respectively, with nitrogen as the carrier gas at a flow rate of 35 mL min^{-1}.

To determine the amount of biomass and MWCNTs washed out from the reactor, total suspended solids (TSS) in the effluent were measured three times a week for each condition. In this procedure, 5 mL of effluent sample was first filtered using a glass fiber filter (ADVANTEC, GC-50) and then dried at 105℃ for 24 h. The total suspended solids were calculated using the following equation:

$$\text{Total Suspended Solids} = \frac{w_2 - w_1}{V_1} \times V_{total} \qquad \text{(Eq.1)}$$

Where, w_1 is the weight of the empty glass fiber filter after drying at 105℃, w_2 is the weight of the dried filtered sample with the filter, V_1 is the volume of the filtered sample (5 mL), and V_{total} is the total volume of the effluent. All measurements were performed in triplicate to ensure accuracy.

It should be noted that due to the experimental failure, not all results are included in this appendix. Instead, a simplified selection of representative results is presented to avoid unnecessary complexity for the reader.

Results and Discussion

Fig 2 (Appx. B) presents the biogas production rate for all conditions up to day 29. The results indicate that during the acclimation phase, biogas production was initially low but gradually stabilized. Among all conditions, the co-immobilized hydrogel achieved stable biogas production the fastest, followed by the hydrogel and MWCNTs conditions, with the control condition taking the longest to stabilize. In the actual experimental phase, when OLR was increased to 2 g-COD L^{-1} day^{-1}, a similar trend was observed: co-immobilized hydrogel achieved stable biogas production first, followed by hydrogel, MWCNTs, and finally the control condition. These results suggest that the proposed co-immobilization method accelerates biogas production stabilization. One possible explanation is that microbe immobilization within the hydrogel concentrates methanogens in a confined space, enabling

them to form stable syntrophic relationship with other microbial communities. In contrast, in the dispersed condition, microbes are more susceptible to washed out or to hydraulic shear stress, which may delay their adaptation and reduce their metabolic activity. Previous studies have shown that the addition of CM can enhance biogas production rates and stabilization (Wang et al., 2021, Xiao et al., 2021). The trend observed in **Fig 2 (Appx. B)** aligns with these findings, as the dispersed MWCNTs condition exhibited faster biogas production stabilization compared to the control. Additionally, when MWCNTs were co-immobilized into the hydrogel, biogas production stabilized even more rapidly. This suggests that the combination of microbial immobilization and CM to facilitate DIET further improves the stabilization process.

Fig 3-A (Appx. B) illustrates the biomass washout from reactor for each condition. These results indicate that the highest to lowest biomass washout followed this order: MWCNTs (33.4%) > Control (25.7%) > Co-immobilized Hydrogel (13%) > Hydrogel (11.2%) on day 30. This may explain the slower biogas production stabilization in the dispersed conditions compared to the immobilized condition. The finding suggests that immobilizing AD microbes in hydrogel helps retain more biomass within the reactor, leading to improved AD performance when used in a long run compared to the conventional dispersed method. **Fig 4 (Appx. B)** presents images of the UASB reactor in each condition on day 0 after the acclimation phase. The MWCNTs condition exhibited flocculated floating sludge, which likely resulted from biogas bubbles being trapped within the sludge, increasing its buoyancy. Notably, this phenomenon was already observed on the second day of the acclimation period in the MWCNTs condition. The presence of MWCNTs likely enhanced biogas production via DIET, but due to the absence of stirring, biogas was not properly release instead being entrapped within the sludge which caused sludge floatation. Consequently, higher biomass and MWCNTs washout were observed in this condition compared to others (**Fig 3-A (Appx. B)**). For the hydrogel condition, more than half of the hydrogel were observed floating. This was likely due to the absence of stirring, which otherwise would have helped release the entrapped biogas through collision-induced permeation. As a result, hydrogel floatation was more pronounced compared to the previous

batch studies (Chapter 5). On the other hand, in the co-immobilized hydrogel condition, most hydrogel remained settled at the bottom of the reactor. This may attribute that the addition of MWCNTs into the hydrogel could enlarge the pore size of the hydrogel, facilitating smoother biogas permeation even without the help of stirring. Nevertheless, even with the floatation of hydrogel, this could be easily overcome by adding a mesh/net in the reactor to prevent washout of hydrogel.

Despite the promising results, the experiment was stopped on day 30 due to inaccurate biogas collection, particularly in the MWCNTs condition. As shown in **Fig 2 (Appx. B)**, both the control and especially MWCNTs conditions exhibited unstable biogas production throughout the experiment. This instability was primarily attributed to poor reactor design, which led to biogas leakage in the dispersed condition. As illustrated in **Fig 4 (Appx. B)**, flocculated floating sludge was observed in both dispersed conditions, with the effect being more severe in the MWCNTs condition. Due to the small effluent outlet of the UASB reactor, the effluent could not be discharged smoothly and occasionally became blocked. As a result, the inoculum volume continued to increase in the reactor until it reached a certain level. At this point, when the pressure differential between the reactor and the effluent outlet exceeded a certain threshold, the accumulated liquid was suddenly expelled in a cyclone-like flow. This rapid discharge created a localized pressure drop, inducing a suction effect that forcibly dragged biogas from the gas bag along with the liquid. Consequently, this phenomenon led to inaccurate biogas measurements, making it difficult to properly compare results across different conditions. As a result, the experiment was discontinued.

Nevertheless, these findings demonstrate the potential of co-immobilized hydrogel in enhancing AD performance by promoting high biomass and CM retention within the reactor. Additionally, both the hydrogel and co-immobilized hydrogel showed no significant difference but appeared unchanged compared to their pre-experiment state, indicating that the durability of hydrogel in a non-stirring reactor like a UASB is likely to be higher (**Fig 5 (Appx. B)**). To accurately assess its effectiveness, a re-evaluation of the co-immobilized hydrogel in a properly designed UASB reactor is necessary for a fair comparison with conventional method.

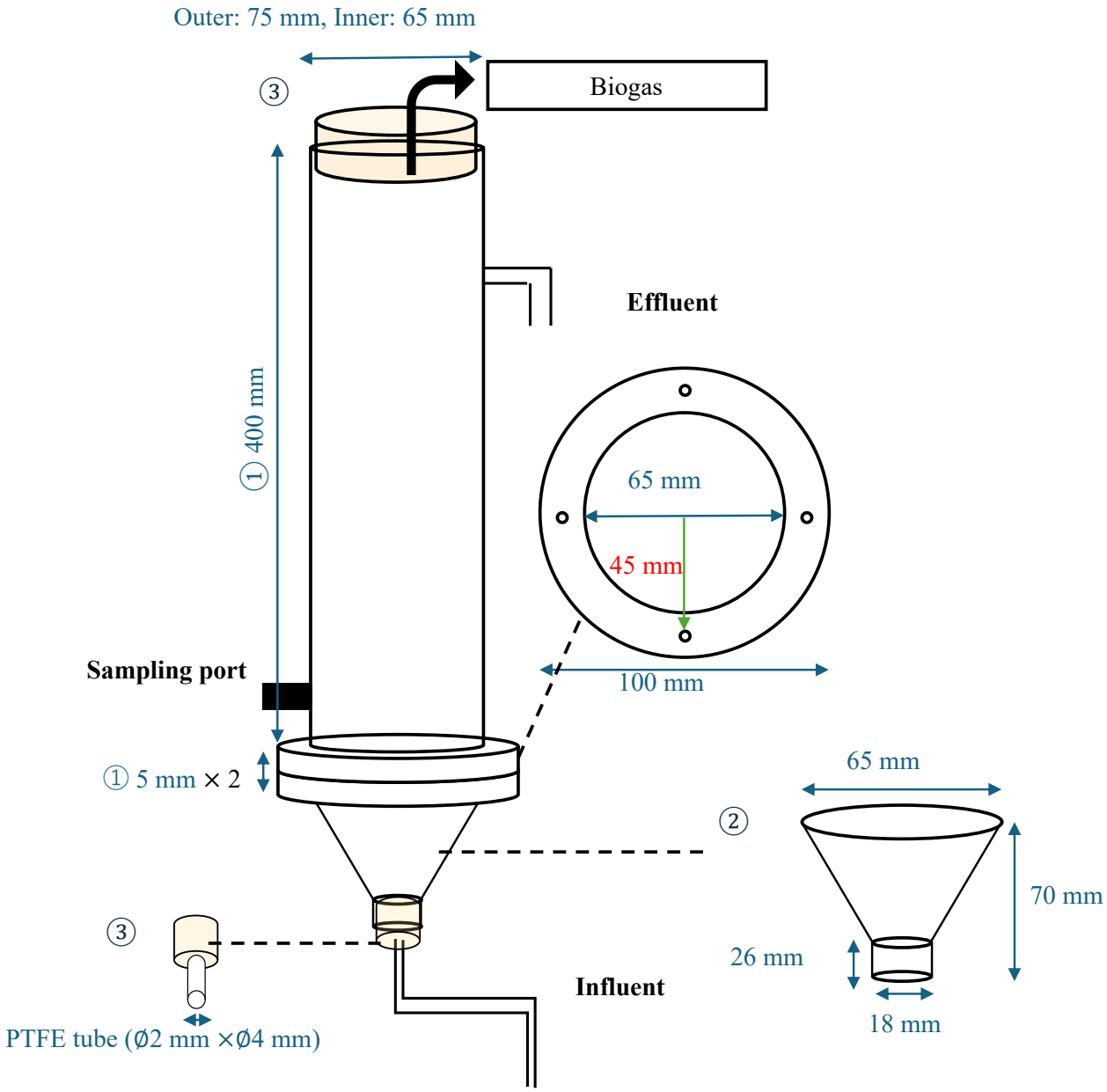

Working volume
1.2 L

Material of reactor
① Arcylic
② Funnel (PP: polypropylene)
③ Silicone rubber stopper

Figure 1 (Appx. B) Schematic design of UASB reactor

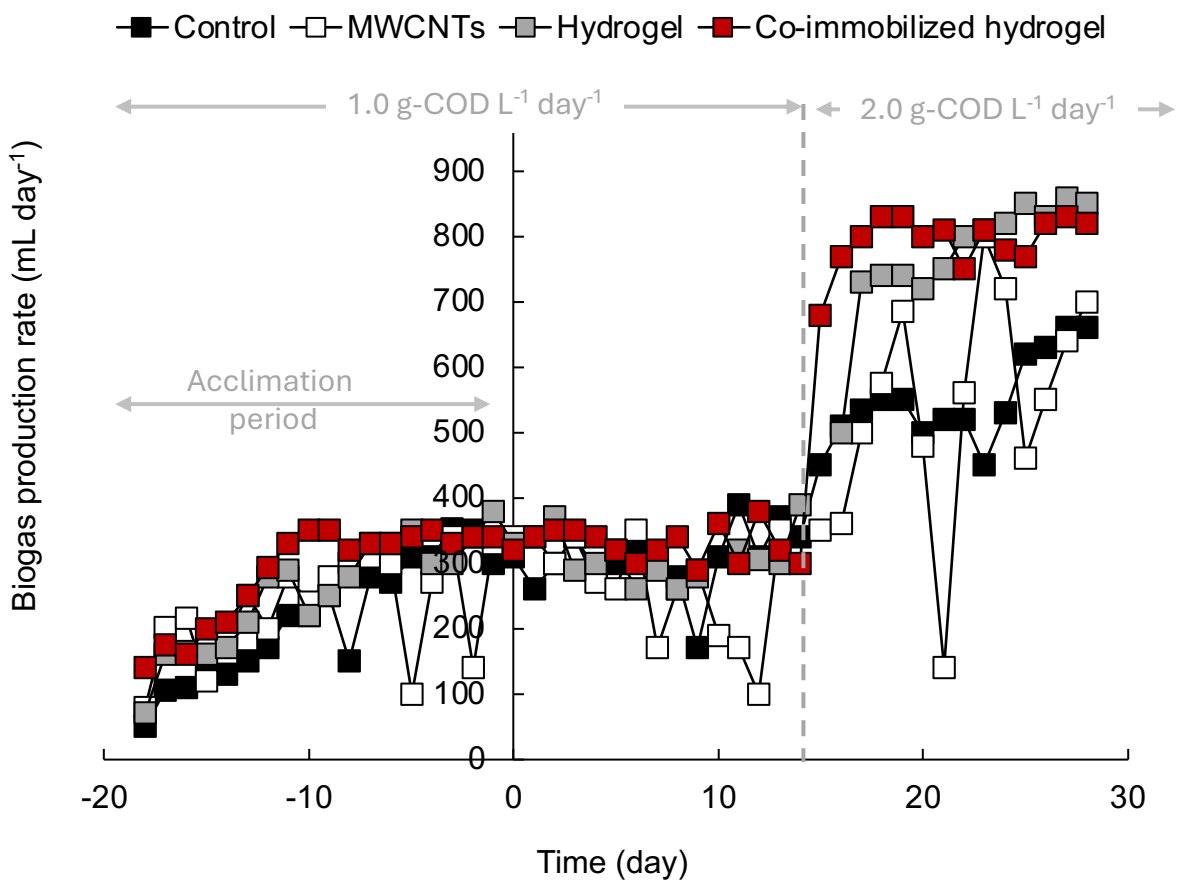

Figure 2 (Appx. B) Biogas production from each condition

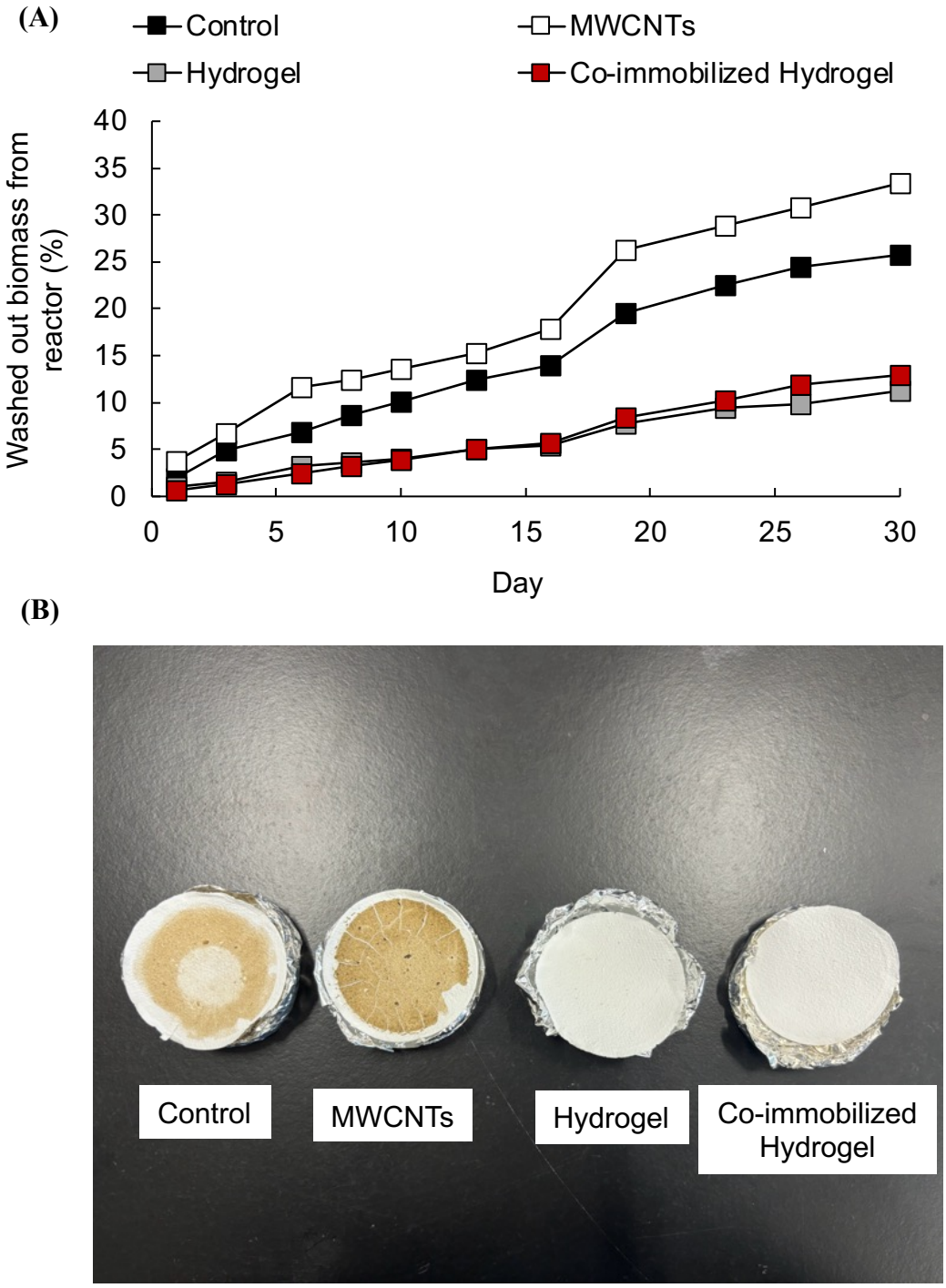

Figure 3 (Appx. B) (A) Amount of washed-out biomass from reactor and (B) image of effluent's suspended solids on filtered paper from each condition

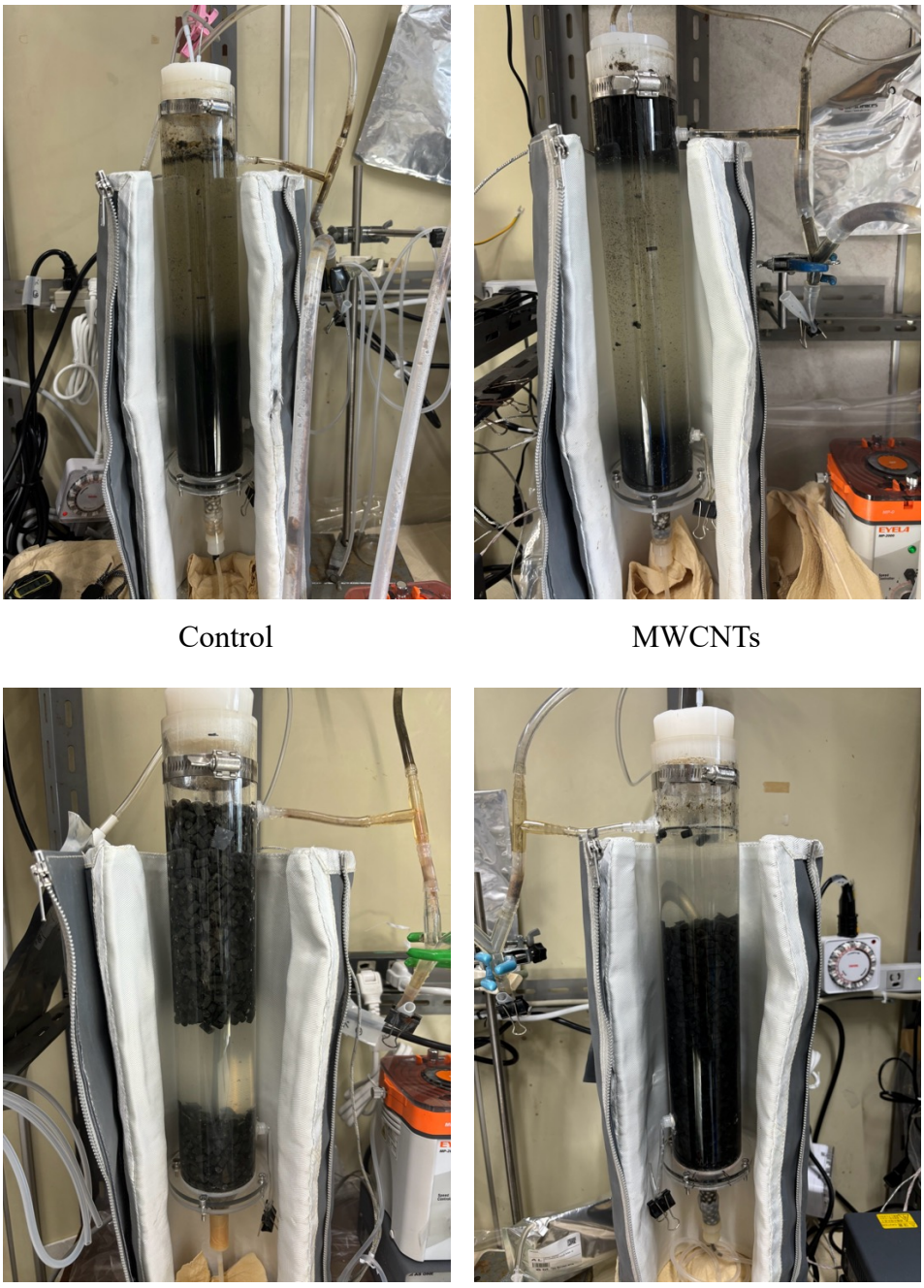

Figure 4 (Appx. B) Images of UASB reactor from each condition in day 0, after acclimation

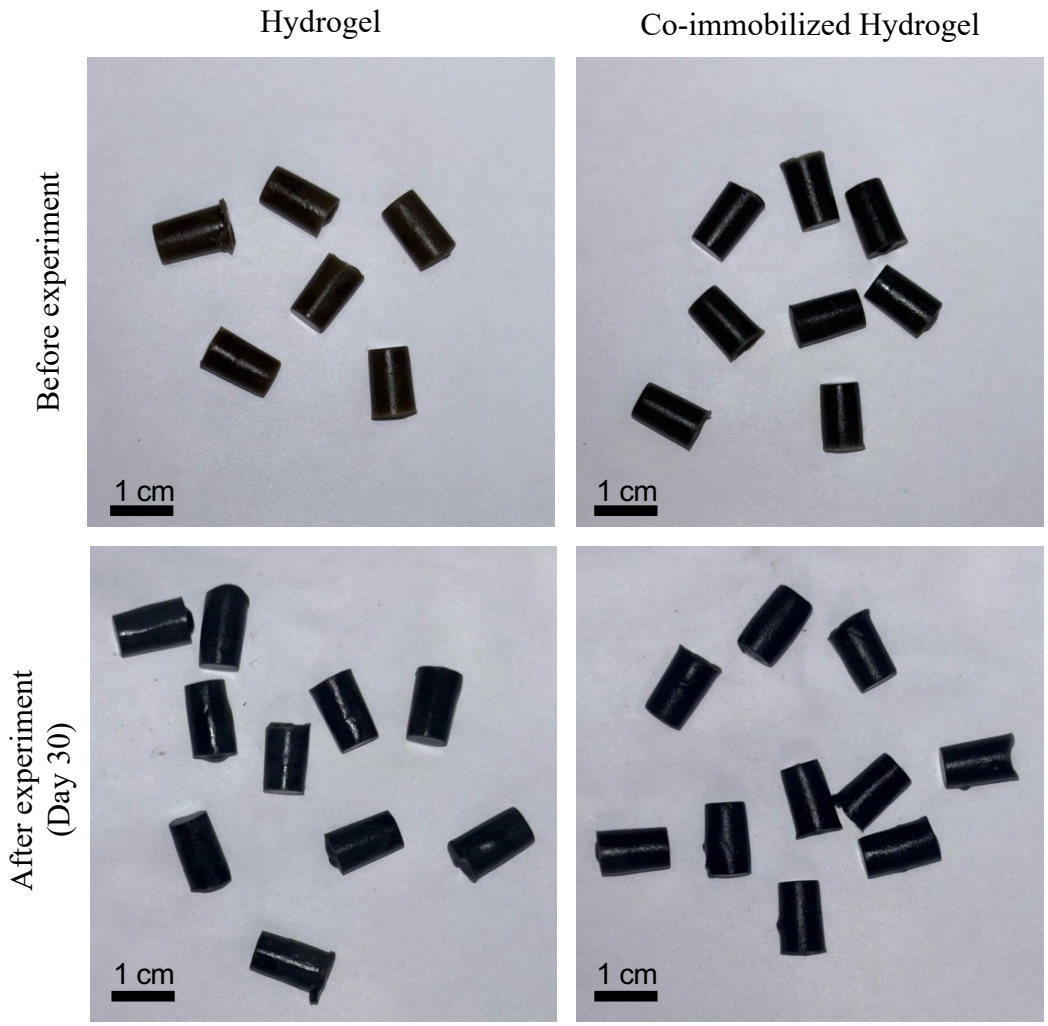

Figure 5 (Appx. B) Image of hydrogel and co-immobilized hydrogel appearance in before and after the experiment

Table 1 (Appx B). Artificial wastewater composition

Component	Concentration (per L)
Ethanol	2.5 mL
Urea	0.23 g
KH_2PO_4	0.11 g
K_2HPO_4	0.17 g
Na_2SO_4	0.05 g
$MgCl_2 \cdot 6H_2O$	0.1 g
$CaCl_2 \cdot 2H_2O$	0.05 g
Trace element solution	10 mL
Vitamin solution	10 mL

Appendix C
Reports on proposed technique tried in semi-continuous experiment

Introduction

In Appendix B, the evaluation of co-immobilized hydrogel in a continuous experiment was not possible due to suboptimal UASB design. Therefore, in this study, co-immobilized hydrogel was assessed in a semi-continuous (sequencing batch reactor) operation instead. Similar to the previous experiment, the OLR was gradually increased until AD failure was observed in each condition to determine the maximum achievable OLR for the proposed technique and to evaluate the durability of the hydrogel.

Materials and Methods

Substrate and inoculum preparation

Mesophilic anaerobic sludge used to treat domestic sewage at the Hokubu Sludge Treatment Centre in Yokohama, Japan, was used as the inoculum for the semi-continuous experiment. Before the experiment, the sludge was left at 37°C temperature room for about a week to naturally degas and remove residue organic matter in the inoculum. The total solid (TS) and volatile solid (VS) contents of the sludge was 23.9 g L^{-1} and 16.8 g L^{-1}, respectively.

The substrate used in this study was similar to the one used in Appendix B, an artificial wastewater by Zhao et al., 2015, with ethanol as the carbon source. The composition of the artificial wastewater is shown in **Table 1 (Appx B)**. Trace elements and vitamin solutions were also added along with the substrate, as described by Morita et al. 2011. The components of the trace element solution were as follows: 0.5 g L^{-1} $MnSO_4 \cdot H_2O$, 0.1 g L^{-1} $FeSO_4 \cdot 7H_2O$, 0.04 g L^{-1} $NiCl_2 \cdot 6H_2O$, 0.05 g L^{-1} $CoCl_2 \cdot 6H_2O$, 0.13 g L^{-1} $ZnCl_2$, 0.01 g L^{-1} $CuSO_4 \cdot 5H_2O$, 0.1 g L^{-1} $AlK(SO_4)_2 \cdot 12H_2O$, 0.01 g L^{-1} H_3BO_3, and 0.025 g L^{-1} $Na_2MoO_4 \cdot 2H_2O$. The components of the vitamin solution were as follow: 0.002 g L^{-1} biotin, 0.005 g L^{-1} pantothenic acid, 0.0001 g L^{-1} B-12, 0.005 g L^{-1} -aminobenzoic acid, 0.005 g L^{-1} thioctic acid, 0.005 g L^{-1} nicotinic acid, 0.005 g L^{-1} thiamine, 0.005 g L^{-1} riboflavin, 0.01

g L^{-1} pyridoxine HCl, and 0.002 g L^{-1} folic acid.

Reactor design and operating condition

The reactors used in this study were prepared from medium-sized glass bottles with a working volume of 1.0 L and sealed with rubber stoppers. Each reactor was equipped with an influent/effluent port and a gas outlet connected to a gas-collecting bag. Four different conditions, similar to those described in Chapter 5, were prepared: (1) Control (dispersed sludge only), (2) MWCNTs (dispersed sludge + 1 g/L MWCNTs), (3) Hydrogel (immobilized AD sludge only), and (4) Co-immobilized Hydrogel (immobilized sludge + 1 g/L MWCNTs). For the dispersed conditions (Control and MWCNTs), each reactor was inoculated with 400 mL of AD sludge and 500 mL of deoxygenated distilled water to achieve a final working volume of 0.9 L. For the immobilized conditions (Hydrogel and Co-immobilized Hydrogel), the preparation was similar, except that the 400 mL of dispersed AD sludge was first immobilized using the method described in Chapter 5. The immobilized sludge was then added to the reactor along with the initial separated supernatant and deoxygenated distilled water to achieve a final working volume of 0.9 L. Before the starting the experiment, all reactors were purged with N_2 gas for 1-2 min to attain an anaerobic phase. All reactors were incubated in a temperature-controlled room at 37°C with a shaking speed of 140 rpm.

The semi-continuous operation was conducted using the following cycle: 10 mins of feeding, 21.6 h of reaction, 2 h of settling, and 10 mins of effluent discharge **(Fig 1 (Appx. C))**. Each reactor was fed daily with 90 mL of artificial wastewater while simultaneously discharging 90 mL of effluent, maintaining a hydraulic retention time (HRT) of 10 days. The initial organic loading rate (OLR) was set at 1.5 g-COD L^{-1} day^{-1} and was gradually increased stepwise until failure of the AD process was observed, allowing determination of the maximum OLR achievable under each condition.

Analytical parameter

TS and VS were measured using the standardized methods of the American Public Health

Association (American Public Health Association, 2005) while pH was measured using a pH meter (Bettler Toledo, S220-Basic). Biogas production was collected daily using gas bags, and the volume was measured with a 1.0 L syringe. The composition of the biogas was analyzed by gas chromatography (Shimadzu Gas Chromatography, GC-2014) equipped with a thermal conductivity detector and an Active Carbon 30/60 packed column. The injector, detector, and column temperatures were maintained at 120°C, 120°C, and 100°C, respectively. The detector current was set to 65 mA, and argon was used as the carrier gas at a flow rate of 40 mL min^{-1}.

Effluent samples were analyzed for ethanol and VFAs concentrations using gas chromatography (Shimadzu Gas Chromatography, GC-2014) equipped with a BX-100 60/80 glass column and a Unisole F-200 30/60 glass column. For ethanol analysis, the injector, detector, and column temperatures were set to 250°C, 110°C, and 110°C, respectively, with nitrogen as the carrier gas at a flow rate of 32 mL min^{-1}. For VFA analysis, the injector, detector, and column temperatures were set to 200°C, 140°C, and 140°C, respectively, with nitrogen as the carrier gas at a flow rate of 35 mL min^{-1}.

At the end of the experiment, the total suspended solids (TSS) in the medium were measured to determine the biomass leakage from the originally immobilized hydrogel in the Hydrogel and Co-immobilized Hydrogel conditions. In this procedure, 5 mL of medium sample was first filtered using a glass fiber filter (ADVANTEC, GC-50) and then dried at 105℃ for 24 h. The total suspended solids were calculated using the following equation:

$$\text{Total Suspended Solids} = \frac{w_2 - w_1}{V_1} \times V_{total} \qquad \text{(Eq.1)}$$

Where w_1 is the weight of the empty glass fiber filter after drting at 105℃, w_2 is the weight of the dried filtered sample with the filter, V_1 is the volume of the filtered sample (5 mL), and V_{total} is the total volume of the medium. All measurements were performed in triplicate to ensure accuracy.

Results and Discussion

Fig 2 (Appx. C) shows the biogas and methane production rates for all conditions up to day 50. The results indicate that biogas production remained relatively stable across all conditions as the OLR was stepwise increased from 1.5 to 6.0 g-COD L^{-1} day^{-1}. However, at OLR 8.0 g-COD L^{-1} day^{-1}, a drastic decrease in biogas production was observed in the control condition, accompanied by ethanol and acetate accumulation **(Fig 3 (Appx. C))** and a pH drop below 6 **(Fig 4 (Appx. C))**. This suggests that the high OLR disrupted intermediate transfer, leading to VFA accumulation and subsequent acidification, ultimately causing system failure. In contrast, the MWCNTs, hydrogel and co-immobilized hydrogel conditions continued to perform efficiently at OLR 8.0-17.0 g-COD L^{-1} day^{-1}, maintaining low ethanol and acetate concentration **(Fig 3 (Appx. C)).** This suggests that DIET was enhanced in these conditions. The MWCNTs likely acted as electron conduits, facilitating faster electron transfer to methanogens, while the hydrogel conditions (despite lacking CM) likely promoted DIET through its microbial proximity, as previously discussed in Chapter 5. However, at OLR 21 g-COD L^{-1} day^{-1}, biogas production started to decline in the MWCNTs condition, while the hydrogel and co-immobilized hydrogel conditions still maintained relatively high production. When OLR was further increased to 25 g-COD L^{-1} day^{-1}, all conditions showed a decline in biogas production, indicating system failure. Interestingly, the failure mechanism differed between the control and the other conditions. In the control, failure was clearly due to acidification, as seen by the significant pH drop (**Fig 4 (Appx. C)**). However, in the MWCNTs, hydrogel and co-immobilized hydrogel conditions, no pH drop was observed at the end of the experiment. Instead, pH increased to >7.9, suggesting that failure was due to ammonia inhibition. Since the nitrogen source used in this experiment was urea, its hydrolysis produced ammonium and increases the pH.

As pH increased, more ammonium was converted into free ammonia, which is toxic to the bacteria and methanogens. Past studies have shown that free ammonia can inhibit microbial activity by diffusing into cell membranes, disrupting proton balance and potassium levels, increasing energy demand for homeostasis, and impairing enzymatic reaction (Yang et al 2024). Based on the VFA

results (**Fig 3 (Appx. C)**), the inhibition in this study likely occurred first in acetogens, as indicated by the accumulation of ethanol before acetate. In contrast, methanogens were inhibited later, as seen by the subsequent accumulation of acetate. A possible explanation to why MWCNTs, hydrogel and co-immobilized hydrogel conditions failed due to ammonia inhibition rather than acidification is the possible prevalence of DIET. The enhanced electron transfer in these conditions led to quicker acetate conversion, preventing excessive acid accumulation and helping to maintain pH stability. However, due to the continuous increase in urea concentration, both pH and free ammonia levels rose, eventually leading to ammonia inhibition and system failure.

An interesting observation from the experiment is that both the immobilized hydrogel and co-immobilized hydrogel conditions continued to produce biogas at high levels at an OLR of 21 g-COD L^{-1} day^{-1}, while the MWCNTs condition began to show a decline in biogas production, despite all three conditions having relatively similar pH levels. This difference in performance can likely be attributed to the immobilization of microbes in hydrogel, which may serve as a protective barrier, reducing their direct exposure to free ammonia. Immobilization in hydrogel may slow the diffusion of ammonia into the hydrogel, allowing the system to maintain activity at higher OLRs. However, when the OLR was increased to 25 g-COD L^{-1} day^{-1}, the concentration of free ammonia in the system reached levels high enough to create a significant concentration gradient. This resulted in a higher diffusion rate of ammonia into the hydrogel, ultimately leading to microbial inhibition. This suggests that while the hydrogel provides some level of protection against ammonia toxicity, its effectiveness diminishes at higher ammonia concentrations. Overall, these results demonstrate that immobilizing AD microbes in hydrogel not only contributes to enhanced AD performance though efficient DIET, but also offer some protection against toxic substances such as free ammonia to a certain extend.

At the end of the experiment, the amount of biomass leaked from the originally immobilized hydrogel was also measured and is shown in **Fig 5 (Appx. C)**. The results indicate that the amount of biomass released from the co-immobilized hydrogel was 1.25 times higher than that from the hydrogel condition. This finding is reasonable, as the addition of MWCNTs interferes with the

crosslinking points of the hydrogel, resulting in larger pore size compared to just immobilizing AD microbes into the hydrogel. Along with the leaked biomass, a significant change in the hydrogel's shape was observed in both conditions at the end of the experiment, with the co-immobilized hydrogel showing more drastic change (**Fig 6 (Appx. C)**). This could explain why no significant increase in menthane production rate was observed, even when MWCNTs were added to the hydrogel (co-immobilized hydrogel), as most of the biomass and MWCNTs were lost in a dispersed form into the medium. It is important to note that no other VFAs (such as propionate, butyrate, etc.) were found in the effluent, other than ethanol and acetate. This suggests that the change in the hydrogel's shape was likely due to mechanical stress from stirring, rather than the breakdown of PVA from microbes. The stirring rate used in this study (140 rpm) was approximately three times higher than in our previous batch studies (50 rpm), which may have accelerated the hydrogel's loss of durability. However, when comparing the hydrogel at mid-experiment (day 30) **(Fig 4 (Appx. C))** to the hydrogel at the end of the experiment in the UASB reactor **(Fig 5 (Appx. B))**, it is evident that despite similar durations of use, the hydrogel in the UASB reactor maintained its shape and appearance much better than the hydrogel used in the stirred reactor. These results suggest that our proposed co-immobilized hydrogel technique may not be suitable for use in continuous stirring reactors due to its low durability. On the other hand, the combined use of co-immobilized hydrogel in UASB reactors may prove more effective, as it appears to retain more biomass and CM while maintain its structural integrity for longer than in stirred reactors.

Conclusion

In this study, co-immobilized hydrogel was evaluated in a semi-continuous operation while gradually increasing the organic loading rate (OLR) to determine its maximum achievable OLR and durability. The results indicate that, except for the control condition, all tested conditions were able to sustain methane fermentation efficiently under high OLR, likely due to the prevalence of DIET. However, system failure at high OLR was more likely caused by free ammonia inhibition due to

elevated pH. Notably, the results suggest that immobilizing anaerobic digestion (AD) microbes within hydrogel can provide protection against inhibitory substances up to a certain extent. Additionally, it is interesting that the hydrogel condition, even without the addition of conductive materials (CM), was able to achieve such high OLR, further demonstrating the significant impact of hydrogel immobilization on enhancing AD performance. However, structural changes in the hydrogel were observed at the end of the experiment, indicating that this immobilization technique may not be suitable for long-term use in a stirred reactor. Moving forward, co-immobilized hydrogel will be reevaluated in a properly designed UASB reactor to provide a more accurate comparison regarding microbial and CM washout, as well as hydrogel durability. Additionally, to mitigate ammonia inhibition, optimizing the C:N ratio or using alternative nitrogen sources instead of urea should be carefully considered.

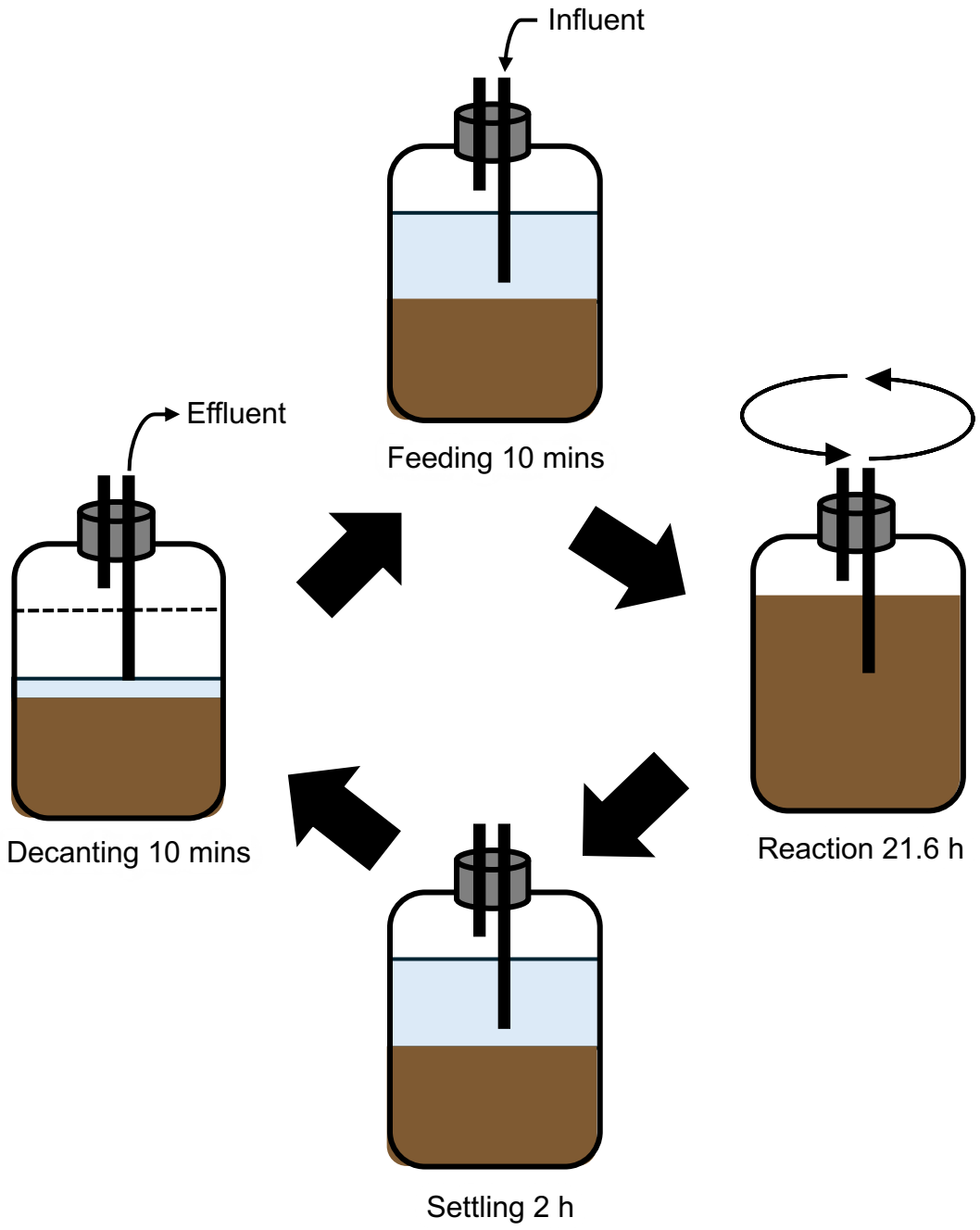

Figure 1 (Appx. C) Schematic of semi-continuous operation

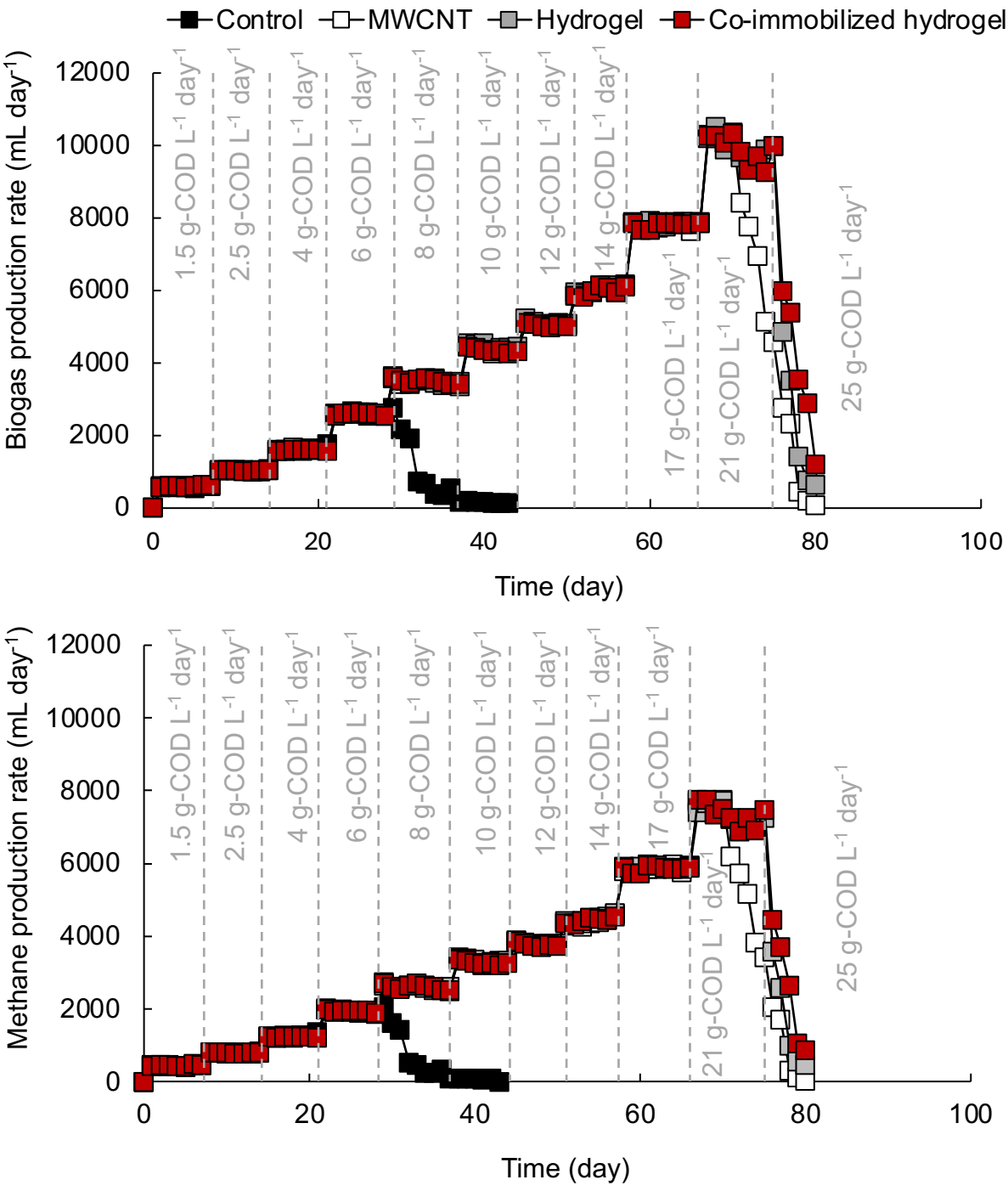

Figure 2 (Appx. C) (A) Biogas production and (B) Methane production rate for each condition

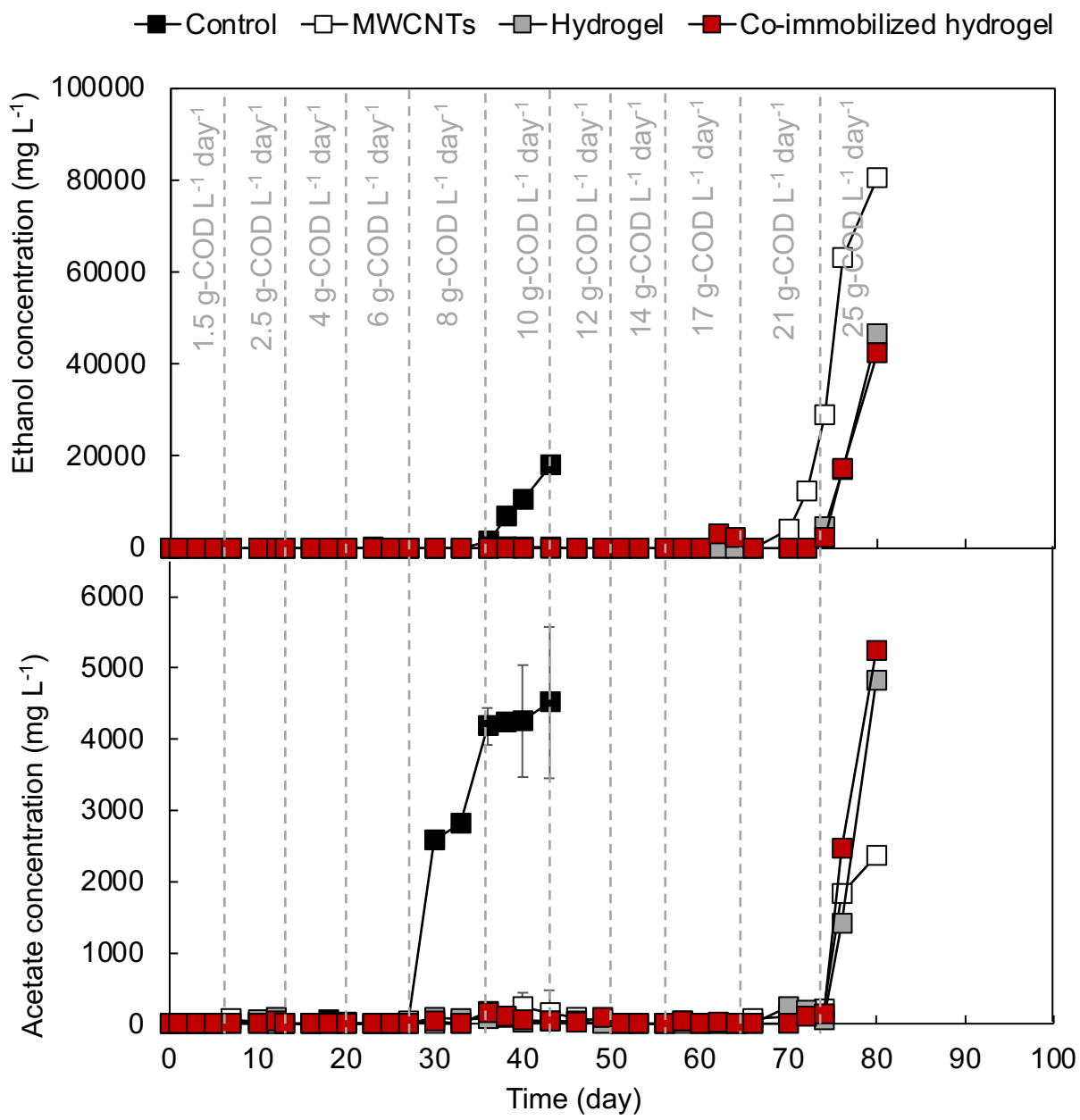

Figure 3 (Appx. C) Ethanol and acetate concentration in effluent for each conditions.

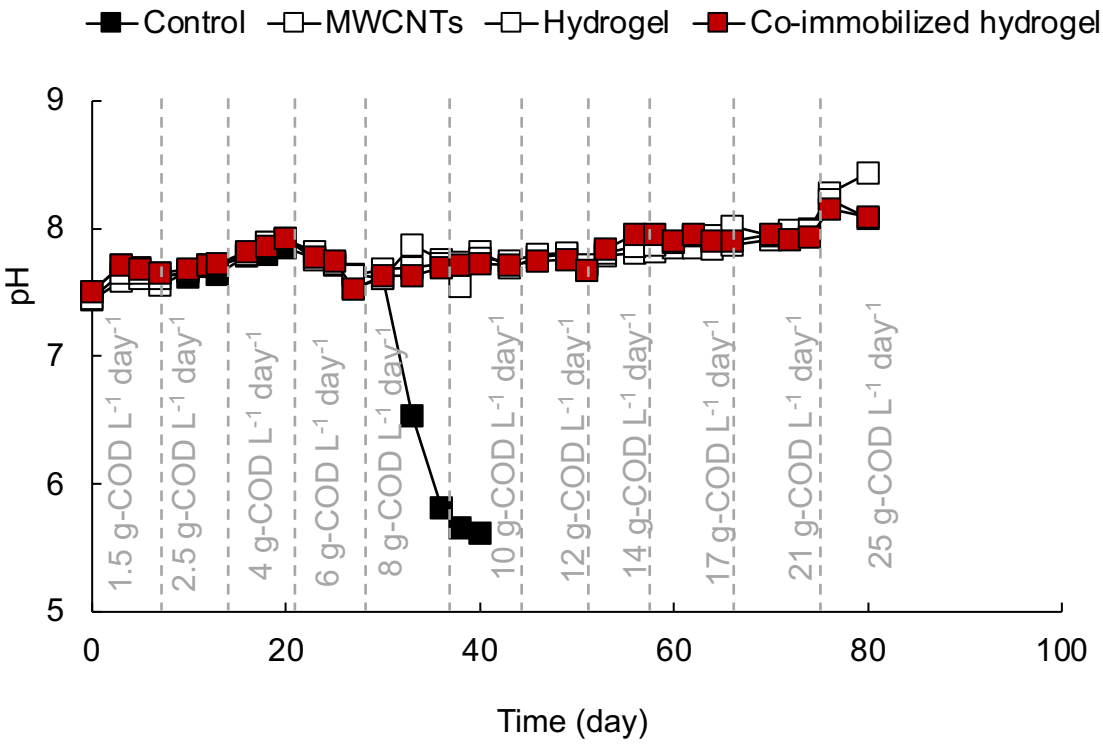

Figure 4 (Appx. C) pH of each conditions' reactor

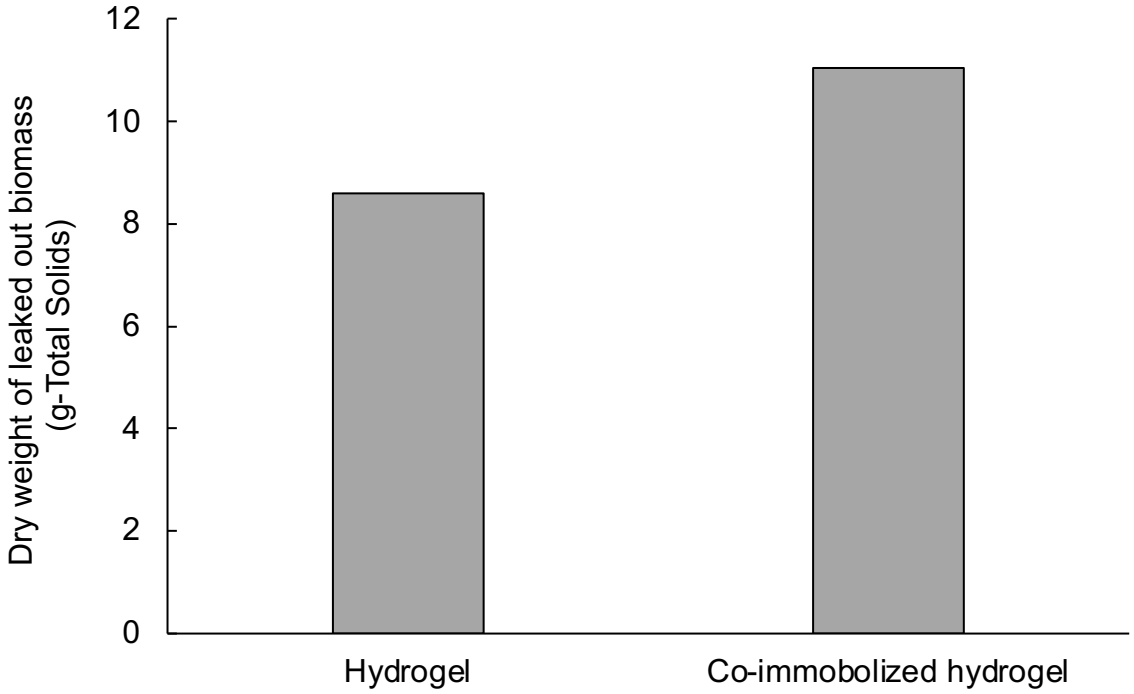

Figure 5 (Appx. C) Amount of leaked out biomass from hydrogel at the end of the experiment

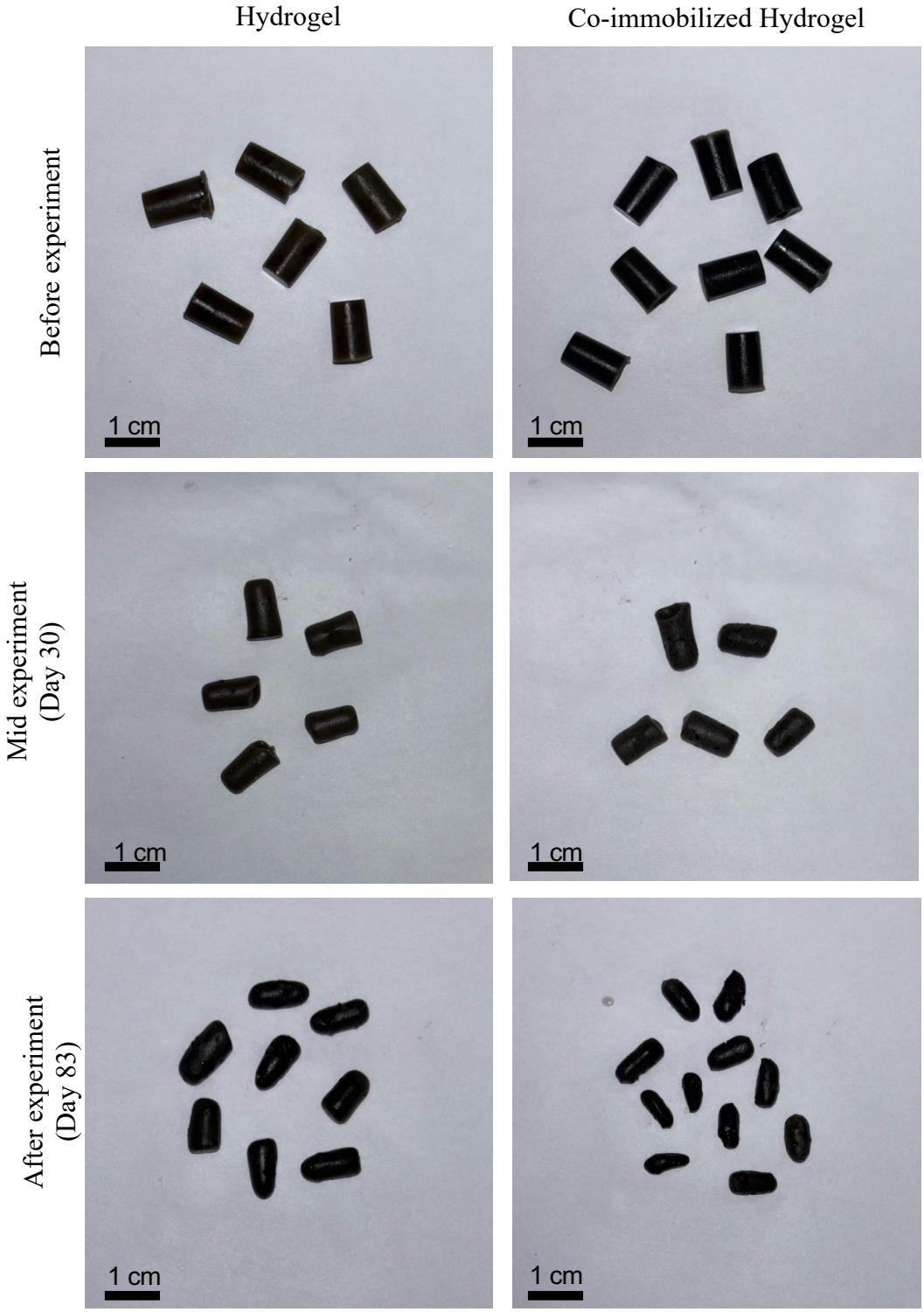

Figure 6 (Appx. B) Image of hydrogel and co-immobilized hydrogel appearance in before , mid and after the experiment

Reference:

Adelnia, H., Ensandoost, R., Moonshi, S. S., Gavgani, J. N., Vasafi, E. I., & Ta, H. T. (2021). Freeze/thawed polyvinyl alcohol hydrogels: Present, past and future. *European Polymer Journal*, *164*, 110974. https://doi.org/10.1016/j.eurpolymj.2021.110974

Ahmad, T., Aadil, R. M., Ahmed, H., Rahman, U. U., Soares, B. C., Souza, S. L., Pimentel, T. C., Scudino, H., Guimarães, J. T., Esmerino, E. A., Freitas, M. Q., Almada, R. B., Vendramel, S. M., Silva, M. C., & Cruz, A. G. (2019). Treatment and utilization of dairy industrial waste: A review. *Trends in Food Science & Technology*, *88*, 361–372. https://doi.org/10.1016/j.tifs.2019.04.003

Ahmed, E., & Rothenberger, A. (2014). Adsorption of volatile hydrocarbons in iron polysulfide chalcogels. *Microporous and Mesoporous Materials*, *199*, 74–82. https://doi.org/10.1016/j.micromeso.2014.08.014

Al-Zuhair, S., & El-Naas, M. (2011). Immobilization of Pseudomonas putida in PVA gel particles for the biodegradation of phenol at high concentrations. *Biochemical Engineering Journal*, *56*(1–2), 46–50. https://doi.org/10.1016/j.bej.2011.05.005

Ambuchi, J. J., Zhang, Z., Shan, L., Liang, D., Zhang, P., & Feng, Y. (2017). Response of anaerobic granular sludge to iron oxide nanoparticles and multi-wall carbon nanotubes during beet sugar industrial wastewater treatment. *Water Research*, *117*, 87–94. https://doi.org/10.1016/j.watres.2017.03.050

Angelidaki, I., & Batstone, D. J. (2010). Anaerobic digestion: process. In *John Wiley & Sons, Ltd eBooks* (pp. 583–600). https://doi.org/10.1002/9780470666883.ch37

APHA, 2005. Standard methods for the examination of Water Environment Federation, Washington DC. https://trove.nla.gov.au/work/16646325?qandversionId=38126605.

Ariyavongvivat, E., Suraraksa, B., & Chaiprasert, P. (2015). Physicochemical and biological characteristics of enhanced anaerobic microbial granulation by synthetic and natural cationic polymers. *Energy Procedia*, *79*, 851–858. https://doi.org/10.1016/j.egypro.2015.11.577

Baek, G., Kim, D., Choi, Y., Cha, J., & Lee, C. (2023). Challenges in engineering direct interspecies electron transfer for enhanced methanogenesis. *Renewable and Sustainable Energy Reviews*, *183*, 113503. https://doi.org/10.1016/j.rser.2023.113503

Baek, G., Kim, J., Cho, K., Bae, H., & Lee, C. (2015). The biostimulation of anaerobic digestion with (semi)conductive ferric oxides: their potential for enhanced biomethanation. *Applied Microbiology and Biotechnology*, *99*(23), 10355–10366. https://doi.org/10.1007/s00253-015-6900-y

Barua, S., & Dhar, B. R. (2017). Advances towards understanding and engineering direct interspecies electron transfer in anaerobic digestion. *Bioresource Technology*, *244*, 698–707. https://doi.org/10.1016/j.biortech.2017.08.023

Baysal, K., Aroguz, A. Z., Adiguzel, Z., & Baysal, B. M. (2013). Chitosan/alginate crosslinked hydrogels: Preparation, characterization and application for cell growth purposes. *International Journal of Biological Macromolecules*, *59*, 342–348. https://doi.org/10.1016/j.ijbiomac.2013.04.073

Beristain-Cardoso, R., Gómez, J., & Méndez-Pampín, R. (2011). Sulfide and ammonium oxidation, acetate mineralization by denitrification in a multipurpose UASB reactor. *Bioresource Technology*, *102*(3), 2549–2554. https://doi.org/10.1016/j.biortech.2010.11.084

Bertin, L., Colao, M. C., Ruzzi, M., & Fava, F. (2004). Performances and microbial features of a granular activated carbon packed-bed biofilm reactor capable of an efficient anaerobic digestion of olive mill wastewaters. *FEMS Microbiology Ecology*, *48*(3), 413–423. https://doi.org/10.1016/j.femsec.2004.03.009

Bertrand, R. L. (2019). LAG phase is a dynamic, organized, adaptive, and evolvable period that prepares bacteria for cell division. *Journal of Bacteriology*, *201*(7). https://doi.org/10.1128/jb.00697-18

Bhattad, U., Venkiteshwaran, K., Cherukuri, K., Maki, J. S., & Zitomer, D. H. (2017). Activity of methanogenic biomass after heat and freeze drying in air. *Environmental Science Water*

Research & Technology, *3*(3), 462–471. https://doi.org/10.1039/c7ew00049a

Bolyen, E., Rideout, J. R., Dillon, M. R., Bokulich, N. A., Abnet, C. C., Al-Ghalith, G. A., Alexander, H., Alm, E. J., Arumugam, M., Asnicar, F., Bai, Y., Bisanz, J. E., Bittinger, K., Brejnrod, A., Brislawn, C. J., Brown, C. T., Callahan, B. J., Caraballo-Rodríguez, A. M., Chase, J., . . . Caporaso, J. G. (2019). Reproducible, interactive, scalable and extensible microbiome data science using QIIME 2. *Nature Biotechnology*, *37*(8), 852–857. https://doi.org/10.1038/s41587-019-0209-9

Bouabidi, Z. B., El-Naas, M. H., & Zhang, Z. (2018). Immobilization of microbial cells for the biotreatment of wastewater: A review. *Environmental Chemistry Letters*, *17*(1), 241–257. https://doi.org/10.1007/s10311-018-0795-7

Brar, S. K., Verma, M., Tyagi, R., & Surampalli, R. (2010). Engineered nanoparticles in wastewater and wastewater sludge – Evidence and impacts. *Waste Management*, *30*(3), 504–520. https://doi.org/10.1016/j.wasman.2009.10.012

Chan, S., Nishi, K., Koyama, M., Toda, T., Matsuyama, T., & Ida, J. (2023). Combined effects of various conductive materials and substrates on enhancing methane production performance. *Biomass and Bioenergy*, *178*, 106977. https://doi.org/10.1016/j.biombioe.2023.106977

Chen, L., Fang, W., Chang, J., Liang, J., Zhang, P., & Zhang, G. (2022). Improvement of direct interspecies electron transfer via adding conductive materials in anaerobic digestion: Mechanisms, performances, and challenges. *Frontiers in Microbiology*, *13*. https://doi.org/10.3389/fmicb.2022.860749

Chen, S., Rotaru, A., Liu, F., Philips, J., Woodard, T. L., Nevin, K. P., & Lovley, D. R. (2014). Carbon cloth stimulates direct interspecies electron transfer in syntrophic co-cultures. *Bioresource Technology*, *173*, 82–86. https://doi.org/10.1016/j.biortech.2014.09.009

Chiellini, E., Corti, A., D'Antone, S., & Solaro, R. (2003). Biodegradation of poly (vinyl alcohol) based materials. *Progress in Polymer Science*, *28*(6), 963–1014. https://doi.org/10.1016/s0079-6700(02)00149-1

Chou, W., Wang, C., Hsu, C., Huang, K., & Liu, T. (2010). Removal of total organic carbon from aqueous solution containing polyvinyl alcohol by electrocoagulation technology. *Desalination*, *259*(1–3), 103–110. https://doi.org/10.1016/j.desal.2010.04.025

Cioabla, A. E., Ionel, I., Dumitrel, G., & Popescu, F. (2012). Comparative study on factors affecting anaerobic digestion of agricultural vegetal residues. *Biotechnology for Biofuels*, *5*(1). https://doi.org/10.1186/1754-6834-5-39

Dang, Y., Holmes, D. E., Zhao, Z., Woodard, T. L., Zhang, Y., Sun, D., Wang, L., Nevin, K. P., & Lovley, D. R. (2016). Enhancing anaerobic digestion of complex organic waste with carbon-based conductive materials. *Bioresource Technology*, *220*, 516–522. https://doi.org/10.1016/j.biortech.2016.08.114

Dang, Y., Sun, D., Woodard, T. L., Wang, L., Nevin, K. P., & Holmes, D. E. (2017). Stimulation of the anaerobic digestion of the dry organic fraction of municipal solid waste (OFMSW) with carbon-based conductive materials. Bioresource Technology, 238, 30–38. https://doi.org/10.1016/j.biortech.2017.04.021

De Bok, F., Plugge, C., & Stams, A. (2004). Interspecies electron transfer in methanogenic propionate degrading consortia. *Water Research*, *38*(6), 1368–1375. https://doi.org/10.1016/j.watres.2003.11.028

Divyalakshmi, P., Murugan, D., Sivarajan, M., Sivasamy, A., Saravanan, P., & Rai, C. L. (2015). In situ disruption approach on aerobic sludge biomass for excess sludge reduction in tannery effluent treatment plant. *Chemical Engineering Journal*, *276*, 130–136. https://doi.org/10.1016/j.cej.2015.04.085

Dong, Y., Zhang, Y., Tu, B., & Miao, J. (2014). Immobilization of ammonia-oxidizing bacteria by calcium alginate. *Ecological Engineering*, *73*, 809–814. https://doi.org/10.1016/j.ecoleng.2014.09.020

Douglas, G. M., Maffei, V. J., Zaneveld, J. R., Yurgel, S. N., Brown, J. R., Taylor, C. M., Huttenhower, C., & Langille, M. G. I. (2020). PICRUSt2 for prediction of metagenome

functions. *Nature Biotechnology*, *38*(6), 685–688. https://doi.org/10.1038/s41587-020-0548-6

Dubé, C., & Guiot, S. R. (2015). Direct Interspecies Electron transfer in Anaerobic digestion: A review. *Advances in Biochemical Engineering, Biotechnology*, 101–115. https://doi.org/10.1007/978-3-319-21993-6_4

Dubé, C., & Guiot, S. R. (2017). Ethanol-to-methane activity of Geobacter-deprived anaerobic granules enhanced by conductive microparticles. *Process Biochemistry*, *63*, 42–48. https://doi.org/10.1016/j.procbio.2017.07.032

Dyksma, S., & Gallert, C. (2022). Effect of magnetite addition on transcriptional profiles of syntrophic Bacteria and Archaea during anaerobic digestion of propionate in wastewater sludge. *Environmental Microbiology Reports*, *14*(4), 664–678. https://doi.org/10.1111/1758-2229.13080

Filman, D. J., Marino, S. F., Ward, J. E., Yang, L., Mester, Z., Bullitt, E., Lovley, D. R., & Strauss, M. (2019). Cryo-EM reveals the structural basis of long-range electron transport in a cytochrome-based bacterial nanowire. *Communications Biology*, *2*(1). https://doi.org/10.1038/s42003-019-0448-9

Gahlot, P., Ahmed, B., Tiwari, S. B., Aryal, N., Khursheed, A., Kazmi, A., & Tyagi, V. K. (2020). Conductive material engineered direct interspecies electron transfer (DIET) in anaerobic digestion: Mechanism and application. *Environmental Technology & Innovation*, *20*, 101056. https://doi.org/10.1016/j.eti.2020.101056

Gardin, H., & Pauss, A. (2001). κ-carrageenan/gelatin gel beads for the co-immobilization of aerobic and anaerobic microbial communities degrading 2,4,6-trichlorophenol under air-limited conditions. *Applied Microbiology and Biotechnology*, *56*(3–4), 517–523. https://doi.org/10.1007/s002530000581

Ghangrekar, M., & Behera, M. (2014). Suspended growth treatment processes. In *Elsevier eBooks* (pp. 74–89). https://doi.org/10.1016/b978-0-12-382182-9.00087-6

Ha, P. T., Lindemann, S. R., Shi, L., Dohnalkova, A. C., Fredrickson, J. K., Madigan, M. T., & Beyenal, H. (2017). Syntrophic anaerobic photosynthesis via direct interspecies electron transfer. *Nature Communications*, *8*(1). https://doi.org/10.1038/ncomms13924

Hassan, C. M., & Peppas, N. A. (2007). Structure and Applications of Poly(vinyl alcohol) Hydrogels Produced by Conventional Crosslinking or by Freezing/Thawing Methods. In *Springer eBooks* (pp. 37–65). https://doi.org/10.1007/3-540-46414-x_2

Holmes, D. E., Shrestha, P. M., Walker, D. J. F., Dang, Y., Nevin, K. P., Woodard, T. L., & Lovley, D. R. (2017). Metatranscriptomic Evidence for Direct Interspecies Electron Transfer between Geobacter and Methanothrix Species in Methanogenic Rice Paddy Soils. *Applied and Environmental Microbiology*, *83*(9). https://doi.org/10.1128/aem.00223-17

Holmes, D., & Smith, J. (2016). Biologically produced methane as a renewable energy source. *Advances in Applied Microbiology*, 1–61. https://doi.org/10.1016/bs.aambs.2016.09.001

Hu, K., Jiang, J., Zhao, Q., Lee, D., Wang, K., & Qiu, W. (2011). Conditioning of wastewater sludge using freezing and thawing: Role of curing. *Water Research*, *45*(18), 5969–5976. https://doi.org/10.1016/j.watres.2011.08.064

Hu, Q., Sun, D., Ma, Y., Qiu, B., & Guo, Z. (2017). Conductive polyaniline nanorods enhanced methane production from anaerobic wastewater treatment. *Polymer*, *120*, 236–243. https://doi.org/10.1016/j.polymer.2017.05.073

Hu, Q., Zhou, N., Gong, K., Liu, H., Liu, Q., Sun, D., Wang, Q., Shao, Q., Liu, H., Qiu, B., & Guo, Z. (2019). Intracellular Polymer Substances Induced Conductive Polyaniline for Improved Methane Production from Anaerobic Wastewater Treatment. *ACS Sustainable Chemistry & Engineering*, *7*(6), 5912–5920. https://doi.org/10.1021/acssuschemeng.8b05847

Huang, W. T., Chang, I. L., Lee, D. J., & Hong, S. G. (1996). Sludge chemical composition changes under uni-directional freezing. *Water Science & Technology*, *34*(3–4). https://doi.org/10.1016/0273-1223(96)00620-8

Isaka, K., Kimura, Y., Osaka, T., & Tsuneda, S. (2012). High-rate denitrification using polyethylene

glycol gel carriers entrapping heterotrophic denitrifying bacteria. *Water Research*, *46*(16), 4941–4948. https://doi.org/10.1016/j.watres.2012.05.050

Jacob, S., Nithianandam, S., Rastogi, S., Sakhuja, S., & Alankar, S. N. S. L. (2021). Handling and treatment strategies of biomedical wastes and biosolids contaminated with SARS-CoV-2 in waste environment. In *Elsevier eBooks* (pp. 207–232). https://doi.org/10.1016/b978-0-323-85780-2.00012-3

Jin, H., He, Z., Ren, Y., Tang, C., Zhou, A., Liu, W., Liang, B., Li, Z., & Wang, A. (2022). Current advances and challenges for direct interspecies electron transfer in anaerobic digestion of waste activated sludge. *Chemical Engineering Journal*, *450*, 137973. https://doi.org/10.1016/j.cej.2022.137973

Joshi, A., Lanjekar, V., Dhakephalkar, P. K., & Dagar, S. S. (2018). Cultivation of multiple genera of hydrogenotrophic methanogens from different environmental niches. *Anaerobe*, *50*, 64–68. https://doi.org/10.1016/j.anaerobe.2018.02.001

Kabisch, A., Otto, A., König, S., Becher, D., Albrecht, D., Schüler, M., Teeling, H., Amann, R. I., & Schweder, T. (2014). Functional characterization of polysaccharide utilization loci in the marine Bacteroidetes 'Gramella forsetii' KT0803. *The ISME Journal*, *8*(7), 1492–1502. https://doi.org/10.1038/ismej.2014.4

Kadimpati, K. K., Mondithoka, K. P., Bheemaraju, S., & Challa, V. R. M. (2012). Entrapment of marine microalga, Isochrysis galbana, for biosorption of Cr(III) from aqueous solution: isotherms and spectroscopic characterization. *Applied Water Science*, *3*(1), 85–92. https://doi.org/10.1007/s13201-012-0062-1

Karolinczak, B., Dąbrowski, W., & Żyłka, R. (2021). Evaluation of dairy wastewater treatment systems using carbon footprint analysis. *Energies*, *14*(17), 5366. https://doi.org/10.3390/en14175366

Kato, S., Hashimoto, K., & Watanabe, K. (2011). Methanogenesis facilitated by electric syntrophy via (semi)conductive iron-oxide minerals. *Environmental Microbiology*, *14*(7), 1646–1654.

https://doi.org/10.1111/j.1462-2920.2011.02611.x

Kato, S., Hashimoto, K., & Watanabe, K. (2012). Microbial interspecies electron transfer via electric currents through conductive minerals. *Proceedings of the National Academy of Sciences*, *109*(25), 10042–10046. https://doi.org/10.1073/pnas.1117592109

Kato, S., Hashimoto, K., & Watanabe, K. (2012). Microbial interspecies electron transfer via electric currents through conductive minerals. *Proceedings of the National Academy of Sciences*, *109*(25), 10042–10046. https://doi.org/10.1073/pnas.1117592109

Khan, A. H., López-Maldonado, E. A., Alam, S. S., Khan, N. A., López, J. R. L., Herrera, P. F. M., Abutaleb, A., Ahmed, S., & Singh, L. (2022). Municipal solid waste generation and the current state of waste-to-energy potential: State of art review. *Energy Conversion and Management*, *267*, 115905. https://doi.org/10.1016/j.enconman.2022.115905

Knight, T., Ronimus, R., Dey, D., Tootill, C., Naylor, G., Evans, P., Molano, G., Smith, A., Tavendale, M., Pinares-Patiño, C., & Clark, H. (2011). Chloroform decreases rumen methanogenesis and methanogen populations without altering rumen function in cattle. *Animal Feed Science and Technology*, *166–167*, 101–112. https://doi.org/10.1016/j.anifeedsci.2011.04.059

Koyama, M., Nagao, N., Syukri, F., Rahim, A. A., Toda, T., Tran, Q. N. M., & Nakasaki, K. (2019). Ammonia recovery and microbial community succession during thermophilic composting of shrimp pond sludge at different sludge properties. *Journal of Cleaner Production*, *251*, 119718. https://doi.org/10.1016/j.jclepro.2019.119718

Kumar, S. (2004). Estimation method for national methane emission from solid waste landfills. *Atmospheric Environment*, *38*(21), 3481–3487. https://doi.org/10.1016/j.atmosenv.2004.02.057

Kurayama, F., Bahadur, N. M., Sato, M., Furusawa, T., & Suzuki, N. (2019). One-step preparation of organic-inorganic hybrid capsules based on simultaneous gelation and silicification. *Engineering Reports*, *1*(4). https://doi.org/10.1002/eng2.12061

Lapébie, P., Lombard, V., Drula, E., Terrapon, N., & Henrissat, B. (2019). Bacteroidetes use

thousands of enzyme combinations to break down glycans. *Nature Communications*, *10*(1). https://doi.org/10.1038/s41467-019-10068-5

Lay, J., Li, Y., & Noike, T. (1998). Mathematical Model for Methane Production from Landfill Bioreactor. *Journal of Environmental Engineering*, *124*(8), 730–736. https://doi.org/10.1061/(asce)0733-9372(1998)124:8(730

Leang, C., Qian, X., Mester, T., & Lovley, D. R. (2010). Alignment of the c -Type Cytochrome OmcS along Pili of Geobacter sulfurreducens. *Applied and Environmental Microbiology*, *76*(12), 4080–4084. https://doi.org/10.1128/aem.00023-10

Lee, J., Kim, E., Han, G., Tongco, J. V., Shin, S. G., & Hwang, S. (2018). Microbial communities underpinning mesophilic anaerobic digesters treating food wastewater or sewage sludge: A full-scale study. *Bioresource Technology*, *259*, 388–397. https://doi.org/10.1016/j.biortech.2018.03.052

Lee, J., Lee, S., & Park, H. (2016). Enrichment of specific electro-active microorganisms and enhancement of methane production by adding granular activated carbon in anaerobic reactors. *Bioresource Technology*, *205*, 205–212. https://doi.org/10.1016/j.biortech.2016.01.054

Lei, Y., Sun, D., Dang, Y., Chen, H., Zhao, Z., Zhang, Y., & Holmes, D. E. (2016). Stimulation of methanogenesis in anaerobic digesters treating leachate from a municipal solid waste incineration plant with carbon cloth. *Bioresource Technology*, *222*, 270–276. https://doi.org/10.1016/j.biortech.2016.10.007

Li, H., Chang, J., Liu, P., Fu, L., Ding, D., & Lu, Y. (2014). Direct interspecies electron transfer accelerates syntrophic oxidation of butyrate in paddy soil enrichments. *Environmental Microbiology*, *17*(5), 1533–1547. https://doi.org/10.1111/1462-2920.12576

Li, L., Liu, H., Chen, Y., Yang, D., Cai, C., Yuan, S., & Dai, X. (2022). Effect of Magnet-Fe3O4 composite structure on methane production during anaerobic sludge digestion: Establishment of direct interspecies electron transfer. *Renewable Energy*, *188*, 52–60. https://doi.org/10.1016/j.renene.2022.01.101

Li, Y., Alaimo, C. P., Kim, M., Kado, N. Y., Peppers, J., Xue, J., Wan, C., Green, P. G., Zhang, R., Jenkins, B. M., Vogel, C. F. A., Wuertz, S., Young, T. M., & Kleeman, M. J. (2019). Composition and Toxicity of Biogas Produced from Different Feedstocks in California. *Environmental Science & Technology*, *53*(19), 11569–11579. https://doi.org/10.1021/acs.est.9b03003

Li, Y., Zhang, Y., Yang, Y., Quan, X., & Zhao, Z. (2017). Potentially direct interspecies electron transfer of methanogenesis for syntrophic metabolism under sulfate reducing conditions with stainless steel. *Bioresource Technology*, *234*, 303–309. https://doi.org/10.1016/j.biortech.2017.03.054

Liu, F., Rotaru, A., Shrestha, P. M., Malvankar, N. S., Nevin, K. P., & Lovley, D. R. (2012). Promoting direct interspecies electron transfer with activated carbon. *Energy & Environmental Science*, *5*(10), 8982. https://doi.org/10.1039/c2ee22459c

Liu, F., Rotaru, A., Shrestha, P. M., Malvankar, N. S., Nevin, K. P., & Lovley, D. R. (2014). Magnetite compensates for the lack of a pilin-associated c-type cytochrome in extracellular

Liu, J., Liu, T., Chen, S., Yu, H., Zhang, Y., & Quan, X. (2020). Enhancing anaerobic digestion in anaerobic integrated floating fixed-film activated sludge (An-IFFAS) system using novel electron mediator suspended biofilm carriers. Water Research, 175, 115697. https://doi.org/10.1016/j.watres.2020.115697

Liu, Y., & Whitman, W. B. (2008). Metabolic, phylogenetic, and ecological diversity of the methanogenic archaea. *Annals of the New York Academy of Sciences*, *1125*(1), 171–189. https://doi.org/10.1196/annals.1419.019

Lonergan, D. J., Jenter, H. L., Coates, J. D., Phillips, E. J., Schmidt, T. M., & Lovley, D. R. (1996). Phylogenetic analysis of dissimilatory Fe(III)-reducing bacteria. *Journal of Bacteriology*, *178*(8), 2402–2408. https://doi.org/10.1128/jb.178.8.2402-2408.1996

Lovley, D. R. (2011). Live wires: direct extracellular electron exchange for bioenergy and the bioremediation of energy-related contamination. *Energy & Environmental Science*, *4*(12), 4896. https://doi.org/10.1039/c1ee02229f

Lovley, D. R. (2017). Syntrophy goes electric: direct interspecies electron transfer. *Annual Review of Microbiology*, *71*(1), 643–664. https://doi.org/10.1146/annurev-micro-030117-020420

Mad-Ali, S., Benjakul, S., Prodpran, T., & Maqsood, S. (2017). Characteristics and gelling properties of gelatin from goat skin as affected by drying methods. *Journal of Food Science and Technology*, *54*(6), 1646–1654. https://doi.org/10.1007/s13197-017-2597-5

Magdum, S. S., Minde, G. P., & Kalyanraman, V. (2013). RAPID DETERMINATION OF INDIRECT COD AND POLYVINYL ALCOHOL FROM TEXTILE DESIZING WASTEWATER. *Pollution Research*, *32*(3). http://works.bepress.com/sandip_magdum/7/

Malvankar, N. S., & Lovley, D. R. (2014). Microbial nanowires for bioenergy applications. *Current Opinion in Biotechnology*, *27*, 88–95. https://doi.org/10.1016/j.copbio.2013.12.003

Martínez, G., Merinero, M., Pérez-Aranda, M., Pérez-Soriano, E., Ortiz, T., Villamor, E., Begines, B., & Alcudia, A. (2020). Environmental Impact of Nanoparticles' application as an Emerging Technology: a review. *Materials*, *14*(1), 166. https://doi.org/10.3390/ma14010166

McIlroy, S. J., Kirkegaard, R. H., Dueholm, M. S., Fernando, E., Karst, S. M., Albertsen, M., & Nielsen, P. H. (2017). Culture-Independent analyses reveal novel anaerolineaceae as abundant primary fermenters in anaerobic digesters treating waste activated sludge. *Frontiers in Microbiology*, *8*. https://doi.org/10.3389/fmicb.2017.01134

Mei, R., Nobu, M. K., Narihiro, T., Yu, J., Sathyagal, A., Willman, E., & Liu, W. (2018). Novel Geobacter species and diverse methanogens contribute to enhanced methane production in media-added methanogenic reactors. Water Research, 147, 403–412. https://doi.org/10.1016/j.watres.2018.10.026

Milano, J., Ong, H. C., Masjuki, H., Chong, W., Lam, M. K., Loh, P. K., & Vellayan, V. (2016). Microalgae biofuels as an alternative to fossil fuel for power generation. *Renewable and Sustainable Energy Reviews*, *58*, 180–197. https://doi.org/10.1016/j.rser.2015.12.150

Morita, M., Malvankar, N. S., Franks, A. E., Summers, Z. M., Giloteaux, L., Rotaru, A. E., Rotaru, C., & Lovley, D. R. (2011). Potential for direct interspecies electron transfer in methanogenic wastewater digester aggregates. *MBio*, *2*(4).

Mostafa, A., Im, S., Song, Y., Ahn, Y., & Kim, D. (2020). Enhanced anaerobic digestion by stimulating DIET reaction. *Processes*, *8*(4), 424. https://doi.org/10.3390/pr8040424

Muralikrishna, I. V., & Manickam, V. (2017). Wastewater treatment Technologies. In *Elsevier eBooks* (pp. 249–293). https://doi.org/10.1016/b978-0-12-811989-1.00012-9

Nageeb, M. (2013). Adsorption Technique for the Removal of Organic Pollutants from Water and Wastewater. In *InTech eBooks*. https://doi.org/10.5772/54048

Nguyen, L. N., Vu, M. T., Johir, M. a. H., Pernice, M., Ngo, H. H., Zdarta, J., Jesionowski, T., & Nghiem, L. D. (2021). Promotion of direct interspecies electron transfer and potential impact of conductive materials in anaerobic digestion and its downstream processing - a critical review. *Bioresource Technology*, *341*, 125847. https://doi.org/10.1016/j.biortech.2021.125847

Nishi, K., Akizuki, S., Toda, T., Matsuyama, T., & Ida, J. (2020). Development of light-shielding hydrogel for nitrifying bacteria to prevent photoinhibition under strong light irradiation. *Process Biochemistry*, *94*, 359–364. https://doi.org/10.1016/j.procbio.2020.04.037

Nishi, K., Akizuki, S., Toda, T., Matsuyama, T., & Ida, J. (2022). Advanced light-tolerant microalgae-nitrifying bacteria consortia for stable ammonia removal under strong light irradiation using light-shielding hydrogel. *Chemosphere*, *297*, 134252. https://doi.org/10.1016/j.chemosphere.2022.134252

Örmeci, B., & Vesilind, P. A. (2001). Effect of dissolved organic material and cations on freeze-thaw conditioning of activated and alum sludges. *Water Research*, *35*(18), 4299–4306.

https://doi.org/10.1016/s0043-1354(01)00174-9

Palacios, P. A., Francis, W. R., & Rotaru, A. (2021). A Win–Loss interaction on FE0 between methanogens and acetogens from a climate lake. *Frontiers in Microbiology*, *12*. https://doi.org/10.3389/fmicb.2021.638282

Pan, X., Zhao, L., Li, C., Angelidaki, I., Lv, N., Ning, J., Cai, G., & Zhu, G. (2020). Deep insights into the network of acetate metabolism in anaerobic digestion: focusing on syntrophic acetate oxidation and homoacetogenesis. *Water Research*, *190*, 116774. https://doi.org/10.1016/j.watres.2020.116774

Pandey, S., & Sarkar, S. (2017). Anaerobic treatment of wastewater using a two-stage packed-bed reactor containing polyvinyl alcohol gel beads as biofilm carrier. *Journal of Environmental Chemical Engineering*, *5*(2), 1575–1585. https://doi.org/10.1016/j.jece.2017.02.013

Park, J., Kang, H., Park, K., & Park, H. (2018). Direct interspecies electron transfer via conductive materials: A perspective for anaerobic digestion applications. *Bioresource Technology*, *254*, 300–311. https://doi.org/10.1016/j.biortech.2018.01.095

Pilarska, A. A., Wolna-Maruwka, A., & Pilarski, K. (2018). Kraft Lignin Grafted with Polyvinylpyrrolidone as a Novel Microbial Carrier in Biogas Production. *Energies*, *11*(12), 3246. https://doi.org/10.3390/en11123246

Pšeja, J., Charvátová, H., Hruzík, P., Hrnčiřík, J., & Kupec, J. (2006). Anaerobic biodegradation of blends based on polyvinyl alcohol. *Journal of Polymers and the Environment*, *14*(2), 185–190. https://doi.org/10.1007/s10924-006-0009-4

Puengrang, P., Suraraksa, B., Prommeenate, P., Boonapatcharoen, N., Cheevadhanarak, S., Tanticharoen, M., & Kusonmano, K. (2020). Diverse Microbial Community Profiles of Propionate-Degrading Cultures Derived from Different Sludge Sources of Anaerobic Wastewater Treatment Plants. *Microorganisms*, *8*(2), 277. https://doi.org/10.3390/microorganisms8020277

Qian, X., Mester, T., Morgado, L., Arakawa, T., Sharma, M. L., Inoue, K., Joseph, C., Salgueiro, C. A., Maroney, M. J., & Lovley, D. R. (2011). Biochemical characterization of purified OmcS, a c-type cytochrome required for insoluble Fe(III) reduction in Geobacter sulfurreducens. *Biochimica Et Biophysica Acta (BBA) - Bioenergetics*, *1807*(4), 404–412. https://doi.org/10.1016/j.bbabio.2011.01.003

Qin, Y., Wang, H., Li, X., Cheng, J. J., & Wu, W. (2017). Improving methane yield from organic fraction of municipal solid waste (OFMSW) with magnetic rice-straw biochar. *Bioresource Technology*, *245*, 1058–1066. https://doi.org/10.1016/j.biortech.2017.09.047

Richter, H., Nevin, K. P., Jia, H., Lowy, D. A., Lovley, D. R., & Tender, L. M. (2009). Cyclic voltammetry of biofilms of wild type and mutant Geobacter sulfurreducens on fuel cell anodes indicates possible roles of OmcB, OmcZ, type IV pili, and protons in extracellular electron transfer. *Energy & Environmental Science*, *2*(5), 506. https://doi.org/10.1039/b816647a

Roquero, D. M., Bollella, P., Katz, E., & Melman, A. (2021). Controlling porosity of calcium alginate hydrogels by interpenetrating polyvinyl Alcohol–Diboronate polymer network. *ACS Applied Polymer Materials*, *3*(3), 1499–1507. https://doi.org/10.1021/acsapm.0c01358

Rossi, E., Becarelli, S., Pecorini, I., Di Gregorio, S., & Iannelli, R. (2022). Anaerobic digestion of the organic fraction of municipal solid waste in Plug-Flow reactors: Focus on bacterial community metabolic pathways. *Water*, *14*(2), 195. https://doi.org/10.3390/w14020195

Rosso, D., Larson, L. E., & Stenstrom, M. K. (2008). Aeration of large-scale municipal wastewater treatment plants: state of the art. *Water Science & Technology*, *57*(7), 973–978. https://doi.org/10.2166/wst.2008.218

Rotaru, A., Shrestha, P. M., Liu, F., Markovaite, B., Chen, S., Nevin, K. P., & Lovley, D. R. (2014a). Direct Interspecies Electron Transfer between Geobacter metallireducens and Methanosarcina barkeri. *Applied and Environmental Microbiology*, *80*(15), 4599–4605. https://doi.org/10.1128/aem.00895-14

Rotaru, A., Shrestha, P. M., Liu, F., Shrestha, M., Shrestha, D., Embree, M., Zengler, K., Wardman, C., Nevin, K. P., & Lovley, D. R. (2014b). A new model for electron flow during anaerobic digestion: direct interspecies electron transfer to Methanosaeta for the reduction of carbon dioxide to methane. *Energy & Environmental Science*, *7*(1), 408–415. https://doi.org/10.1039/c3ee42189a

Sakai, S., Ehara, M., Tseng, I., Yamaguchi, T., Bräuer, S. L., Cadillo-Quiroz, H., Zinder, S. H., & Imachi, H. (2012). Methanolinea mesophila sp. nov., a hydrogenotrophic methanogen isolated from rice field soil, and proposal of the archaeal family Methanoregulaceae fam. nov. within the order Methanomicrobiales. *INTERNATIONAL JOURNAL OF SYSTEMATIC AND EVOLUTIONARY MICROBIOLOGY*, *62*(Pt_6), 1389–1395. https://doi.org/10.1099/ijs.0.035048-0

Salvador, A. F., Martins, G., Melle-Franco, M., Serpa, R., Stams, A. J., Cavaleiro, A. J., Pereira, M. A., & Alves, M. M. (2017). Carbon nanotubes accelerate methane production in pure cultures of methanogens and in a syntrophic coculture. *Environmental Microbiology*, *19*(7), 2727–2739. https://doi.org/10.1111/1462-2920.13774

Satani, H., Kuwata, M., Ishii, H., Inoue, T., & Shimizu, A. (2020). Preparation of SEM hydrogel samples using a high pressure water freeze fracture method. *High Pressure Research*, *41*(1), 97–108. https://doi.org/10.1080/08957959.2020.1863399

Senko, O., Gladchenko, M., Maslova, O., & Efremenko, E. (2019). Long-Term storage and use of artificially immobilized anaerobic sludge as a powerful biocatalyst for conversion of various wastes including those containing xenobiotics to biogas. *Catalysts*, *9*(4), 326. https://doi.org/10.3390/catal9040326

Sharma, D., Mahajan, R., & Goel, G. (2018). Insights into direct interspecies electron transfer mechanisms for acceleration of anaerobic digestion of wastes. *International Journal of Environmental Science and Technology*, *16*(4), 2133–2142. https://doi.org/10.1007/s13762-018-2065-4

Shrestha, P. M., & Rotaru, A. (2014). Plugging in or going wireless: strategies for interspecies electron transfer. *Frontiers in Microbiology*, *5*. https://doi.org/10.3389/fmicb.2014.00237

Sitthi, S., Hatamoto, M., Watari, T., & Yamaguchi, T. (2020). Enhancing anaerobic syntrophic propionate degradation using modified polyvinyl alcohol gel beads. *Heliyon*, *6*(12), e05665. https://doi.org/10.1016/j.heliyon.2020.e05665

Smith, K. S., & Ingram-Smith, C. (2007). Methanosaeta, the forgotten methanogen? *Trends in Microbiology*, *15*(4), 150–155. https://doi.org/10.1016/j.tim.2007.02.002

Springael, K. (2019). Alginate-based encapsulation of microbial granules as a protective means to reduce stress during anaerobic digestion (Master's thesis). Ghent University. https://libstore.ugent.be/fulltxt/RUG01/002/785/122/RUG01-002785122_2019_0001_AC.pdf

Stauffer, S. R., & Peppas, N. A. (1992). Poly(vinyl alcohol) hydrogels prepared by freezing-thawing cyclic processing. Polymer Science and Engineering, 18, 3932–3936. https://cpsm.kpi.ua/polymer/1992/18/3932-3936.pdf

Storck, T., Virdis, B., & Batstone, D. J. (2015). Modelling extracellular limitations for mediated versus direct interspecies electron transfer. *The ISME Journal*, *10*(3), 621–631. https://doi.org/10.1038/ismej.2015.139

Ta, D., Lin, C., Ta, T., & Chu, C. (2020). Biohythane production via single-stage fermentation using gel-entrapped anaerobic microorganisms: Effect of hydraulic retention time. *Bioresource Technology*, *317*, 123986. https://doi.org/10.1016/j.biortech.2020.123986

Thomashow, M. F. (1998). Role of Cold-Responsive Genes in plant freezing tolerance1. *PLANT PHYSIOLOGY*, *118*(1), 1–8. https://doi.org/10.1104/pp.118.1.1

Tian, T., Qiao, S., Li, X., Zhang, M., & Zhou, J. (2016). Nano-graphene induced positive effects on methanogenesis in anaerobic digestion. *Bioresource Technology*, *224*, 41–47. https://doi.org/10.1016/j.biortech.2016.10.058

Tiwari, S. B., Dubey, M., Ahmed, B., Gahlot, P., Khan, A. A., Rajpal, A., Kazmi, A., & Tyagi, V. K. (2021). Carbon-based conductive materials facilitated anaerobic co-digestion of agro waste

under thermophilic conditions. *Waste Management*, *124*, 17–25. https://doi.org/10.1016/j.wasman.2021.01.032

Tsou, Y., Khoneisser, J., Huang, P., & Xu, X. (2016). Hydrogel as a bioactive material to regulate stem cell fate. Bioactive Materials, 1(1), 39–55. https://doi.org/10.1016/j.bioactmat.2016.05.001

Tuyen, N., Ryu, J., Yae, J., Kim, H., Hong, S., & Ahn, D. (2018). Nitrogen removal performance of anammox process with PVA–SA gel bead crosslinked with sodium sulfate as a biomass carrier. *Journal of Industrial and Engineering Chemistry*, *67*, 326–332. https://doi.org/10.1016/j.jiec.2018.07.004

Van Pham, D., & Bach, L. T. (2014). Immobilized bacteria by using PVA (Polyvinyl alcohol) crosslinked with Sodium sulfate. *International Journal of Science and Engineering*, *7*(1). https://doi.org/10.12777/ijse.7.1.41-47

Viggi, C. C., Rossetti, S., Fazi, S., Paiano, P., Majone, M., & Aulenta, F. (2014). Magnetite particles triggering a faster and more robust syntrophic pathway of methanogenic propionate degradation. *Environmental Science & Technology*, *48*(13), 7536–7543. https://doi.org/10.1021/es5016789

Wang, G., Fu, P., Su, Y., Zhang, B., Zhang, M., Li, Q., Zhang, J., Li, Y., & Chen, R. (2024). Comparing the mechanisms of syntrophic volatile fatty acids oxidation and methanogenesis recovery from ammonia stress in regular and biochar-assisted anaerobic digestion: Different roads lead to the same goal. *Journal of Environmental Management*, *352*, 120041. https://doi.org/10.1016/j.jenvman.2024.120041

Wang, J., Fan, Y., & Chen, Y. (2021). Nitrogen removal performance and characteristics of gel beads immobilized anammox bacteria under different PVA:SA ratios. *Water Environment Research*, *93*(9), 1627–1639. https://doi.org/10.1002/wer.1547

Wang, N., Yuan, T., Ko, J. H., Shi, X., & Xu, Q. (2020). Enhanced syntrophic metabolism of propionate and butyrate via nickel-containing activated carbon during anaerobic digestion. *Journal of Material Cycles and Waste Management*, *22*(5), 1529–1538.

https://doi.org/10.1007/s10163-020-01037-y

Wang, Y., Yuan, C., Cui, B., & Liu, Y. (2018). Influence of cations on texture, compressive elastic modulus, sol-gel transition and freeze-thaw properties of kappa-carrageenan gel. *Carbohydrate Polymers*, *202*, 530–535. https://doi.org/10.1016/j.carbpol.2018.08.146

Wang, Z., Wang, T., Si, B., Watson, J., & Zhang, Y. (2021). Accelerating anaerobic digestion for methane production: Potential role of direct interspecies electron transfer. *Renewable and Sustainable Energy Reviews*, *145*, 111069. https://doi.org/10.1016/j.rser.2021.111069

Wenjie, Z., Dunqiu, W., Yasunori, K., Taichi, Y., Li, Z., & Kenji, F. (2008). PVA-gel beads enhance granule formation in a UASB reactor. *Bioresource Technology*, *99*(17), 8400–8405. https://doi.org/10.1016/j.biortech.2008.02.040

Wu, K. A., & Wisecarver, K. D. (1992). Cell immobilization using PVA crosslinked with boric acid. *Biotechnology and Bioengineering*, *39*(4), 447–449. https://doi.org/10.1002/bit.260390411

Wu, Z., Li, Z., Liu, Q., & Yang, Z. (2023). Magnetite-boosted syntrophic conversion of acetate to methane during thermophilic anaerobic digestion. *Water Science & Technology*, *89*(1), 160–169. https://doi.org/10.2166/wst.2023.421

Xiao, L., Lichtfouse, E., & Kumar, P. S. (2021). Advantage of conductive materials on interspecies electron transfer-independent acetoclastic methanogenesis: A critical review. *Fuel*, *305*, 121577. https://doi.org/10.1016/j.fuel.2021.121577

Xu, H., Wang, C., Yan, K., Wu, J., Zuo, J., & Wang, K. (2016). Anaerobic granule-based biofilms formation reduces propionate accumulation under high H 2 partial pressure using conductive carbon felt particles. *Bioresource Technology*, *216*, 677–683. https://doi.org/10.1016/j.biortech.2016.06.010

Yan, W., Shen, N., Xiao, Y., Chen, Y., Sun, F., Tyagi, V. K., & Zhou, Y. (2017). The role of conductive materials in the start-up period of thermophilic anaerobic system. *Bioresource Technology*, *239*, 336–344. https://doi.org/10.1016/j.biortech.2017.05.046

Yang, C., Wu, T., Chen, H., Hsieh, T., Ho, K., & Kuo, C. (2011). Platinum Particles Embedded into

Nanowires of Polyaniline Doped With Poly(Acrylic Acid-co-Maleic Acid) as Electrocatalyst for Methanol Oxidation. *International Journal of Electrochemical Science*, *6*(5), 1642–1654. https://doi.org/10.1016/s1452-3981(23)15099-1

Yang, P., Tan, G. A., Aslam, M., Kim, J., & Lee, P. (2019). Metatranscriptomic evidence for classical and RuBisCO-mediated CO2 reduction to methane facilitated by direct interspecies electron transfer in a methanogenic system. *Scientific Reports*, *9*(1). https://doi.org/10.1038/s41598-019-40830-0

Yang, Z., Xu, X., Guo, R., Fan, X., & Zhao, X. (2015). Accelerated methanogenesis from effluents of hydrogen-producing stage in anaerobic digestion by mixed cultures enriched with acetate and nano-sized magnetite particles. *Bioresource Technology*, *190*, 132–139. https://doi.org/10.1016/j.biortech.2015.04.057

Yang, J., Zhang, J., Du, X., Gao, T., Cheng, Z., Fu, W., & Wang, S. (2024). Ammonia inhibition in anaerobic digestion of organic waste: a review. *International Journal of Environmental Science and Technology*. https://doi.org/10.1007/s13762-024-06029-1

Ye, R., Jin, Q., Bohannan, B., Keller, J. K., McAllister, S. A., & Bridgham, S. D. (2012). pH controls over anaerobic carbon mineralization, the efficiency of methane production, and methanogenic pathways in peatlands across an ombrotrophic–minerotrophic gradient. *Soil Biology and Biochemistry*, *54*, 36–47. https://doi.org/10.1016/j.soilbio.2012.05.015

Yin, Q., Yang, S., Wang, Z., Xing, L., & Wu, G. (2018). Clarifying electron transfer and metagenomic analysis of microbial community in the methane production process with the addition of ferroferric oxide. *Chemical Engineering Journal*, *333*, 216–225. https://doi.org/10.1016/j.cej.2017.09.160

Yuan, H., Wang, X., Lin, T. Y., Kim, J., & Liu, W. T. (2021). Disentangling the syntrophic electron transfer mechanisms of Candidatus geobacter eutrophica through electrochemical stimulation and machine learning. *Scientific Reports*, *11*(1). https://doi.org/10.1038/s41598-021-94628-0

Zaks, D. P. M., Winchester, N., Kucharik, C. J., Barford, C. C., Paltsev, S., & Reilly, J. M. (2011). Contribution of anaerobic digesters to emissions mitigation and electricity generation under U.S. climate policy. *Environmental Science & Technology*, *45*(16), 6735–6742. https://doi.org/10.1021/es104227y

Zhang, J., & Lu, Y. (2016). Conductive Fe3O4 Nanoparticles Accelerate Syntrophic Methane Production from Butyrate Oxidation in Two Different Lake Sediments. *Frontiers in Microbiology*, *7*. https://doi.org/10.3389/fmicb.2016.01316

Zhang, K., Deng, Y., Liu, Z., Feng, Y., Hu, C., & Wang, Z. (2023). Biochar facilitated direct interspecies electron transfer in anaerobic digestion to alleviate antibiotics inhibition and enhance methanogenesis: a review. *International Journal of Environmental Research and Public Health*, *20*(3), 2296. https://doi.org/10.3390/ijerph20032296

Zhang, K., Zhang, Y., Ouyang, X., Li, J., Liao, J., You, A., Yue, X., Xie, G., Liang, J., & Li, J. (2019). Genome-Centered Metagenomics Analysis Reveals the Microbial Interactions of a Syntrophic Consortium during Methane Generation in a Decentralized Wastewater Treatment System. *Applied Sciences*, *10*(1), 135. https://doi.org/10.3390/app10010135

Zhang, Q., Li, R., Guo, B., Zhang, L., & Liu, Y. (2021). Thermophilic co-digestion of blackwater and organic kitchen waste: Impacts of granular activated carbon and different mixing ratios. Waste Management, 131, 453–461. https://doi.org/10.1016/j.wasman.2021.06.024

Zhang, S., Chang, J., Lin, C., Pan, Y., Cui, K., Zhang, X., Liang, P., & Huang, X. (2017). Enhancement of methanogenesis via direct interspecies electron transfer between Geobacteraceae and Methanosaetaceae conducted by granular activated carbon. *Bioresource Technology*, *245*, 132–137. https://doi.org/10.1016/j.biortech.2017.08.111

Zhang, Y., Zhang, L., Guo, B., Zhou, Y., Gao, M., Sharaf, A., & Liu, Y. (2020). Granular activated carbon stimulated microbial physiological changes for enhanced anaerobic digestion of municipal sewage. *Chemical Engineering Journal*, *400*, 125838. https://doi.org/10.1016/j.cej.2020.125838

Zhao, Z., Wang, J., Li, Y., Zhu, T., Yu, Q., Wang, T., Liang, S., & Zhang, Y. (2019). Why do DIETers like drinking: Metagenomic analysis for methane and energy metabolism during anaerobic digestion with ethanol. *Water Research*, *171*, 115425. https://doi.org/10.1016/j.watres.2019.115425

Zhao, Z., Zhang, Y., Holmes, D. E., Dang, Y., Woodard, T. L., Nevin, K. P., & Lovley, D. R. (2016a). Potential enhancement of direct interspecies electron transfer for syntrophic metabolism of propionate and butyrate with biochar in up-flow anaerobic sludge blanket reactors. *Bioresource Technology*, *209*, 148–156. https://doi.org/10.1016/j.biortech.2016.03.005

Zhao, Z., Zhang, Y., Woodard, T., Nevin, K., & Lovley. (2015). Enhancing syntrophic metabolism in up-flow anaerobic sludge blanket reactors with conductive carbon materials. *Bioresource Technology*, *191*, 140–145. https://doi.org/10.1016/j.biortech.2015.05.007

Zhao, Z., Zhang, Y., Yu, Q., Dang, Y., Li, Y., & Quan, X. (2016b). Communities stimulated with ethanol to perform direct interspecies electron transfer for syntrophic metabolism of propionate and butyrate. *Water Research*, *102*, 475–484. https://doi.org/10.1016/j.watres.2016.07.005

Zheng, S., Li, Z., Zhang, P., Wang, B., Zhang, P., & Feng, Y. (2020). Multi-walled carbon nanotubes accelerate interspecies electron transfer between Geobacter cocultures. *Bioelectrochemistry*, *131*, 107346. https://doi.org/10.1016/j.bioelechem.2019.107346

Zheng, S., Zhang, H., Li, Y., Zhang, H., Wang, O., Zhang, J., & Liu, F. (2015). Co-occurrence of Methanosarcina mazei and Geobacteraceae in an iron (III)-reducing enrichment culture. *Frontiers in Microbiology*, *6*. https://doi.org/10.3389/fmicb.2015.00941

Zhou, J., Smith, J. A., Li, M., & Holmes, D. E. (2023). Methane production by Methanothrix thermoacetophila via direct interspecies electron transfer with Geobacter metallireducens. *mBio*. https://doi.org/10.1128/mbio.00360-23

Zhuang, H., Xie, Q., Shan, S., Fang, C., Ping, L., Zhang, C., & Wang, Z. (2020). Performance, mechanism and stability of nitrogen-doped sewage sludge based activated carbon supported

magnetite in anaerobic degradation of coal gasification wastewater. *The Science of the Total Environment*, *737*, 140285. https://doi.org/10.1016/j.scitotenv.2020.140285

Zhuang, L., Ma, J., Yu, Z., Wang, Y., & Tang, J. (2018). Magnetite accelerates syntrophic acetate oxidation in methanogenic systems with high ammonia concentrations. *Microbial Biotechnology*, *11*(4), 710–720. https://doi.org/10.1111/1751-7915.13286

Zhuang, L., Tang, J., Wang, Y., Hu, M., & Zhou, S. (2015). Conductive iron oxide minerals accelerate syntrophic cooperation in methanogenic benzoate degradation. *Journal of Hazardous Materials*, *293*, 37–45. https://doi.org/10.1016/j.jhazmat.2015.03.039